

**OCRWM**

**DESIGN CALCULATION OR ANALYSIS COVER SHEET**

1. QA: N/A  
2. Page 1 of 214

3. System Subsurface Tunneling System	4. Document Identifier 800-KMC-SSD0-00700-000-00A
5. Title Ground Control for Non-Emplacement Drifts for LA	
6. Group Design and Engineering/Geotechnical Group	
7. Document Status Designation <input checked="" type="checkbox"/> Preliminary <input type="checkbox"/> Final <input type="checkbox"/> Cancelled	

8. Notes/Comments

Carlos Carranza-Torres, Branko Damjanac, Marc Ruest, and David Sainsbury of Itasca Consulting Group, Inc. provided technical support and numerical analyses presented in Sections 6.4 and 6.5.

This calculation supercedes the calculation previously issued under DI: 800-K0C-TUG0-00100-000-00B. However, the computer input and output files from previous versions are not superseded. In this calculation, the materials from the previous version are incorporated and the stability analysis for interburden pillar between access drift to intake Shaft #1 and two underlying exhaust mains is added. "PC drift" is changed to "observation drift" throughout the text. Some minor editorial changes are made. All changes to the previous calculation are indicated by vertical bars in the margin adjacent to the revised material.

Attachments	Total Number of Pages
None	N/A

**RECORD OF REVISIONS**

9. No.	10. Reason For Revision	11. Total # of Pgs.	12. Last Pg. #	13. Originator (Print/Sign/Date)	14. Checker (Print/Sign/Date)	15. QER (Print/Sign/Date)	16. Approved/Accepted (Print/Sign)	17. Date
00A	Initial Issue	214	214	David H. Tang SIGNATURE ON FILE 2/25/04	Yimine Sun SIGNATURE ON FILE 2/25/04	N/A	Fei Duan SIGNATURE ON FILE	2/26/04

#### **DISCLAIMER**

This report was prepared as an account of work sponsored by an agency of the United States Government. Neither the United States Government nor any agency thereof, nor any of their employees, nor any of their contractors, subcontractors or their employees, makes any warranty, express or implied, or assumes any legal liability or responsibility for the accuracy, completeness, or any third party's use or the results of such use of any information, apparatus, product, or process disclosed, or represents that its use would not infringe privately owned rights. Reference herein to any specific commercial product, process, or service by trade name, trademark, manufacturer, or otherwise, does not necessarily constitute or imply its endorsement, recommendation, or favoring by the United States Government or any agency thereof or its contractors or subcontractors. The views and opinions of authors expressed herein do not necessarily state or reflect those of the United States Government or any agency thereof.

## CONTENTS

	<b>Page</b>
ACRONYMS AND ABBREVIATIONS .....	16
1. PURPOSE .....	17
2. QUALITY ASSURANCE .....	18
3. COMPUTER SOFTWARE AND MODEL USAGE .....	19
3.1 FLAC COMPUTER SOFTWARE .....	19
3.2 FLAC3D COMPUTER SOFTWARE .....	19
3.3 3DEC COMPUTER CODE .....	20
3.4 SPREADSHEET SOFTWARE .....	20
4. INPUTS .....	21
4.1 DATA AND PARAMETERS .....	21
4.1.1 Rock Mass Mechanical Properties .....	21
4.1.1.1 Lithophysal Rock .....	21
4.1.1.2 Non-lithophysal Rock .....	21
4.1.2 Rock Mass Density .....	22
4.1.3 Dimensions and Properties for Fully Grouted Rock Bolts .....	22
4.1.4 Dimension and Properties for Shotcrete .....	22
4.1.5 Dimensions and Properties for Stainless Steel Super Swellex Bolts .....	22
4.1.6 Seismic Velocity History .....	22
4.1.7 Rock Mass Thermal Expansion Coefficients .....	23
4.1.8 Rock Mass Mechanical Properties of TCw Thermal Mechanical Unit .....	26
4.2 DESIGN CRITERIA AND CONSTRAINTS .....	26
4.2.1 Criteria .....	26
4.2.2 Constraints .....	27
4.3 CODES AND STANDARDS .....	28
5. ASSUMPTIONS .....	29
5.1 INITIAL GROUND RELAXATION .....	29
5.2 AVERAGE DEPTH OF REPOSITORY HOST HORIZON .....	29
5.3 HORIZONTAL-TO-VERTICAL IN SITU STRESS RATIOS .....	29
5.4 TENSILE STRENGTH OF LITHOPHYSAL ROCK .....	30
5.5 LIMIT AXIAL FORCE FOR STAINLESS STEEL SUPER SWELLEX BOLTS ...	30
5.6 TENSILE STRENGTH IN THE 3DEC SIMULATIONS .....	30
5.7 PROPERTIES OF INTERFACE BETWEEN SHOTCRETE AND ROCK .....	30
5.8 GROUND SUPPORT TYPES .....	30
6. GROUND SUPPORT DESIGN .....	32
6.1 INTRODUCTION .....	32
6.2 REPOSITORY HOST HORIZON AND GEOTECHNICAL CHARACTERIZATION .....	33
6.3 GROUND SUPPORT FUNCTIONS .....	33

6.4	EMPIRICAL METHODS.....	37
6.4.1	Geomechanics Rock Mass Classification System.....	37
6.4.2	NGI Rock Mass Classification System.....	38
6.4.3	Empirical Analysis of Ground Support Need.....	41
6.5	ANALYTICAL METHODS.....	47
6.5.1	Modeling of Non-Emplacement Drifts.....	47
6.5.1.1	Modeling of Access and Exhaust Mains and Turnouts.....	47
6.5.1.2	Modeling of Intersections between Access Mains and Turnouts and between Exhaust Mains and Emplacement Drifts.....	48
6.5.1.3	Modeling of Observation Drift.....	50
6.5.1.4	Modeling of TBM Launch Chamber.....	50
6.5.1.5	Modeling of North Portal.....	50
6.5.1.6	Modeling of Interburden Pillar between Shaft Access and Exhaust Mains.....	50
6.5.2	Loading and Boundary Conditions.....	50
6.5.2.1	In Situ Loads.....	51
6.5.2.2	Operation Loads.....	67
6.5.2.3	Seismic Loads.....	67
6.5.2.4	Thermal Loads.....	68
6.5.2.5	Boundary Conditions.....	69
6.5.3	Stability of Unsupported Non-Emplacement Drifts.....	70
6.5.3.1	In Situ Stress Loading Condition.....	70
6.5.3.2	Thermal Loading Condition.....	118
6.5.3.3	Seismic Loading Condition.....	136
6.5.3.4	Ground Reaction Curves.....	163
6.5.4	Ground Support Systems for Non-Emplacement Drifts.....	167
6.5.4.1	Candidate Ground Support System.....	167
6.5.4.2	Candidate Ground Support Materials.....	167
6.5.5	Stability of Supported Non-Emplacement Drifts.....	168
6.5.5.1	Mechanical Properties of Fully Grouted Rock Bolts and Swellex Bolts.....	169
6.5.5.2	In Situ Stress Loading Condition.....	170
6.5.5.3	Thermal Loading Condition.....	174
6.5.5.4	Seismic Loading Condition.....	175
6.6	UNCERTAINTY DISCUSSION.....	203
6.6.1	Uncertainties with Empirical Approach.....	203
6.6.2	Uncertainties with Numerical Modeling Method.....	203
6.6.3	Uncertainties with Input Data.....	204
7.	SUMMARY AND CONCLUSIONS.....	206
7.1	SUMMARY.....	206
7.2	STABILITY OF UNSUPPORTED NON-EMPLACEMENT DRIFTS.....	206
7.3	GROUND SUPPORT SYSTEM FOR NON-EMPLACEMENT DRIFTS.....	208
7.4	STABILITY OF SUPPORTED NON-EMPLACEMENT DRIFTS.....	209
8.	REFERENCES.....	211
8.1	DOCUMENTS CITED.....	211

8.2	CODES, STANDARDS, REGULATIONS, AND PROCEDURES.....	213
8.3	SOURCE DTNS .....	214

**FIGURES**

	<b>Page</b>
Figure 4-1. Time Histories of Velocity Components of Seismic Motion for Mean Annual Exceedance Probability of: (a) $1 \times 10^{-4}$ ; (b) $5 \times 10^{-4}$ .....	25
Figure 5-1. Illustration of Shotcreted Areas at Intersections .....	31
Figure 6-1. Underground Layout and Geological Units by Panel .....	35
Figure 6-2. Lithophysae and Fracturing in the Tptpl Unit.....	36
Figure 6-3. Fractures in the Wall of the ECRB in the Tptpmn Unit.....	36
Figure 6-4. Estimated Ground Support Needs Based on Q Index .....	40
Figure 6-5. Ground Support Needs for Rock Mass Categories 1 to 5 for Access and Exhaust Mains.....	43
Figure 6-6. Ground Support Needs for Rock Mass Categories 1 to 5 for Turnouts .....	44
Figure 6-7. Ground Support Needs for Rock Mass Categories 1 to 5 for Typical Intersection.....	44
Figure 6-8. Ground Support Needs for Rock Mass Categories 1 to 5 for Largest Intersection.....	45
Figure 6-9. FLAC Model of Access and Exhaust Mains.....	49
Figure 6-9A. FLAC Model of Turnouts with Rock Bolts .....	49
Figure 6-10. 3DEC Model Configuration of Intersection at Location A.....	53
Figure 6-10A. 3DEC Model Configuration of Intersection at Location C .....	54
Figure 6-11. FLAC3D Model Configuration of Intersection at Location C.....	55
Figure 6-11A. Perspective View of Intersection at Location C in FLAC3D Model .....	55
Figure 6-12. 3DEC Model Geometry and Dimension for Intersection at Location A .....	56
Figure 6-13. Geometry of 3DEC Model for Intersection at Location B.....	57
Figure 6-13A. Geometry of 3DEC Model for Intersection at Location D.....	58
Figure 6-14. Geometry of Two-dimensional Model of Observation Drift and Emplacement Drift.....	59
Figure 6-14A. Grid of Two-dimensional Model of Observation Drift and Emplacement Drift.....	59
Figure 6-15. Geometry of Intersection of Observation Drift with Exhaust Main .....	60
Figure 6-15A. Geometry of 3DEC Model for Intersection between Observation Drift and Exhaust Main .....	61
Figure 6-16. Geometry of Two-dimensional Model of TBM Launch Chamber .....	62
Figure 6-16A. Grid of Two-dimensional Model of TBM Launch Chamber .....	62
Figure 6-17. a) Isometric and b) Plan Views of North Portal Model .....	63
Figure 6-17A. a) Frontal Cross-sectional (C <sub>1</sub> -C <sub>1</sub> ') and b) Longitudinal Cross-sectional (L-L') Views of North Portal Model.....	64
Figure 6-17B. Configuration of 3DEC Model for Interburden Pillar between Access Drift to Intake Shaft #1 and Exhaust Mains .....	65
Figure 6-17C. Geometry of 3DEC Model for Interburden Pillar between Access Drift to Intake Shaft #1 and Exhaust Mains .....	66
Figure 6-18. Displacements at Access and Exhaust Mains for Lithophysal Cat. 1 Rock.....	73
Figure 6-19. Contours of Safety Factor around Unsupported Access/Exhaust Main for Lith. Cat. 1 Rock.....	79
Figure 6-20. Contours of Safety Factor around Unsupported Access/Exhaust Main for N. Lith. Cat. 1 Rock.....	79

Figure 6-21. Contours of Safety Factor around Unsupported Turnout for Lith. Cat. 1 Rock .....	80
Figure 6-22. Contours of Safety Factor around Unsupported Turnout for N. Lith. Cat. 1 Rock .....	80
Figure 6-23. Intersection A: Displacement Field in Vertical Section 1 for Lith. Cat. 1 Rock .....	81
Figure 6-24. Intersection A: Displacement Field in Vertical Section 1 for N. Lith. Cat. 1 Rock .....	81
Figure 6-25. Intersection A: Displacement Field in Vertical Section 2 for Lith. Cat. 1 Rock .....	82
Figure 6-26. Intersection A: Displacement Field in Vertical Section 2 for N. Lith. Cat. 1 Rock .....	82
Figure 6-27. Intersection A: Vertical Displacement along Vertical Line through Point A .....	83
Figure 6-28. Intersection A: Potential Yield Zone in Vertical Section 2 for Lith. Cat. 1 Rock .....	83
Figure 6-29. Intersection A: Potential Yield Zone in Vertical Section 2 for N. Lith. Cat. 1 Rock .....	84
Figure 6-30. Intersection C: Displacement Field in Vertical Section 1 for Lith. Cat. 1 Rock.....	84
Figure 6-31. Intersection C: Displacement Field in Vertical Section 1 for N. Lith. Cat. 1 Rock .....	85
Figure 6-32. Intersection C: Displacement Field in Vertical Section 2 for Lith. Cat. 1 Rock.....	85
Figure 6-33. Intersection C: Displacement Field in Vertical Section 2 for N. Lith. Cat. 1 Rock .....	86
Figure 6-34. Intersection C: Vertical Displacement along Vertical Line through Point A .....	86
Figure 6-35. Intersection C: Potential Yield Zone in Vertical Section 1 for Lith. Cat. 1 Rock .....	87
Figure 6-36. Intersection C: Potential Yield Zone in Vertical Section 1 for N. Lith. Cat. 1 Rock .....	87
Figure 6-37. Intersection C: Contours of Vertical Displacements and Stress Fields in Vertical Section 1 for Lith. Cat. 1 Rock Using FLAC3D.....	88
Figure 6-38. Intersection A: Stress Field in Vertical Section 1 for Lith. Cat. 1 Rock.....	89
Figure 6-39. Intersection A: Stress Field in Vertical Section 1 for N. Lith. Cat. 1 Rock.....	89
Figure 6-40. Intersection A: Stress Field in Vertical Section 2 for Lith. Cat. 1 Rock.....	90
Figure 6-41. Intersection A: Stress Field in Vertical Section 2 for N. Lith. Cat. 1 Rock.....	90
Figure 6-42. Intersection A: Factor of Safety in Vertical Section 2 for Lith. Cat. 1 Rock.....	91
Figure 6-43. Intersection A: Factor of Safety in Vertical Section 2 for N. Lith. Cat. 1 Rock.....	91
Figure 6-44. Intersection A: Compressive and Tensile Stresses in Vertical Section 2 for Lith. Cat. 1 Rock.....	92
Figure 6-45. Intersection A: Average Pillar Stress vs. Distance from the Pillar Tip.....	92
Figure 6-46. Intersection A: Potential Yield Zone in Horizontal Section for Lith. Cat. 1 Rock .....	93
Figure 6-47. Intersection A: Potential Yield Zone in Horizontal Section for N. Lith. Cat. 1 Rock .....	93
Figure 6-48. Intersection C: Stress Field in Vertical Section 1 for Lith. Cat. 1 Rock .....	94
Figure 6-49. Intersection C: Stress Field in Vertical Section 1 for N. Lith. Cat. 1 Rock .....	94
Figure 6-50. Intersection C: Stress Field in Vertical Section 2 for Lith. Cat. 1 Rock .....	95
Figure 6-51. Intersection C: Stress Field in Vertical Section 2 for N. Lith. Cat. 1 Rock .....	95
Figure 6-52. Intersection C: Factor of Safety in Vertical Section 2 for Lith. Cat. 1 Rock.....	96
Figure 6-53. Intersection C: Factor of Safety in Vertical Section 2 for N. Lith. Cat. 1 Rock .....	96

Figure 6-54. Intersection C: Average Pillar Stress vs. Distance from Pillar Tip.....	97
Figure 6-55. Intersection C: Potential Yield Zone in Horizontal Section for Lith. Cat. 1 Rock.....	97
Figure 6-56. Intersection C: Potential Yield Zone in Horizontal Section for N. Lith. Cat. 1 Rock.....	98
Figure 6-57. Intersection B: Displacement Field in Vertical Section 1 for Lith. Cat. 1 Rock.....	98
Figure 6-58. Intersection D: Displacement Field in Vertical Section 1 for N. Lith. Cat. 1 Rock.....	99
Figure 6-59. Intersection B: Stress Field in Vertical Section 1 for Lith. Cat. 1 Rock.....	99
Figure 6-60. Intersection D: Stress Field in Vertical Section 1 for N. Lith. Cat. 1 Rock.....	100
Figure 6-61. Intersection B: Factor of Safety in Vertical Section 1 for Lith. Cat. 1 Rock.....	100
Figure 6-62. Intersection D: Factor of Safety in Vertical Section 1 for N. Lith. Cat. 1 Rock.....	101
Figure 6-63. Intersection B: Potential Yield Zone in Vertical Section 1 for Lith. Cat. 1 Rock.....	101
Figure 6-64. Intersection D: Potential Yield Zone in Vertical Section 1 for N. Lith. Cat. 1 Rock.....	102
Figure 6-65. Intersection B: Potential Yield Zone in Horizontal Section for Lith. Cat. 1 Rock.....	102
Figure 6-66. Intersection D: Potential Yield Zone in Horizontal Section for N. Lith. Cat. 1 Rock.....	103
Figure 6-66A. Displacements due to Excavations of Observation Drift and Emplacement Drift.....	103
Figure 6-66B. Contours of Major Principal Stress after Excavation of Observation Drift and Emplacement Drift.....	104
Figure 6-66C. Potential Yield Zone after Excavation of Observation Drift and Emplacement Drift.....	104
Figure 6-66D. Factor of Safety after Excavation of Observation Drift and Emplacement Drift.....	105
Figure 6-66E. Displacement Field in Vertical Section 1 at Intersection between Observation Drift and Exhaust Main.....	105
Figure 6-66F. Displacement Field in Vertical Section 2 at Intersection between Observation Drift and Exhaust Main.....	106
Figure 6-66G. Potential Yield Zone in Intersection between Observation Drift and Exhaust Main in Section 1.....	106
Figure 6-66H. Potential Yield Zone in Intersection between Observation Drift and Exhaust Main in Section 2.....	107
Figure 6-66I. Factor of Safety in Intersection between Observation Drift and Exhaust Main in Section 1.....	107
Figure 6-66J. Factor of Safety in Intersection between Observation Drift and Exhaust Main in Section 2.....	108
Figure 6-66K. Displacements due to Excavation of TBM Launch Chamber.....	108
Figure 6-66L. Contours of Major Principal Stress after Excavation of TBM Launch Chamber.....	109
Figure 6-66M. Potential Yield Zone after Excavation of TBM Launch Chamber.....	109
Figure 6-66N. Factor of Safety after Excavation of TBM Launch Chamber.....	110

Figure 6-66O. Factor of Safety after Excavation of North Portal Starter Tunnel: a) Horizontal Cross-section at Elevation 1128 m, and b) Longitudinal Cross-section L-L' .....	111
Figure 6-66P. Major Principal Stresses after Excavation of North Portal Starter Tunnel for Cross-sections: a) C <sub>1</sub> -C <sub>1</sub> ' and b) C <sub>2</sub> -C <sub>2</sub> ' .....	112
Figure 6-66Q. Displacement Field after Excavation of North Portal Starter Tunnel for Cross-sections: a) C <sub>1</sub> -C <sub>1</sub> ' and b) C <sub>2</sub> -C <sub>2</sub> ' .....	113
Figure 6-66R. Displacement Field in Vertical Section 1 for Lith. Cat. 1 Rock at Interburden Area .....	114
Figure 6-66S. Displacement Field in Vertical Section 2 for Lith. Cat. 1 Rock at Interburden Area .....	114
Figure 6-66T. Stress Field in Vertical Section 1 for Lith. Cat. 1 Rock at Interburden Area .....	115
Figure 6-66U. Stress Field in Vertical Section 2 for Lith. Cat. 1 Rock at Interburden Area .....	115
Figure 6-66V. Factor of Safety in Vertical Section 1 for Lith. Cat. 1 Rock at Interburden Area .....	116
Figure 6-66W. Factor of Safety in Vertical Section 2 for Lith. Cat. 1 Rock at Interburden Area .....	116
Figure 6-66X. Potential Yield Zone in Vertical Section 1 for Lith. Cat. 1 Rock at Interburden Area .....	117
Figure 6-66Y. Potential Yield Zone in Vertical Section 2 for Lith. Cat. 1 Rock at Interburden Area .....	117
Figure 6-67. Intersection B: Temperature Field in Vertical Section 1 after 3 Years of Heating .....	120
Figure 6-68. Intersection B: Temperature Field in Vertical Section 1 after 20 Years of Heating .....	120
Figure 6-69. Intersection B: Temperature History at Points 1, 2 and 3 .....	121
Figure 6-70. Intersection D: Temperature History at Points 1, 2 and 3 .....	121
Figure 6-71. Intersection B: Time History of Major Principal Stresses for Lith. Cat. 1 Rock .....	122
Figure 6-72. Intersection B: Time History of Major Principal Stresses for Lith. Cat. 5 Rock .....	122
Figure 6-73. Intersection D: Time History of Major Principal Stresses for N. Lith. Cat. 1 Rock .....	123
Figure 6-74. Intersection D: Time History of Major Principal Stresses for N. Lith. Cat. 5 Rock .....	123
Figure 6-75. Intersection B: Factor of Safety in Vertical Section 1 for Lith. Cat. 1 Rock after 1 Year of Heating .....	124
Figure 6-76. Intersection B: Factor of Safety in Vertical Section 1 for Lith. Cat. 1 Rock after 50 Years of Heating .....	124
Figure 6-77. Intersection D: Factor of Safety in Vertical Section 1 for N. Lith. Cat. 1 Rock after 1 Year of Heating .....	125
Figure 6-78. Intersection D: Factor of Safety in Vertical Section 1 for N. Lith. Cat. 1 Rock after 50 Years of Heating .....	125
Figure 6-79. Intersection B: Potential Yield Zone in Vertical Section 1 for Lith. Cat. 1 Rock after 50 Years of Heating .....	126

Figure 6-80. Intersection D: Potential Yield Zone in Vertical Section 1 for N. Lith. Cat. 1 Rock after 50 Years of Heating .....	126
Figure 6-81. Intersection B: Time History of Vertical Displacement at Point 1 for Lith. Rock .....	127
Figure 6-82. Intersection D: Time History of Vertical Closure at Point 1 for N. Lith. Rock.....	127
Figure 6-82A. Temperature Contours around Observation Drift after 50 Years of Heating.....	128
Figure 6-82B. Temperature Histories at Three Points around Observation Drift during 50 Years of Heating .....	128
Figure 6-82C. Major Principal Stresses at Three Points around Observation Drift during 50 Years of Heating .....	129
Figure 6-82D. Potential Yield Zone around Observation Drift after 50 Years of Heating .....	129
Figure 6-82E. Factor of Safety around Observation Drift after 50 Years of Heating .....	130
Figure 6-82F. Displacement Histories at Three points around Observation Drift during 50 Years of Heating .....	130
Figure 6-82G. Potential Yield Zone at Intersection between Observation Drift and Exhaust Main in Vertical Section 1 after 50 Years of Heating.....	131
Figure 6-82H. Potential Yield Zone at Intersection between Observation Drift and Exhaust Main in Vertical Section 2 after 50 Years of Heating.....	131
Figure 6-82I. Factor of Safety at Intersection between Observation Drift and Exhaust Main in Vertical Section 1 after 50 Years of Heating .....	132
Figure 6-82J. Factor of Safety at Intersection between Observation Drift and Exhaust Main in Vertical Section 2 after 50 Years of Heating .....	132
Figure 6-82K. Temperature Field in Vertical Section 1 after 3 Years of Heating at Interburden Area .....	133
Figure 6-82L. Temperature Field in Vertical Section 1 after 20 Years of Heating at Interburden Area .....	133
Figure 6-82M. Temperature Histories at Various Points at Interburden Area .....	134
Figure 6-82N. Histories of Major Principal Stresses for Lith. Cat. 1 Rock at Interburden Area.....	134
Figure 6-82O. Safety Factor in Vertical Section 1 for Lith. Cat. 1 Rock after 1 Year of Heating at Interburden Area.....	135
Figure 6-82P. Safety Factor in Vertical Section 1 for Lith. Cat. 1 Rock after 50 Years of Heating at Interburden Area.....	135
Figure 6-82Q. Potential Yield Zone in Vertical Section 1 for Lith. Cat. 1 after 50 Years of Heating.....	136
Figure 6-83. Intersection A: Potential Yield Zone in Vertical Section 2 for Lith. Cat. 1 Rock under In Situ and Seismic Loads.....	137
Figure 6-84. Intersection A: Potential Yield Zone in Vertical Section 2 for N. Lith. Cat. 1 Rock under In Situ and Seismic Loads .....	138
Figure 6-85. Intersection A: Potential Yield Zone in Horizontal Section for Lith. Cat. 1 Rock under In Situ and Seismic Loads .....	138
Figure 6-86. Intersection A: Potential Yield Zone in Horizontal Section for N. Lith. Cat. 1 Rock under In Situ and Seismic Loads .....	139
Figure 6-87. Intersection A: Stress Field in Vertical Section 2 for Lith. Cat. 1 Rock under In Situ and Seismic Loads.....	139

Figure 6-88. Intersection A: Stress Field in Vertical Section 2 for N. Lith. Cat. 1 Rock under In Situ and Seismic Loads .....	140
Figure 6-89. Intersection A: Factor of Safety in Vertical Section 2 for Lith. Cat. 1 Rock under In Situ and Seismic Loads .....	140
Figure 6-90. Intersection A: Compressive and Tensile Stresses in Vertical Section 2 for Lith. Cat. 1 Rock under In Situ and Seismic Loads.....	141
Figure 6-91. Intersection A: Average Pillar Stress vs. Distance from Pillar Tip under In Situ and Seismic Loading .....	141
Figure 6-92. Intersection A: Velocity Histories in x, y and z Direction near Point A for Lith. Cat. 1 Rock.....	142
Figure 6-93. Intersection A: Vertical Displacements along Vertical Line through Point A under Static and Seismic Loads .....	142
Figure 6-94. Intersection B: Velocity Histories in X, Y and Z Directions near Point 1 for Lith. Cat. 1 Rock.....	143
Figure 6-95. Intersection D: Velocity Histories in X, Y and Z Directions near Point 1 for N. Lith. Cat. 1 Rock.....	144
Figure 6-96. Intersection B: Potential Yield Zone in Vertical Section 1 for Lith. Cat. 1 Rock under In Situ and Seismic Loads.....	144
Figure 6-97. Intersection D: Potential Yield Zone in Vertical Section 1 for N. Lith. Cat. 1 Rock under In Situ and Seismic Loads.....	145
Figure 6-98. Intersection B: Potential Yield Zone in Horizontal Section for Lith. Cat. 1 Rock under In Situ and Seismic Loads.....	145
Figure 6-99. Intersection D: Potential Yield Zone in Horizontal Section for N. Lith. Cat. 1 Rock under In Situ and Seismic Loads.....	146
Figure 6-100. Intersection B: Factor of Safety in Vertical Section 1 for Lith. Cat. 1 Rock under In Situ and Seismic Loads .....	146
Figure 6-101. Intersection D: Factor of Safety in Vertical Section 1 for N. Lith. Cat. 1 Rock under In Situ and Seismic Loads.....	147
Figure 6-101A. Potential Yield Zone around Observation Drift after Seismic Shaking.....	148
Figure 6-101B. Factor of Safety around Observation Drift after Seismic Shaking.....	148
Figure 6-101C. Velocity Histories of Point at Crown of Observation Drift during Seismic Shaking .....	149
Figure 6-101D. Stress Histories of Points at Observation Drift during Seismic Shaking.....	149
Figure 6-101E. Potential Yield Zone in Intersection between Observation Drift and Exhaust Main in Vertical Section 1 after Seismic Shaking.....	150
Figure 6-101F. Potential Yield Zone in Intersection between Observation Drift and Exhaust Main in Vertical Section 2 after Seismic Shaking.....	150
Figure 6-101G. Factor of Safety in Intersection between Observation Drift and Exhaust Main in Vertical Section 1 after Seismic Shaking.....	151
Figure 6-101H. Factor of Safety in Intersection between Observation Drift and Exhaust Main in Vertical Section 2 after Seismic Shaking.....	151
Figure 6-101I. Potential Yield Zone around TBM Launch Chamber after Seismic Shaking.....	153
Figure 6-101J. Factor of Safety around TBM Launch Chamber after Seismic Shaking.....	154
Figure 6-101K. Velocity Histories of Point at Crown of TBM Launch Chamber after Seismic Shaking.....	154

Figure 6-101L. Stress Histories at Three Points around TBM Launch Chamber after Seismic Shaking.....	155
Figure 6-101M. Velocity Histories in X, Y, and Z Directions at Ground Surface.....	155
Figure 6-101N. Velocity Histories in X, Y, and Z Directions at Crown of Starter Tunnel.....	156
Figure 6-101O. Factor of Safety after 19.84 Seconds of Ground Shaking: a) Horizontal Cross-section at Elevation 1128 m; and b) Longitudinal Cross-section L-L' .....	157
Figure 6-101P. Major Principal Stresses after 19.84 Seconds of Ground Shaking for Cross-sections: a) C <sub>1</sub> -C <sub>1</sub> ' and b) C <sub>2</sub> -C <sub>2</sub> ' .....	158
Figure 6-101Q. Factor of Safety at End of Ground Shaking: a) Horizontal Cross-section at Elevation 1128 m; and b) Longitudinal Cross-section L-L' .....	159
Figure 6-101R. Major Principal Stresses at End of Ground Shaking for Cross-sections: a) C <sub>1</sub> -C <sub>1</sub> ' and b) C <sub>2</sub> -C <sub>2</sub> ' .....	160
Figure 6-101S. Velocity Histories in X, Y, and Z Directions near Point 1 for Lith. Cat. 1 Rock at Interburden Area.....	161
Figure 6-101T. Potential Yield Zone in Vertical Section 1 for Lith. Cat. 1 Rock under In Situ and Seismic Loading at Interburden Area.....	161
Figure 6-101U. Potential Yield Zone in Vertical Section 2 for Lith. Cat. 1 Rock under In Situ and Seismic Loading at Interburden Area.....	162
Figure 6-101V. Safety Factor in Vertical Section 1 for Lith. Cat. 1 Rock under In Situ and Seismic Loading at Interburden Area .....	162
Figure 6-101W. Safety Factor in Vertical Section 2 for Lith. Cat. 1 Rock under In Situ and Seismic Loading at Interburden Area .....	163
Figure 6-102. Ground Reaction Curves for Unsupported Access and Exhaust Mains: (a) Roof; (b) Wall.....	165
Figure 6-103. Ground Reaction Curves for Unsupported Turnouts: (a) Roof; (b) Wall.....	166
Figure 6-104. Ground Support System in Access or Exhaust Mains .....	169
Figure 6-105. Ground Support System in Turnouts.....	170
Figure 6-105A. Isometric View of Shotcrete and Rockbolts in North Portal Model .....	174
Figure 6-106. Displacements around Supported Access Main for Lith. Cat. 1 Rock.....	178
Figure 6-107. Axial Force along Bolts at Access Main for Lith. Cat. 1 Rock .....	178
Figure 6-108. Contours of Safety Factor around Supported Access/Exhaust Main for Lith. Cat. 1 Rock.....	179
Figure 6-109. Contours of Safety Factor around Supported Access/Exhaust Main for N. Lith. Cat. 1 Rock.....	179
Figure 6-110. Contours of Safety Factor around Supported Turnout for Lith. Cat. 1 Rock.....	180
Figure 6-111. Contours of Safety Factor around Supported Turnout for N. Lith. Cat. 1 Rock.....	180
Figure 6-112. Axial Forces in Bolts along the Access Main after Excavation.....	181
Figure 6-113. Axial Forces in Bolts along the Access Main after Excavation of First Turnout.....	181
Figure 6-114. Plan View: Axial Forces in Bolts along the Access Main after Excavation of First Turnout.....	182
Figure 6-115. Plan View: Axial Forces in Bolts along the Access Main after Excavation of both Turnouts.....	182
Figure 6-116. Displacement in Vertical Section 2 through First Intersection: a) before, b) after Excavation of Second Turnout .....	183

Figure 6-117. Axial Forces in Bolts along Exhaust Main after Excavation .....	184
Figure 6-118. Plan View of Axial Forces in Bolts along Exhaust Main after Excavation .....	184
Figure 6-119. Axial Forces in Bolts along Exhaust Main after Excavation of Exhaust Main and Emplacement Drift .....	185
Figure 6-120. Axial Forces in Bolts along Emplacement Drift after Excavation of Exhaust Main and Emplacement Drift .....	185
Figure 6-121. Plan View of Axial Forces in Bolts along Exhaust Main after Excavation of Exhaust Main and Emplacement Drift .....	186
Figure 6-121A. Bolt Forces in Observation Drift after Excavation of Emplacement Drift .....	186
Figure 6-122. Time History of Bolt Forces at Exhaust Main and Emplacement Drift during Preclosure .....	187
Figure 6-123. Intersection B: Forces in Bolts along Exhaust Main after 5 Years of Heating .....	187
Figure 6-124. Intersection B: Forces in Bolts along Exhaust Main after 50 Years of Heating .....	188
Figure 6-125. Plan view of Forces in Bolts along Exhaust Main after 50 Years of Heating .....	188
Figure 6-125A. Bolt Forces in Observation Drift after 50 Years of Heating .....	189
Figure 6-125B. Bolt Forces in Three Points of Observation Drift after 50 Years of Heating .....	189
Figure 6-125C. Potential Yield Zone around Observation Drift after 50 Years of Heating .....	190
Figure 6-126. Plan View of Rock Bolts and Shotcrete at Intersection of Access Main and Turnout .....	190
Figure 6-127. Perspective View along Access Main showing Geometry of Shotcrete .....	191
Figure 6-128. Axial Forces in Bolts along Access Main before Ground Shaking .....	191
Figure 6-129. Axial Forces in Bolts along Access Main after 40 seconds of Ground Shaking .....	192
Figure 6-130. Axial Forces in Bolts along Access Main at End of Ground Shaking .....	192
Figure 6-131. Contours of Major Principal Stresses in Shotcrete after 40 Seconds of Ground Shaking .....	193
Figure 6-132. Contours of Major Principal Stresses in Shotcrete at End of Ground Shaking .....	193
Figure 6-133. Forces in Bolts along Exhaust Main after 40 Seconds of Ground Shaking .....	194
Figure 6-134. Bolt forces in Observation Drift after Seismic Shaking .....	194
Figure 6-135. Histories of Forces in Three Bolts in Observation Drift during Seismic Shaking .....	195
Figure 6-136. Potential Yield Zone around Observation Drift after Seismic Shaking .....	195
Figure 6-137. Plan View of Bolt Forces in Intersection between Observation Drift and Exhaust Main after 50 Years of Heating .....	196
Figure 6-138. Bolt Forces in Intersection between Observation Drift and Exhaust Main after 50 Years of Heating – View along Exhaust Main .....	196
Figure 6-139. Bolt Forces in Intersection between Observation Drift and Exhaust Main after 50 Years of Heating – View along Observation Drift .....	197
Figure 6-140. Plan View of Bolt Forces in Intersection between Observation Drift and Exhaust Main after 40 Seconds of Seismic Shaking .....	197
Figure 6-141. Plan View of Bolt Forces in Intersection between Observation Drift and Exhaust Main at End of Seismic Shaking .....	198
Figure 6-142. Bolt Forces in TBM Launch Chamber after Seismic Shaking .....	198
Figure 6-143. Histories of Forces in Three Bolts in TBM Launch Chamber during Seismic Shaking .....	199

Figure 6-144. Potential Yield Zone around TBM Launch Chamber after Seismic Shaking.....	199
Figure 6-145. Bolt Forces in North Portal after 19.84 Seconds of Ground Shaking.....	200
Figure 6-146. Bolt Forces in North Portal at End of Ground Shaking .....	200
Figure 6-147. Contours of a) Major and b) Minor Principal Membrane Stresses in Shotcrete after 19.84 Seconds of Ground Shaking .....	201
Figure 6-148. Contours of a) Major and b) Minor Principal Membrane Stresses in Shotcrete at End of Ground Shaking .....	202

## TABLES

	<b>Page</b>
Table 4-1. Rock Mass Mechanical Properties for Lithophysal Rock .....	21
Table 4-2. Rock Mass Mechanical Properties for Non-lithophysal Rock .....	22
Table 4-3. Dimensions and Properties of Fully Grouted Rock Bolts .....	23
Table 4-4. Dimension and Properties of Shotcrete .....	23
Table 4-5. Dimensions and Properties for Stainless Steel Super Swellex Rock Bolts .....	24
Table 4-6. Coefficients of Thermal Expansion for TSw2 Unit .....	26
Table 4-7. Rock Mass Mechanical Properties of the TCw Unit .....	26
Table 6-1. Estimate of Ground Support Needs Based on RMR System .....	39
Table 6-2. RMR and Q Values for Non-lithophysal Rock .....	42
Table 6-3. Equivalent Dimension $D_e$ and Bolt Length for Various Openings .....	42
Table 6-4. Ground Support Needs for Access and Exhaust Mains based on Q Values .....	45
Table 6-5. Ground Support Needs for Turnouts based on Q Values .....	46
Table 6-6. Ground Support Needs for Typical Intersections based on Q Values .....	46
Table 6-7. Ground Support Needs for Large Intersections based on Q Values .....	46
Table 6-8. Boundary Conditions for 3DEC Analysis .....	70
Table 6-9. Unsupported Access and Exhaust Mains and Turnouts - Results for In Situ Stress Loading Condition from FLAC .....	72

## ACRONYMS AND ABBREVIATIONS

3DEC	3-Dimensional Distinct Element Code
ASM	American Society for Metals
ASTM	American Society for Testing and Materials
BSC	Bechtel SAIC Company, LLC.
DOE	U.S. Department of Energy
DTN	Data Tracking Number
ECRB	Enhanced Characterization of the Repository Block
EDZ	Excavation-disturbed Zone
ESF	Exploratory Studies Facility
ESR	Excavation Support Ratio
FLAC	Fast Lagrangian Analysis of Continua
FLAC3D	Fast Lagrangian Analysis of Continua in 3 Dimensions
GRC	Ground Reaction Curve
LA	License Application
NGI	Norwegian Geotechnical Institute
NUFT	Nonisothermal Unsaturated-saturated Flow and Transport
Q	Rock Mass Quality Index
QARD	Quality Assurance Requirements and Description
PC	Performance Confirmation
RMR	Rock Mass Rating
RQD	Rock Quality Designation
RHH	Repository Host Horizon
SCM	Software Configuration Management
SF	Safety Factor
SRF	Stress Reduction Factor
TBM	Tunnel Boring Machine
TDMS	Technical Data Management System
WWF	Welded Wire Fabric
YMP	Yucca Mountain Project

## **1. PURPOSE**

The purpose of this calculation is to analyze the stability of repository non-emplacement drifts during the preclosure period, and to provide a final ground support method for non-emplacement drifts for the License Application (LA). This calculation will provide input for the development of LA documents.

The scope of this calculation is limited to the non-emplacement drifts including access mains, ramps, exhaust mains, turnouts, intersections between access mains and turnouts, and intersections between exhaust mains and emplacement drifts, portals, TBM launch chambers, observation drift and test alcove in the performance confirmation (PC) facilities, etc. The calculation is limited to the non-emplacement drifts subjected to a combined loading of in-situ stress, seismic stress, and/or thermal stress. Other effects such as hydrological and chemical effects are not considered in this analysis.

## 2. QUALITY ASSURANCE

This calculation is developed in accordance with AP-3.12Q, *Design Calculations and Analyses*. In accordance with the Q-list (BSC 2003d, p. A-7), the ground control system for non-emplacment drifts is designated as 'not important to waste isolation', and 'not important to safety', and the Safety Category (SC) is 'Non-SC'. Therefore, this calculation is not subjected to the requirements of the *Quality Assurance Requirements and Description* (QARD) (DOE 2003).

### **3. COMPUTER SOFTWARE AND MODEL USAGE**

Three commercially available computer programs, FLAC (Fast Lagrangian Analysis of Continua), FLAC3D (Fast Lagrangian Analysis of Continua in 3 Dimensions), and 3DEC (3-Dimensional Distinct Element Code) are used in this calculation. Descriptions of these codes and their qualification status are provided in the following subsections.

#### **3.1 FLAC COMPUTER SOFTWARE**

FLAC Version 4.0 (STN: 10167-4.0-00) is a two-dimensional explicit finite difference code which simulates the behavior of structures built of soil, rock, or other materials subjected to static, dynamic, and thermally-induced loads (Itasca Consulting Group 2002). Modeled materials respond to applied forces or boundary restraints according to prescribed linear or non-linear stress/strain laws and undergo plastic flow when a limiting yield condition is reached. FLAC is based upon a Lagrangian scheme, which is well suited for large deflections and has been used primarily for analysis and design in mine engineering and underground construction. The explicit time-marching solution of the full equations of motion, including inertial terms, permits the analysis of progressive failure and collapse. A detailed discussion on the general features and fields of the FLAC computer software applications is presented in the User's Manual (Itasca Consulting Group 2002).

FLAC was used in mechanical analyses in this calculation. All input and output files for this software item used in this calculation have been archived on CD-ROMs and will be submitted to the Record Processing Center (RPC) as part of the records package for this calculation. The results are presented and described in Section 6.

FLAC Version 4.0 was obtained from the Software Configuration Management (SCM) in accordance with the AP-SI.1Q procedure. FLAC is installed and run on stand-alone PCs with Windows 2000 operating systems. FLAC Version 4.0 was qualified for use in design in accordance with the AP-SI.1Q procedure. FLAC was appropriate for the applications used in this analysis, and used within the range of validation, as specified in the software qualification documentation.

#### **3.2 FLAC3D COMPUTER SOFTWARE**

The FLAC3D Version 2.1 (STN: 10502-2.1-00) is a three-dimensional explicit finite difference program for solving complex problems in geotechnical, civil, and mining engineering. FLAC3D simulates the behavior of three-dimensional structures built of soil, rock, or other materials that undergo plastic flow when a limiting yield condition is reached. The explicit, Lagrangian calculation scheme and the mixed-discretization zoning technique ensure that plastic collapse and flow are modeled very accurately. A detailed discussion on the general features and fields of the FLAC3D computer software applications is presented in the User's Manual (Itasca Consulting Group 2002).

FLAC3D was used in mechanical analysis in this calculation. All input and output files for this software item used in this calculation have been archived on CD-ROMs and will be submitted to

the RPC as part of the records package for this calculation. The results are presented and described in Section 6.

FLAC3D Version 2.1 was obtained from the SCM in accordance with the AP-SI.1Q procedure. FLAC3D is installed and run on stand-alone PCs with Windows 2000 operating systems. FLAC3D Version 2.1 was qualified for use in design in accordance with the AP-SI.1Q procedure. FLAC was appropriate for the applications used in this calculation, and used within the range of validation, as specified in the software qualification documentation.

### **3.3 3DEC COMPUTER CODE**

3DEC Version 2.01 (STN: 10025-2.01-00) is a three-dimensional computer code based on the distinct element method for discontinuum modeling. In 3DEC, the discontinuous medium is presented as an assemblage of discrete blocks. Individual blocks behave as either rigid or deformable material; deformable blocks are subdivided into a mesh of finite difference elements. 3DEC is based on a Lagrangian calculation scheme that is well-suited to model the large deformations of blocks in a system. A detailed discussion on the general features and fields of 3DEC computer software applications is presented in the User's Manual (Itasca Consulting Group 2002).

3DEC was used in coupled thermomechanical and seismic analyses in this calculation. All input and output files for this software item used in this calculation have been archived on CD-ROMs and will be submitted to the RPC as part of the records package for this calculation. The results are presented and described in Section 6.

3DEC Version 2.01 was obtained from the SCM in accordance with the AP-SI.1Q procedure. 3DEC is installed and run on stand-alone PCs with Windows 2000 operating systems. It is noted that in this calculation all computer runs using 3DEC were conducted in batch mode. 3DEC Version 2.01 was qualified for use in design in accordance with the AP-SI.1Q procedure. 3DEC was appropriate for the applications used in this calculation, and used within the range of validation, as specified in the software qualification documentation.

### **3.4 SPREADSHEET SOFTWARE**

Microsoft Excel 97 SR-2 spreadsheet software was used in displaying some of the FLAC, FLAC3D, and 3DEC results graphically. In this application, results from the FLAC, FLAC3D, or 3DEC analyses were used as inputs, and outputs were charts or figures. There are no formulas used in the spreadsheets. Microsoft Excel 97 SR-2 is an exempt software product in accordance with the AP-SI.1Q procedure.

## 4. INPUTS

This section presents the data and parameters, criteria, and codes and standards used in the calculation.

### 4.1 DATA AND PARAMETERS

#### 4.1.1 Rock Mass Mechanical Properties

##### 4.1.1.1 Lithophysal Rock

Rock mass properties for lithophysal rock are listed in Table 4-1. Note that all data are obtained from Table 5-8 of *Input Parameters for Ground Support Design* (BSC 2003a) except that values of bulk modulus and shear modulus are calculated based on values of modulus of elasticity and Poisson's ratio in Table 4-1 and from equations 14 and 13, p. 111 of Jaeger and Cook 1979. The values of modulus of elasticity are expressed to two decimal points, which is also consistent with other values including decimal numbers.

Table 4-1. Rock Mass Mechanical Properties for Lithophysal Rock

Parameter	Lithophysal Rock (Ttptpul and Ttptpl)					
	1	2	3	4	5	6
Rock Mass Lithophysal Porosity Category	1	2	3	4	5	6
Lithophysal Porosity (%)	25-30	20-25	15-20	10-15	<10	N/A
Poisson's Ratio	0.22	0.22	0.22	0.22	0.22	0.22
Modulus of Elasticity (GPa)*	1.92	6.37	10.82	15.26	19.71	1.0
Bulk Modulus (GPa)	1.14	3.79	6.44	9.08	11.73	0.60
Shear Modulus (GPa)	0.79	2.61	4.43	6.25	8.08	0.41
Cohesion (MPa)	2.07	3.11	4.14	5.18	6.21	1.24
Friction Angle (degrees)	45	45	45	45	45	45
Unconfined Compressive Strength (MPa)	10	15	20	25	30	6

Source: BSC 2003a, Table 5-8. Note: \* Values are calculated to second digit based on Eq. I.11.1 of BSC 2003a.

##### 4.1.1.2 Non-lithophysal Rock

Rock mass properties for non-lithophysal rock (Ttptpmn) are listed in Table 4-2. These values are determined based on the rock mass classification. Details on how these values are estimated are presented in the *Subsurface Geotechnical Parameters Report* (BSC 2003c, Section 8.5, Table 8-41).

Table 4-2. Rock Mass Mechanical Properties for Non-lithophysal Rock

Parameter	Non-lithophysal Rock (Ttptmn)				
	1	2	3	4	5
Rock Mass Quality Category	1	2	3	4	5
Cumulative Frequency Distribution (%)	10	30	50	70	90
Geologic Strength Index (GSI)	50.48	55.49	59.03	62.33	66.79
Rock Mass Quality (Q' or Q <sub>p</sub> )	2.05	3.59	5.31	7.67	12.58
Elastic Modulus (GPa)	10.25	13.66	16.74	20.23	26.18
Poisson's Ratio <sup>b</sup>	0.19	0.19	0.19	0.19	0.19
Bulk Modulus (GPa) <sup>a</sup>	5.51	7.34	9.00	10.88	14.08
Shear Modulus (GPa) <sup>a</sup>	4.31	5.74	7.03	8.50	11.00
Global Compressive Strength (MPa)	33.50	39.67	44.42	49.50	57.71
Cohesion (MPa)	7.60	8.69	9.53	10.39	11.75
Friction Angle (degrees)	40.15	42.29	43.64	44.92	46.66
Tensile Strength (MPa)	0.08	0.12	0.16	0.21	0.32

Source: BSC 2003c, Section 8.5, Table 8-41.

Note: <sup>a</sup> Bulk modulus and shear modulus are calculated based on equation described in Section 4.1.1.1. <sup>b</sup> Based on Sec. 8.5.2.3 of BSC 2003c

#### 4.1.2 Rock Mass Density

A rock mass saturated bulk density of 2,410 kg/m<sup>3</sup> is used to estimate overburden and in situ stress state. This value is for the rock unit of Ttptln, and is the highest value of lithostratigraphic units (BSC 2001, Table 4-2). Therefore, use of this value is conservative for the purpose of this calculation.

#### 4.1.3 Dimensions and Properties for Fully Grouted Rock Bolts

The dimensions and properties of fully grouted rock bolts are shown in Table 4-3.

#### 4.1.4 Dimension and Properties for Shotcrete

The dimension and properties of shotcrete are shown in Table 4-4.

#### 4.1.5 Dimensions and Properties for Stainless Steel Super Swellex Bolts

Stainless steel Super Swellex rock bolts are proposed for use in emplacement drifts. The dimensions and mechanical properties of stainless steel Super Swellex bolts are listed in Table 4-5.

#### 4.1.6 Seismic Velocity History

Seismic velocity histories for the mean annual exceedance probability of 1 x 10<sup>-4</sup> (10,000 years) at repository horizon and 5 x 10<sup>-4</sup> (2,000 years) for the surface facilities area are shown in Figures 4-1a (DTN: MO0306SDSAVDTH.000) and 4-1b (DTN: MO0310SDSTMHIS.003),

respectively. Details on how these seismic velocity histories are applied in numerical calculations are discussed in Section 6.5.2.3.

#### 4.1.7 Rock Mass Thermal Expansion Coefficients

The coefficients of thermal expansion for rock mass at TSw2 thermal mechanical unit is shown in Table 4-6.

Table 4-3. Dimensions and Properties of Fully Grouted Rock Bolts

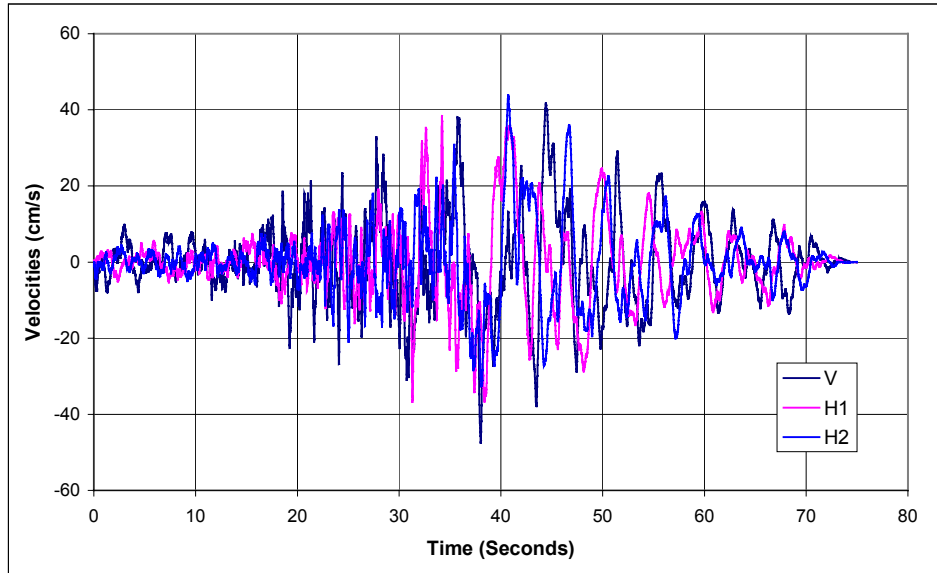
Parameter	Value	Source and Remark
Diameter of Rock Bolt (m)	0.0254	Converted from a diameter of 1 inch (1 in $\times$ 0.0254 m/in = 0.0254 m)
Thickness of Grout Annulus (m)	0.00635	Converted from a thickness of 0.25 in (0.25 in $\times$ 0.0254 m/in = 0.00635 m)
Length of Rock Bolts (m)	3 - 5	3 m in typical non-emplacement drifts and increase up to 5 m in intersection area
Spacing between bolts and rows (m)	1.25	Spacing may be changed to 1.5 m if necessary
Perimeter of Rock Bolt (m)	0.08	Calculated: $p = \pi D = 3.1415 \times 0.0254 = 0.08$ m
Allowable Axial Force (kN) <sup>a</sup>	264	Based on the yield strength (force) of 264 kN (DSI 2002, Dywidag threadbar)
Modulus of Elasticity of Steel (GPa)	200	AISC 1997, p. 1-117 (29,000 x1000/(145x 10 <sup>6</sup> ))
Modulus of Elasticity of Grout (GPa)	14	Onofrei et al. 1993, Figure 33, p. 60
Poisson's Ratio of Grout	0.25	Set to be the same as concrete (see Merritt 1983, p. 6-8)
Grout Unconfined Compressive Strength (MPa)	90	Onofrei et al. 1993, Figure 27b, p. 52
Bond Stiffness of Grout (N/m/m)	$8.68 \times 10^8$	Calculated using Equation 3 of Ruest and Martin 2002
Bond Strength of Grout (cohesion) (N/m)	$1.9 \times 10^{5a}$ $3.0 \times 10^{5b}$	Based on recommendation by Hutchinson and Diederichs (1996, Figure 2.6.13). <sup>a</sup> for lith. Cat. 1 tuff, <sup>b</sup> for non lith. Cat. 1 tuff. See discussion in Sec. 6.5.5.1.

Table 4-4. Dimension and Properties of Shotcrete

Parameter	Value	Source
Thickness of Shotcrete (m)	0.1	Converted from a thickness of 4 in (4 in $\times$ 0.0254 m/in = 0.102 m)
Elastic Modulus $E$ (GPa)	29	Based on mean value in Sec. 1.7 of ACI 506R-90(95)
Poisson's Ratio $\nu$	0.25	Assumed same as concrete, Merritt (1983, p. 6-8)

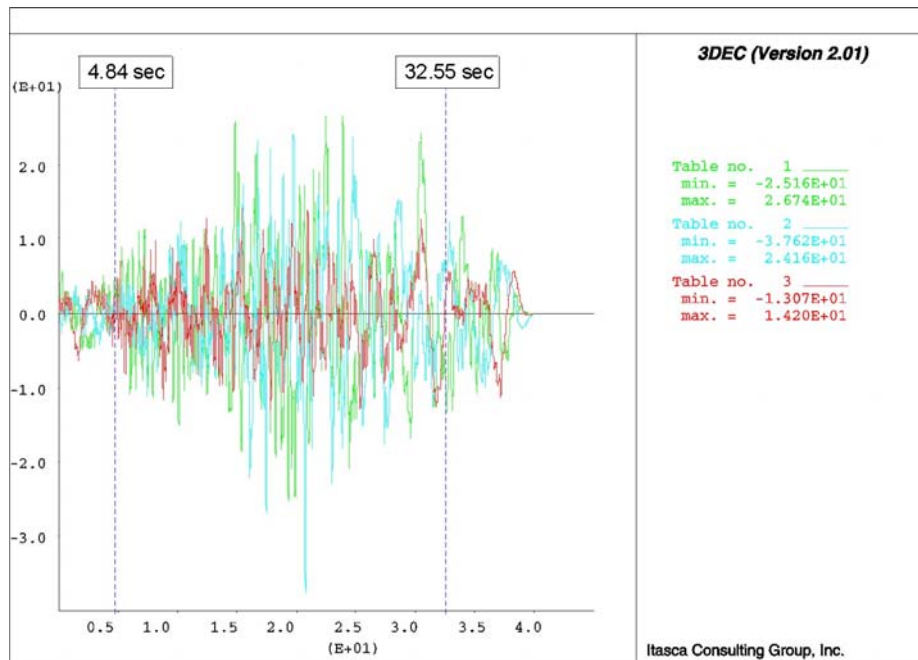
Table 4-5. Dimensions and Properties for Stainless Steel Super Swellex Rock Bolts

<b>Parameter</b>	<b>Value</b>	<b>Source</b>
Diameter of Rock Bolt (m)	0.054	Atlas Copco 2003, p. 10.
Thickness of (m)	0.003	Atlas Copco 2003, p. 10.
Young's Modulus of Stainless Steel (GPa)	200	The value is 193 GPa for 316 type stainless steel based on Table 21, p. 871 of ASM International 1990. It is rounded off to 200 GPa for conservatism.
Limit Axial Force (kN)	260	See Assumption 5.5.
Bond Stiffness (N/m/m)	$3 \times 10^8$	See Section 6.5.5.1.
Bond Strength (N/m)	$2.75 \times 10^5$	See Section 6.5.5.1.



Source: DTN: MO0306SDSAVDTH.000

(a)



Source: DTN: MO0402SDSTMHIS.004

(b)

Figure 4-1. Time Histories of Velocity Components of Seismic Motion for Mean Annual Exceedance Probability of: (a)  $1 \times 10^{-4}$ ; (b)  $5 \times 10^{-4}$

Table 4-6. Coefficients of Thermal Expansion for TSw2 Unit

Temperature	Coefficient of thermal expansion
°C	1/°C
0-50	$7.14 \times 10^{-6}$
50-75	$7.47 \times 10^{-6}$
75-100	$7.46 \times 10^{-6}$
100-500	$9.07 \times 10^{-6}$

Source: DTN: SNL01B05059301.006

#### 4.1.8 Rock Mass Mechanical Properties of TCw Thermal Mechanical Unit

Table 4-7 lists the rock mass mechanical properties for the TCw thermal mechanical unit. The mechanical properties are from Table 5-9 of BSC 2003a.

Table 4-7. Rock Mass Mechanical Properties of the TCw Unit

Thermal Mechanical Unit	TCw	
Density (kg/m <sup>3</sup> )	2310	
Rock Mass Quality (RMQ)	1	5
Modulus of Elasticity (GPa)	7.33	29.36
Poisson's Ratio	0.21	0.21
Cohesion (MPa)	1.5	3.9
Friction Angle (degrees)	54	57
Tensile Strength (MPa)	0.97	2.35

Source: BSC 2003a, Table 5-9

## 4.2 DESIGN CRITERIA AND CONSTRAINTS

### 4.2.1 Criteria

The following criteria are applicable to the design of ground support system in non-emplacment drifts:

**4.2.1.1** The ground control system shall be designed to maintain adequate operating envelopes through permanent closure for access mains, exhaust air mains and miscellaneous openings (Minwalla 2003, Section 4.5.2.1).

**4.2.1.2** The ground control system shall accommodate geologic mapping of 100 percent of non-emplacment openings (Minwalla 2003, Section 4.5.2.1).

- 4.2.1.3 The system shall be designed for the appropriate worst case combination of in situ, thermal, seismic, construction, and operational loads (Minwalla 2003, Section 4.5.2.1).
- 4.2.1.4 The ground control system for non-emplacements openings shall be designed for safety factors compatible with maintenance plans (Minwalla 2003, Section 4.5.2.1).
- 4.2.1.5 The ground control system shall use materials having acceptable long-term effects on waste isolation (Minwalla 2003, Section 4.5.2.2).
- 4.2.1.6 The ground control system shall be designed to withstand a design basis earthquake (Minwalla 2003, Section 4.5.2.2).
- 4.2.1.7 The ground control system shall be designed to prevent rock falls that could potentially result in personnel injury (Minwalla 2003, Section 4.5.2.3).
- 4.2.1.8 The ground control system shall accommodate the maintenance of non-emplacements openings (Minwalla 2003, Section 4.5.2.6).

## 4.2.2 Constraints

The following design constraints are applicable to the ground support system in non-emplacements drifts:

### 4.2.2.1 Diameters of Emplacement Drift and Access/Exhaust Main

The diameter of emplacement drift is 5.5 m and the diameter of access mains and exhaust mains is 7.62 m (BSC 2004, Table 1).

### 4.2.2.2 Turnout Drift Dimension

The turnout has a horseshoe shape in cross-section (8 m wide and 7 m high). The excavation springline is 3 m above the sill and the turnout crown section has a radius of 4 m (BSC 2004, Figure 3 and Table 1).

### 4.2.2.3 Dimension and Configuration of Observation Drift and Test Alcove

Both observation drift and test alcove have a horseshoe shape in cross-section (5 m wide and 5 m high). The observation drift is parallel to the emplacement drift in the plan view. Horizontal spacing, center-to-center, between the observation drift and the emplacement drift is 20 m. Along most of its length the vertical distance between the crown of the observation drift and the floor of the emplacement drift is 10 m. (Note that observation drift is below the emplacement drift). See Figures 6-15 and 6-15A for illustration of observation drift configuration. The test alcove is below the emplacement drift with a minimum of 10 m from crown to invert (BSC 2003e, Section 8.5).

#### **4.2.2.4 TBM Launch Chamber Dimension and Configuration**

The TBM launch chamber is a horseshoe-shaped underground excavation. It is 11 m × 11 m in cross-section and 20-m long. It will be excavated by conventional drill-and-blast method (BSC 2003e, Section 8.3).

#### **4.2.2.5 North Portal Starter Tunnel Dimension and Configuration**

The North Portal Starter Tunnel was excavated nominally 9.8 (rounded-off to 10) m high by 9.9 (rounded-off to 10) m wide in an arched shape. It was constructed by conventional drill-and-blast method. (CRWMS M&O 1997, Section 7.1). The length of Starter Tunnel is about 60 m (BSC 2003e, Figure 3).

### **4.3 CODES AND STANDARDS**

The codes and standards applicable to ground support system in non-emplacment drifts are as listed below.

#### **4.3.1 American Society for Testing and Materials (ASTM)**

ASTM A 36/  
A 36M-03a      *Standard Specification for Carbon Structural Steel*

ASTM A 82-97a      *Standard Specification for Steel Wire, Plain, for Concrete Reinforcement*

ASTM A 242/  
A 242M-03a      *Standard Specification for High-Strength Low-Alloy Structural Steel*

ASTM A 588/  
A 588M-03      *Standard Specification for High-Strength Low-Alloy Structural Steel with 50 ksi [345MPa] Minimum Yield Point to 4-in. [100-mm] Thick*

ASTM F 432-95      *Standard Specification for Roof and Rock Bolts and Accessories*  
(Reapproved 2001)

#### **4.3.2 American Institute of Steel Construction (AISC)**

AISC 1997      *Manual of Steel Construction – Allowable Stress Design*

#### **4.3.3 American Concrete Institute (ACI)**

ACI 506R-90 (95)      *Guide to Shotcrete*

ACI 506.2-95      *Specification for Shotcrete*

## 5. ASSUMPTIONS

The following assumptions were made in this calculation:

### 5.1 INITIAL GROUND RELAXATION

An initial ground relaxation value of 75 percent is assumed and used in the ground support analysis for the fully-grouted rock bolting in non-emplacment drifts. This ground relaxation value results in 25 percent of the pre-excavation in situ stress being imposed on the ground support system. This same ground relaxation value for rock bolts is also confirmed from ground control analysis for emplacement drifts (see Section 6.1.5 of BSC 2003f). This is considered adequate since the initial relaxation will likely be completed before the final support installed. Used in Section 6.

An initial ground relaxation value of 100 percent is assumed and used in the ground support analysis for the final shotcrete lining in non-emplacment drifts. This value is considered to be adequate because the shotcrete lining will usually be installed after the drift excavation. Any rock deformation induced by the excavation will most likely be complete well before the application of the shotcreting. Used in Section 6.

### 5.2 AVERAGE DEPTH OF REPOSITORY HOST HORIZON

The average depth of repository host horizon is assumed to be 400 m measured from the center of an emplacement drift (BSC 2003a, Tables 5-2a to 5-2c). Depth of emplacement drifts varies from drift to drift. The depths near the centers of Panels 1, 3 East and 3 West are approximately 296 m, 259 m, and 372 m, respectively. The depths of emplacement drifts range from 215 to 450 m with the majority between 300 to 400 m. In a recent scoping analysis on emplacement drift stability, it was indicated that the results for the maximum value of 450 m would be similar to those for the bounding case of 400 m (BSC 2003g, Section 4.2.1). Since non-emplacment drifts are in the same horizon as that for emplacement drifts, it is therefore, considered adequate to make the same assumption for the purpose of this calculation. Used in Section 6.

### 5.3 HORIZONTAL-TO-VERTICAL IN SITU STRESS RATIOS

The major horizontal principal stress with a direction of N15°E is 62% of the vertical stress whereas the minor horizontal principal stress with a direction of N75°W is 36% of the vertical stress. This is according to the in situ stress measurement by hydraulic fracturing in a test hole located in the TSw2 unit (SNF37100195002.001). This assumption is used for 3-dimensional modeling in Section 6.

The horizontal-to-vertical in situ stress ratios ( $K_0$ ) is assumed to be 0.5 for two-dimensional modeling. This value is approximately the average of the minimum and maximum  $K_0$  values for the 3-dimensional modeling.

This assumption is considered adequate for the purpose of this calculation. Used in Section 6.

#### **5.4 TENSILE STRENGTH OF LITHOPHYSAL ROCK**

Tensile strength is assumed to be equal to a half of cohesion for various categories of the lithophysal rock. For example, tensile strength of category 1 rock mass is equal to 1.04 MPa since cohesion for this category rock mass is 2.07 MPa as indicated in Table 4-1. This value is about 10% of the corresponding unconfined compressive strength value, and is considered reasonable for the lithophysal rock mass. Used in Section 6.

#### **5.5 LIMIT AXIAL FORCE FOR STAINLESS STEEL SUPER SWELLEX BOLTS**

The limit axial force for stainless steel Super Swellex bolts is assumed to be 260 kN in the calculation. Used in Section 6.

The tensile strength of stainless steel 316 is 620 MPa (ASTM A 276-03, Table 2, p. 4). The limit axial force of 260 kN is calculated from  $620 \times 10^6 \times \pi / 4 \times (0.054^2 - 0.048^2) / 1000 = 298$  kN and using a reduction factor for conservatism. It is considered adequate for the purpose of this calculation.

#### **5.6 TENSILE STRENGTH IN THE 3DEC SIMULATIONS**

To avoid large, unrealistic deformation of zones around the boundary of the excavation that yield in tension due to numerical simulation, tensile strength in the 3DEC simulations was assumed to be infinitely large. This assumption is to facilitate numerical convergence without sacrificing the drift response. This is considered adequate for the purpose of this calculation. Used in Section 6.

#### **5.7 PROPERTIES OF INTERFACE BETWEEN SHOTCRETE AND ROCK**

The properties of interface between shotcrete and rock are assumed as follows: cohesion –  $1 \times 10^9$  Pa, angle of friction –  $45^\circ$ , bond stiffness –  $2 \times 10^9$  N/m/m, bond shear strength –  $2 \times 10^9$  N/m, and tensile strength –  $1 \times 10^9$  Pa. Used in Section 6.

These property values are assumed in 3DEC modeling. Since shotcrete is assumed to be linearly elastic and the interface between shotcrete and rock is intimate and cannot break. It is considered adequate for the purpose of this calculation.

#### **5.8 GROUND SUPPORT TYPES**

The following ground support systems are assumed for non-emplacment drifts in this calculation. Used throughout.

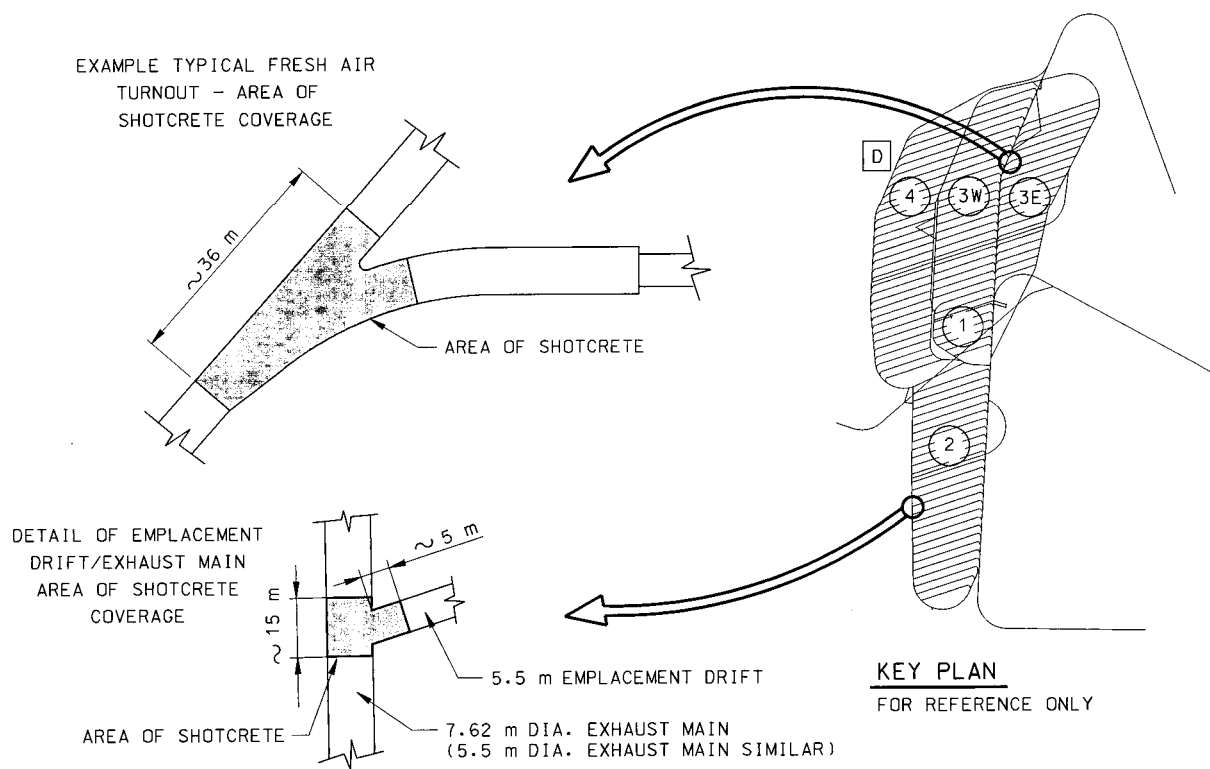
Non-emplacment openings except intersections between access mains and turnouts or between exhaust mains and emplacment drifts, ramps, and starter tunnel – fully grouted bolts with heavy duty welded wire fabric (WWF).

Intersections between access mains and turnouts or between exhaust mains and emplacment drifts, ramps and starter tunnel - fully grouted bolts with fiber-reinforced shotcrete, and lattice girders as necessary for roof span control. It should be noted that stainless steel Super Swellex bolts are used at the small intersection area inside the emplacment drifts, which is consistent with the current ground support design in emplacment drifts. A very small amount of shotcrete

is used in this portion of emplacement drift for enhancing the opening stability. However, shotcrete might not be used if this small amount of cementitious material would cause significant impact on waste package performance. Figure 5-1 illustrates shotcreted area at the intersections with fresh air turnout (i.e., between access main and turnout) and exhaust air turnout (i.e., between exhaust main and emplacement drift). Note that shotcrete area will cover the crown and extend below the springline covering an arc of about  $240^\circ$  for circular openings and  $2/3$  of the total surface area in horseshoe-shaped openings.

For the ground support at North Portal, fully grouted rock bolts with fiber-reinforced shotcrete will be installed around the portal frontal and lateral faces.

The above ground support systems are developed based on the current ground support design concept, the majority of which are also similar to the ones assumed in Section 5.2 of *Committed Ground Support Materials for LA Design* (BSC 2004), and are considered appropriate for this calculation.



Note: Plan view of underground layout is for illustration only. The correct layout is shown in Figure 6-1

Source: BSC 2004, Figure 4

Figure 5-1. Illustration of Shotcreted Areas at Intersections

## 6. GROUND SUPPORT DESIGN

### 6.1 INTRODUCTION

This calculation provides the technical basis for the design of the ground control systems for non-emplacement drifts for License Application (LA). In the design of permanent underground facilities, the ground support needs are determined using several available methods, i.e., empirical methods, observational approach, and analytical methods (Bieniawski 1984, p. 35). The design and construction of an underground high-level nuclear waste repository facility introduce unique challenges that are not commonly experienced for other subsurface facilities. For example, the presence of high level nuclear waste and the resultant thermal loading conditions introduce a series of additional requirements to the overall design and construction of the facility in addition to the waste isolation requirements. In situ (excavation) loads, potential loads from repository operations, and loads due to seismic loading conditions during an earthquake must also be addressed in the design.

The non-emplacement drift ground support design effort includes both empirical and analytical methods, coupled by observational approach (i.e., engineering experience). The empirical methods are primarily used for assessing the needs for ground support of non-emplacement drifts as well as for its selection. Design issues such as personnel safety, constructibility, and geologic mapping requirements should be factored into the design of the ground support system at this approach. However, due to the complexity of the problem involved with ground support design for nuclear waste repository, the repository ground control design effort will focus mainly on analytical methods by using computer programs to evaluate the stability of unsupported and supported openings. Applicable thermal and seismic loads will be considered in the design in addition to the in situ loading conditions. The best available experience of drift stability for the repository host rock can be obtained from observation of stability condition of openings in the Exploratory Studies Facility (ESF) and the Enhanced Characterization of the Repository Block (ECRB), which will also be discussed.

The non-emplacement drifts include all other repository underground openings that will not be used for waste emplacement, such as mains, exhaust mains, ventilation shafts and raises, emplacement drift turnouts, and intersections between turnouts and mains, etc. For non-emplacement drifts, both the initial and final ground support systems will be developed, but only the final ground support systems will be discussed in this calculation. Also, as indicated in Section 1, the ground support design in this calculation will include access mains, exhaust mains, turnouts, ramps, intersections between access mains and turnouts and between exhaust mains and emplacement drifts, observation drift, TBM launch chambers, and portals.

It should be noted that the design for initial ground support installed during excavation is not included in this calculation. Initial ground support is placed in close proximity to the advancing tunnel face for worker safety and prevention of equipment from damage due to rock fall until the permanent support system is installed. Note that initial ground support may become the final ground support depending on its type and tunnel construction method. Usually, the initial ground support system consists of rock bolts and wire mesh but it may change depending on local ground condition and excavation method. In this calculation, no credit or account will be

given for the initial ground support in modeling the final ground support systems for non-emplacement drifts.

## 6.2 REPOSITORY HOST HORIZON AND GEOTECHNICAL CHARACTERIZATION

In order to design the ground support system in non-emplacement drifts, it is important to understand the environment in which these drifts will be located.

According to the *Underground Layout Configuration* calculation (BSC 2003e, Section 7.1.7), the repository host horizon (RHH) will be located in the lower part of the lithophysal zone of the densely welded devitrified lithophysal-rich tuff unit and the entire densely welded devitrified lithophysal-poor tuff unit of the Topopah Spring Tuff. The RHH contains four lithostratigraphic units, namely the upper lithophysal unit (Ttpul), the middle non-lithophysal unit (Ttpmn), the lower lithophysal unit (Ttpll), and the lower non-lithophysal unit (Ttpln). The underground layout and the geological units within each panel is shown in Figure 6-1 (BSC 2003e, Figure II-2). Of the total emplacement areas, approximately 85% will lie within the Ttpll and Ttpul units combined and the rest 15% will be located in the Ttpmn and Ttpln units. In the lithophysal rock, 95% of the emplacement area lies in the Ttpll unit whereas in the non-lithophysal rock, 83% of the emplacement area lies in the Ttpmn unit (BSC 2003e, Table II-2). In other words, among the area for non-emplacement drifts, the primary tuff rock units for lithophysal and non-lithophysal rocks are Ttpll and Ttpmn units, respectively.

Geological mapping was conducted in the ESF tunnel and the ECRB drift to characterize the rock units within the RHH. The data collected were analyzed using two empirical rock mass classification systems, the Geomechanics Rock Mass Rating (RMR) system (Bieniawski 1989) and the Rock Mass Quality (Q) system of Norwegian Geotechnical Institute (NGI) (Barton et al. 1974). The geotechnical characteristics of the Ttpll and Ttpmn units are summarized as follows (Board 2003, Section 3.4):

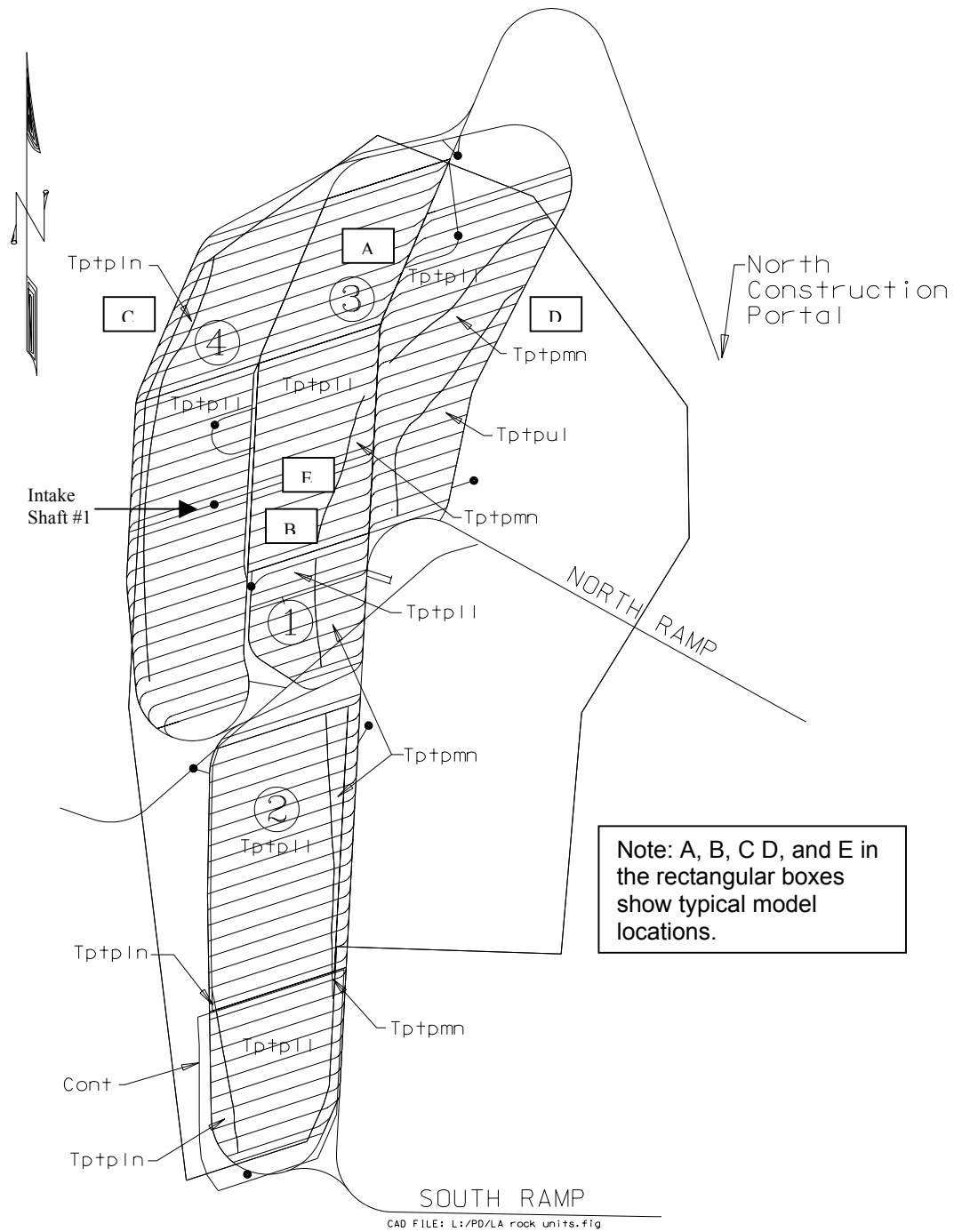
***Ttpll Unit.*** The Ttpll unit has a horizontal RQD rating of 42 (poor), a Q rating of 7.9 (fair), and a RMR value of 57 (fair). Its content of lithophysae varies from 5 to 30 percent by volume, with a size ranging from 5 to 130 cm. The larger lithophysal cavities tend to be irregular or ellipsoidal features that exhibit prismatic fracturing. The unit has an average of two plus random joint sets; however no keyblock problems are expected. Typical lithophysae and fracturing in the Ttpll are shown in Figure 6-2.

***Ttpmn Unit.*** The Ttpmn unit has a mean horizontal RQD rating ranging from 60 to 62 (fair), and a RMR value of 60 (fair). It is characterized by less than 3 percent lithophysae by volume. This unit has an average of three to three plus random joint sets, with predominately two vertical joint sets and one horizontal joint set. The horizontal joint set, or vapor-phase partings, is the primary cause of potential formation of keyblocks. A typical fracture pattern in the Ttpmn unit is shown in Figure 6-3.

## 6.3 GROUND SUPPORT FUNCTIONS

Ground support for non-emplacement drifts has the following functional and performance requirements (see Section 4.2.1 and Board 2003, Section 7.3):

- Ensure stable conditions for operational worker safety
- Prevent rock deformation to acceptable levels so that operational envelopes are maintained
- Allow for geological mapping, performance confirmation activities (which may include remote observation and possible field testing), waste retrieval operations, and closure operations (which may include installation of permanent drip shields)
- Prevent for rock falls that could potentially result in personnel injury
- Use materials with acceptable long-term effects on waste isolation
- Accommodate the planned or unplanned maintenance over the operational life of the repository.



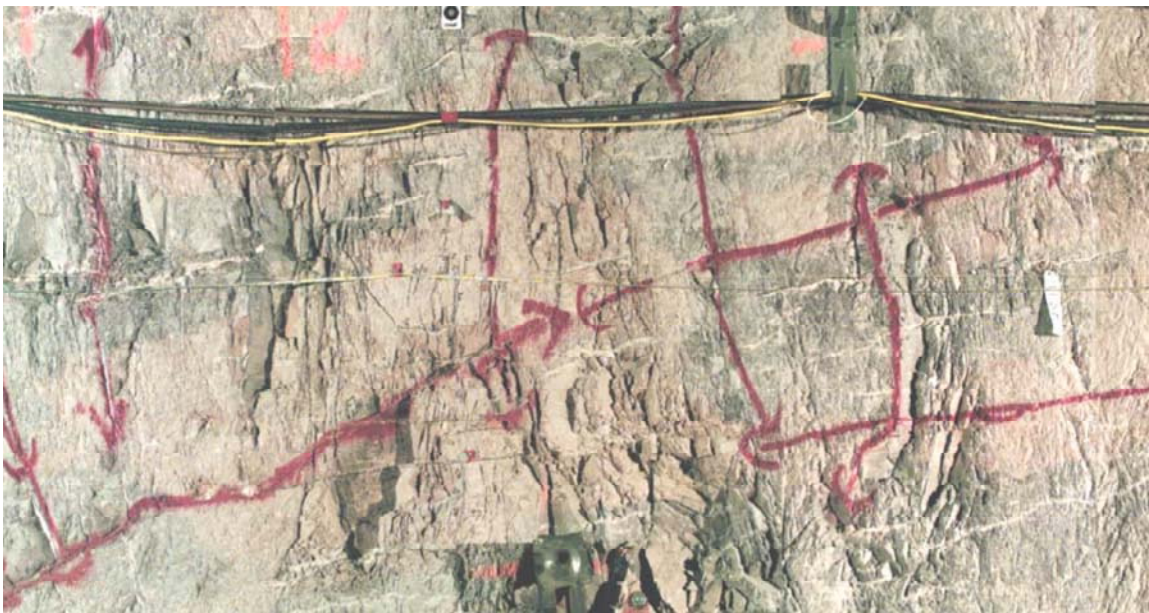
Source: BSC 2003e, Figure II-2.

Figure 6-1. Underground Layout and Geological Units by Panel



Source: Board 2003, Figure 10b

Figure 6-2. Lithophysae and Fracturing in the TptplI Unit



00266DC\_007.ai

Source: Board 2003, Figure 8

Figure 6-3. Fractures in the Wall of the ECRB in the Tptpmn Unit

## 6.4 EMPIRICAL METHODS

Empirical methods are usually applicable to designing tunnels in mining and civil engineering. The empirical approach relies on rock mass classification systems. Generally, these systems allow rock properties and geologic conditions shown in samples taken from boreholes, scanline, full-peripheral mapping, detailed test surveys, and certain outcrops at the planned site, to be compared with similar information compiled and categorized from existing underground facilities. Based on this comparison, support requirements or needs can be estimated.

To date, many rock mass classification systems have been proposed, such as systems by Deere and Deere (1988), Wickham et al. (1972), Bieniawski (1989), Barton et al. (1974), and Barton (2002). Two common classification systems were recommended in the *Drift Design Methodology and Preliminary Application for the Yucca Mountain Site Characterization Project* (Hardy and Bauer 1991, p. 6-6) and in the *Support of Underground Excavations in Hard Rock* (Hoek et al. 2000, p. 44). These two classification systems are the RMR value developed by Bieniawski (1989), and the Q value developed by Barton (see Barton 2002). Both methods incorporate geological, geometric and design/engineering parameters in arriving at quantitative value of their rock mass quality (Hoek et al. 2000, p. 44). The latter system was used in designing the ESF, and the successful performance of that facility has lead to adoption of this system for analysis of ground control elements for SR (BSC 2001, p. 50). These two classification systems are briefly described in the following sections. A detailed description of them can be found in Bieniawski (1989) and Barton et al. (1974), respectively.

### 6.4.1 Geomechanics Rock Mass Classification System

The Rock Mass Rating (RMR) system, otherwise known as the Geomechanics Classification, was developed by Bieniawski during 1972 – 1973 (Bieniawski 1989, p. 51). The following six parameters are used to classify a rock mass using the RMR system (Bieniawski 1989, p. 52):

1. Uniaxial compressive strength of rock material
2. Rock quality designation (RQD)
3. Spacing of discontinuities
4. Condition of discontinuities
5. Groundwater conditions
6. Orientation of discontinuities

These parameters not only are measurable in the field but can also be obtained from borings. Joints are the major factor in this classification system; four of the six parameters (RQD, joint spacing, joint conditions, and orientation of joints) are related to joint characteristics. Increments of rock mass rating corresponding to each parameter are summed to determine RMR.

The RMR values for various rock units at the repository host horizon are generally available from data collected in the ESF and ECRB. In case these RMR values are not available, empirical correlation can be used to estimate RMR values based on known deformation modulus of rock mass. The empirical correlation used in this calculation is as follows (Barton 2002, p. 193, Eq. 8):

$$RMR = 40 \log E_m + 10 \quad (\text{Eq. 6-1})$$

where  $E_m$  = deformation modulus of rock mass in GPa

Once the RMR values are determined, the rock mass quality for each rock unit considered can be judged based on the guidelines provided by Bieniawski (1989, Tables 4.1 and 4.2). Recommendation for the excavation scheme and rock support needs can be made by following the guidelines presented in Table 6-1 (Bieniawski 1989, Table 4.4). Details on how to apply the RMR classification system to the preliminary design of ground support for rock tunnels such as those in repository non-emplacement drifts can be found in the *Engineering Rock Mass Classifications* (Bieniawski 1989, Section 4).

#### 6.4.2 NGI Rock Mass Classification System

The NGI rock mass classification or the rock mass quality Q system, developed in earlier 1970s by Barton (2002, p. 187), is commonly used in the design of rock support for tunnels and large underground chambers. The six parameters in the NGI system include 1) RQD, 2) joint set number ( $J_n$ ), 3) joint roughness number ( $J_r$ ), 4) joint alteration number ( $J_a$ ), 5) joint water reduction factor ( $J_w$ ), and 6) stress reduction factor (SRF).

These parameters chosen to describe the rock mass quality Q are combined in the following way (Barton et al. 1974, Eq. 1):

$$Q = \left( \frac{RQD}{J_n} \right) \left( \frac{J_r}{J_a} \right) \left( \frac{J_w}{SRF} \right) \quad (\text{Eq. 6-2})$$

The three ratios in the equation - RQD/ $J_n$ ,  $J_r/J_a$ , and  $J_w/SRF$  - represent block size, minimum inter-block shear strength, and active stress, respectively (Barton et al. 1974, p. 202).

Similar to the RMR values, Q indices for various rock units at the repository host horizon are generally available from the ESF and ECRB. In case these Q indices are not available, empirical correlation can be used to estimate Q indices based on given rock mass modulus. The empirical correlation used in this calculation is as follows (Hoek et al. 2000, Eqs. 8.16 and 8.19):

$$Q = Q' \times \frac{J_w}{SRF} = e^{\frac{RMR-44}{9}} \times \frac{J_w}{SRF} \quad (\text{Eq. 6-3})$$

where

$$Q' = \left( \frac{RQD}{J_n} \right) \left( \frac{J_r}{J_a} \right)$$

The RMR value in Eq. 6-3 is estimated from the given deformation modulus of rock mass using Eq. 6-1.

Table 6-1. Estimate of Ground Support Needs Based on RMR System

Rock mass class	Excavation	Rock bolts (20 mm diameter, fully grouted)	Shotcrete	Steel sets
I - Very good rock <i>RMR</i> : 81-100	Full face, 3 m advance.	Generally no support required except spot bolting.		
II - Good rock <i>RMR</i> : 61-80	Full face, 1-1.5 m advance. Complete support 20 m from face.	Locally, bolts in crown 3 m long, spaced 2.5 m with occasional wire mesh.	50 mm in crown where required.	None.
III - Fair rock <i>RMR</i> : 41-60	Top heading and bench 1.5-3 m advance in top heading. Commence support after each blast. Complete support 10 m from face.	Systematic bolts 4 m long, spaced 1.5 - 2 m in crown and walls with wire mesh in crown.	50-100 mm in crown and 30 mm in sides.	None.
IV - Poor rock <i>RMR</i> : 21-40	Top heading and bench 1.0-1.5 m advance in top heading. Install support concurrently with excavation, 10 m from face.	Systematic bolts 4-5 m long, spaced 1-1.5 m in crown and walls with wire mesh.	100-150 mm in crown and 100 mm in sides.	Light to medium ribs spaced 1.5 m where required.
V - Very poor rock <i>RMR</i> : < 20	Multiple drifts 0.5-1.5 m advance in top heading. Install support concurrently with excavation. Shotcrete as soon as possible after blasting.	Systematic bolts 5-6 m long, spaced 1-1.5 m in crown and walls with wire mesh. Bolt invert.	150-200 mm in crown, 150 mm in sides, and 50 mm on face.	Medium to heavy ribs spaced 0.75 m with steel lagging and forepoling if required. Close invert.

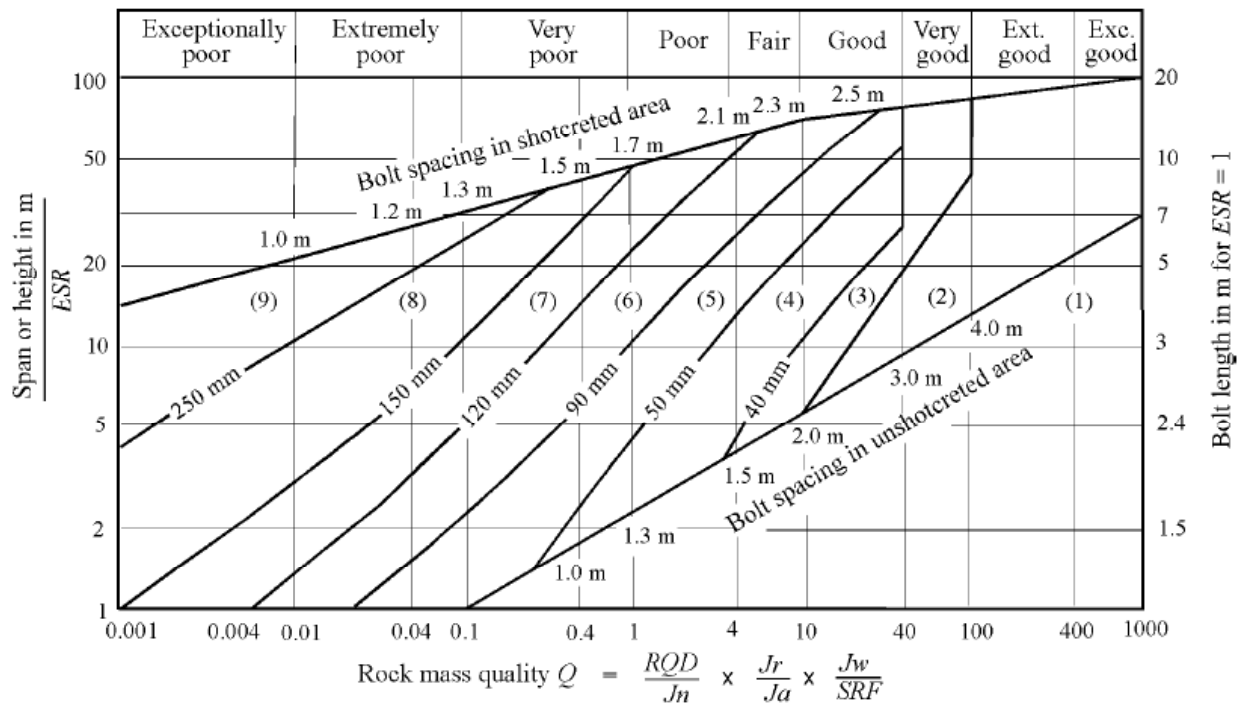
Source: Bieniawski 1989, Table 4.4.

The Q index is used with the Equivalent Dimension, defined as the largest of span, diameter, and height divided by the excavation support ratio (ESR). ESR is roughly analogous to the inverse of the factor of safety used in engineering design. The ESR reflects the degree of safety and ground support required for an excavation as determined by the purpose, presence of machinery, personnel, etc., to meet safety requirements. In essence, the safety factor of an opening can be increased by reducing the ESR value. The ESR values for various underground openings can be estimated based on Barton et al. (1974, Table 7). For example, the *ESR* for the access and exhaust mains and the turnouts, classified as “access tunnels”, is taken to be 1.3; the intersections are assigned a value of 1.0.

The Equivalent Dimension is plotted against Q on the design chart, Figure 6-4, to determine the required ground support need (Hoek et al. 2000, Figure 4.3).

The NGI rock mass classification system provides guidance on bolt spacing, bolt length, and shotcrete thickness, based on the rock mass quality index (Q) and the opening dimensions. The length L of rockbolts can be estimated from the excavation width B and ESR (Hoek et al. 2000, Eq. 4-3):

$$L = \frac{2 + 0.15B}{ESR} \quad (\text{Eq. 6-4})$$



**REINFORCEMENT CATEGORIES**

- |   |   |
|---|---|
| <ul style="list-style-type: none"> <li>1) Unsupported</li> <li>2) Spot bolting</li> <li>3) Systematic bolting</li> <li>4) Systematic bolting with 40-100 mm unreinforced shotcrete</li> </ul> | <ul style="list-style-type: none"> <li>5) Fibre reinforced shotcrete, 50 - 90 mm, and bolting</li> <li>6) Fibre reinforced shotcrete, 90 - 120 mm, and bolting</li> <li>7) Fibre reinforced shotcrete, 120 - 150 mm, and bolting</li> <li>8) Fibre reinforced shotcrete, &gt; 150 mm, with reinforced ribs of shotcrete and bolting</li> <li>9) Cast concrete lining</li> </ul> |
|---|---|

Source: Hoek et al. 2000, Figure 4.3.

Figure 6-4. Estimated Ground Support Needs Based on Q Index

### 6.4.3 Empirical Analysis of Ground Support Need

Results of the empirical analysis based on the RMR and Q approaches for non-emplacment drifts in the non-lithophysal rock are presented in the following. Note that the empirical analysis is only considered for access/exhaust mains, intersections between access mains and emplacement drift turnouts, and intersections between exhaust mains and emplacement drifts, which comprise of majority of non-emplacment drifts; observation drift, TBM launch chambers, and portals are not included. The methods used are described in Sections 6.4.1 and 6.4.2.

For the non-emplacment drifts excavated in the lithophysal rock, however, use of the RMR or Q approach for the ground support design is non-conventional, and there are no sufficient data or field experiences available to support this application. This is primarily due to the fact that the lithophysal rock contains air-filled large cavities and is hard to be characterized using the RMR or Q index since a RQD value is defined for a rock with fractures not with voids. Therefore, these empirical methods are not used in this calculation for evaluating the requirements of ground support for non-emplacment drifts in the lithophysal rock. Selection of ground support methods for this rock type is based on experiences and observations from the construction of the ESF and the ECRB tunnels, and assessment from numerical analyses.

Based on Geomechanics Rock Mass Classification approach, the ground support need for non-lithophysal rock in non-emplacment drifts can be estimated based on Table 6-1. First, RMR values are calculated from  $E_m$  (elastic modulus) values shown in Table 4-2 based on Eq. 6-1. It needs to be noted that RMR values are not available, so the correlation between RMR and  $E_m$  is used. Table 6-2 shows the RMR values (under third column) for rock mass categories 1 to 5.

By comparing RMR values for various rock mass categories shown in Table 6-2 with those in Table 6-1, the following ground support needs are estimated: bolt lengths range from 3 m in the good rock (categories 4-5) to 4 m in the fair rock (categories 1-3). Bolt spacing ranges from 2.5 m in the good rock to 1.5 - 2 m in the fair rock. In the good rock, 50-mm of shotcrete is recommended where required. In the fair rock, 50-100 mm of shotcrete in crown with 30-mm in the sides is recommended. It should be noted that Bieniawski's recommendations for ground support shown in Table 6-1 was based on a 10-m wide, horseshoe-shaped tunnel (Bieniawski 1984, Table 6.11). Because this span is larger than those of the excavations outside the intersection, and because the support was designed for a civil application, the estimated ground support needs are considered very conservative for use at Yucca Mountain.

For NGI Rock Mass Classification approach, Q values for various rock mass categories need to be calculated. The following steps are needed for estimating the Q values:

- Calculate the RMR values (note that RMR values are already calculated, see the previous paragraph).
- Determine the unconfined compressive strength ( $\sigma_c$ ) of intact non-lithophysal rock (Tptpmn), which is about 207 MPa (BSC 2003a, Table 5-5).

- Estimate the major principal stress ( $\sigma_1$ ) of rock adjacent to non-emplacment drifts, which is estimated to be about 20 to 56 MPa (see Section 6.5.3.1).
- Calculate the ratio  $\sigma_v/\sigma_1$  to be in the ranges of 4 to 10.
- Assign SRF value according to Table 4.6 of the *Support of Underground Excavations in Hard Rock* (Hoek et al. 2000, p. 43). A SRF value ranging from 0.5 to 2 is considered appropriate.

Based on Eq. 6-3 and  $J_w$  of 1, Q values are calculated for rock mass categories 1 to 5 and listed in Table 6-2 (under fifth column).

The lengths of rock bolts calculated based on Eq. 6-4 for various roof spans and ESR values are shown in Table 6-3. Note that equivalent dimension,  $D_e$ , is obtained by dividing the span, B, by ESR (Hoek et al. 2000, p. 39).

Table 6-2. RMR and Q Values for Non-lithophysal Rock

Category	$E_m$ (GPa)	RMR	SRF	Q
1	10.25	50	0.5 – 2.0	0.97 – 3.90
2	13.66	55	0.5 – 2.0	1.70 – 6.79
3	16.74	59	0.5 – 2.0	2.65 – 10.59
4	20.23	62	0.5 – 2.0	3.69 – 14.78
5	26.18	67	0.5 – 2.0	6.44 – 25.76

Table 6-3. Equivalent Dimension  $D_e$  and Bolt Length for Various Openings

Opening Types	Span (m)	ESR	$D_e$ (m)	Bolt Length (m)
Access and Exhaust Main	7.62	1.3	5.9	2.4
Turnout	8.00	1.3	6.2	2.5
Intersection (Typical)	13.5	1.0	13.5	4.0
Intersection (largest)	22.0	1.0	22.0	5.3

Figures 6-5 through 6-8 are plots of ground support needs for various rock mass categories for access/exhaust mains, turnouts, typical intersection, and largest intersection, respectively. These plots are derived based on  $D_e$  and Q values listed in Table 6-3.

Tables 6-4 through 6-7 show the ground support needs for various non-emplacment drift excavations under rock mass categories 1 to 5 as determined from Figures 6-5 through 6-8. Based on these tables, the estimated ground support needs can be summarized as follows:

- For access and exhaust mains: bolt length - 2.4 m, bolt spacing - 1.7 m to 2.7 m, unreinforced shotcrete - 40 to 50 mm thick for category 1 rock whereas none to 50 mm thick for categories 2 to 4 rock, and no shotcrete for category 5 rock.
- For turnouts: bolt length - 2.5 m, bolt spacing - 1.7 m to 2.7 m, unreinforced shotcrete - 40 to 50 mm thick for category 1 rock whereas none to 50 mm thick for categories 2 to 4 rock, and no shotcrete for category 5 rock.
- For intersections: bolt length – 4.0 m to 5.3 m, bolt spacing - 1.7 m to 2.7 m, fiber-reinforced shotcrete - 40 to 120 mm thick for categories 1 to 3 rock whereas unreinforced shotcrete none to 90 mm thick for categories 4 and 5 rock.

As discussed in Section 6.2, typical rock conditions in non-lithophysal rock (Tptpmn) are close to fair and good (Geomechanics RMR approach, see Table 6-1) or support categories 3 and 4 (NGI Q approach, see Figure 6-4). Therefore, by comparing the recommendations made by both RMR and Q approaches, use of pattern bolting with 3 m long, spaced at 1.25 to 1.5 m, in conjunction with 40 to 50 mm thick shotcrete is considered adequate for access and exhaust mains and turnouts. Note that since use of shotcrete is only limited to intersections in non-emplacement drifts, use of shotcrete in access and exhaust mains and turnouts outside of intersection area is replaced by the heavy duty welded wire fabric (Assumption 5.8). For ground support needs at intersections, use of pattern bolting with bolt length of 5 m, spaced at 1.25 to 1.5 m, and in conjunction with 100 mm thick fiber-reinforced shotcrete is considered adequate.

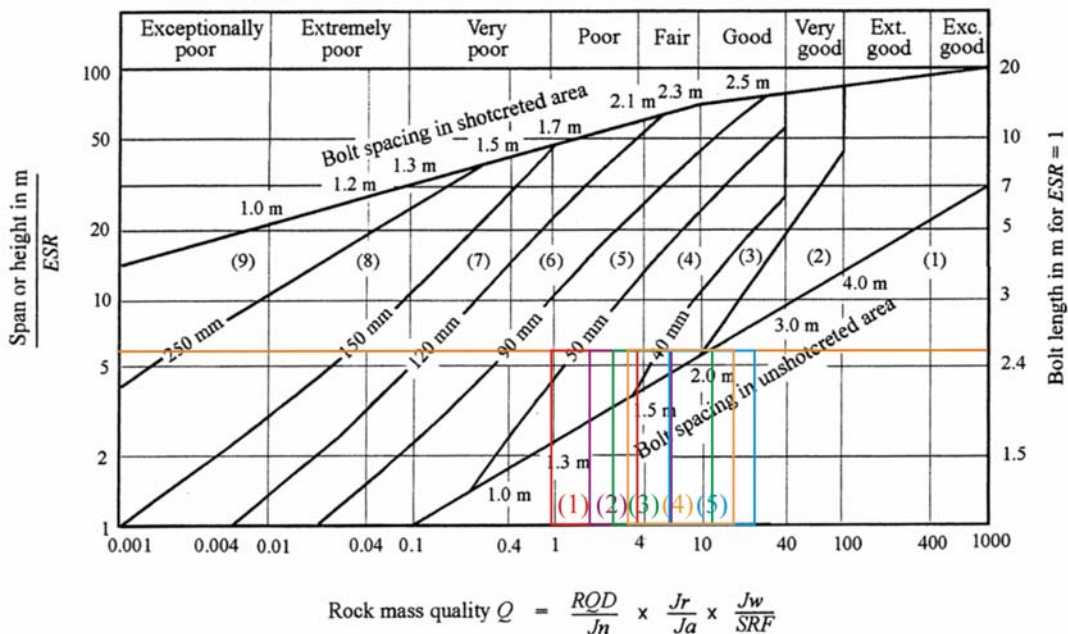


Figure 6-5. Ground Support Needs for Rock Mass Categories 1 to 5 for Access and Exhaust Mains

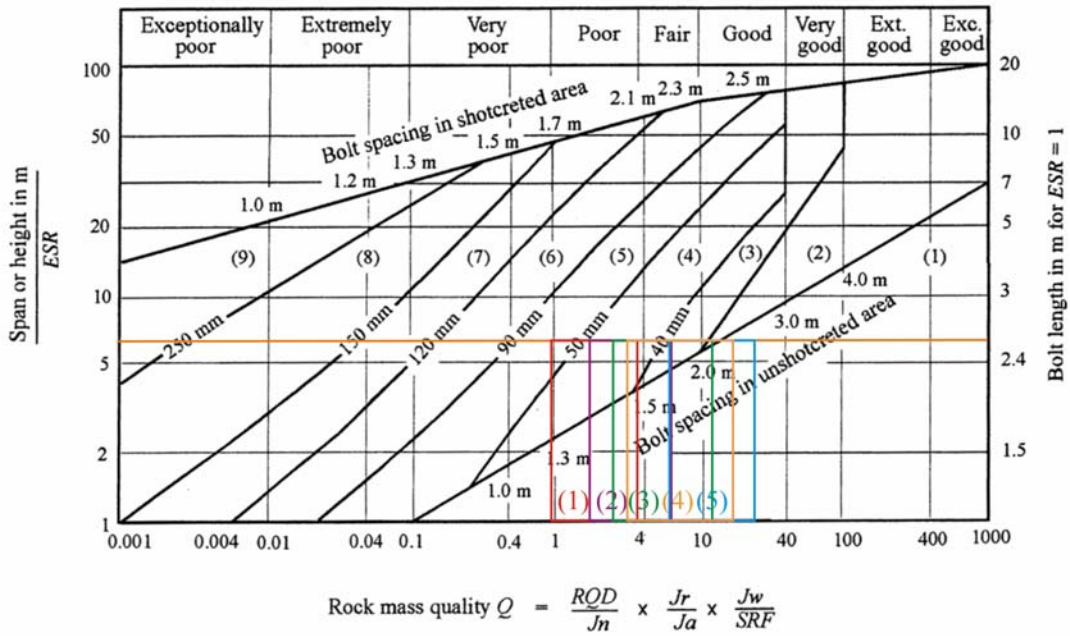


Figure 6-6. Ground Support Needs for Rock Mass Categories 1 to 5 for Turnouts

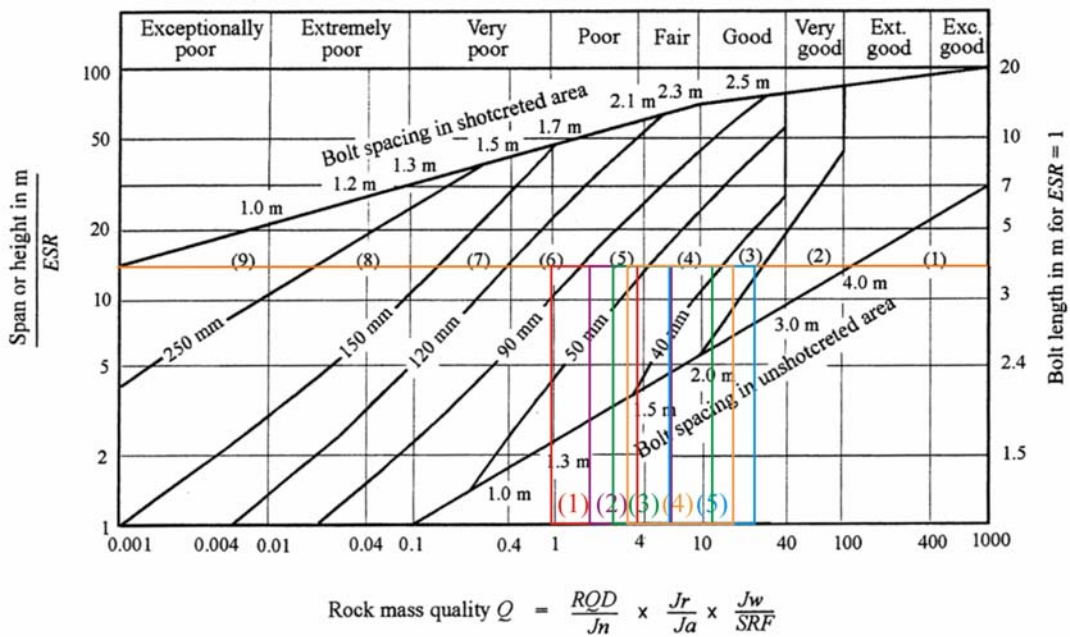


Figure 6-7. Ground Support Needs for Rock Mass Categories 1 to 5 for Typical Intersection

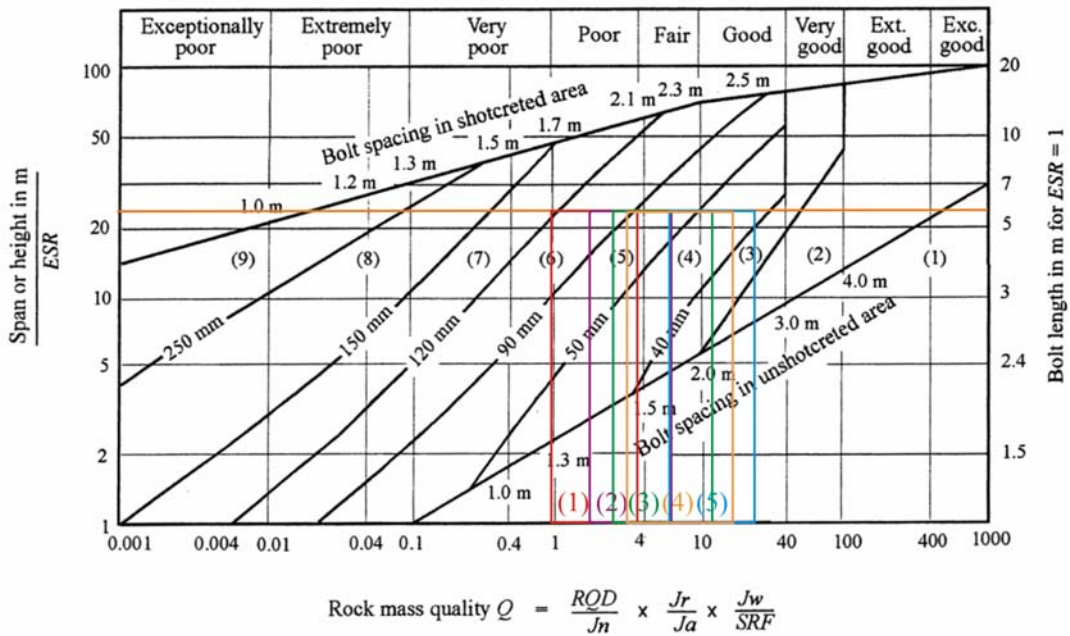


Figure 6-8. Ground Support Needs for Rock Mass Categories 1 to 5 for Largest Intersection

Table 6-4. Ground Support Needs for Access and Exhaust Mains based on Q Values

Category	Bolt Spacing (m)	Bolt Length (m)	Shotcrete Thickness (mm)	Other
1	1.7 – 2.1	2.4	40 – 50	none
2	1.8 – 2.2	2.4	none – 50	none
3	1.9 – 2.3	2.4	none - 40	none
4	2.0 – 2.4	2.4	none – 40	none
5	2.2 – 2.7	2.4	none	none

Table 6-5. Ground Support Needs for Turnouts based on Q Values

Category	Bolt Spacing (m)	Bolt Length (m)	Shotcrete Thickness (mm)	Other
1	1.7 – 2.1	2.5	40 – 50	none
2	1.8 – 2.3	2.5	none – 50	none
3	1.9 – 2.3	2.5	none – 40	none
4	2.0 – 2.4	2.5	none – 40	none
5	2.2 – 2.7	2.5	none	none

Table 6-6. Ground Support Needs for Typical Intersections based on Q Values

Category	Bolt Spacing (m)	Bolt Length (m)	Shotcrete Thickness (mm)	Other
1	1.7 – 2.1	4.0	50 – 90	Fibers
2	1.8 – 2.3	4.0	40 – 90	Fibers
3	1.9 – 2.3	4.0	40 – 90	none
4	2.0 – 2.4	4.0	40 – 90	none
5	2.2 – 2.7	4.0	none – 50	none

Table 6-7. Ground Support Needs for Large Intersections based on Q Values

Category	Bolt Spacing (m)	Bolt Length (m)	Shotcrete Thickness (mm)	Other
1	1.7 – 2.1	5.3	90 – 120	Fibers
2	1.8 – 2.3	5.3	50 – 120	Fibers
3	1.9 – 2.3	5.3	40 – 90	Fibers
4	2.0 – 2.4	5.3	40 – 90	none
5	2.2 – 2.7	5.3	40 – 50	none

## **6.5 ANALYTICAL METHODS**

The computer modeling techniques serve as an analytical basis for assessing the opening shape and determining the general stress distribution around the tunnel opening in underground design. In repository ground support design, numerical analyses will play an important role in determining and evaluating the effects of the seismic and thermal loading conditions.

For the non-emplacement drift ground support analysis, a series of computer analyses are conducted and presented here to simulate the in situ, seismic, and/or thermal loading conditions. Note that in all numerical modeling cases the thermal loading is only applicable to exhaust mains and their intersections with emplacement drifts. An in situ thermal test has been conducting in the ESF to provide an experimental basis for evaluating the thermal-hydrological-geomechanical-geochemical behavior at the site. The response of the host rock and ground support components to temperatures higher than the anticipated in the repository will provide knowledge about the response of the surrounding rock and the ground support components when subjected to high temperatures.

In general, non-emplacement drift stability analyses include computer simulation of unsupported and supported openings. For unsupported openings, stability analysis includes the excavation of the non-emplacement drifts in a gravity-stressed rock medium, followed by seismic analysis. For stability analysis of exhaust mains and intersection between them and emplacement drifts, the introduction of elevated temperatures to simulate the waste emplacement process will follow in situ stress loading and seismic loading. For stability analyses of supported openings, the approach is the same as that for unsupported openings except that the final ground support system is incorporated into the modeling during the excavation process and, therefore, is subjected to in situ, thermal loading (only for intersections between exhaust mains and emplacement drifts, intersection between exhaust main and observation drift, and interburden area between access to intake shaft #1 and exhaust mains), and seismic loading.

### **6.5.1 Modeling of Non-Emplacement Drifts**

#### **6.5.1.1 Modeling of Access and Exhaust Mains and Turnouts**

For non-emplacement drifts such as access mains, exhaust mains, and turnouts, which have relatively large distance in longitudinal axis compared with its cross-sectional area, a two-dimensional computer modeling is appropriate. Two-dimensional continuum approach will be used for the ground support design calculation for these openings. This is considered adequate and consistent with the conventional practice in mining or tunneling industry.

In a continuum approach, the geologic features, such as fractures or lithophysae, in the rock mass are “lumped” into a thermomechanical constitutive model that represents the overall equivalent effect of these features. In a discontinuum approach, fractures or lithophysae are modeled explicitly as interfaces or cavities. The difference between these techniques is therefore the level of detail that is necessary in the model to adequately capture the deformation and failure mechanisms (Board 2003, Section 5.3.1). From a ground support design perspective, stability of non-emplacement drifts is judged by overall rock mass displacements and stresses. Two-dimensional continuum approach that uses equivalent rock mass properties and constitutive

model may provide good tools for bounding analyses and also allow ease of parametric examination and model interpretation. Therefore, it is appropriate for use in ground support design related analyses.

The FLAC computer code is employed in the two-dimensional analyses. In FLAC models, rock mass properties that reflect the effects of lithophysae and fractures on rock mass properties are used. These property values are presented in Tables 4-1 and 4-2 for the lithophysal and non-lithophysal rocks, respectively. The behavior of rock mass is judged using the Mohr-Coulomb yield criterion. Figure 6-9 illustrates the configuration of a FLAC model for access and exhaust mains. Figure 6-9A shows the FLAC model for turnout with rock bolts installed. To make the calculation more efficient, symmetry across the opening centerline is invoked, i.e., only half of the opening and the surrounding rock is modeled. The vertical dimension of the model is 100 m, and the horizontal is 50 m. Determination of the model dimension depends on requirements on accuracy and computational efforts. In general, the boundary effect is negligible if the model dimension is at least five times the size of an opening to be analyzed.

#### **6.5.1.2 Modeling of Intersections between Access Mains and Turnouts and between Exhaust Mains and Emplacement Drifts**

Because the geometry of the intersections is three-dimensional, the numerical analysis was conducted using the three-dimensional codes 3DEC and FLAC3D. Most of the analysis was carried out using 3DEC, which has the advantage of generating model geometry easily and quickly. Note that 3DEC is a discontinuum code, but in the simulations of intersections, the blocks were glued together to behave effectively as a continuum. Thus, the local stability of blocks created by joints around the excavation was not considered. It should also be noted that, because of the tetrahedral zones with constant strain used in 3DEC, the calculation of plastic deformation is sometimes inaccurate. The advantage of FLAC3D is that it performs more accurate calculations of plastic deformation, particularly in the case of softening plasticity. Because FLAC3D models for such complex geometries as those of the intersections are very time consuming to generate, only location C was analyzed with FLAC3D. The objective was to verify the 3DEC results.

The geometries of two layouts A and C for intersections of access mains and turnouts as represented in the 3DEC model (showing the tunnels only, i.e., the surrounding rock mass is hidden) are shown in Figures 6-10 and 6-10A. The locations of the vertical section planes and profiles in which some of the results are presented are indicated in the figures. The geometry of the FLAC3D model for location C is shown in Figures 6-11 and 6-11A. The access main has a circular cross-section with a diameter of 7.62 m. The turnout has a horseshoe shape in the cross-section of 8 m wide and 7 m high. The floors of the two tunnels are at the same elevation. The dimensions of the entire model for both locations are 200 m × 200 m in plan and 100 m in height. The geometry of the entire 3DEC model for location A is shown in Figure 6-12.

The geometries of the model for locations B and D for intersections of exhaust mains and the emplacement drifts are shown in Figures 6-13 and 6-13A. In both cases, the model size is 200 m × 81 m in plan and 100 m in height. The typical dimension for exhaust main is 7.62m except in Panel 1 of the repository, where it is 5.5 m. However, throughout the analyses it was

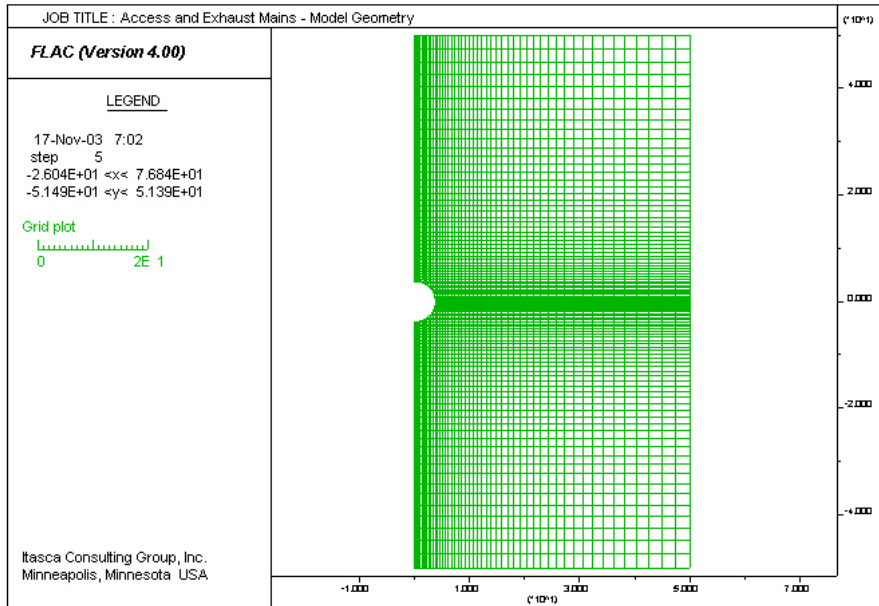


Figure 6-9. FLAC Model of Access and Exhaust Mains

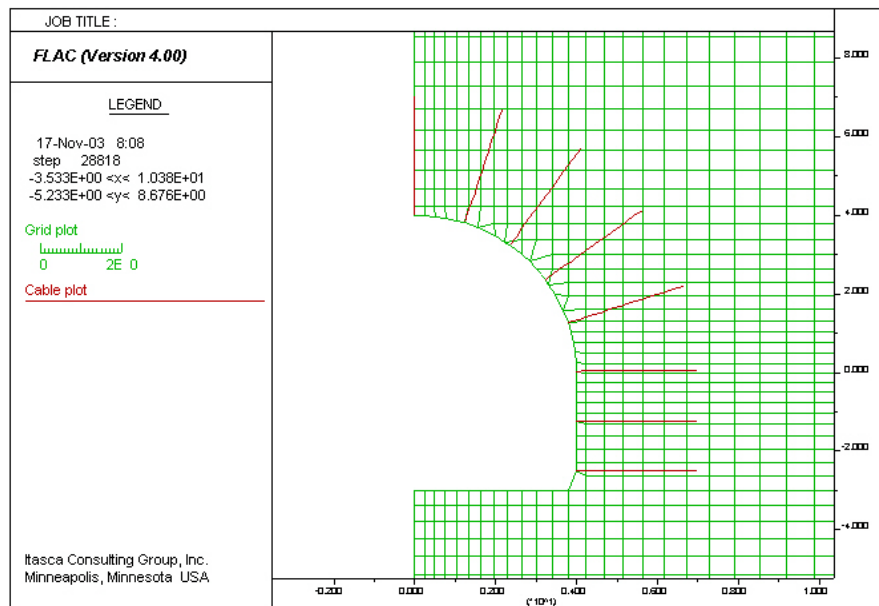


Figure 6-9A. FLAC Model of Turnouts with Rock Bolts

assumed that diameter of the exhaust main is 7.62 m, a conservative condition (resulting in larger spans) with regard to stability of the excavations. The symmetry condition, assumed on the vertical planes at mid-distance between the emplacement drifts, simplifies calculation of the thermal stresses.

### **6.5.1.3 Modeling of Observation Drift**

Two geometrical dispositions of the observation drift were analyzed. A typical cross-section when the observation drift is parallel to the emplacement drift is analyzed using a two-dimensional FLAC model. The geometry of the model and computational grid are shown in Figures 6-14 and 6-14A. The intersection of the observation drift with the exhaust main, accounting also for the interaction with the nearest emplacement drift, is analyzed in a three-dimensional 3DEC model. The geometry of the observation drift in the intersection with exhaust main and the geometry of the 3DEC model are shown in Figures 6-15 and 6-15A.

### **6.5.1.4 Modeling of TBM Launch Chamber**

The TBM launch chamber was analyzed using a two-dimensional FLAC model. Figures 6-16 and 6-16A show the geometry and grid of the model in a cross-section normal to the chamber axis.

### **6.5.1.5 Modeling of North Portal**

Figure 6-17 shows isometric and plan views of the 3DEC model of the North Portal. The model was constructed based on available topographical information and cross-sections of the portal region. Cross-sections  $C_1-C_1'$  and  $L-L'$ , indicated in Figure 6-17, are shown in Figures 6-17Aa and 6-17Ab.

### **6.5.1.6 Modeling of Interburden Pillar between Shaft Access and Exhaust Mains**

The location of the 3DEC model for interburden pillar between shaft access and exhaust mains is shown in location E in Figure 6-1. At this location, the access drift to #1 intake shaft overlies the two parallel exhaust mains. In plan view, the first drift intersects with the two exhaust mains. From three-dimensional viewpoint, these three drifts are not intersecting. The interburden between the first drift and the latter two drifts is about 10 m and the diameter of each of these drifts is 7.62 m. The model size is 200 m  $\times$  81 m in plan and 100 m in height. Figures 6-17B and 6-17C show the configuration and geometry of the 3DEC model. Note that only unsupported drifts were modeled for this case.

## **6.5.2 Loading and Boundary Conditions**

In designing the repository openings, stresses resulting from four sources must be considered: in situ (including excavation effects), construction and operation activities, thermal (nuclear waste), and seismic. In situ stresses are present before drift excavation and will be altered in the vicinity of openings during repository excavation. The stresses during construction, such as installation activities (e.g. jacking process) or stresses due to equipment movement such as TBM weight during mining, must be considered in the design of the ground support systems. The stresses due

to repository operations such as loads caused by gantry weight or waste package weight may also need to be considered in the design. Thermal stresses will occur after waste emplacement, and the timing and magnitude of the temperature-induced loads at any particular location in the repository are primarily dependent on the position relative to the stored waste packages. The magnitude of earthquake-induced stress and the duration of the earthquake event are a function of the intensity of the earthquake, the distance from the event to the repository, and the direction and size of the seismic wave relative to the opening. The applicability and magnitude of some of the design loads will vary depending on the type of ground support system. Some of the loads, such as thermal loads, will only apply to the final ground support system. In the following sections, a description for each design load type is presented.

### 6.5.2.1 In Situ Loads

The virgin stress field existing before excavation is the in situ or geostatic state of rock stress. Excavation of repository openings will disturb the surrounding in situ stress field. The stability of the opening will depend on the concentrations of excavation-induced stress and rock mass deformation behavior. For repository openings, computer simulation of the excavation process will be used to assess the stability. In situ stress estimates, opening dimensions, rock mass bulk density, rock mass elastic moduli, and rock mass strength parameters for the failure or yield criteria are required to perform the analyses.

The in situ stress state at the repository has not been measured directly and will vary from location to location. For the initial state of stress, the vertical stress ( $\sigma_v$ ) at some point is caused by the overburden weight and is given as

$$\sigma_v = -\sum_{i=1}^n \rho_i g h_i \quad (\text{Eq. 6-5})$$

where  $\rho_i$  ( $\text{kg/m}^3$ ) is average bulk density of the  $i$ th layer of rock mass,  $h_i$  (m) is thickness of the  $i$ th layer of rock mass above an opening,  $g$  ( $\text{m/s}^2$ ) is the gravitational acceleration, and  $n$  is the total number of overlying layers of rock mass.

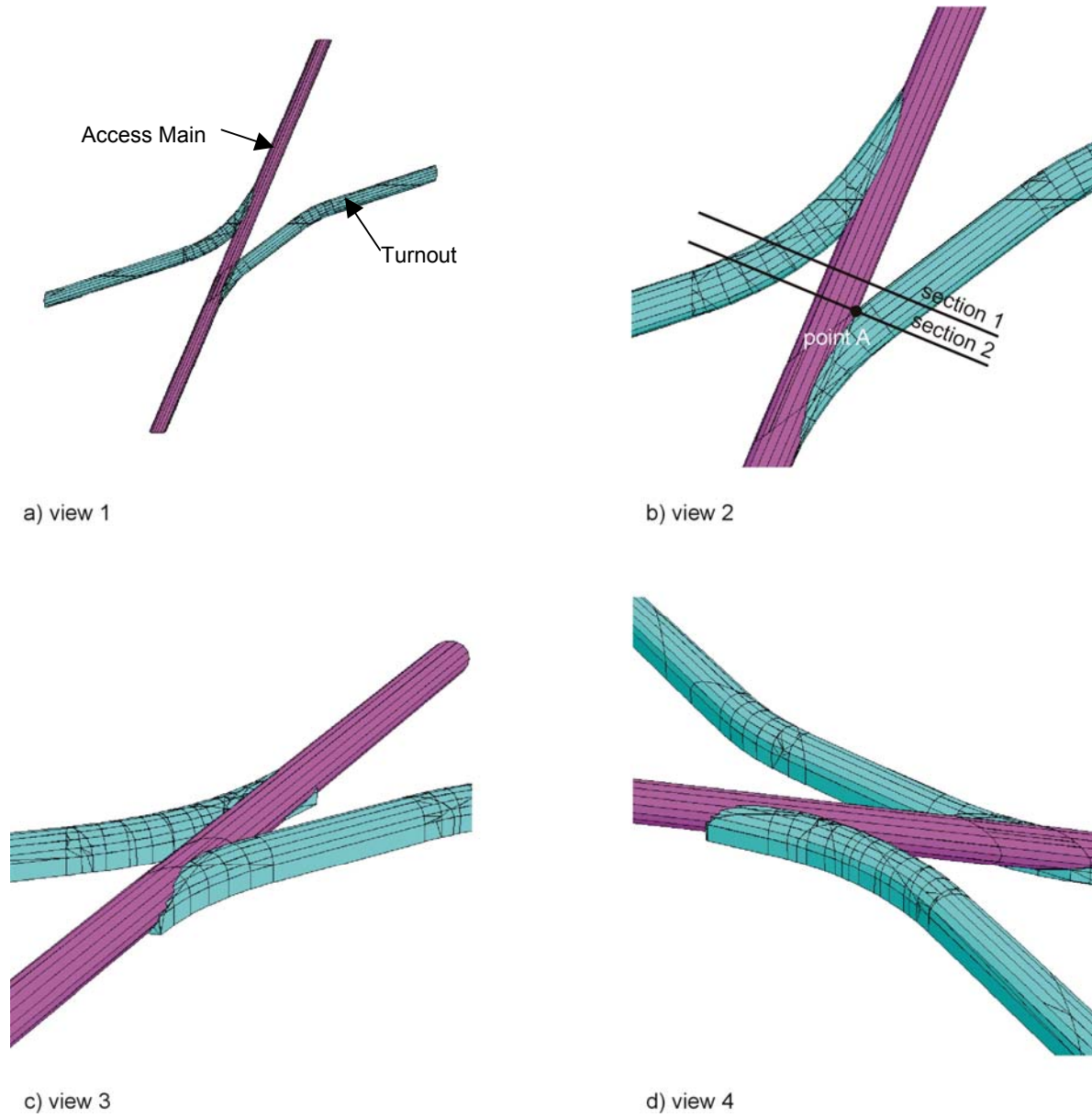
Average initial horizontal stress ( $\sigma_h$ ) at the same location is estimated as:

$$\sigma_h = K_0 \sigma_v \quad (\text{Eq. 6-6})$$

where  $K_0$  = horizontal-to-vertical stress ratio, dimensionless.

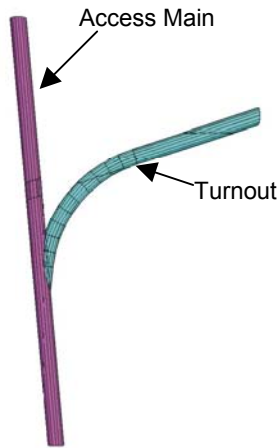
The vertical in-situ stress is gravitational, and it is the major principal stress. In this calculation, the average rock density of  $2410 \text{ kg/m}^3$  (Section 4.1.2) is assumed to estimate the overburden and in situ stress state for modeling all non-emplacement drifts except North Portal, in which a density of  $2310 \text{ kg/m}^3$  (see Table 4-7) is used. For 3DEC modeling, the major horizontal principal stress is 62% of the vertical stress whereas the minor horizontal principal stress is 36% of the vertical stress (Section 5.3). This is according to the in situ stress measurement by hydraulic fracturing in a test hole located in the TSw2 unit (SNF37100195002.001). For FLAC modeling, the horizontal-to-vertical stress ratio is 0.5 (Assumption 5.3). The overburden weight is applied as a stress boundary condition at the top of the model.

In evaluation of the stresses induced by excavation in the ground support components for the non-emplacment drifts, an initial ground relaxation value of 75 percent is used. This results in 25 percent of the pre-excavation in situ stress being imposed on the ground support system (Section 5.1). This value is considered to be conservative to account for the effect of face advance and stand-off between the face and the installed rock bolts. Any rock deformation induced by the excavation will most likely be complete well before the installation of the final ground support. Also, as discussed in Assumption 5.1, an initial ground relaxation value of 100 percent is assumed and used in the ground support analysis for the final shotcrete lining in non-emplacment drifts. In other words, there will be no pre-excavation in situ stress being imposed on the shotcrete system.

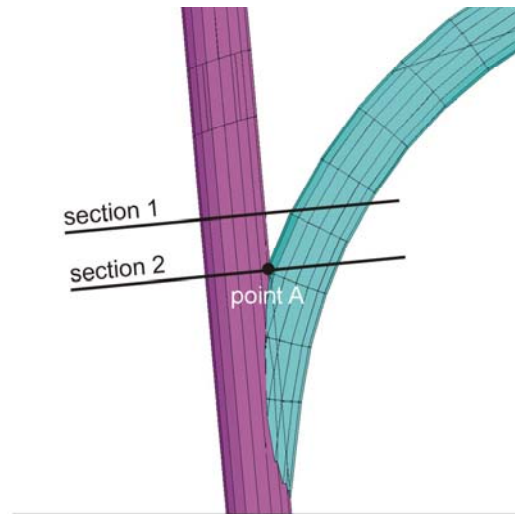


Note: the distance between sections 1 and 2 is 6.2 m.

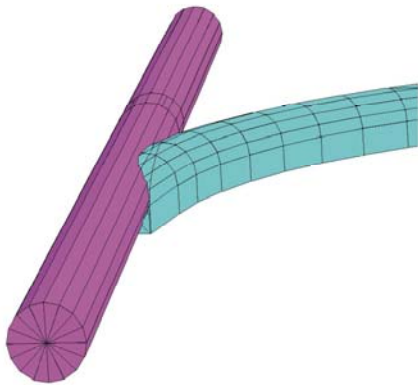
Figure 6-10. 3DEC Model Configuration of Intersection at Location A



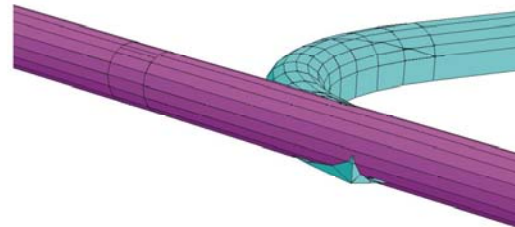
a) view 1



b) view 2



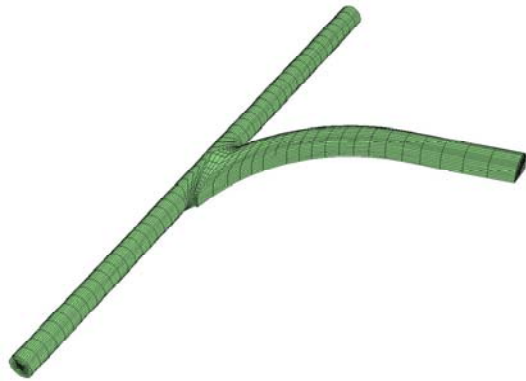
c) view 3



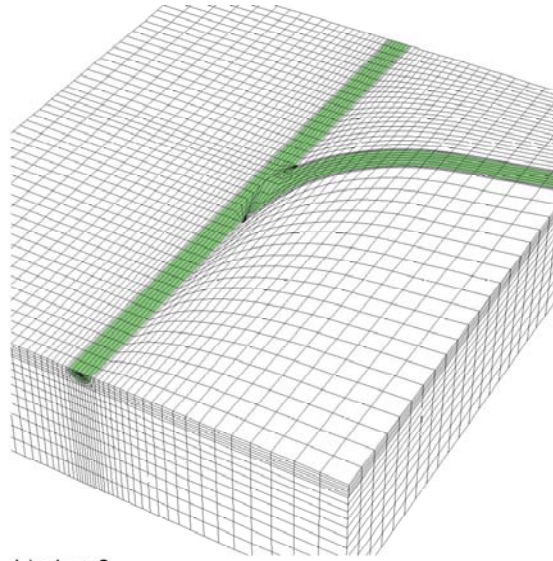
d) view 4

Note: the distance between sections 1 and 2 is 14.8 m.

Figure 6-10A. 3DEC Model Configuration of Intersection at Location C

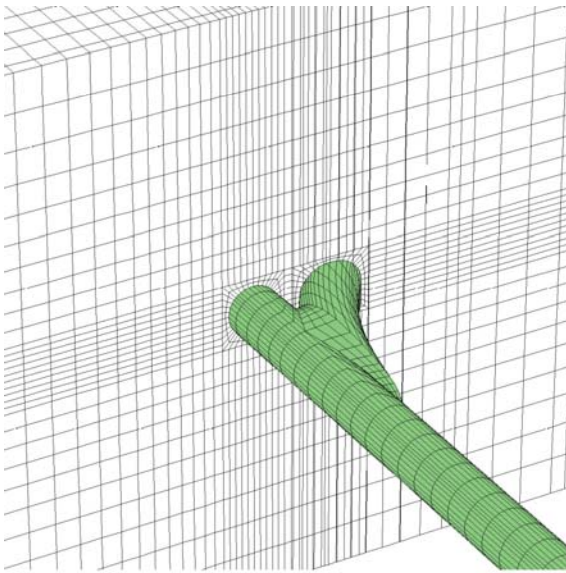


a) view 1

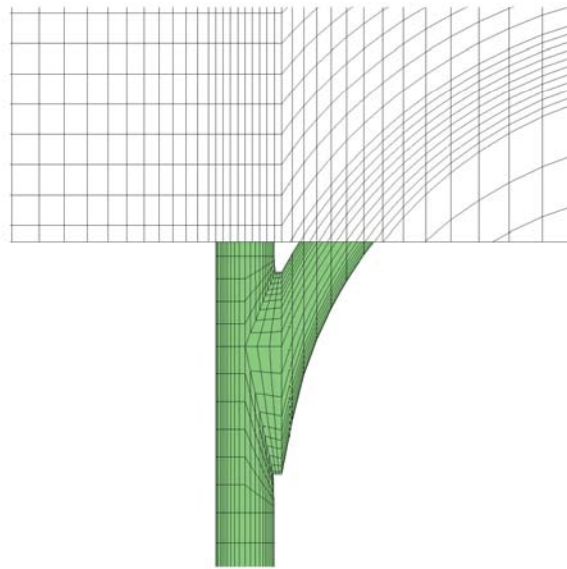


b) view 2

Figure 6-11. FLAC3D Model Configuration of Intersection at Location C

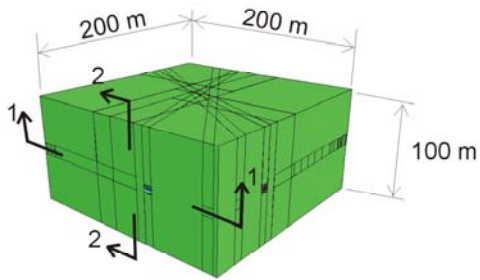


a) view 1

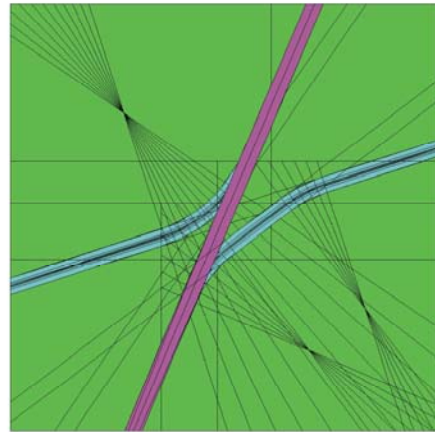


b) view 2

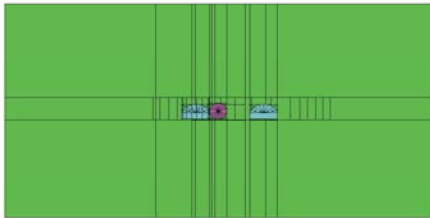
Figure 6-11A. Perspective View of Intersection at Location C in FLAC3D Model



a) isometric view

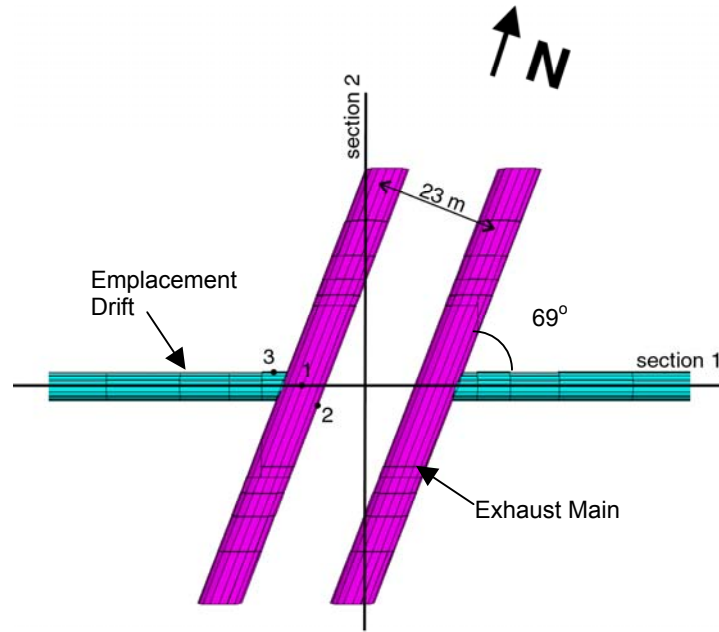


b) section 1

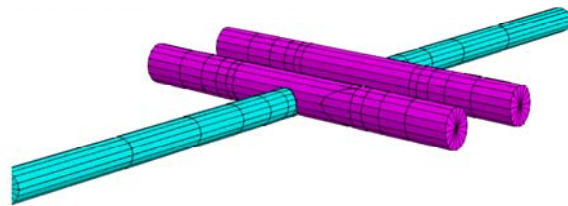


c) section 2

Figure 6-12. 3DEC Model Geometry and Dimension for Intersection at Location A

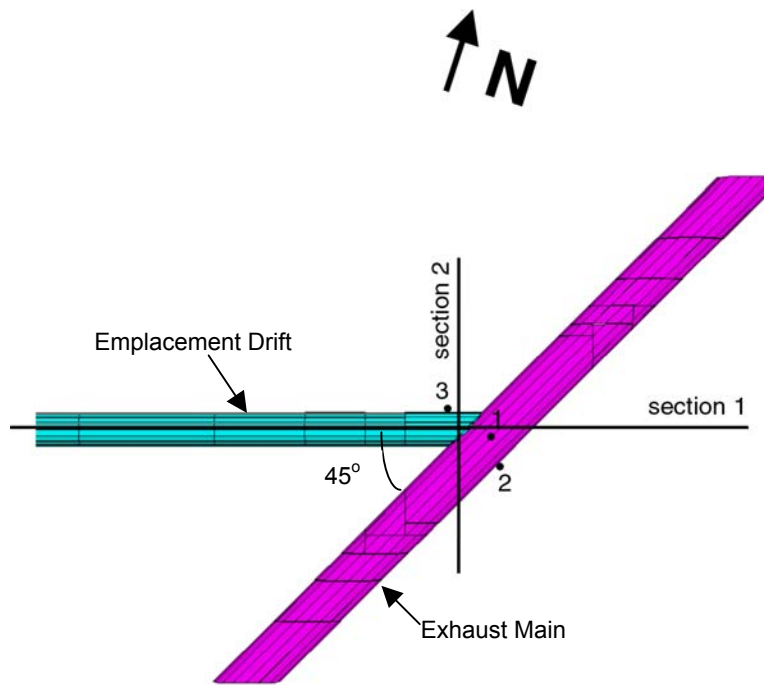


a) view 1

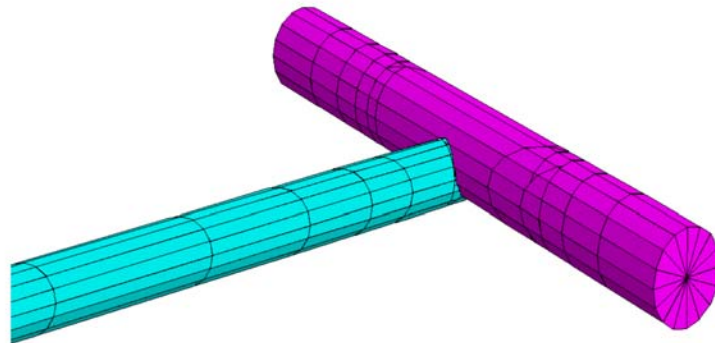


b) view 2

Figure 6-13. Geometry of 3DEC Model for Intersection at Location B



a) view 1



b) view 2

Figure 6-13A. Geometry of 3DEC Model for Intersection at Location D

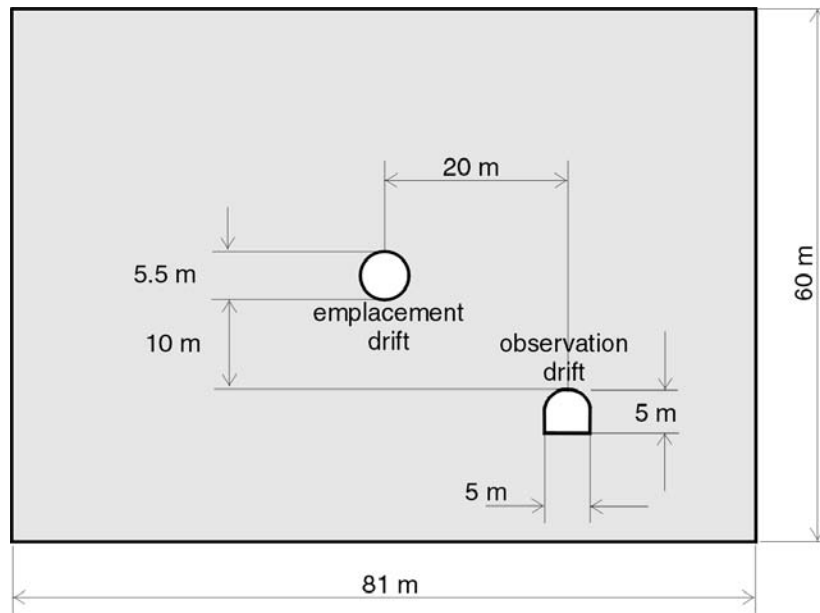


Figure 6-14. Geometry of Two-dimensional Model of Observation Drift and Emplacement Drift

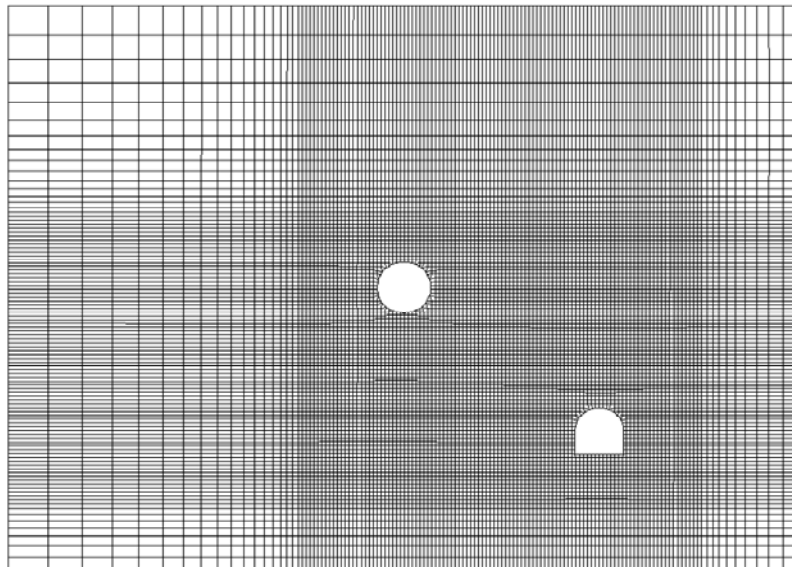


Figure 6-14A. Grid of Two-dimensional Model of Observation Drift and Emplacement Drift

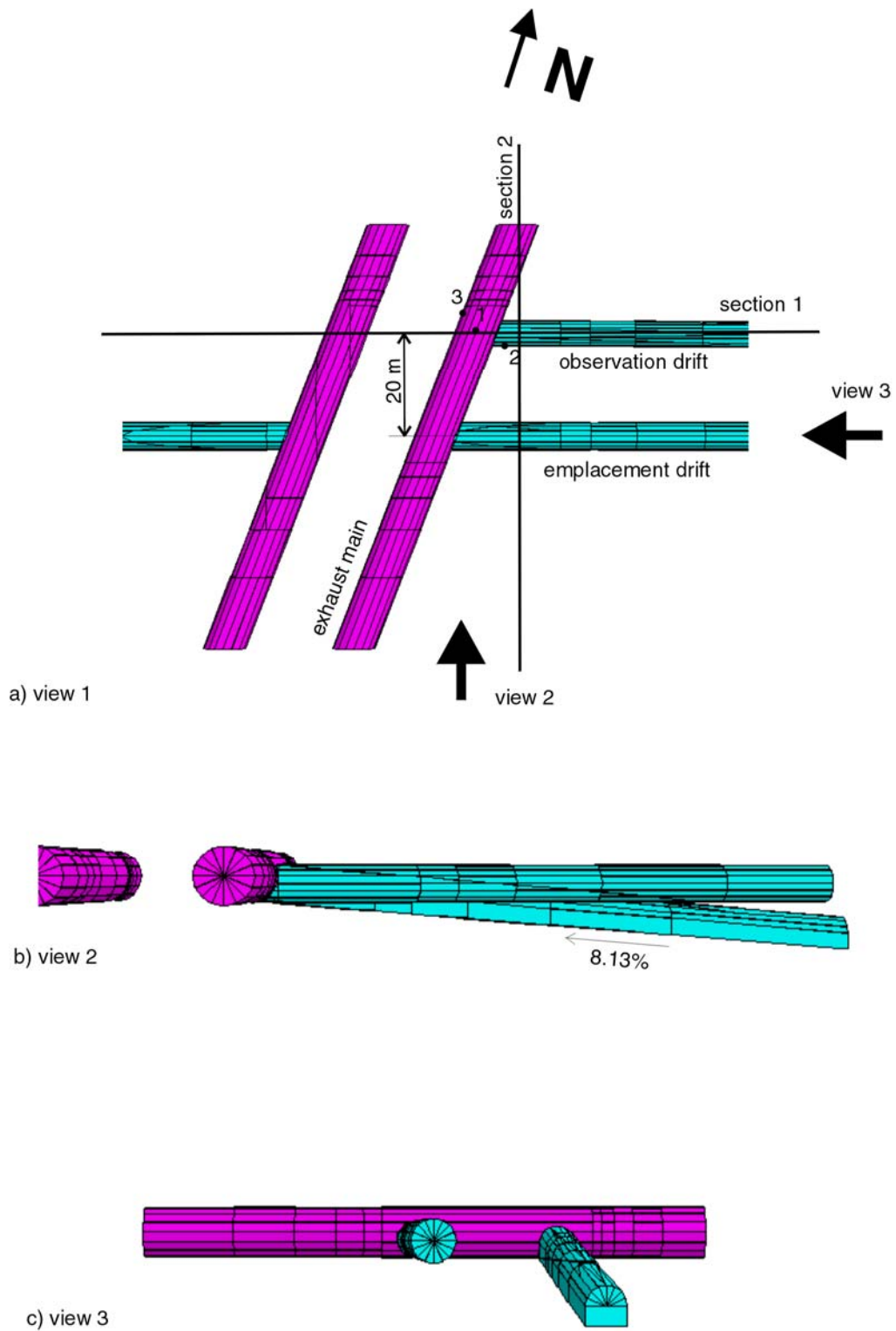
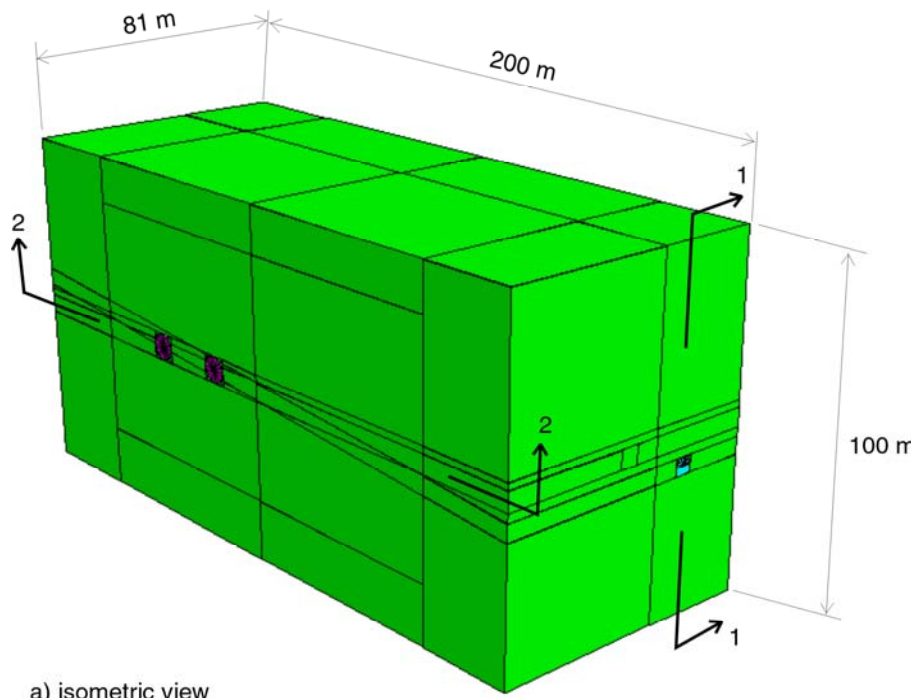
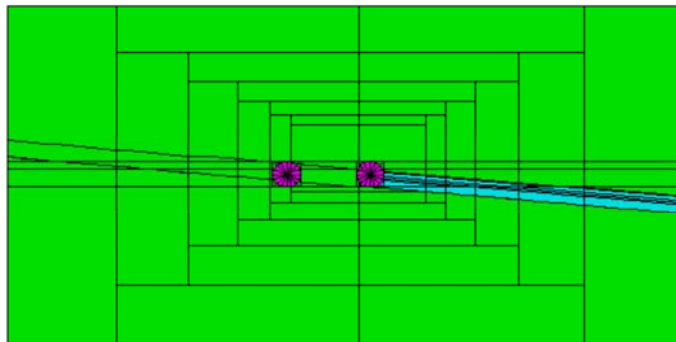


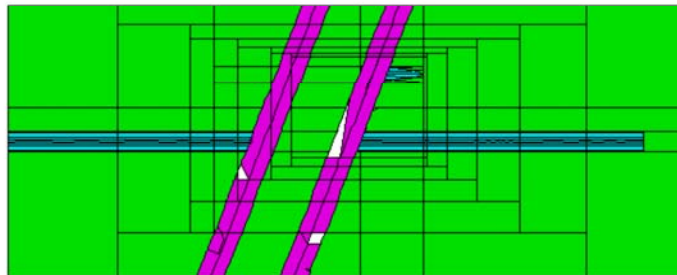
Figure 6-15. Geometry of Intersection of Observation Drift with Exhaust Main



a) isometric view



b) section 1



c) section 2

Figure 6-15A. Geometry of 3DEC Model for Intersection between Observation Drift and Exhaust Main

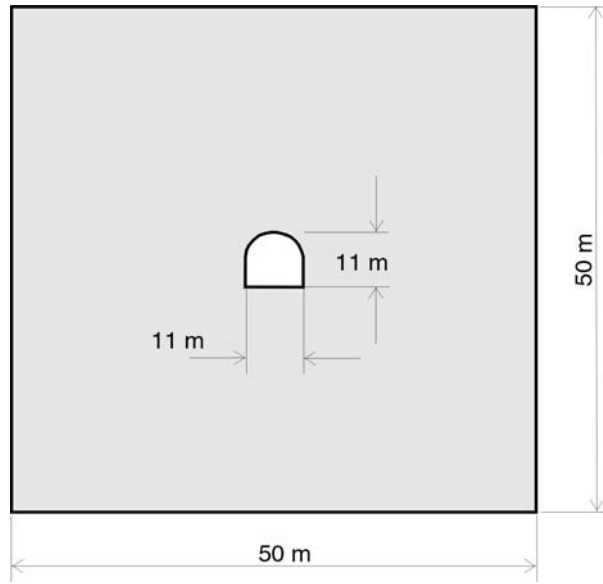


Figure 6-16. Geometry of Two-dimensional Model of TBM Launch Chamber

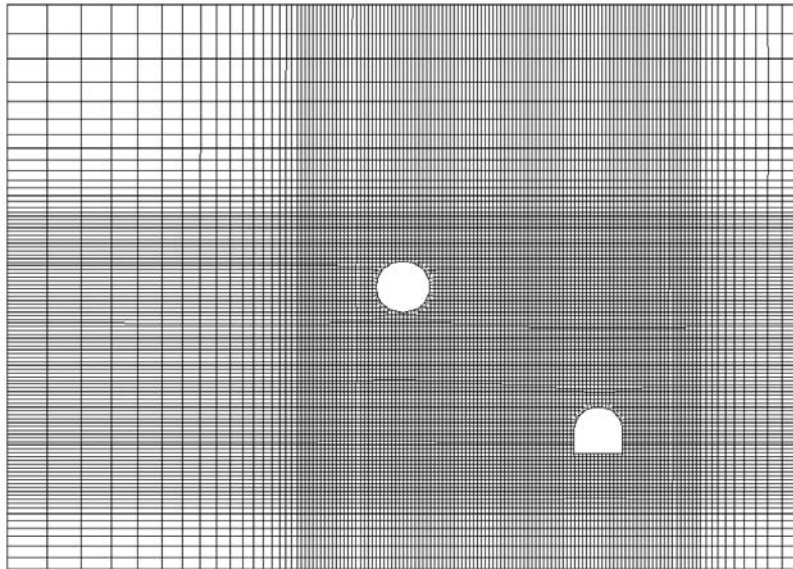


Figure 6-16A. Grid of Two-dimensional Model of TBM Launch Chamber

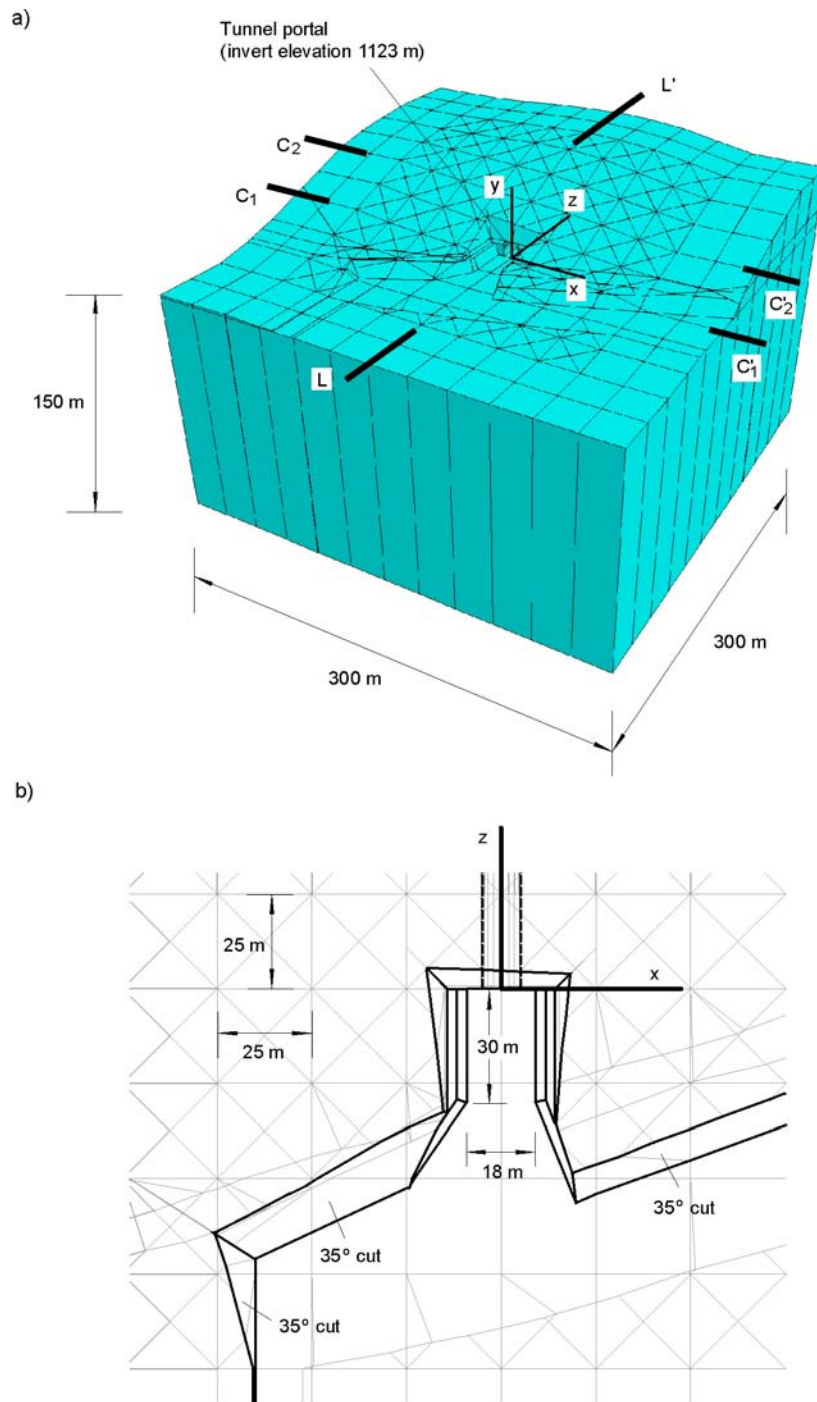
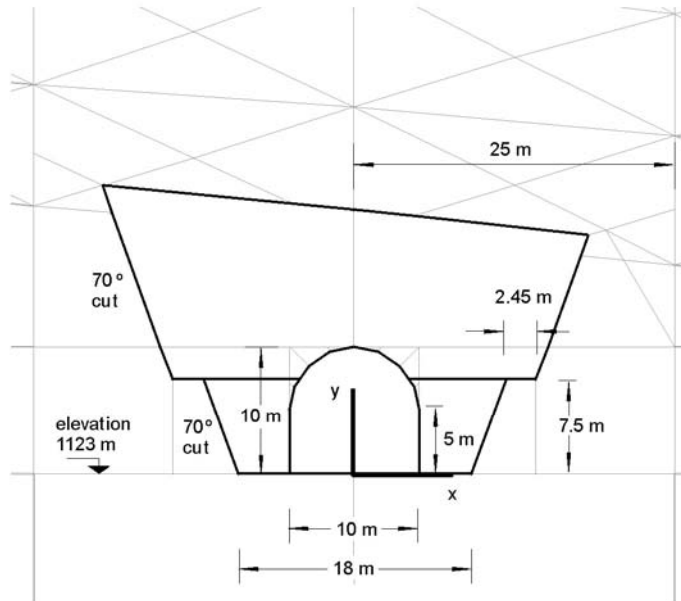


Figure 6-17. a) Isometric and b) Plan Views of North Portal Model

a)



b)

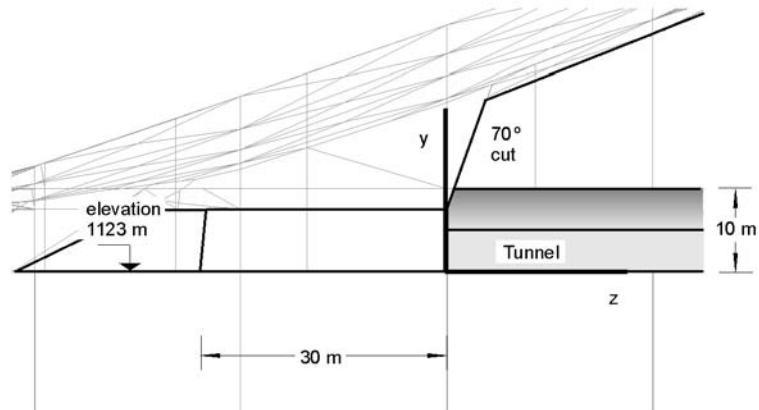


Figure 6-17A. a) Frontal Cross-sectional (C<sub>1</sub>-C<sub>1</sub>') and b) Longitudinal Cross-sectional (L-L') Views of North Portal Model

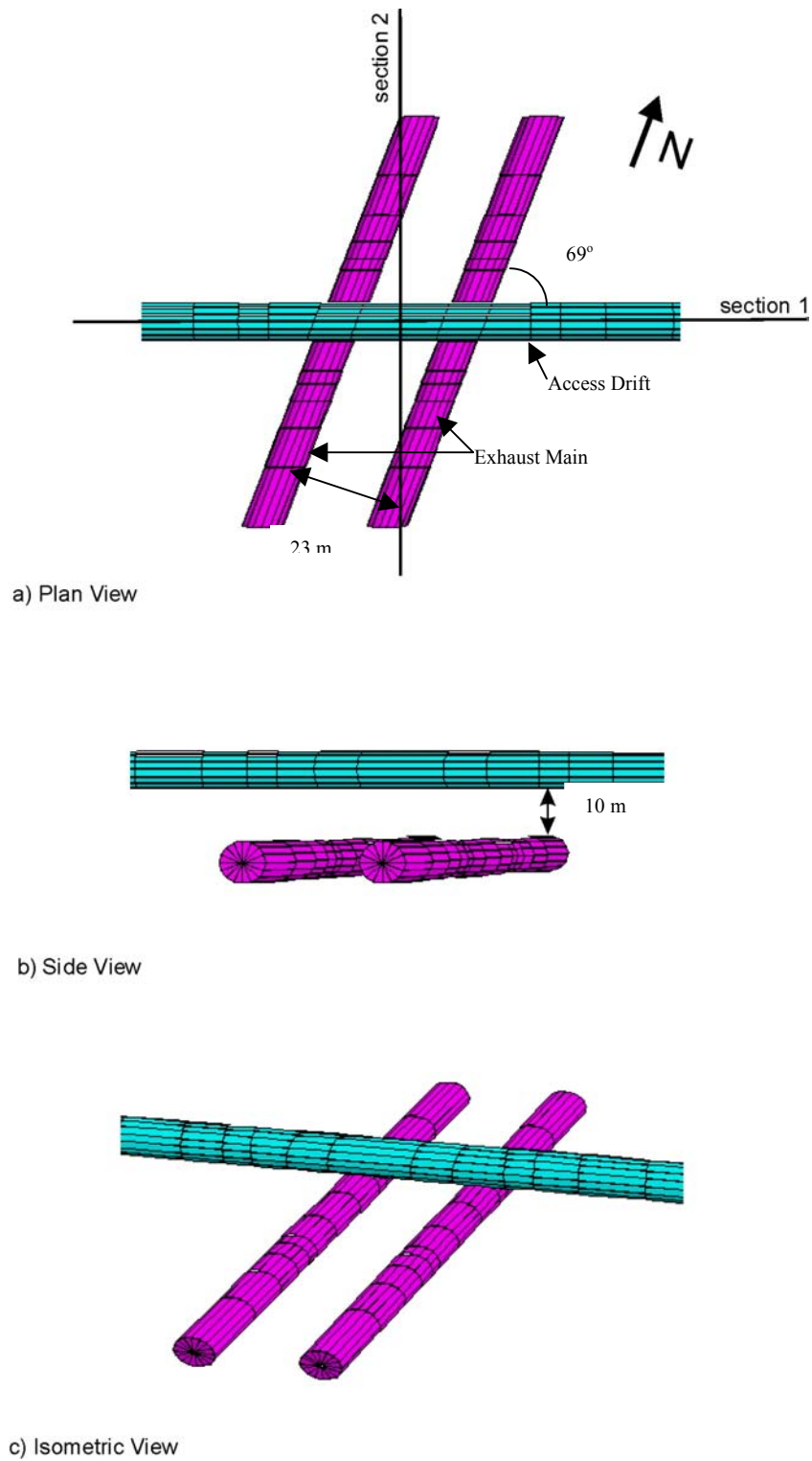
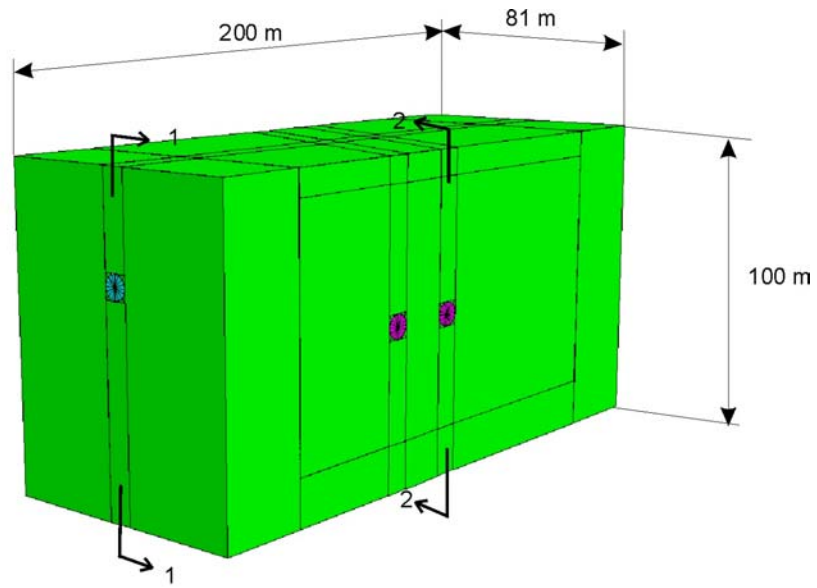
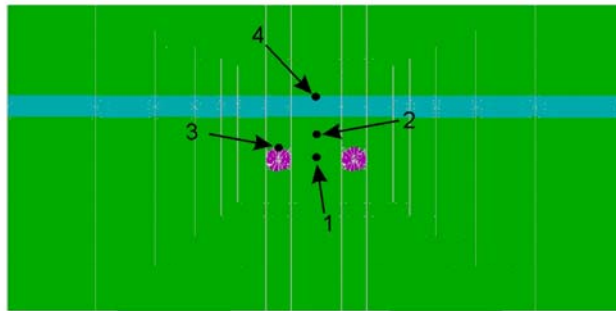


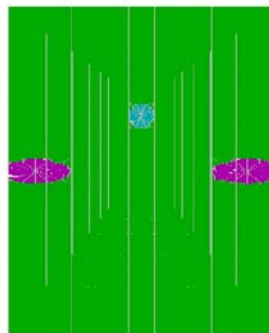
Figure 6-17B. Configuration of 3DEC Model for Interburden Pillar between Access Drift to Intake Shaft #1 and Exhaust Mains



a) isometric view



b) section 1



c) section 2

Figure 6-17C. Geometry of 3DEC Model for Interburden Pillar between Access Drift to Intake Shaft #1 and Exhaust Mains

### **6.5.2.2 Operation Loads**

Operational loads, such as waste package weight and invert material weight, are not considered in this calculation due to the preliminary nature of the design. Exclusion of these loads was believed to result in an overestimate of the inward rock displacements (particularly below the springline) since these loads are expected to offset some of the displacements caused by excavation and heating (note that heating is only considered for those areas in the proximity of emplacement drifts and exhaust mains or directly connected with them).

### **6.5.2.3 Seismic Loads**

Ground motions associated with earthquakes are required to be considered in the design of the repository underground openings. The critical ground motions for subsurface design are ground velocity and acceleration.

In contrast to surface structures, underground structures such as tunnels and their lining or reinforcement systems are constrained by the surrounding medium and do not move independently of the surrounding rock. In reality, the underground structures display significantly greater degrees of redundancy due to the confinement from the ground compared to surface structures, which are generally unsupported above their foundation. Therefore, for underground openings, the surrounding rock acts as a support during a seismic event. Case history studies of underground openings which have been subjected to seismic activities are generally used in practice to provide a basis for ground support design. Forty-one (out of seventy-one) cases of observed damage to rock tunnels from earthquake movements were compared to calculate peak surface motions to determine damage thresholds (Dowding 1979). The tunnels were built between late 1800s and the 1960s, and, thus, represent a wide variety of construction methods. It is shown that peak surface accelerations which cause heavy damage to surface structures, cause only minor damage to tunnels. For accelerations up to 0.19g and velocities up to 20 cm/s, no damage was experienced even for unsupported openings. Minor damage (new cracks and minimal rock fall) was observed for accelerations up to 0.5g and velocities up to about 90 cm/s.

Other than case history studies, there are no empirical or closed-form solutions available to assess seismic effects on underground openings. Limited progress has been made in seismic design methodology for underground tunnels, possibly because of favorable performance data. The lack of applicable codes in the past has led to widely varied measures of precaution taken by different engineers. Moreover, the development of pertinent computer codes, as well as vast improvements in computational capacities of hardware, provides effective tools for seismic design of underground openings. For ground support analysis for LA, fully dynamic analyses will be performed to simulate seismic effects and assess opening stability.

Dynamic loading was applied at the bottom of the model, propagating vertically upwards. Although the dynamic loading was specified as velocity time histories, it was numerically applied at the bottom model boundary as stress boundary condition by using formulas developed for plane waves in elasto-dynamics with the direct relation between velocity and stress given as follows (Itasca Consulting Group 2002, Manuals/3DEC/Optional Features/Section 2: Dynamic Analysis, Section 2.6):

$$\begin{aligned}\sigma_y &= 2\rho C_p v_v \\ \sigma_{xy} &= 2\rho C_s v_{h1} \\ \sigma_{zy} &= 2\rho C_s v_{h2}\end{aligned}\quad (\text{Eq. 6-7})$$

where  $\rho$  is material density;  $C_p$  and  $C_s$  are P and S wave velocity, respectively; and  $v_v$  and  $v_{h1}$  and  $v_{h2}$  are vertical and horizontal velocity components. The factor 2 in Equation 6-7 is due to quiet boundaries.

Seismic load used corresponds to a mean annual exceedance probability of  $1 \times 10^{-4}$  (10,000 years) and  $5 \times 10^{-4}$  (2,000 years) as mentioned in Section 4.1.5. Note that seismic load for a mean annual exceedance probability of  $1 \times 10^{-4}$  is used in all models except for North Portal, in which seismic load for a mean annual exceedance probability of  $5 \times 10^{-4}$  is used (the  $1 \times 10^{-4}$  ground motion for North Portal is not available). Seismic load is considered in both 3DEC and FLAC3D models by applying seismically-induced stresses to the lower boundary of a model. Both P- and S-waves are applied simultaneously. In order to reduce computer computational time, only portion of the velocity time histories that cover 5 to 95% of energy bracket is used. Note that below and beyond this bracket dynamic amplitudes are significantly low. The duration corresponding to this portion of velocity time histories for 10,000 and 2,000 year return periods are from 9.78 to 58.79 seconds (DTN: MO0306SDSAVDTH.000) and 4.84 to 32.55 seconds (DTN: MO0402SDSTMHIS.004), respectively.

#### 6.5.2.4 Thermal Loads

Thermally induced stresses are generated by thermal expansion of the rock mass due to the thermal energy released from the stored nuclear waste. Thermal stresses at any location depend on the proximity and timing of waste emplacement, the waste heat generation, the age of the waste, packaging and emplacement configuration, and the thermomechanical properties of the rock mass.

Heat transfer process due to heat decay of the waste packages in the emplacement drift is a complicated thermal process. During the preclosure period, the heat transfer process is dictated by the thermal radiation from the waste package to the drift wall, convection due to the preclosure ventilation, and the thermal conduction of heat into the rock mass around the drift. The convective heat transfer occurs due to the temperature difference between the airflow and surfaces of the waste package and the drift wall. The temperature difference was originated by the thermal radiation from the waste package to drift wall.

It should be noted that thermal loading is only considered in evaluating the stability analysis for intersections between exhaust mains and emplacement drifts, observation drift, intersection between observation drift and exhaust main, and interburden pillar between access to intake shaft #1 and exhaust mains.

The exhaust mains are located near (intersecting) the emplacement drifts. After waste emplacement, the exhaust mains and the intersections between the exhaust mains and the emplacement drifts will be subjected to the thermal stresses. The temperature change and thermal stresses will be different around the intersection at location B (in the middle of the repository) and at location D (at the edge of the repository). The evolution of the temperature field around the intersections (both locations B and D) was calculated by the NUFT code. Temperature changes at the edge of the repository (location D) are overpredicted by NUFT's two-dimensional results (because emplacement drift is assumed to be infinitely long in 2-D model whereas there is no emplacement drift on the other side of exhaust main at location D), resulting in conservative estimate of stress increase (and more unfavorable stability conditions). The temperature fields (at 1, 2, 3, 5, 10, 20, 30 and 50 years) from the NUFT code (BSC 2003g, Section 6.4.1) were imported into 3DEC in order to calculate the thermal stress around the excavations, according to the following formula (Itasca Consulting Group 2002, Manuals/3DEC/Optional Features/Section 1: Thermal Option, Section 1.2.3):

$$\Delta\sigma_{ij} = \delta_{ij} 3K\alpha(T)\Delta T \quad (\text{Eq. 6-8})$$

where  $\Delta\sigma_{ij}$  is the stress change,  $\delta_{ij}$  is the Kronecker delta,  $K$  is the bulk modulus of the rock mass,  $\alpha(T)$  is the coefficient of the linear thermal expansion, a function of temperature (as listed in Table 4-5), and  $\Delta T$  is the temperature change.

3DEC was used to model the effects of the thermal stress on stability and deformation of the intersections between emplacement drifts and exhaust mains. The thermal expansion of the ground support was not accounted for. In general, this approximation results in conservative estimate of the load in the rock bolts for the preclosure. For the purpose of this calculation, it is considered adequate.

#### 6.5.2.5 Boundary Conditions

The boundary conditions for 3DEC computer analysis are presented in Table 6-8. At the in situ loading stage and the later thermal loading period, fixed velocity at lateral and bottom boundaries were used to ensure boundary effect does not affect the stress distribution around the opening. The prescribed temperatures generated from NUFT at various time periods were incorporated into 3DEC model to evaluate the thermomechanical behavior. For the dynamic analysis, non-reflecting boundary is used for both the top and bottom of the model, whereas free-field boundary is imposed at the lateral perimeter of the model. The free-field boundaries ensure that plane waves propagating upward suffer no distortion at the boundary. At the dynamic loading stage, the seismic load is considered in the 3DEC models by applying seismically-induced stresses (both normal and shear tractions) to the lower boundary of a model. FLAC and FLAC3D are used for static analysis in this calculation. Their boundary conditions are the same as those for 3DEC model.

Table 6-8. Boundary Conditions for 3DEC Analysis

Boundary	Static Analysis Stage	Dynamic Analysis Stage
Lateral	Fixed at the direction normal to the face	Free-Field boundary
Bottom	Fixed at the vertical direction	Non-reflecting boundary
Top	Applied pressure at the vertical direction	Non-reflecting boundary
Drift Wall	Free	Non-reflecting boundary

### 6.5.3 Stability of Unsupported Non-Emplacement Drifts

This section presents the results of assessment of stability of unsupported non-emplacement drifts. The assessment is based on numerical analysis using the FLAC, 3DEC, and FLAC3D computer codes. The analysis evaluates displacement and stress in the vicinity of an unsupported non-emplacement drift, factor of safety, ground reaction curves (GRC), and temperature increases in rock following waste emplacement.

#### 6.5.3.1 In Situ Stress Loading Condition

The effect of the rock mass quality variability within the lithophysal and non-lithophysal units at the repository level was accounted for by considering different rock mass categories. There are six categories in the lithophysal unit and five categories in the non-lithophysal units. The rock mass properties for different categories listed in Tables 4-1 and 4-2 for the lithophysal and non-lithophysal rock mass, respectively, are determined by rock mass characterization based on laboratory and in-situ testing. In this calculation, the computer simulations for all non-emplacement openings except for North Portal were mainly carried out for the most conservative conditions, category 1 rock (the poorest quality rock mass), both in lithophysal and non-lithophysal units. Stability analysis for category 5 rock (the strongest quality rock mass) was also included for access and exhaust mains. Category 6 rock is considered representative of extremely poor quality lithophysal rock mass in the disturbed rock zone around excavations. Therefore, it was not considered in the simulations because it would result in excessively conservative, unrealistic predictions of deformation and damage of the rock mass. A Mohr-Coulomb, elastic-plastic constitutive model was assumed for all simulations. It should be noted that in computer simulations for North Portal the properties considered for the rock are those of the poorest quality rock mass (i.e., category 1) in the TCw unit (see Table 4-7).

##### 6.5.3.1.1 Access and Exhaust Mains and Turnouts

Table 6-9 summarizes the results of unsupported access and exhaust mains and turnouts for drift displacement and rock stresses induced by excavation. For access and exhaust mains, the horizontal displacement varies from 6.4 mm for lithophysal category 1 rock to 0.3 mm for non-

lithophysal category 5 rock. The vertical displacement is estimated to range from 32.8 mm for lithophysal category 1 rock to 2.3 mm for non-lithophysal category 5 rock. For turnouts, the horizontal displacement for lithophysal category 1 rock is 9.0 mm and 1.3 mm for non-lithophysal category 1 rock. The vertical displacement for lithophysal category 1 rock is 36.2 mm and 6.5 mm for non-lithophysal category 1 rock. Note that the sign convention in FLAC is that positive displacement signifies displacement in positive X or Y direction. Thus, the above mentioned vertical and horizontal displacement are moving in downward and inward directions, respectively. Also, all the maximum vertical displacements occur at the crown whereas the maximum horizontal displacements at springline. Figure 6-18 shows the displacements around access mains for lithophysal category 1 rock. The largest displacement of 32.8 mm occurs at the crown. The results show the effect of rock mass quality on the drift deformation.

The maximum tangential stress for access and exhaust mains varies from about 20 MPa in compression occurring near the skin of springline to about 5 MPa in compression occurring near the skin of crown. The maximum tangential stress for turnouts varies from 18 MPa in compression for non-lithophysal category 1 rock occurring near the skin of springline to about 5 MPa in compression occurring near the skin of crown. The stresses at the crown are much smaller than those at the springline. The minor principal (radial) stresses are about 1 MPa or lower, which are much lower than those of the maximum tangential stresses.

Figures 6-19 and 6-20 show the contours of safety factor (SF) against Mohr-Coulomb shear failure around the unsupported access/exhaust mains for category 1 rock in lithophysal and non-lithophysal units, respectively. The SF in this case is defined as the ratio of shear strength to the shear stress on the potential failure plane. For lithophysal rock, a very narrow zone adjacent to wall (about 0.2 m into wall) is shown with potential yield. At distance of 1.5 m into wall SF increases to 2. For non-lithophysal rock, almost no yield is observed near the wall and SF increases to 2 with a very short distance (about 0.2 m) into wall. Figures 6-21 and 6-22 show the contours of safety factors around the unsupported turnouts for category 1 rock in lithophysal and non-lithophysal units, respectively. The distribution of SF contours is similar to those of access mains except the extent is a little larger, which is mainly due to the stress concentration at 90° angle intersection between sidewall and invert. There is no indication of instability of the rock surrounding the access/exhaust mains and turnouts.

### **6.5.3.1.2 Intersections**

#### **6.5.3.1.2.1 Intersection between Access Main and Turnout**

Stability of the intersections in the lithophysal and non-lithophysal rock mass for in-situ stress conditions, assuming no ground support, is analyzed for two layouts at locations A and C. The intersection at location C represents a typical layout; the intersection at location A represents the critical conditions with respect to the maximum span of the roof and stress concentrations in the pillars.

Table 6-9. Unsupported Access and Exhaust Mains and Turnouts - Results for In Situ Stress Loading Condition from FLAC

Items	Access/Exhaust Mains		Access/Exhaust Mains		Turnouts	
	L. Cat. 1	NL. Cat. 1	L. Cat. 5	NL. Cat. 5	L. Cat. 1	NL. Cat. 1
Horizontal Displacement (mm)	-6.4	-0.8	-0.5	-0.3	-9.0	-1.3
Vertical Displacement (mm)	-32.8	-5.9	-3.1	-2.3	-36.2	-6.5
Major Principal (Tangential) Stress near Crown (MPa)	-5.3	-5.3	-5.3	-5.3	-5.3	-5.3
Minor Principal (Radial) Stress near Crown (MPa)	-0.5	-0.4	-0.4	-0.4	-0.2	-0.2
Major Principal (Tangential) Stress near Springline (MPa)	-19.0	-21.5	-21.5	-21.5	-11.0	-18.0
Minor Principal (Radial) Stress at Springline (MPa)	-1.0	-1.2	-1.2	-1.2	-0.2	-0.3

Note: a) L – lithophysal, NL – non-lithophysal, b) The vertical displacement occurs at crown whereas horizontal displacement at springline.

To avoid large, unphysical deformation of zones around the boundary of the excavation that yield in tension, tensile strength in the 3DEC simulations was assumed to be infinitely large. Simulation of the intersection at location C in the lithophysal rock mass category 1 was conducted with both 3DEC and FLAC3D. In the FLAC3D simulation the rock mass was assumed to have no tensile strength. The results of 3DEC (with infinite rock mass tensile strength) and FLAC3D (with no tensile strength) are compared to demonstrate that the assumption used in the 3DEC model has little effect on the results (see Figure 6-37 and discussion in Section 6.5.3.1.2.1.1).

The results for the intersection at the location A (hereinafter called intersection A) and at the location C (hereinafter called intersection C) are shown in Figures 6-23 through 6-56. For both units (lithophysal and non-lithophysal) and both intersection locations (A and C), the figures include the plots of:

1. Displacement fields in two vertical sections 1 and 2 (see section location in Figures 6-11 and 6-12);
2. Displacement profile along the vertical line through the point A (see Point A location in Figures 6-11 and 6-12);
3. Stress fields in the same vertical sections as for the displacement fields;
4. Average pillar stress as a function of the distance from the tip (Point A). The stresses were averaged over the entire pillar width and height for a 2-m long segments measured radially from the pillar tip; and
5. Potential yield zones in the horizontal and the vertical sections.

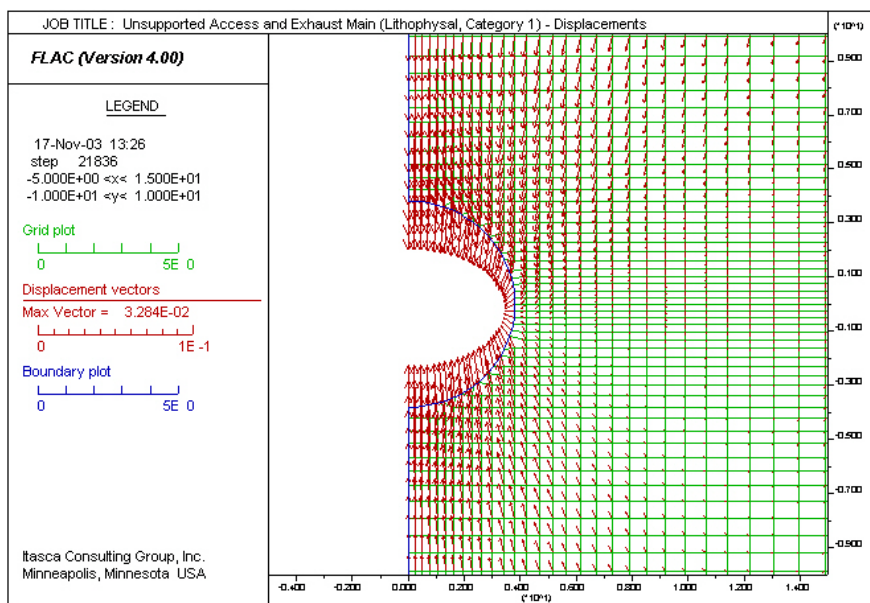


Figure 6-18. Displacements at Access and Exhaust Mains for Lithophysal Cat. 1 Rock

### 6.5.3.1.2.1.1 Rock Displacements

Figures 6-23 and 6-24 show displacement fields in vertical section 1 at intersection A for category 1 rock of lithophysal and non-lithophysal rock, respectively. For the same intersection, Figures 6-25 and 6-26 show displacement fields in vertical section 2 for category 1 rock of lithophysal and non-lithophysal rock, respectively. Note that vertical section 1 cuts across two turnouts and one access main as well as two very narrow pillars. Vertical section 2 cuts through the intersecting access main and turnout, one narrow pillar, and another turnout. The important features of these two sections are: section 1 cuts through very narrow pillar whereas section 2 cuts through an opening with large roof span. The results show that the maximum displacement in lithophysal rock occurs at the intersection area with large roof span with a value of 7.21 cm. The maximum displacement in non-lithophysal rock at the same location is 1.12 cm. Figure 6-27 shows the vertical displacements along the vertical line through point A in section 2. The profiles of the vertical displacement along the vertical line through point A show a gradual increase in displacements approaching the back of the intersection. There is no indication of large displacement gradients, which is a consequence of distressing and loosening of potentially unstable ground. As shown in this figure, the displacements for lithophysal category 5 rock are smaller than those of non-lithophysal category 1 rock. The major reason is that the elastic modulus of the former is larger than that of the latter. Relatively large displacements for the lithophysal category 1 rock mass result from the very low elastic modulus assigned to the lithophysal category 1 rock mass. These observations are confirmed with plots of the rock mass

regions that deformed plastically, as shown in Figures 6-28 and 6-29. Plastic deformation extends to approximately 1 m from the drift walls in the lithophysal, category 1 rock mass. There is practically no plastic deformation around the drifts in the non-lithophysal rock mass.

Similar results are predicted for intersection C as shown in Figures 6-30 through 6-36. However, since each access main only intersects with one turnout and the roof span at intersection C is smaller, the corresponding opening displacements are smaller compared with those of intersection A. For instance, the maximum displacements in lithophysal and non-lithophysal rock occur at section 2 (i.e., with large roof span) and are 6.4 and 1 cm, respectively. The maximum displacements in lithophysal and non-lithophysal rock occur at section 1 are 4.8 and 0.8 cm, respectively. Figure 6-37a shows the contour plots of vertical displacements at section 1 for lithophysal category 1 rock based on FLAC3D results. The maximum displacements at the crown area range from 4.0 to 5.2 cm and are comparable to that of 3DEC results. (Note that Figure 6-37b shows the contour plots of stress field at section 1 for lithophysal category 1 rock based on FLAC3D results. The range of stress fields and distribution in this figure is comparable to that of Figure 6-48.) The results justify the use of 3DEC and the assumption of infinite tensile strength in the analyses of deformation and stability of the intersections (also see discussion in Section 6.5.3.1.2.1).

#### **6.5.3.1.2.1.2 Stresses in Rock Adjacent to Openings**

Figures 6-38 and 6-39 show stress fields in vertical section 1 at intersection A for category 1 rock of lithophysal and non-lithophysal rock, respectively. For the same intersection, Figures 6-40 and 6-41 show stress fields in vertical section 2 for category 1 rock of lithophysal and non-lithophysal rock, respectively. The results indicate that the maximum compressive stress occurs near the sidewall or in the pillar between adjacent openings and slight destressing above crown and below invert. The highest compressive stress of 56 MPa occurs near the sidewall of the opening at intersection area with large roof span in non-lithophysal category 1 rock. Note that this stress value is larger than the unconfined compressive strength of the rock mass (see Table 4-2). This result does not mean that rock will fail at that location since the rock mass in situ is under confined condition. Yet, it does indicate that there is a potential for rock spalling near the sidewall, which is also revealed in Figures 6-42 and 6-43. In these two figures, the contours of safety factors ranging from 1 to 1.6 are observed along the sidewalls of the openings, especially more evident for lithophysal rock. Figure 6-44 shows the stress field with indication of tensile stresses in vertical section 2 for lithophysal category 1 rock. A very narrow region of tensile stress is observed in the crown and the invert area. There are no indications of large-scale instability of the roof even in category 1, lithophysal rock mass. It is possible that a limited volume of the rock mass becomes unstable due to local structures unaccounted for in this analysis (continuum approach) if the intersections are unsupported. The designed ground support in the intersection will be needed to prevent any such rockfall.

Stability of the pillar between the access main and the turnout can be assessed based on a plot of average pillar stress (shown in Figure 6-45) and plots of regions of plastic deformation (i.e., potential yield zone) shown in the horizontal section in Figures 6-46 and 6-47 (note that the similar plots in vertical section are shown in Figures 6-28 and 6-29). The stress concentrations will cause damage and fracturing of the pillar. The extent of the damage will depend on the

quality of the rock mass. The calculations predict pillar damage to extend 8 m from the tip in the lithophysal rock mass, category 1. In good quality lithophysal rock mass and non-lithophysal rock mass the pillar will be damaged to a distance of approximately 3 m from the tip. However, in reality, the pillars will be rounded to a distance from the tip where the major damage is observed. It is not needed (and probably impossible) to create the pillar tip. If rounding of the pillars is not performed during excavation, it will take place naturally by broken ground falling off. The pillars will eventually attain the stable geometry. It seems, from the numerical results, that the rounding length should not be larger than 5 m in the poorest quality lithophysal rock mass. If the additional ground support is used the pillar rounding length could be reduced even more.

Similar results are predicted for intersection C as shown in Figures 6-48 through 6-56. However, since each access main only intersects with one turnout and the roof span at intersection area is smaller, the corresponding rock stresses are smaller compared with those of intersection A. There are no indications of large-scale instability of the roof even in category 1, lithophysal rock mass. It is possible that a limited volume of the rock mass becomes unstable due to local structures unaccounted for in this analysis (continuum approach) if the intersections are unsupported. The designed ground support in the intersection will be needed to prevent any such rockfall. The pillar stability for intersection C should be achieved as long as the pillar tip is going to be rounded off as discussed above for intersection A.

#### **6.5.3.1.2.1.3 Discussion**

The 3DEC models predict similar deformation and stability conditions for intersections at locations A and C. The rock mass deformation around intersections will be predominantly elastic. The plastic deformation is expected to extend approximately 1 m from the drift walls into the rock mass, in the worst case, for the poorest quality rock mass. A relatively large displacement of 7 cm predicted for the lithophysal, category 1 rock mass (see Figure 6-25), is a consequence of the very low Young's modulus used. There are no indications of loosening and instability of the rock mass in the crown for any of the analyzed cases. The roof in the intersections appears to be stable, even for the largest spans.

The tips of the pillars between the access main and the turnouts will be damaged due to stress concentrations. The extent of this damage from the pillar tip will depend on the rock mass quality. Rounding of the pillars and additional ground support will resolve the problem of pillar instability.

#### **6.5.3.1.2.2 Intersection between Exhaust Main and Emplacement Drift**

Two intersection layouts, B and D, were analyzed as being representative of the extreme conditions existing in the exhaust main intersections from the perspective of excavation stability. The diameter of the exhaust main is 7.62 m — except in Panel 1 of the repository, where it is 5.5 m. Throughout the analyses presented in this calculation, it was assumed that diameter of the exhaust main is 7.62 m, a conservative condition (resulting in larger spans) with regard to stability of the excavations.

The results of the stability analysis of unsupported intersections at locations B and D are shown in Figures 6-57 through 6-66. The analysis was carried out for categories 1 and 5 in both lithophysal (location B) and non-lithophysal (location D) rock masses, representing the variability of rock mass quality at the repository horizon. The results are presented here for category 1 only. The rock mass around the intersections in category 5 deforms elastically at both locations. The modeling sequence followed the expected construction sequence: the exhaust mains were excavated prior to excavation of the emplacement drifts. The presented results are for the final stage of the excavation.

The maximum vertical displacement in the roof is 4.3 cm in the poorest-quality lithophysal rock mass (Figure 6-57). The maximum displacements in the non-lithophysal rock mass are predicted to be less than 1 cm (Figure 6-58 for all categories). The intersections cause stress concentrations in excess of 25 MPa (see Figures 6-59 and 6-60) in the walls of the exhaust main. However, stress tensors colored by the factor-of-safety with respect to a Mohr-Coulomb yield condition (shown in Figures 6-61 and 6-62), and the extent of the rock mass that undergoes plastic deformation in the vertical and horizontal sections (shown in Figures 6-63 through 6-66) indicate that deformation of the rock mass around the intersections will be predominantly elastic. There is a narrow (less than a meter) region of the rock mass around the exhaust main at location B for category 1 that yields (Figure 6-63). However, the effect of the interaction between the exhaust main and the emplacement drift on the extent of rock mass yielding is negligible. The sharp angle between the exhaust main and the emplacement drift creates a pillar (Figure 6-66) between these two excavations. At the most, the rock mass yields 1 m from the tip of the pillar, indicating that rounding the pillar tip would resolve any potential problems.

### **6.5.3.1.3 Observation Drift**

The model results for the typical cross-section perpendicular to the observation drift axis are shown in Figures 6-66A to 6-66D. The maximum displacements predicted for the observation drift are similar to those for the emplacement drift (for the same rock-mass quality), of the order of 0.03 m, because the sizes of both tunnels are similar. The plot of the contours of the major principal stress (Figure 6-66B) clearly shows that, for a given distance, two excavations (the emplacement drift and the observation drift) do not interact with each other. The predicted extent of the damage of the rock mass (Figure 6-66C) surrounding the observation drift and the emplacement drift is similar. There is a little more damage in the walls and the floor of the observation drift because of mechanically less-favorable shape (i.e., flat walls and corners). However, the factor-of-safety with respect to Mohr-Coulomb shear failure (Figure 6-66D) increases very quickly as a function of distance from the drift boundary; the factor-of-safety is larger than 2 only a couple of meters from the drift walls.

The results of modeling the intersection between the observation drift and the exhaust main are presented in Figures 6-66E to 6-66J. The maximum displacements (Figures 6-66E and 6-66F) are comparable to predictions of the two-dimensional model because of the larger span of the exhaust main (7.62 m). However, for the analyzed conditions, there are no indications of stability problems in the intersection. The regions of the rock mass that undergo plastic deformation are confined to the vicinity of the excavations (Figures 6-66G and 6-66H). The extent of damage

does not increase in the intersection, and it does not seem that the excavations interact with each other. The pillar between the observation drift and the exhaust main appears (in the vertical section 2) to be almost completely elastic. Factor-of-safety with respect to Mohr-Coulomb shear failure is larger than 2 (Figures 6-66I and 6-66J) except in close vicinity of the excavations.

#### **6.5.3.1.4 TBM Launch Chamber**

The larger span of the TBM launch chamber (11 m) compared to other excavation considered (i.e., emplacement drifts, access mains) results in larger displacements due to excavation and relaxation of the in situ stresses. The maximum displacement is 0.055 m (Figure 6-66K). The stress state around the chamber (Figure 6-66L) is similar to the stress state around the observation drift (Figure 6-66B), because two excavations have the same shape. Consequently, the size of the region of the rock mass undergoing inelastic deformation (Figure 6-66M), when scaled with characteristic dimension of the excavation, is the same for the launch chamber as for the observation drift. Because the span (or height) of the launch chamber is approximately two times of the span of the observation drift, the depth of the damaged rock in the wall of the launch chamber is about 2 m, compared to the depth of about 1 m predicted in the wall of the observation drift. Outside the yielded region, the factor-of-safety to shear failure increases rapidly as a function of distance from the drift wall (Figure 6-66N), indicating overall stability of the excavation.

#### **6.5.3.1.5 North Portal**

The model results under static in situ conditions after both the slope and the starter tunnel are excavated are shown in Figures 6-66O to 6-66Q. The stress state is completely elastic. Small overburden and slope heights result in stresses (Figure 6-66P) that are small compared to cohesion, even in the case of the poorest-quality rock mass, category 1, which was considered in the calculation. The factor-of-safety with respect to Mohr-Coulomb shear failure is quite large (approximately 5) throughout the entire model (see Figure 6-66O). The displacement field shown in Figure 6-66Q is due to the excavation of the starter tunnel only. The magnitude of the displacements is very small, of the order of 0.002 m or less. It appears from the results of the numerical modeling that the North Portal and the starter tunnel would be stable for the considered mechanical properties of the rock mass even if no ground support was used.

#### **6.5.3.1.6 Interburden Pillar between Shaft Access and Exhaust Mains**

The results of the interburden pillar stability analysis are shown in Figures 6-66R through 6-66Y. The results are for the final stage of the excavation. The maximum vertical displacement in the exhaust mains (crown and floor) is approximately 3.0 cm. In the access drift, the maximum vertical displacement of 4.3 cm (Figures 6-66R and 6-66S) occurs in the crown of drift.

The excavation of drifts causes maximum stress concentrations of approximately 25 and 23 MPa (see Figures 6-66T and 6-66U) in the walls of the exhaust mains and access drift, respectively. However, safety factors with respect to the Mohr-Coulomb yield condition averaging 1 to 3 are shown for the rock immediately surrounding the drifts (shown in Figures 6-66V and 6-66W). In addition, a minor extent of the rock mass yielding is shown in Figures 6-66X and 6-66Y.

Therefore, the results indicate that deformation of the rock mass around the drifts and in the pillar between the drifts will be predominantly elastic.

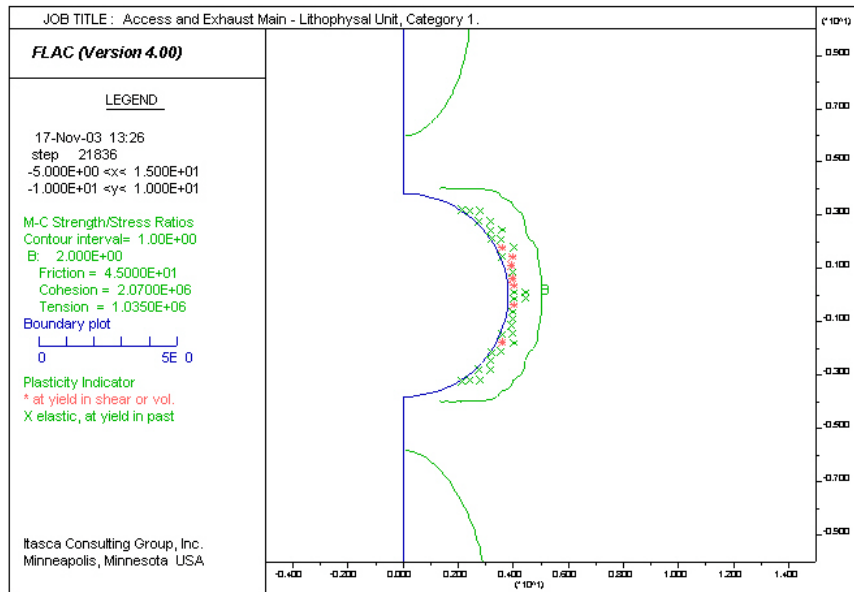


Figure 6-19. Contours of Safety Factor around Unsupported Access/Exhaust Main for Lith. Cat. 1 Rock

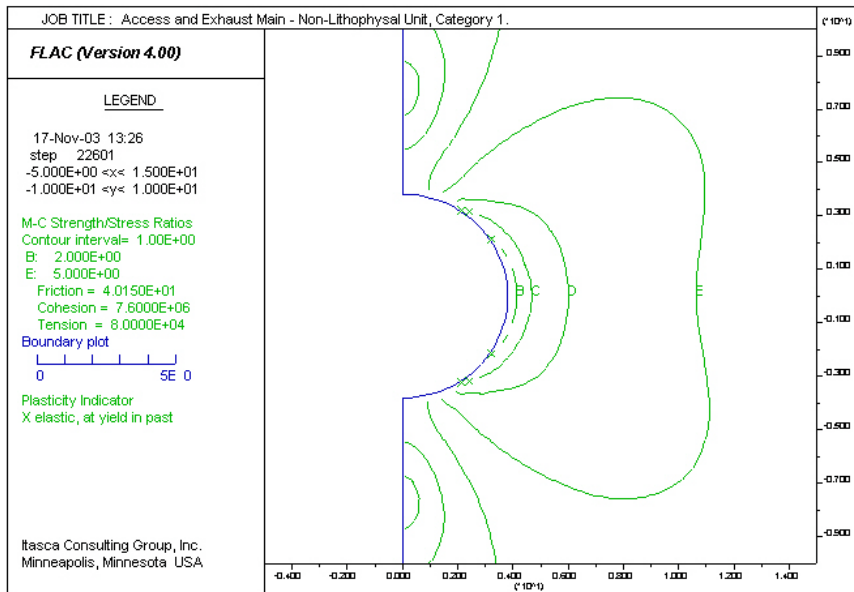


Figure 6-20. Contours of Safety Factor around Unsupported Access/Exhaust Main for N. Lith. Cat. 1 Rock

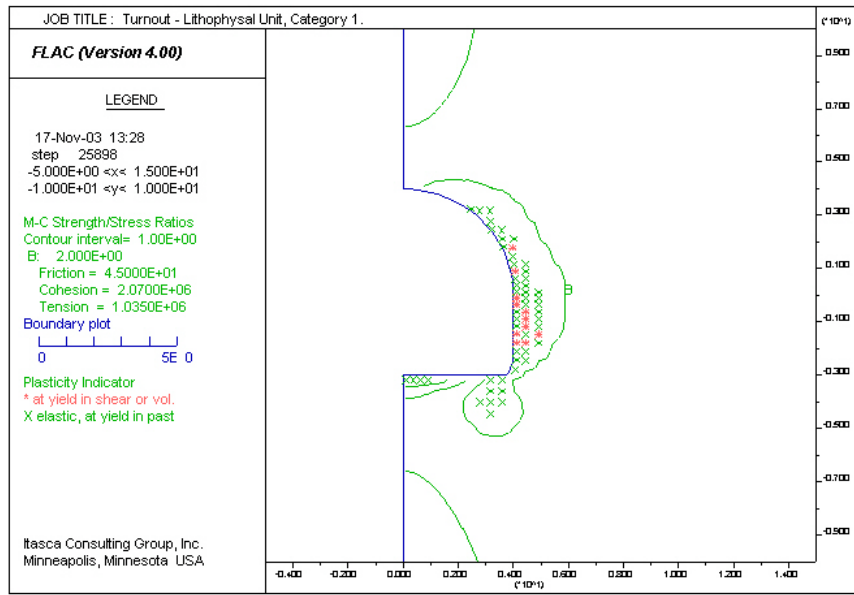


Figure 6-21. Contours of Safety Factor around Unsupported Turnout for Lith. Cat. 1 Rock

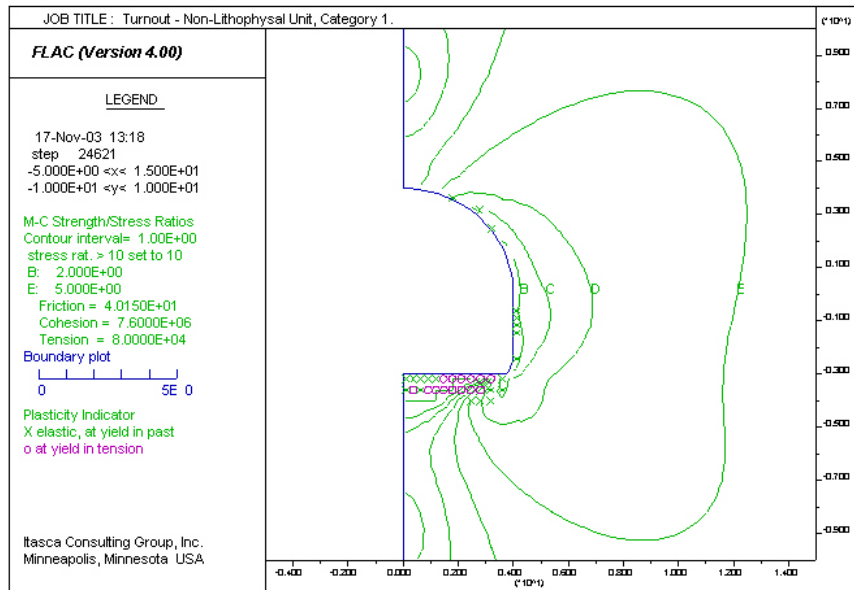


Figure 6-22. Contours of Safety Factor around Unsupported Turnout for N. Lith. Cat. 1 Rock

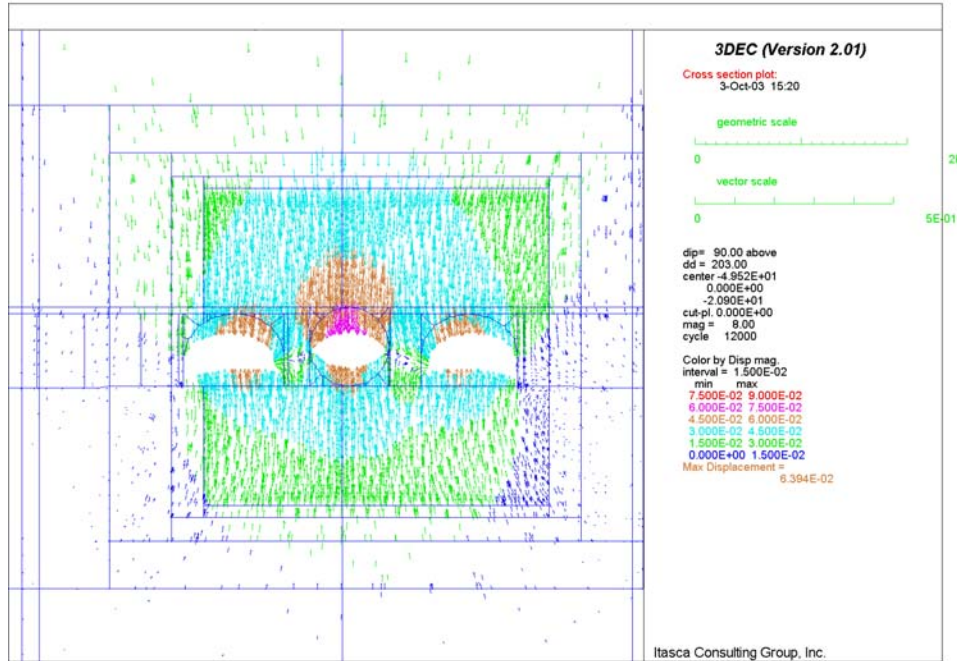


Figure 6-23. Intersection A: Displacement Field in Vertical Section 1 for Lith. Cat. 1 Rock

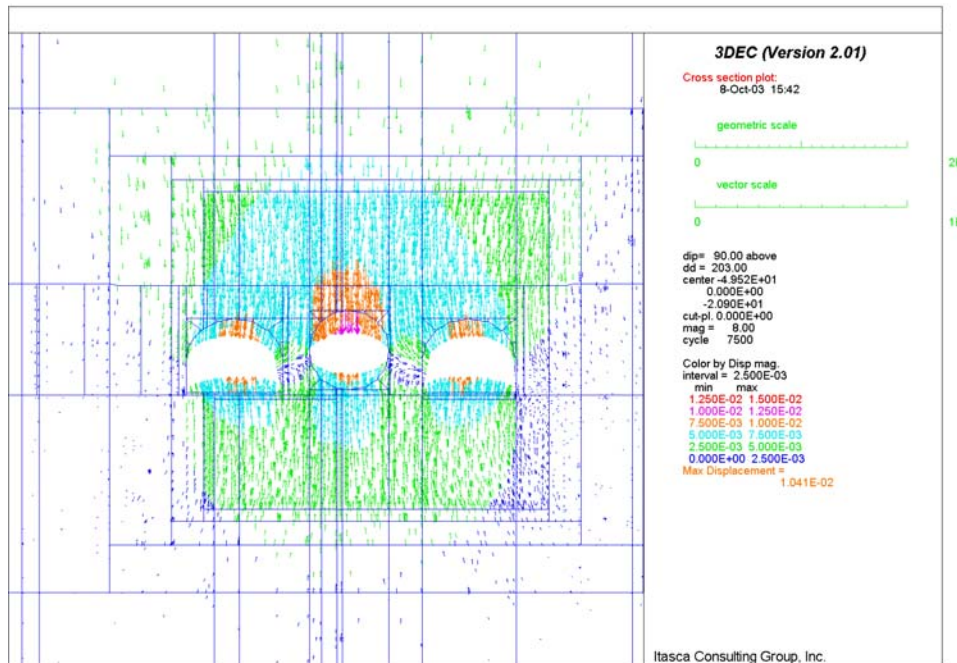


Figure 6-24. Intersection A: Displacement Field in Vertical Section 1 for N. Lith. Cat. 1 Rock

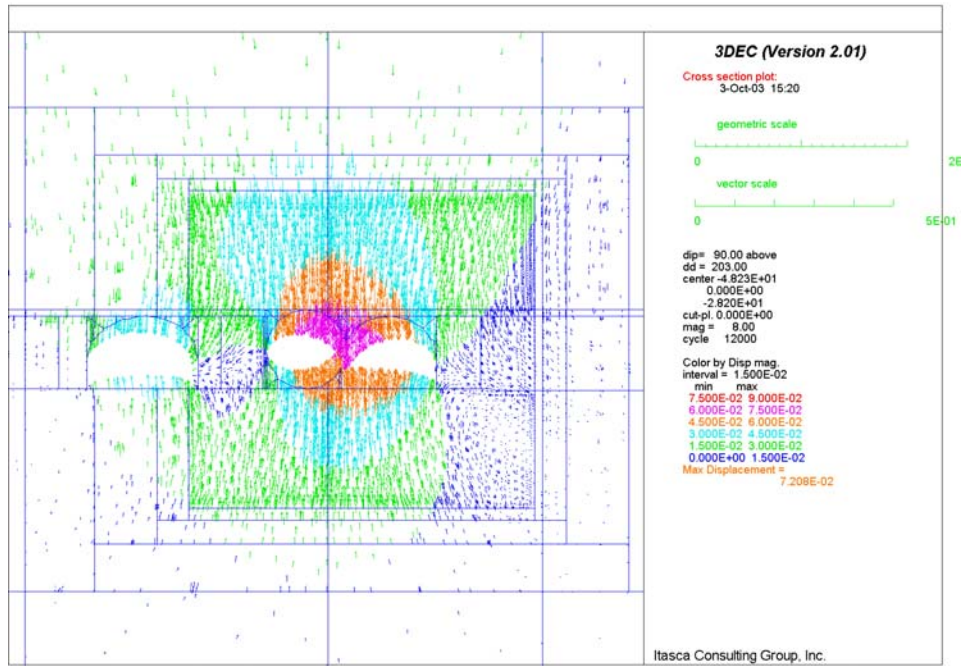


Figure 6-25. Intersection A: Displacement Field in Vertical Section 2 for Lith. Cat. 1 Rock

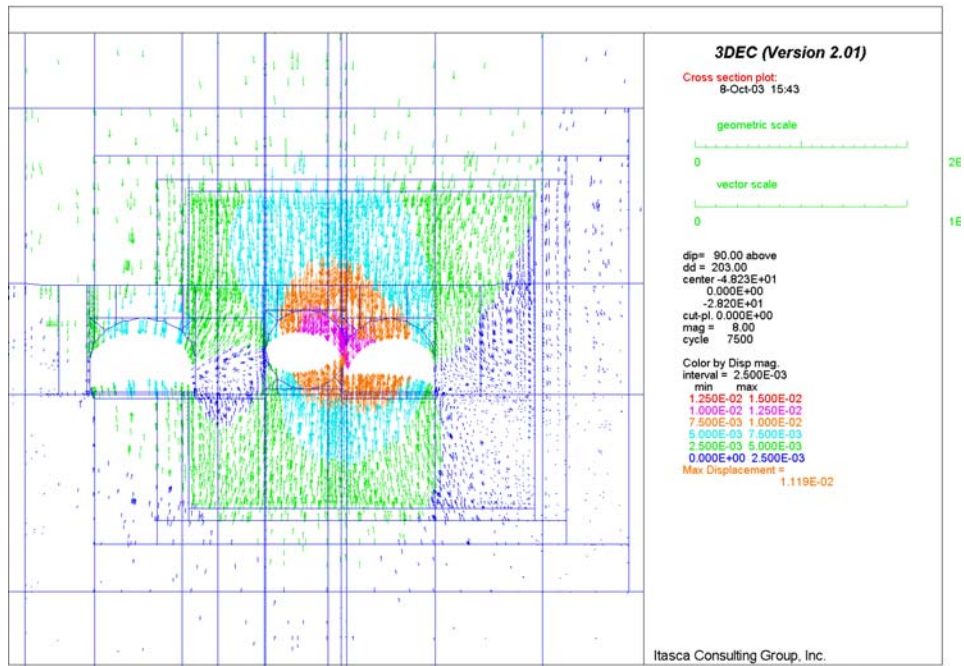


Figure 6-26. Intersection A: Displacement Field in Vertical Section 2 for N. Lith. Cat. 1 Rock

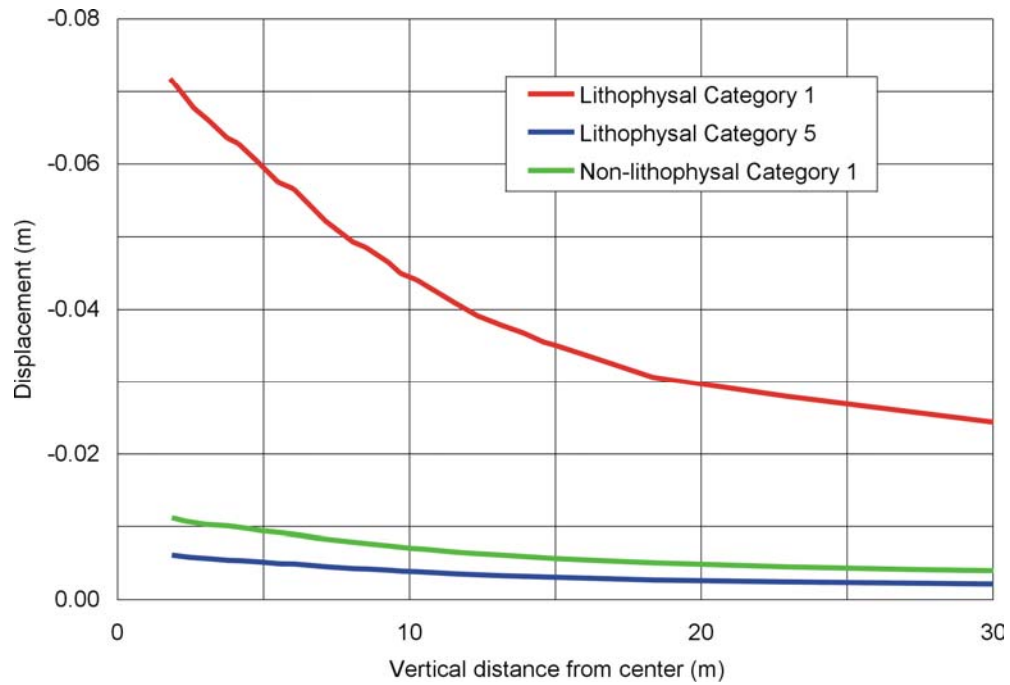


Figure 6-27. Intersection A: Vertical Displacement along Vertical Line through Point A

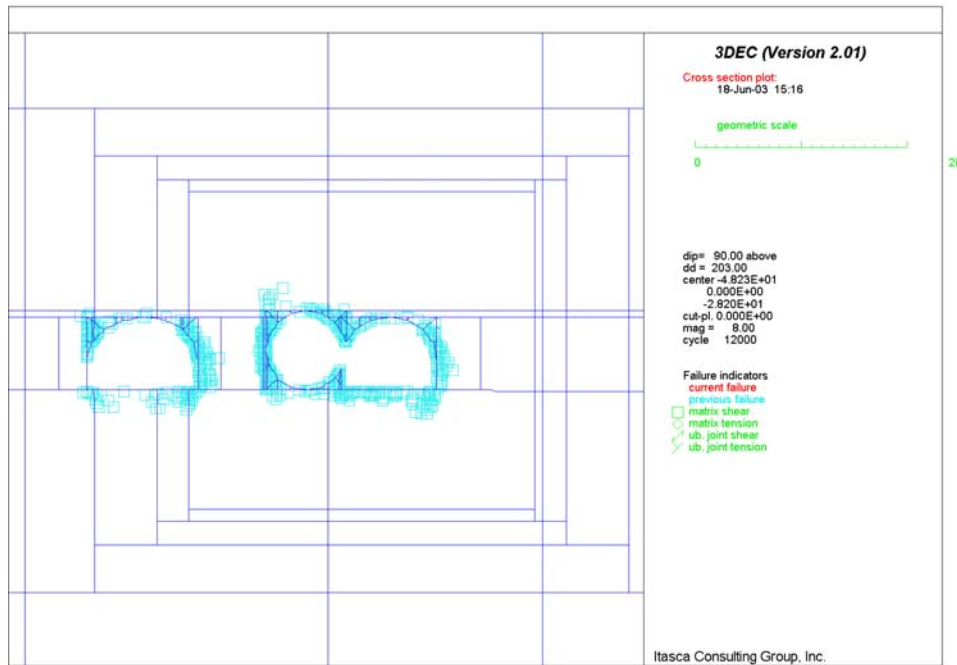


Figure 6-28. Intersection A: Potential Yield Zone in Vertical Section 2 for Lith. Cat. 1 Rock

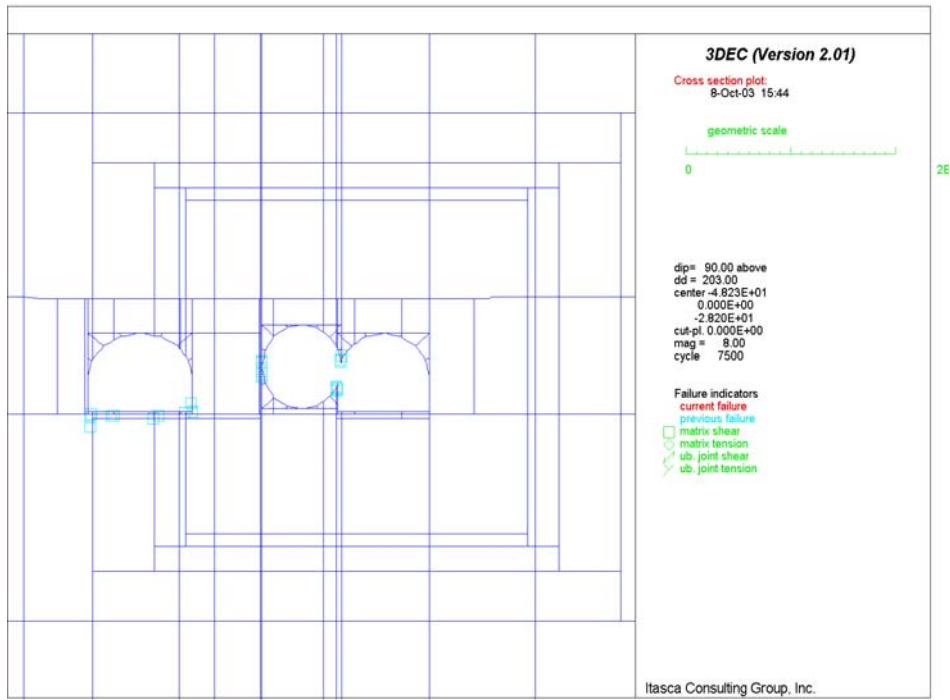


Figure 6-29. Intersection A: Potential Yield Zone in Vertical Section 2 for N. Lith. Cat. 1 Rock

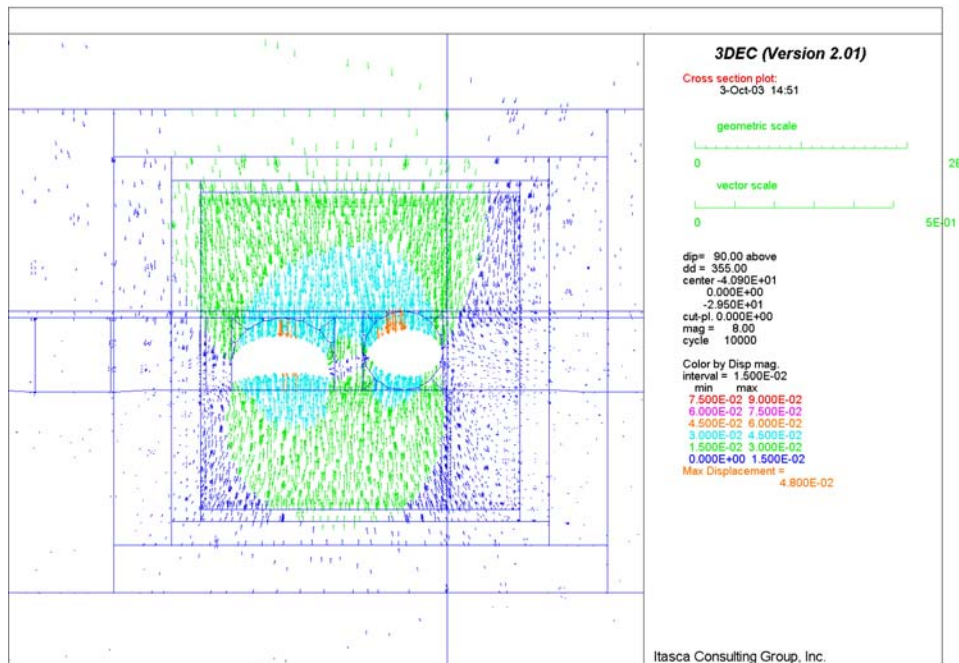


Figure 6-30. Intersection C: Displacement Field in Vertical Section 1 for Lith. Cat. 1 Rock

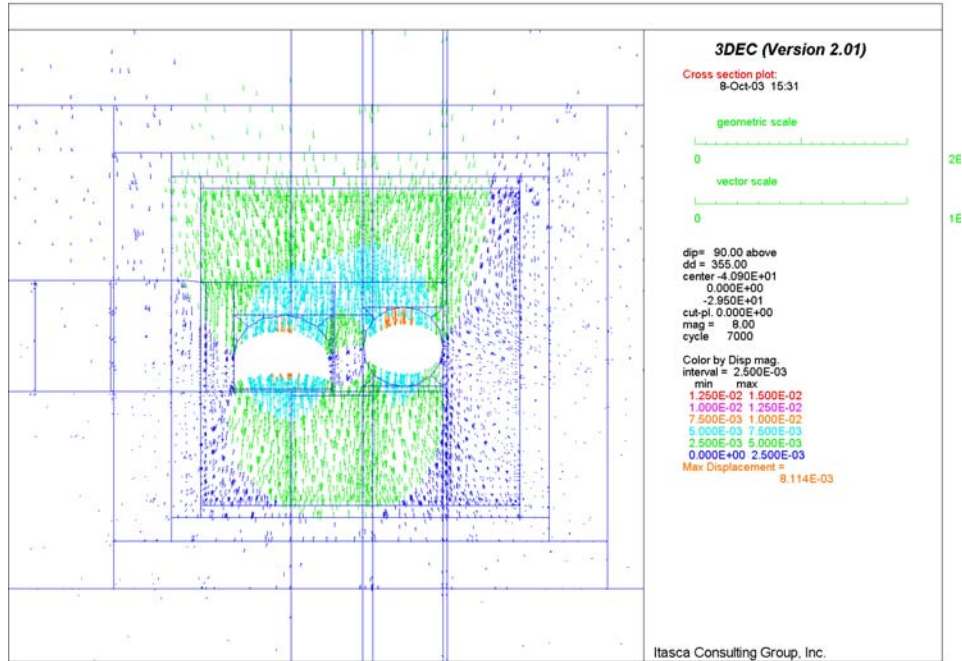


Figure 6-31. Intersection C: Displacement Field in Vertical Section 1 for N. Lith. Cat. 1 Rock

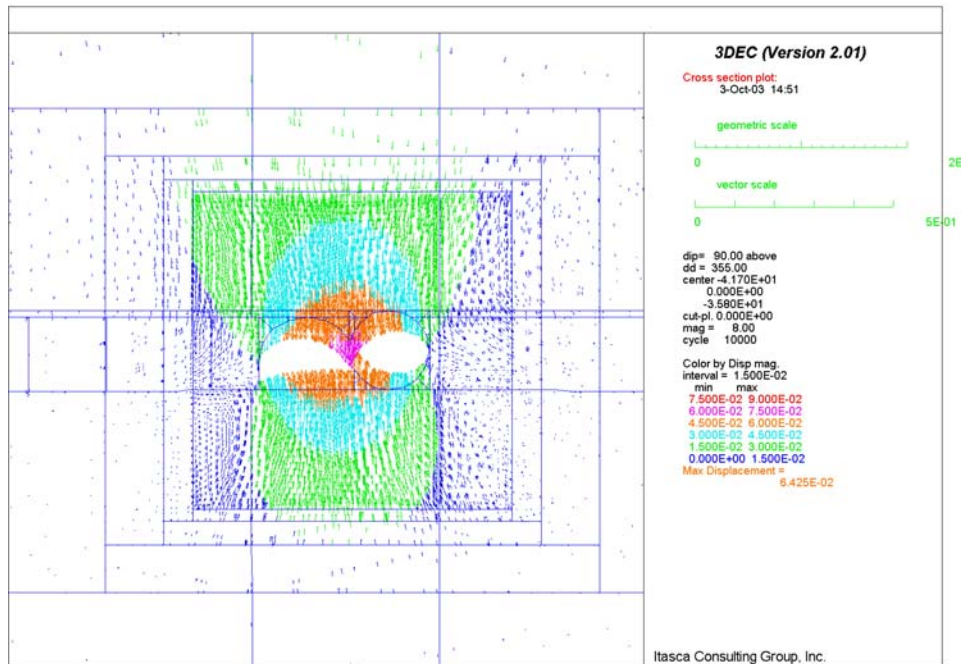


Figure 6-32. Intersection C: Displacement Field in Vertical Section 2 for Lith. Cat. 1 Rock

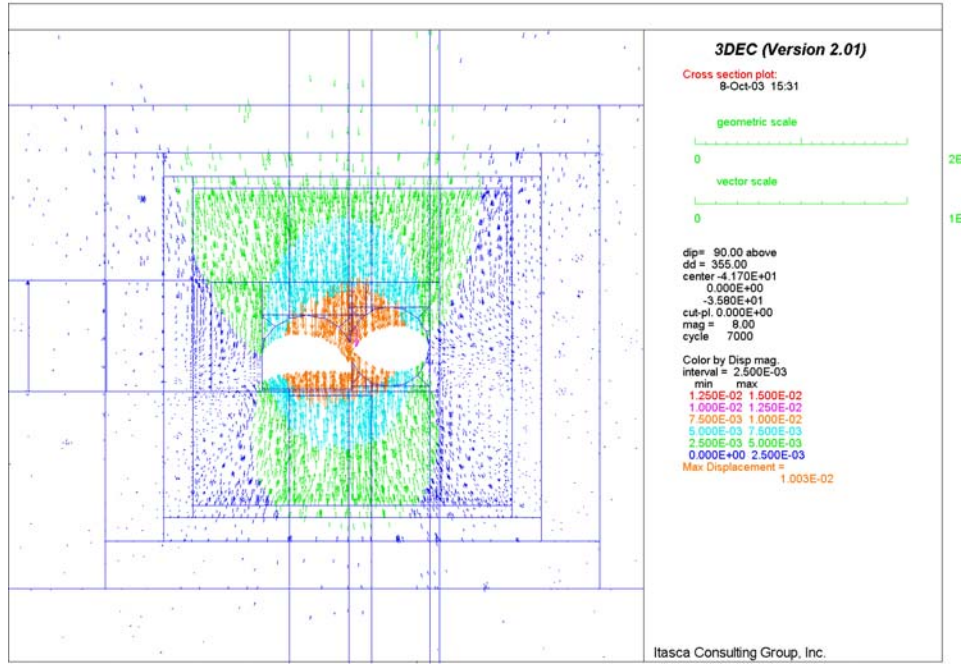


Figure 6-33. Intersection C: Displacement Field in Vertical Section 2 for N. Lith. Cat. 1 Rock

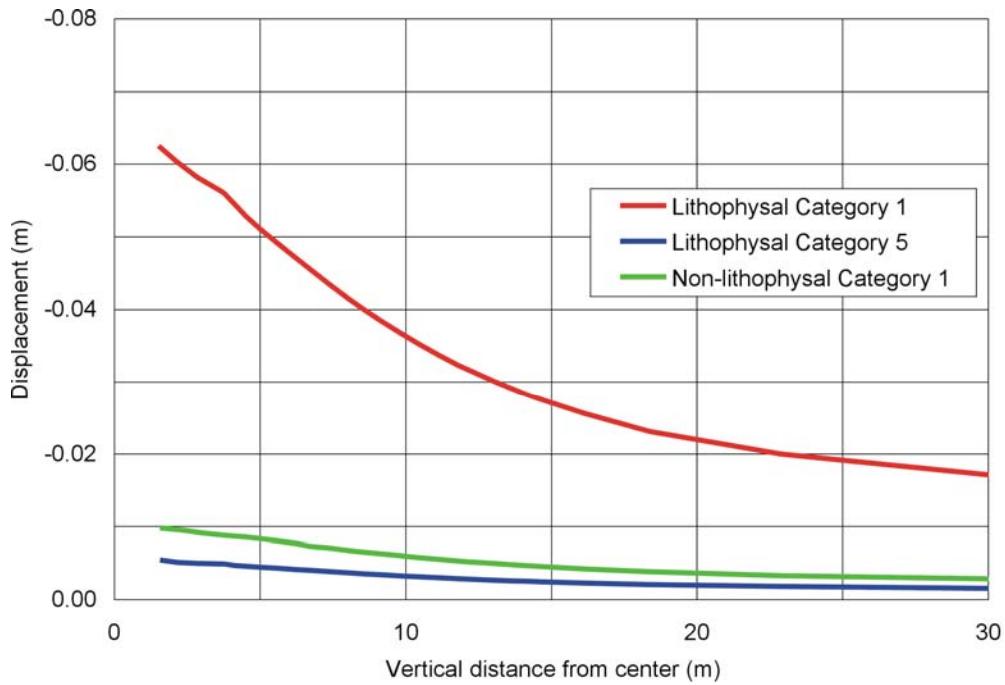


Figure 6-34. Intersection C: Vertical Displacement along Vertical Line through Point A

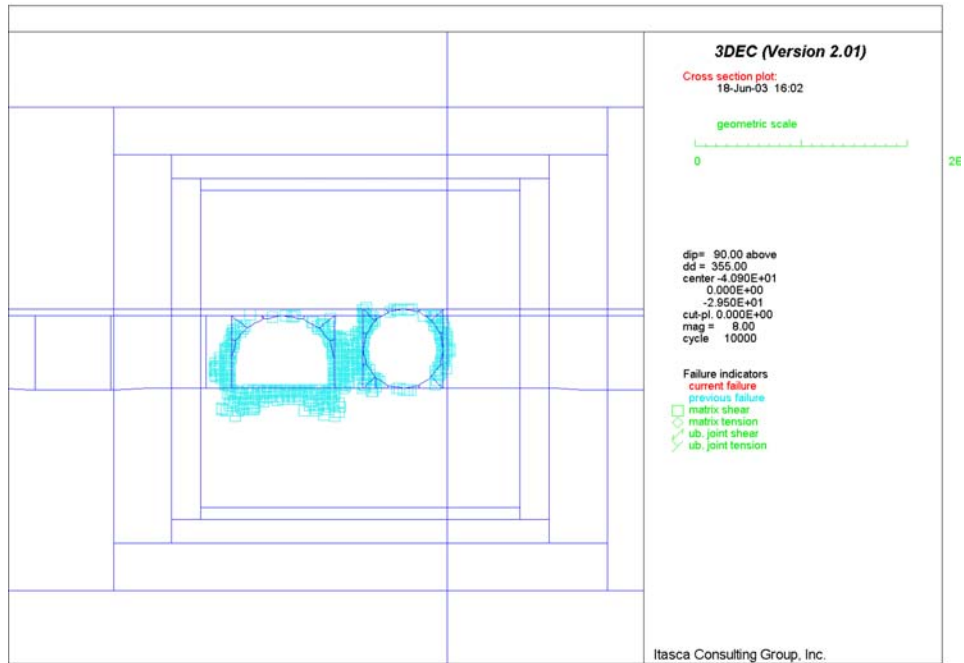


Figure 6-35. Intersection C: Potential Yield Zone in Vertical Section 1 for Lith. Cat. 1 Rock

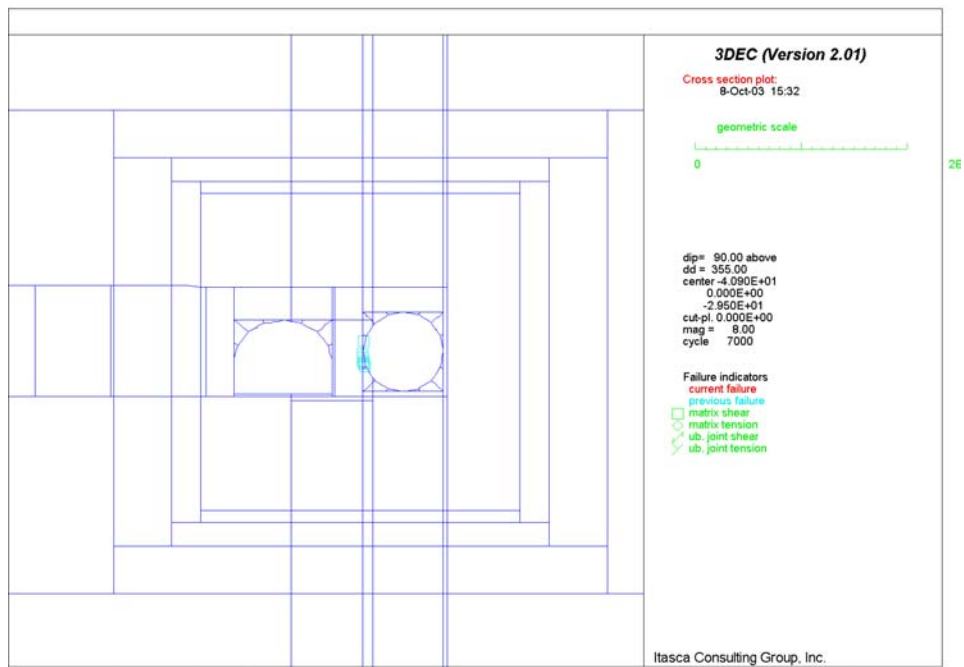
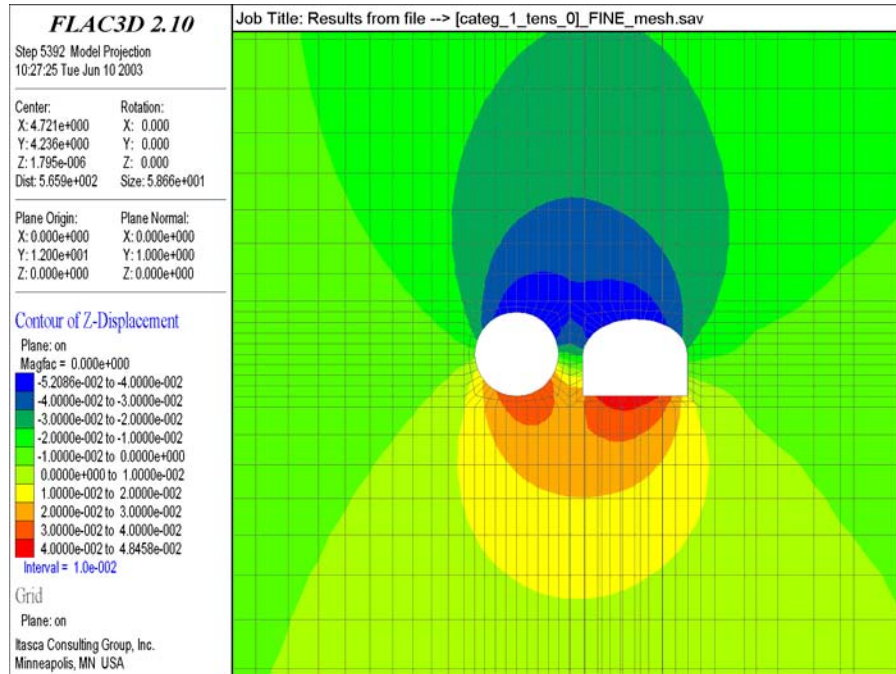
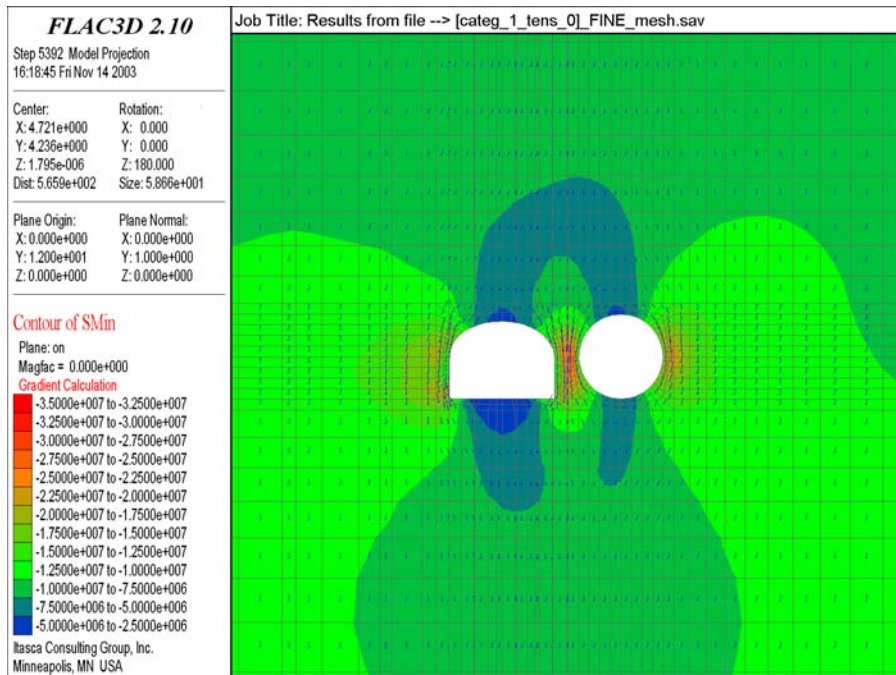


Figure 6-36. Intersection C: Potential Yield Zone in Vertical Section 1 for N. Lith. Cat. 1 Rock



(a) Vertical Displacements



(b) Stress Fields

Figure 6-37. Intersection C: Contours of Vertical Displacements and Stress Fields in Vertical Section 1 for Lith. Cat. 1 Rock Using FLAC3D

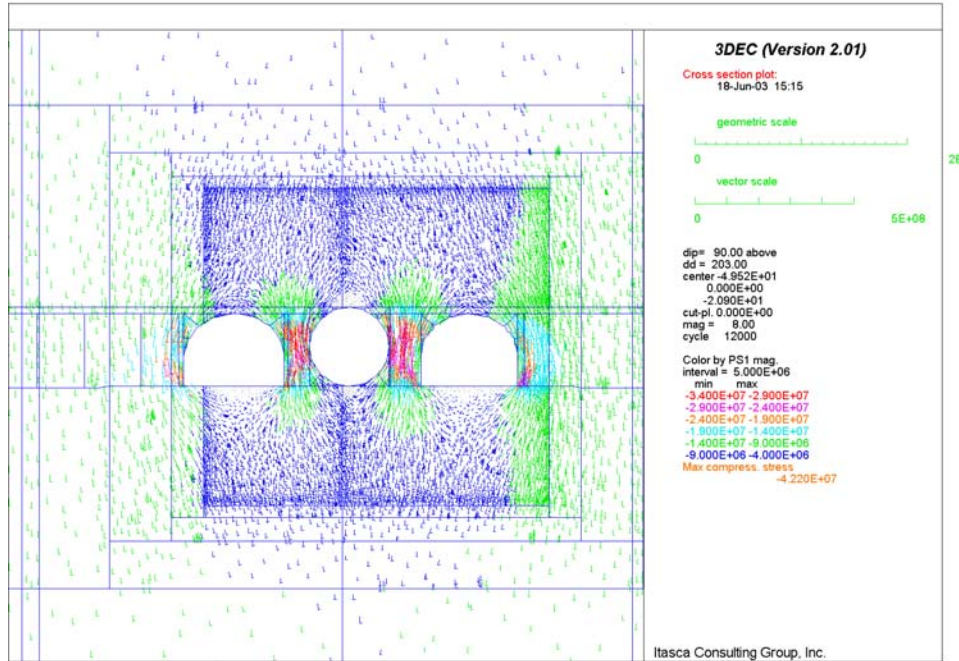


Figure 6-38. Intersection A: Stress Field in Vertical Section 1 for Lith. Cat. 1 Rock

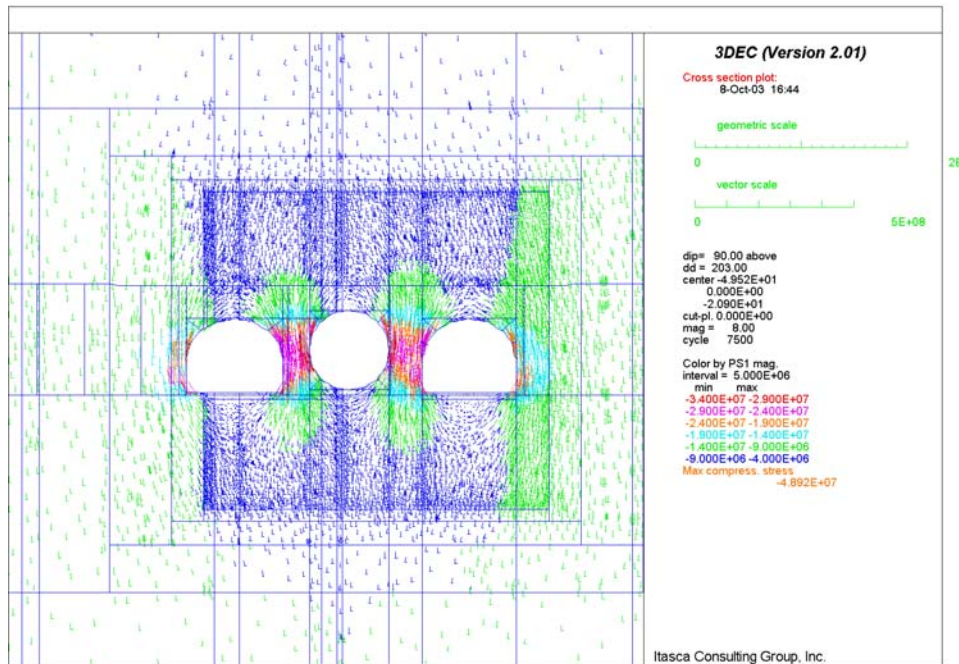


Figure 6-39. Intersection A: Stress Field in Vertical Section 1 for N. Lith. Cat. 1 Rock

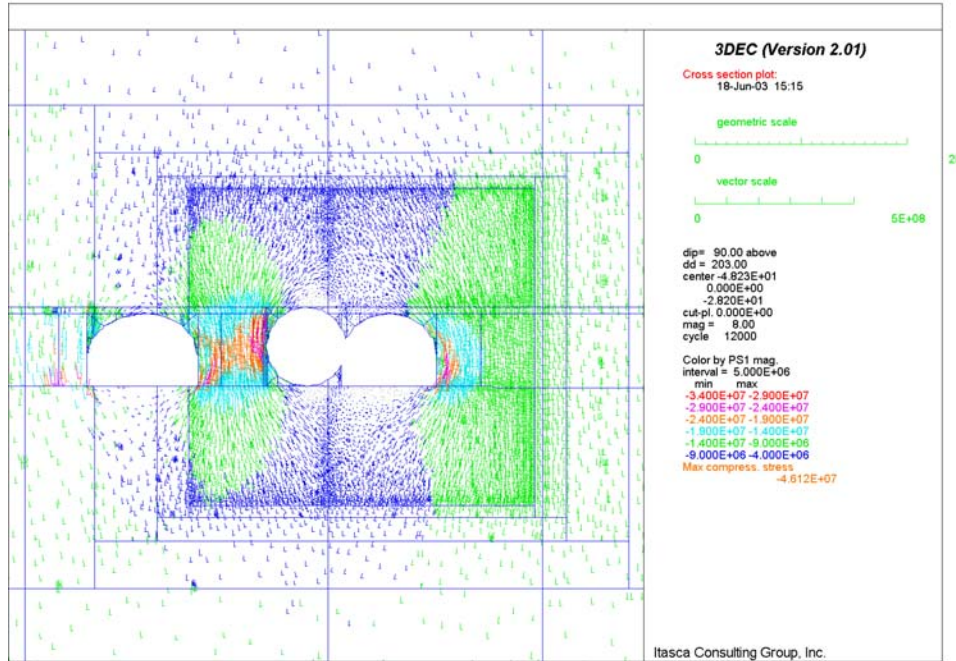


Figure 6-40. Intersection A: Stress Field in Vertical Section 2 for Lith. Cat. 1 Rock

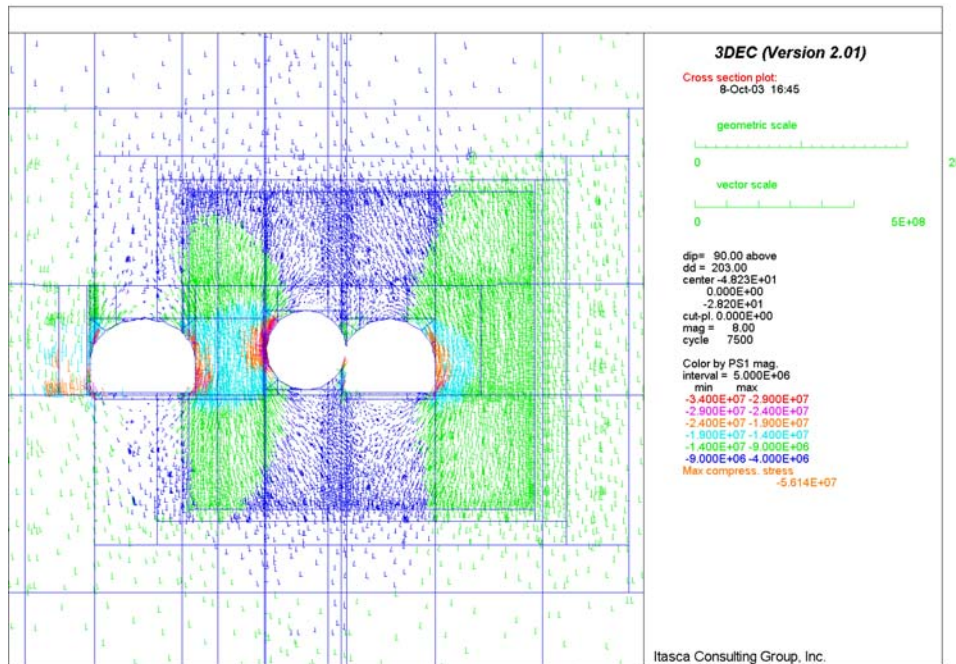


Figure 6-41. Intersection A: Stress Field in Vertical Section 2 for N. Lith. Cat. 1 Rock

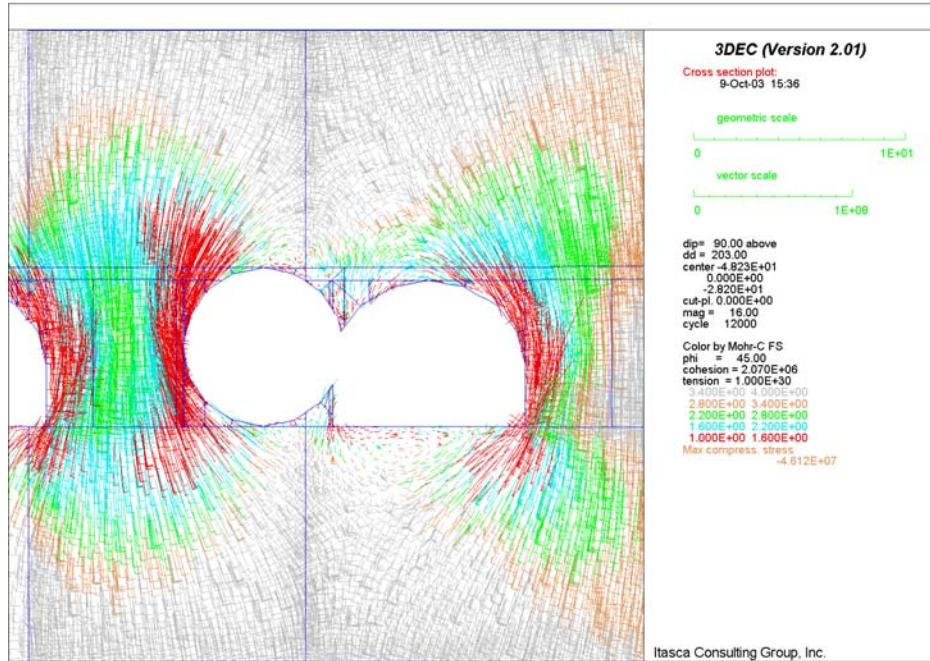


Figure 6-42. Intersection A: Factor of Safety in Vertical Section 2 for Lith. Cat. 1 Rock

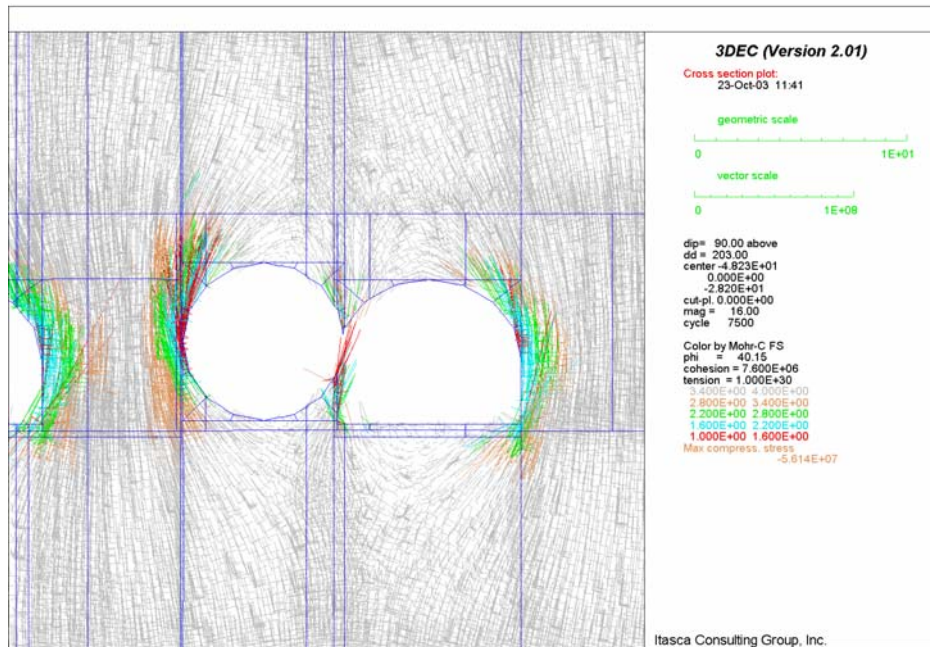


Figure 6-43. Intersection A: Factor of Safety in Vertical Section 2 for N. Lith. Cat. 1 Rock

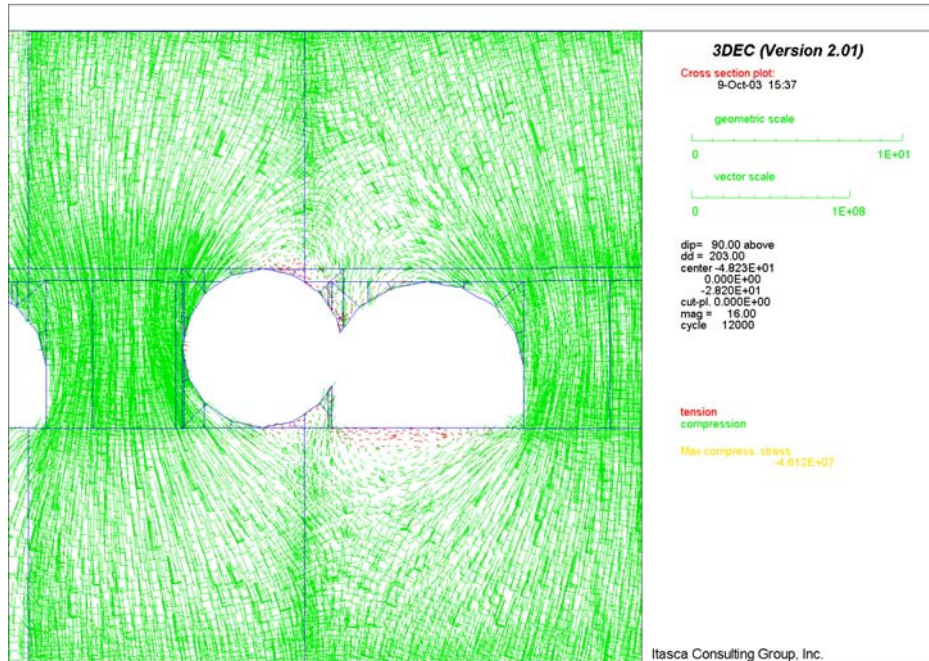


Figure 6-44. Intersection A: Compressive and Tensile Stresses in Vertical Section 2 for Lith. Cat. 1 Rock

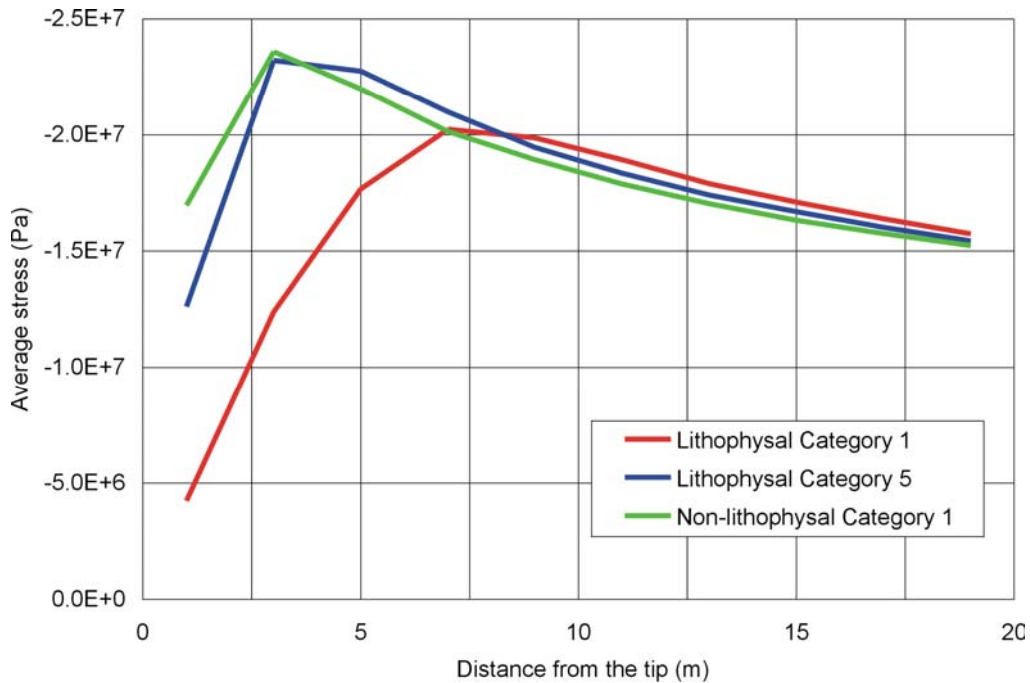


Figure 6-45. Intersection A: Average Pillar Stress vs. Distance from the Pillar Tip

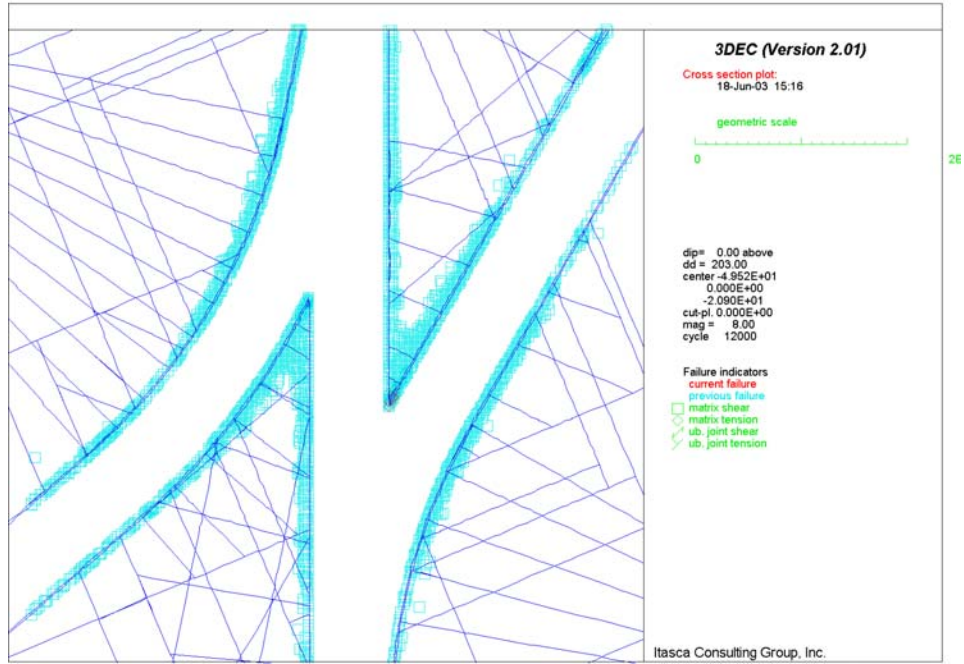


Figure 6-46. Intersection A: Potential Yield Zone in Horizontal Section for Lith. Cat. 1 Rock

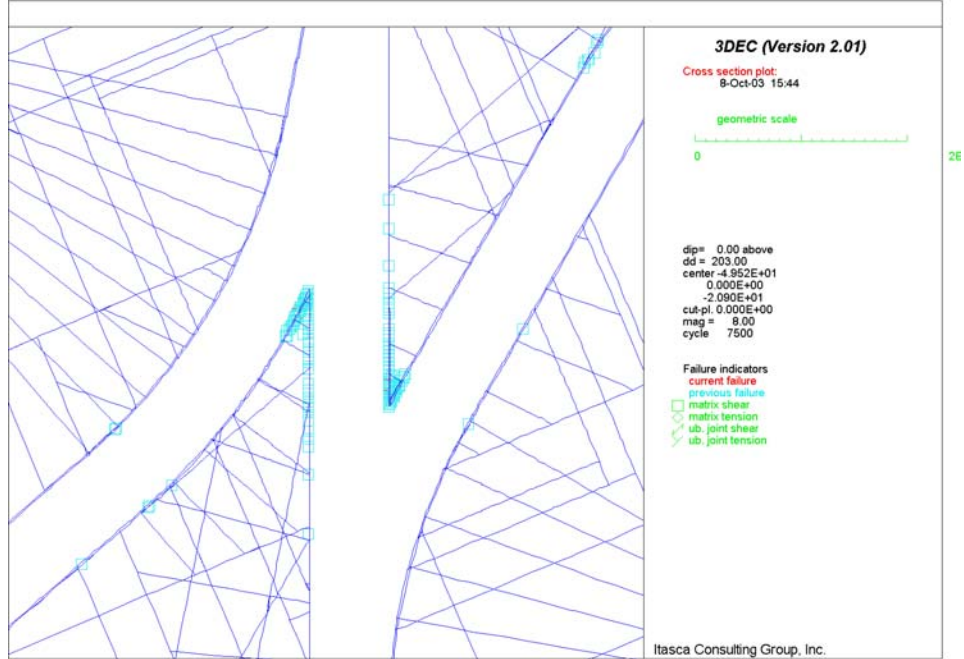


Figure 6-47. Intersection A: Potential Yield Zone in Horizontal Section for N. Lith. Cat. 1 Rock

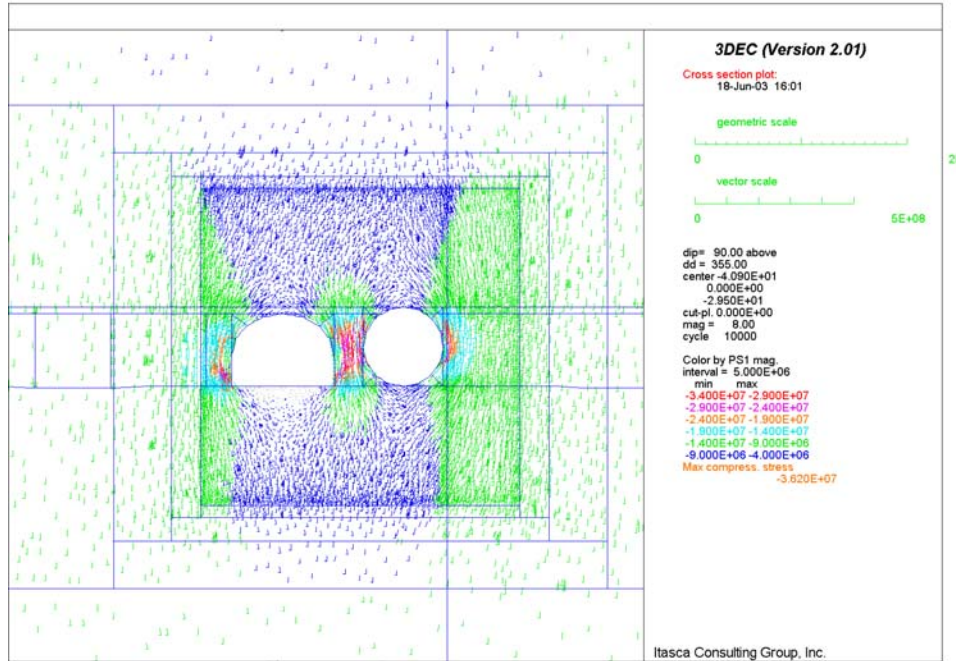


Figure 6-48. Intersection C: Stress Field in Vertical Section 1 for Lith. Cat. 1 Rock

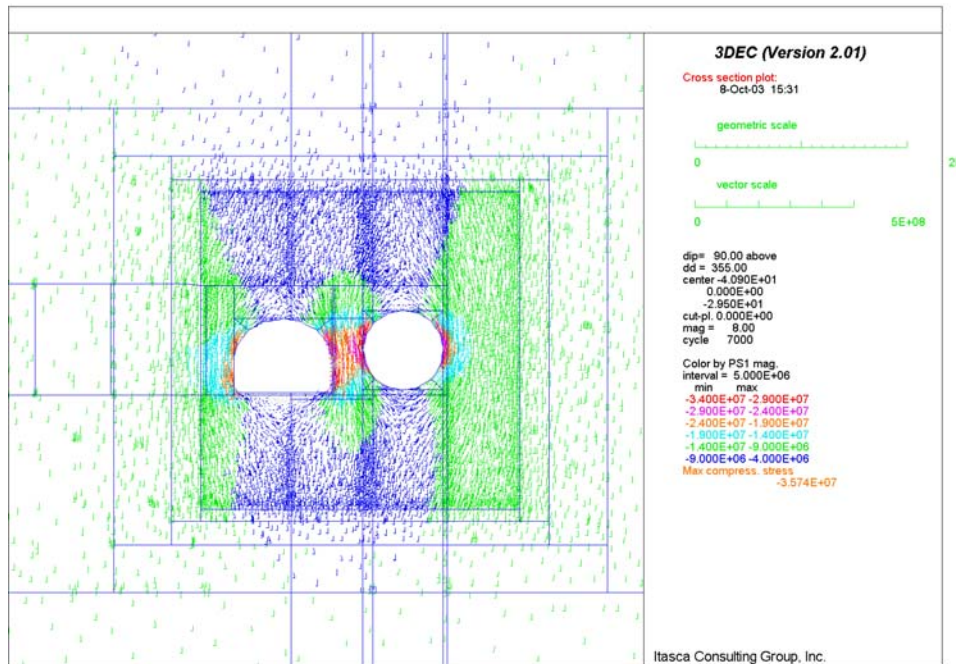


Figure 6-49. Intersection C: Stress Field in Vertical Section 1 for N. Lith. Cat. 1 Rock

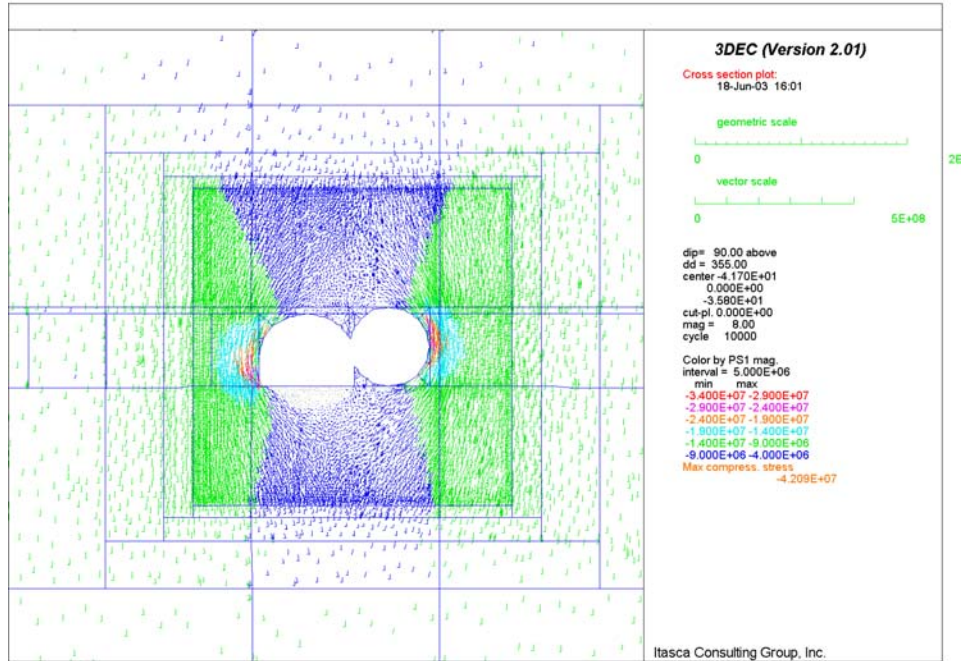


Figure 6-50. Intersection C: Stress Field in Vertical Section 2 for Lith. Cat. 1 Rock

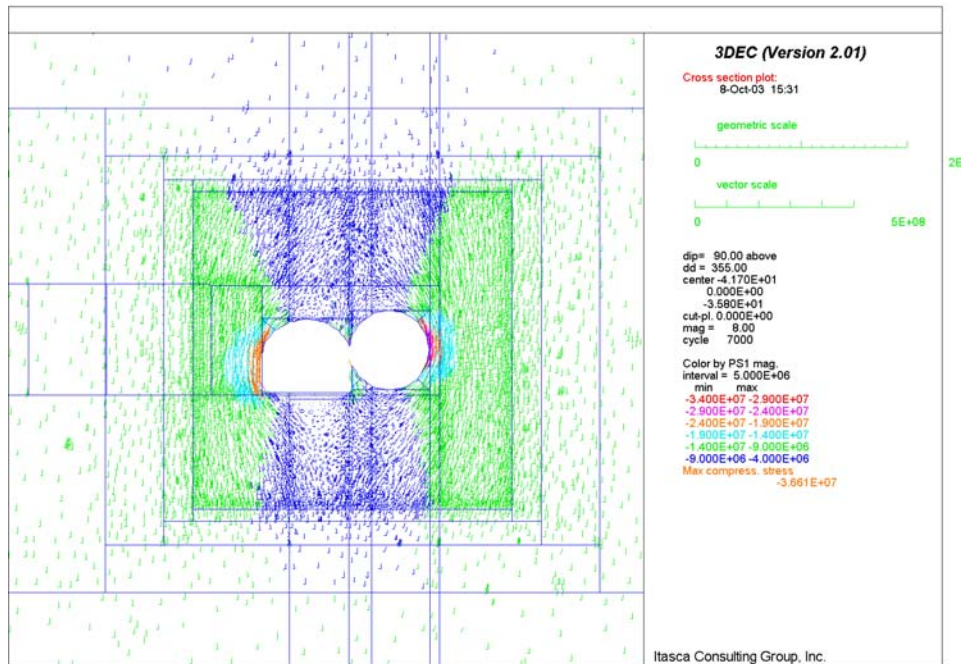


Figure 6-51. Intersection C: Stress Field in Vertical Section 2 for N. Lith. Cat. 1 Rock

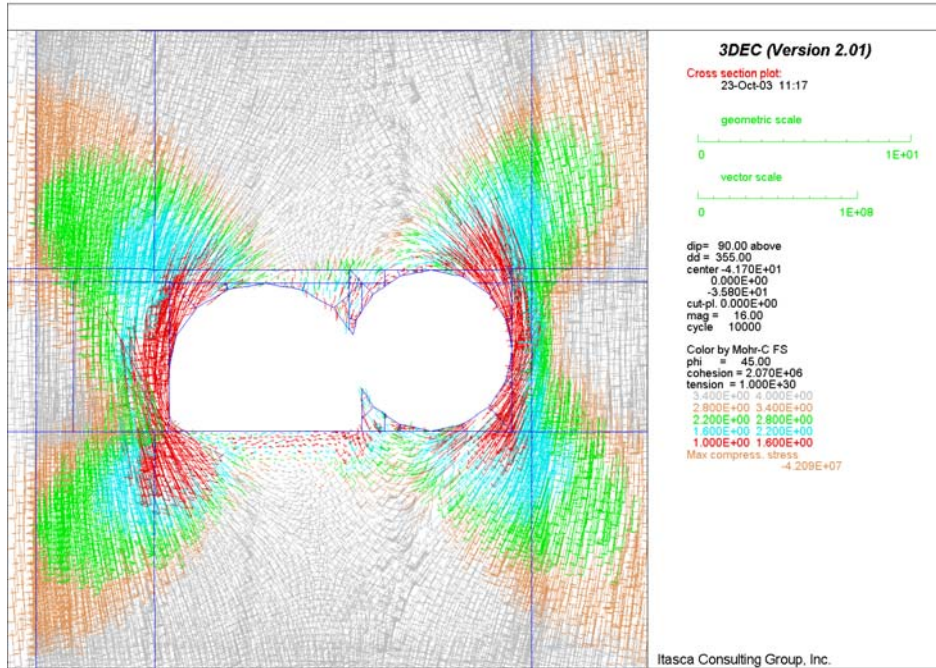


Figure 6-52. Intersection C: Factor of Safety in Vertical Section 2 for Lith. Cat. 1 Rock

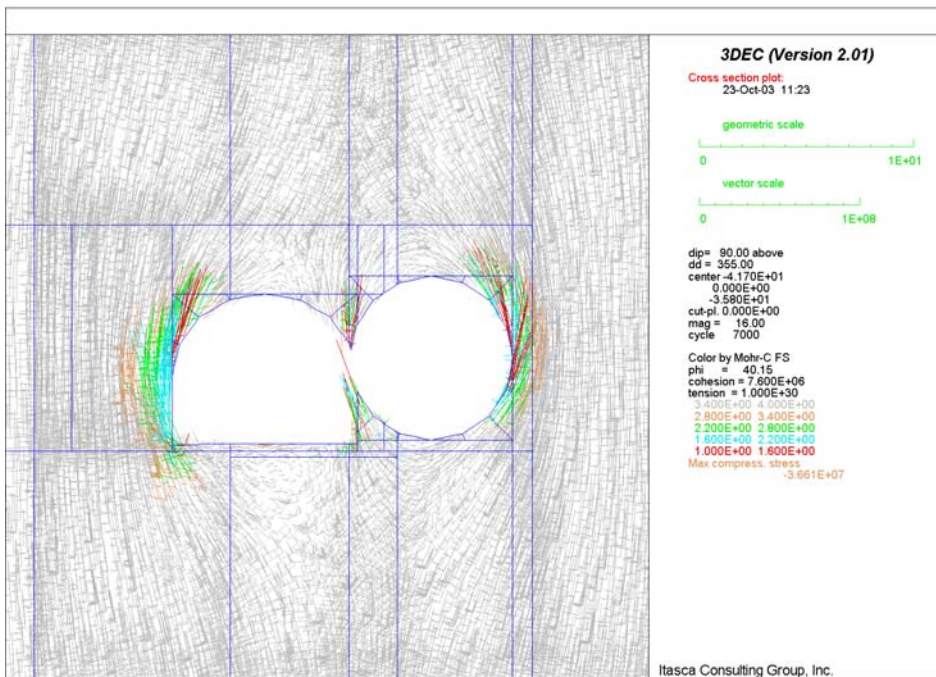


Figure 6-53. Intersection C: Factor of Safety in Vertical Section 2 for N. Lith. Cat. 1 Rock

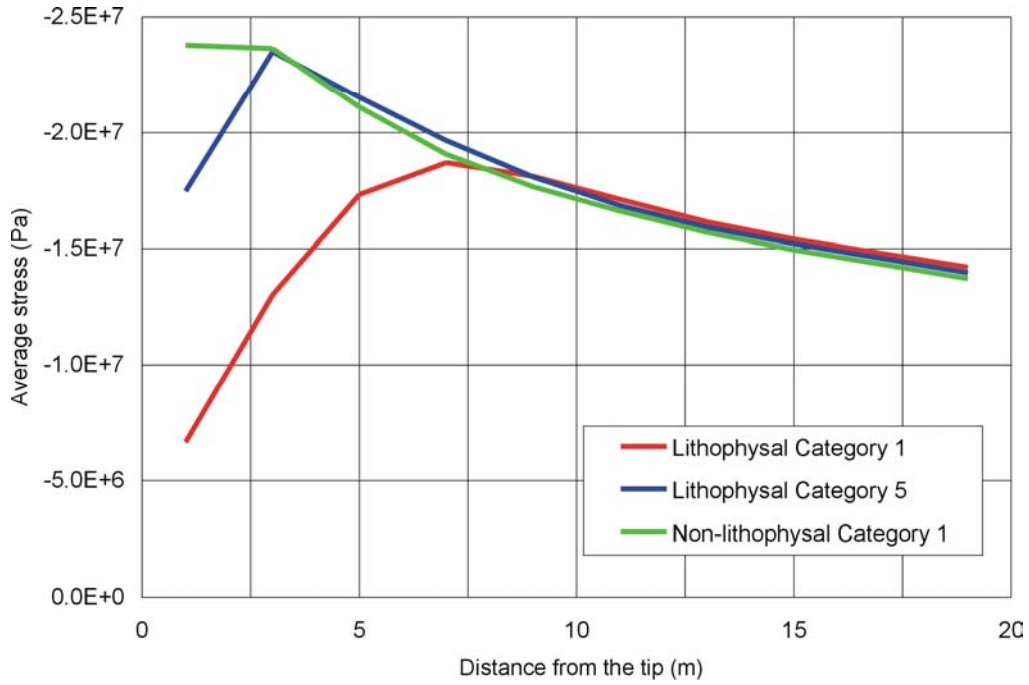


Figure 6-54. Intersection C: Average Pillar Stress vs. Distance from Pillar Tip

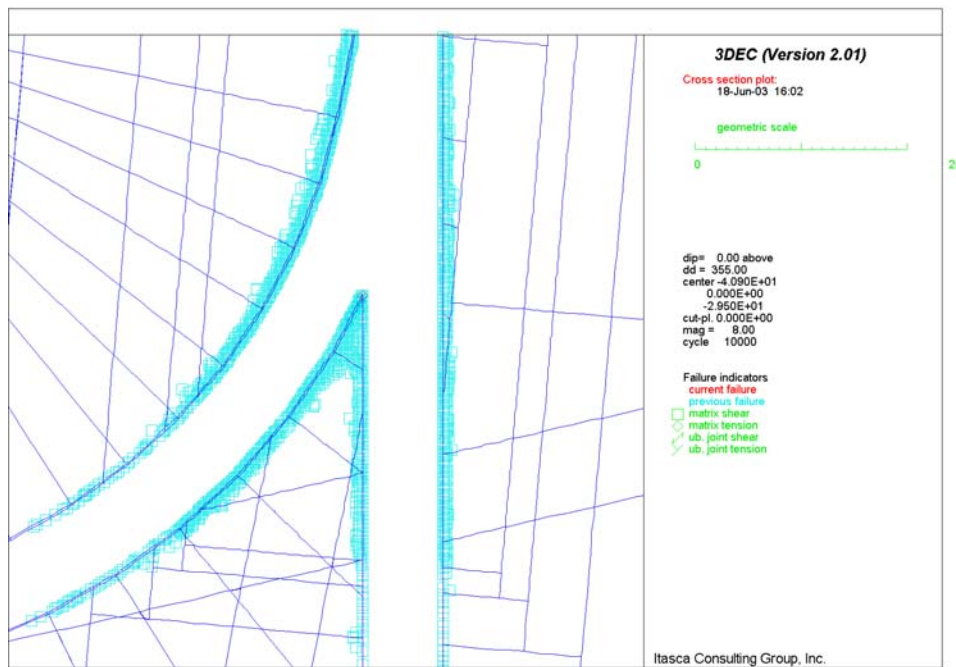


Figure 6-55. Intersection C: Potential Yield Zone in Horizontal Section for Lith. Cat. 1 Rock

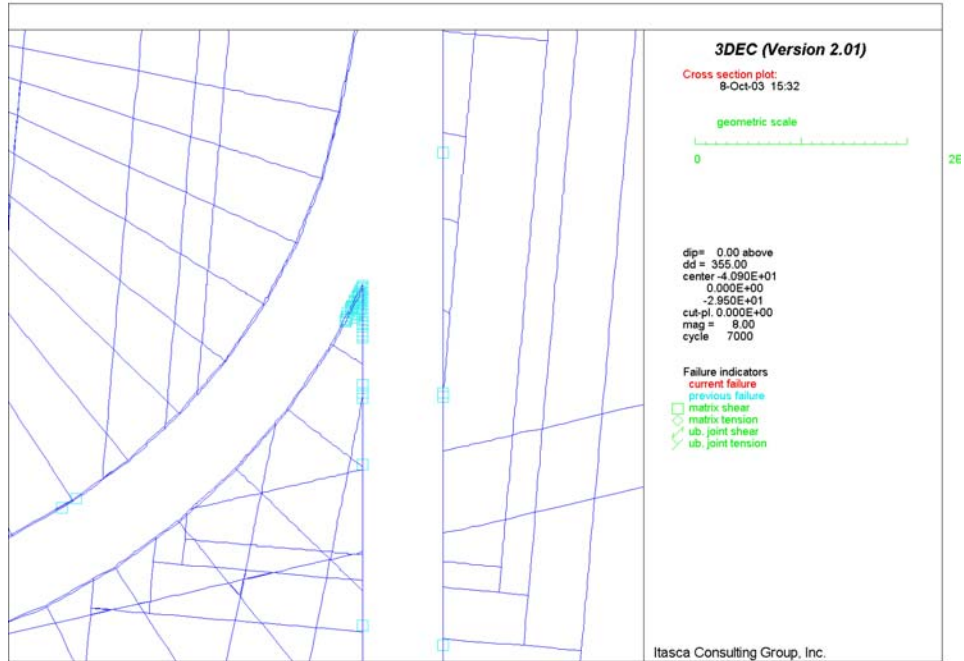


Figure 6-56. Intersection C: Potential Yield Zone in Horizontal Section for N. Lith. Cat. 1 Rock

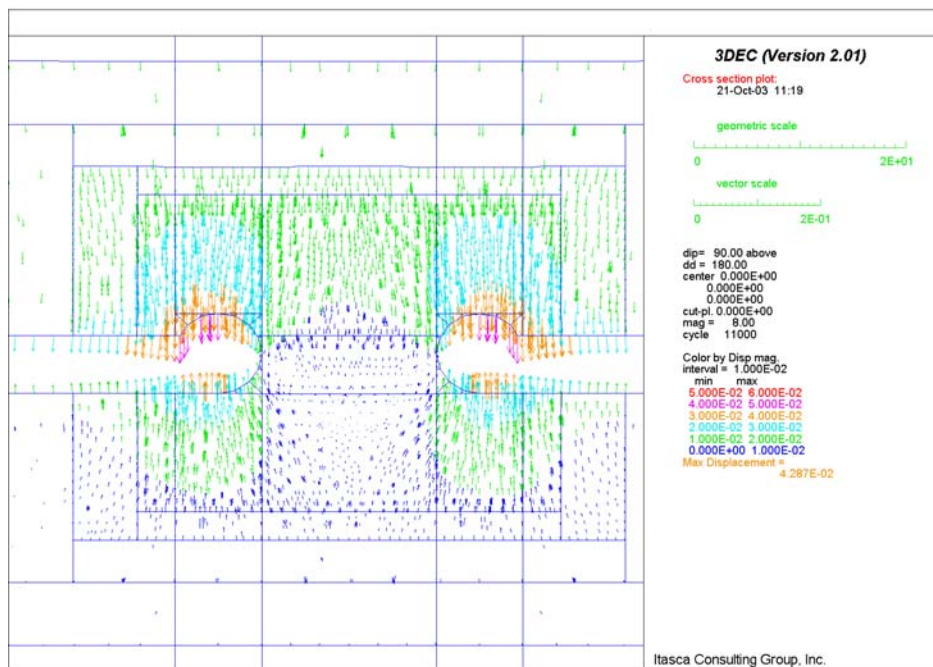


Figure 6-57. Intersection B: Displacement Field in Vertical Section 1 for Lith. Cat. 1 Rock

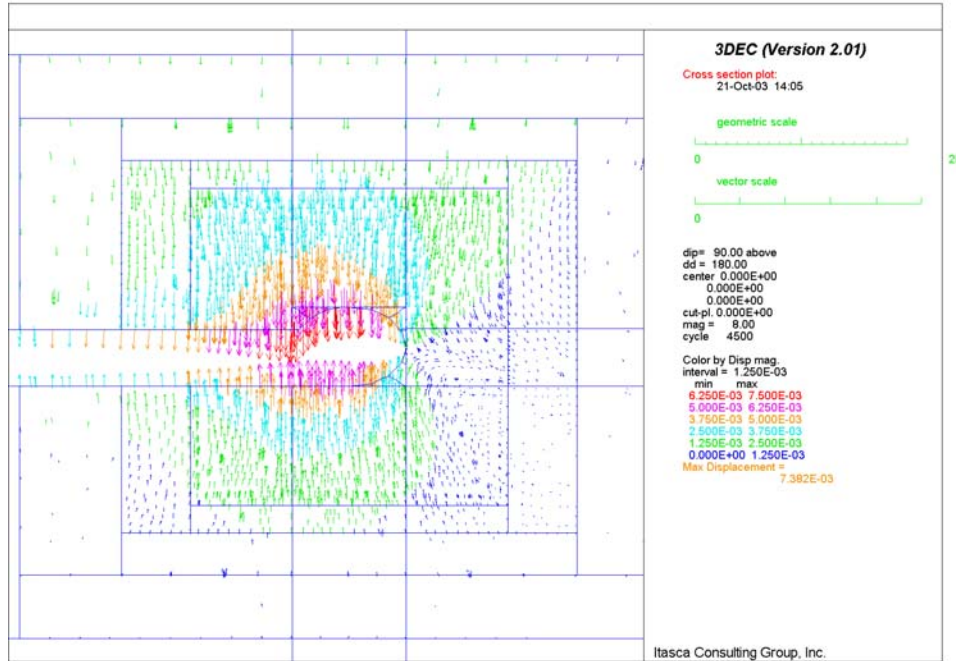


Figure 6-58. Intersection D: Displacement Field in Vertical Section 1 for N. Lith. Cat. 1 Rock

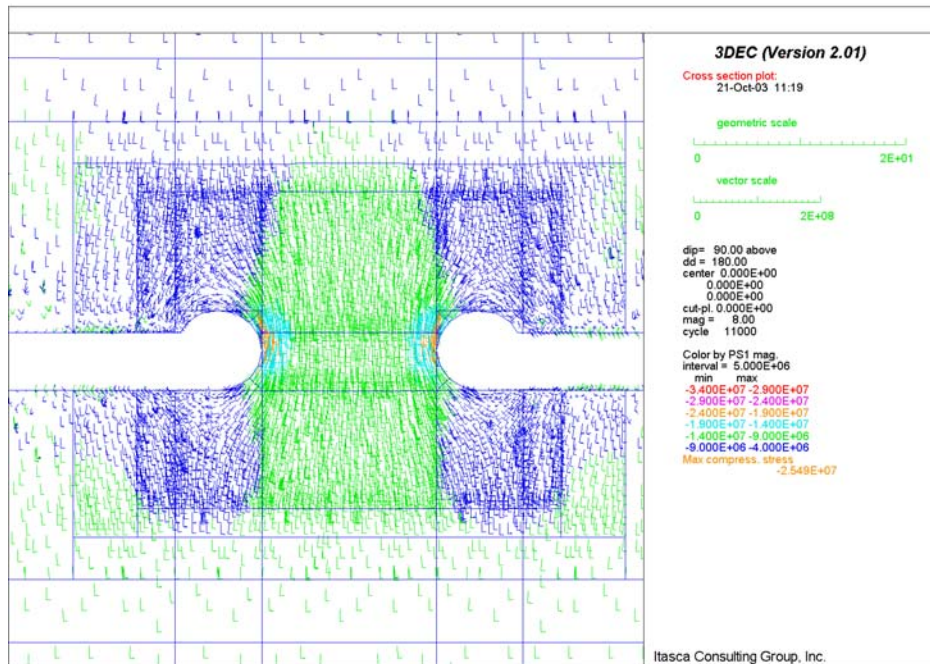


Figure 6-59. Intersection B: Stress Field in Vertical Section 1 for Lith. Cat. 1 Rock

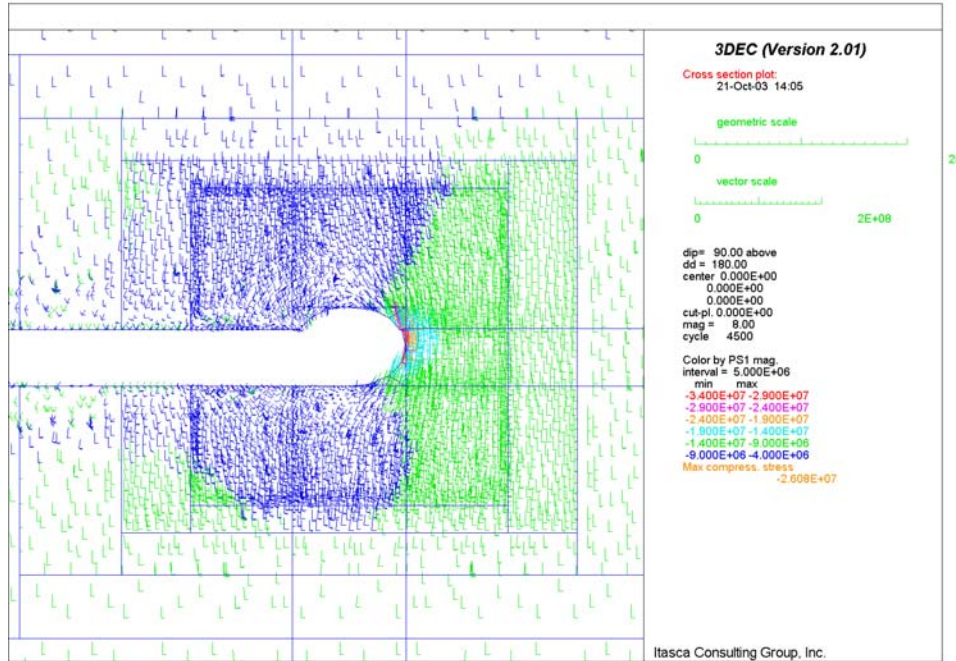


Figure 6-60. Intersection D: Stress Field in Vertical Section 1 for N. Lith. Cat. 1 Rock

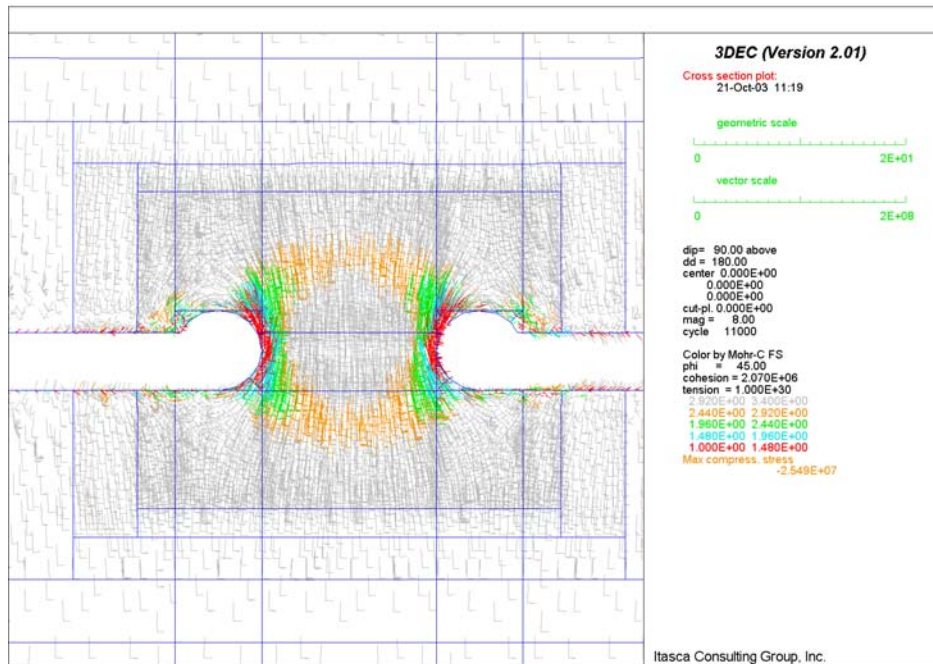


Figure 6-61. Intersection B: Factor of Safety in Vertical Section 1 for Lith. Cat. 1 Rock

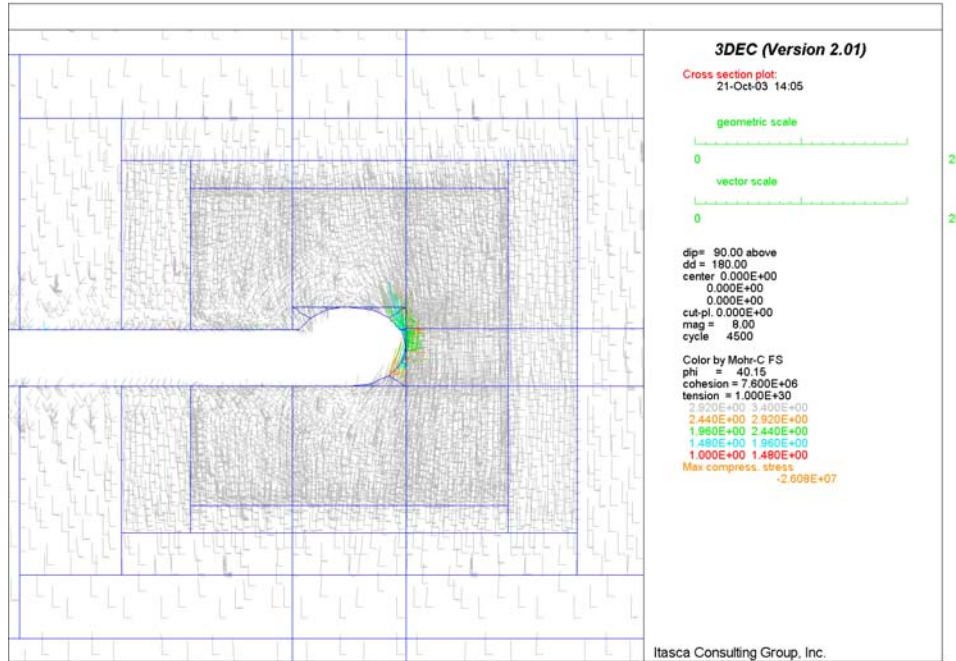


Figure 6-62. Intersection D: Factor of Safety in Vertical Section 1 for N. Lith. Cat. 1 Rock

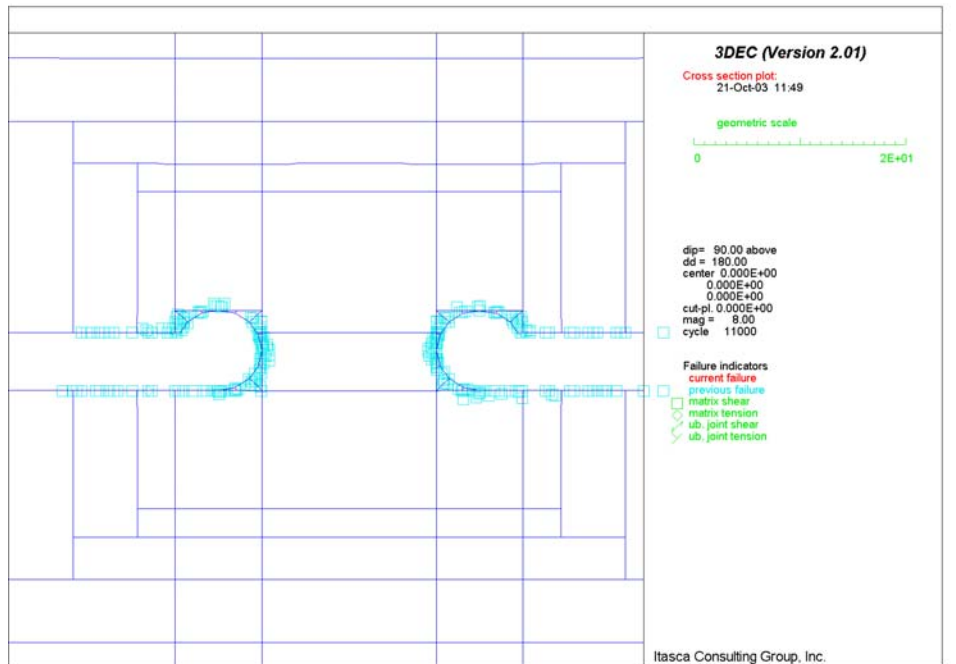


Figure 6-63. Intersection B: Potential Yield Zone in Vertical Section 1 for Lith. Cat. 1 Rock

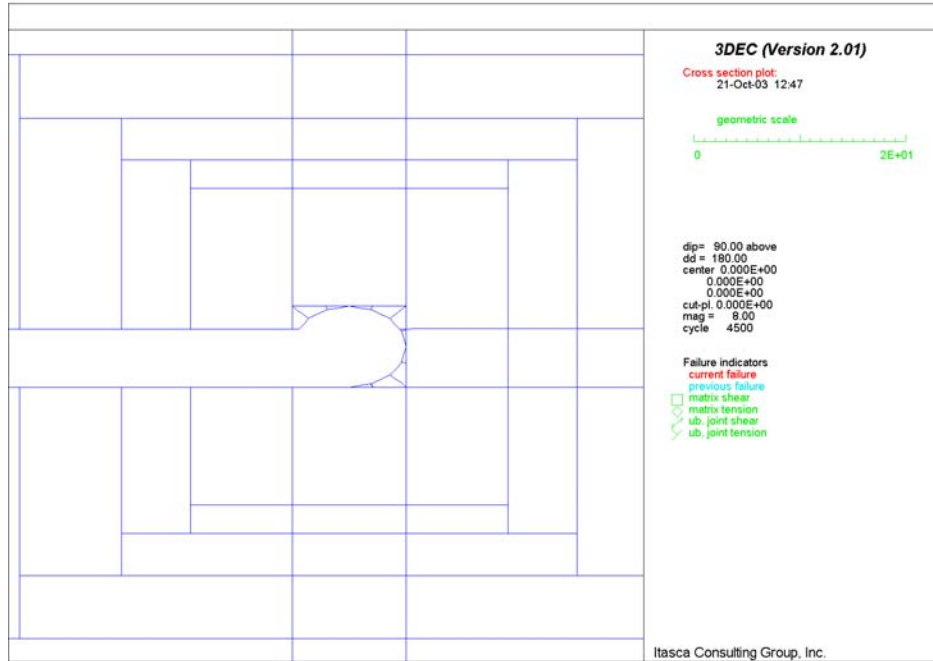


Figure 6-64. Intersection D: Potential Yield Zone in Vertical Section 1 for N. Lith. Cat. 1 Rock

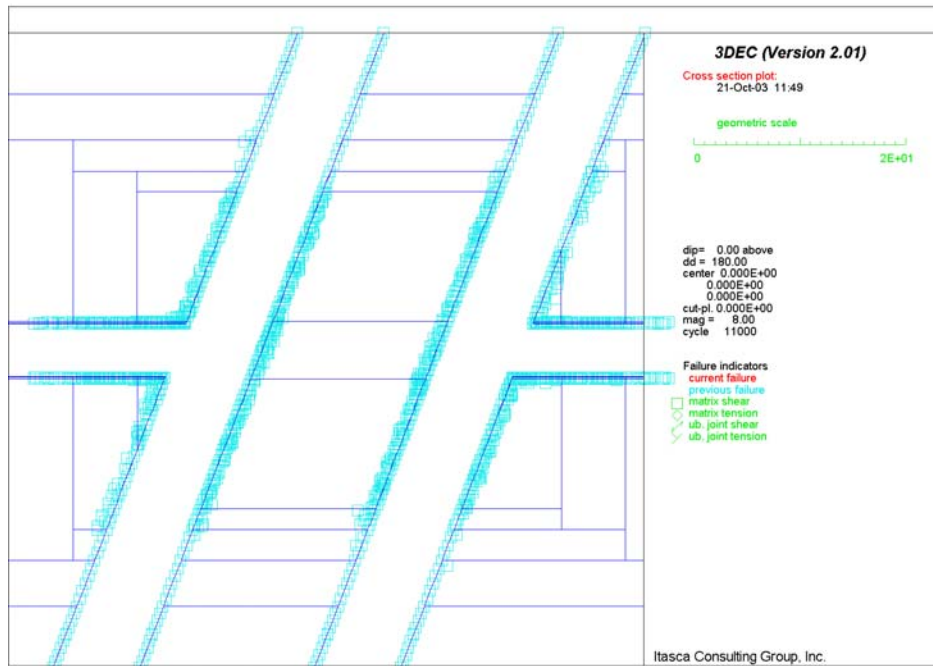


Figure 6-65. Intersection B: Potential Yield Zone in Horizontal Section for Lith. Cat. 1 Rock

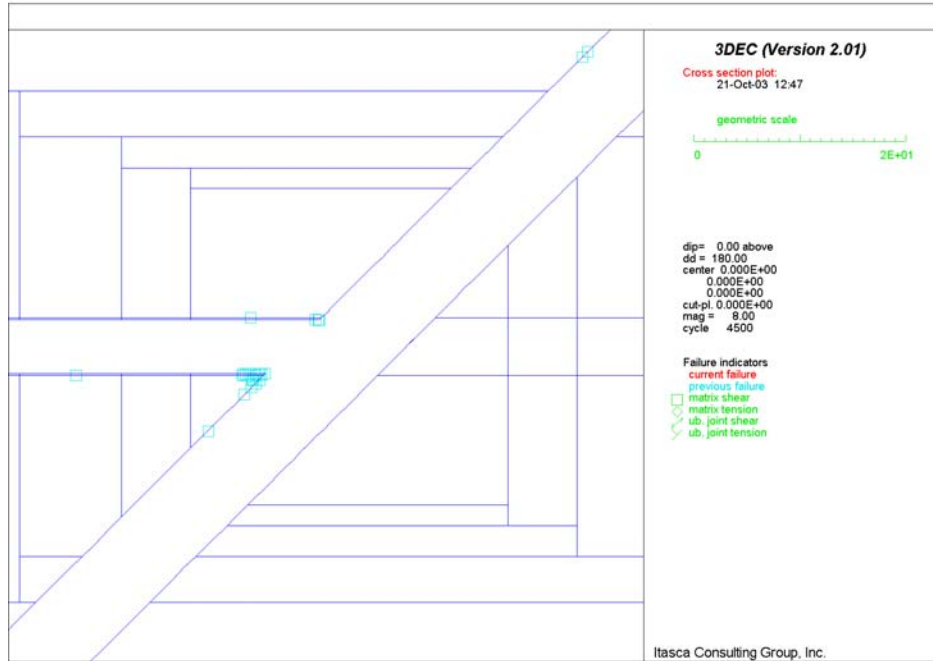


Figure 6-66. Intersection D: Potential Yield Zone in Horizontal Section for N. Lith. Cat. 1 Rock

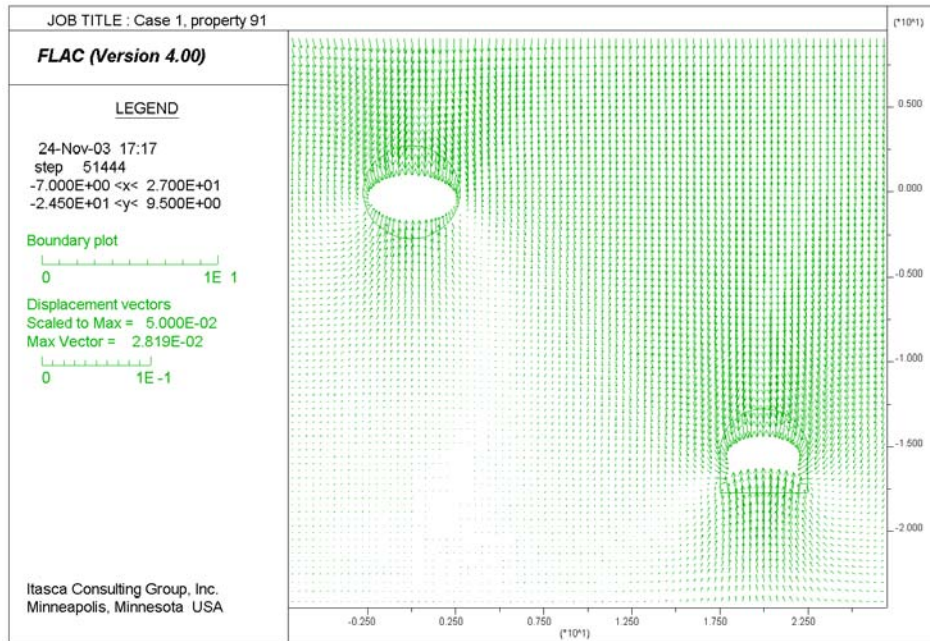


Figure 6-66A. Displacements due to Excavations of Observation Drift and Emplacement Drift

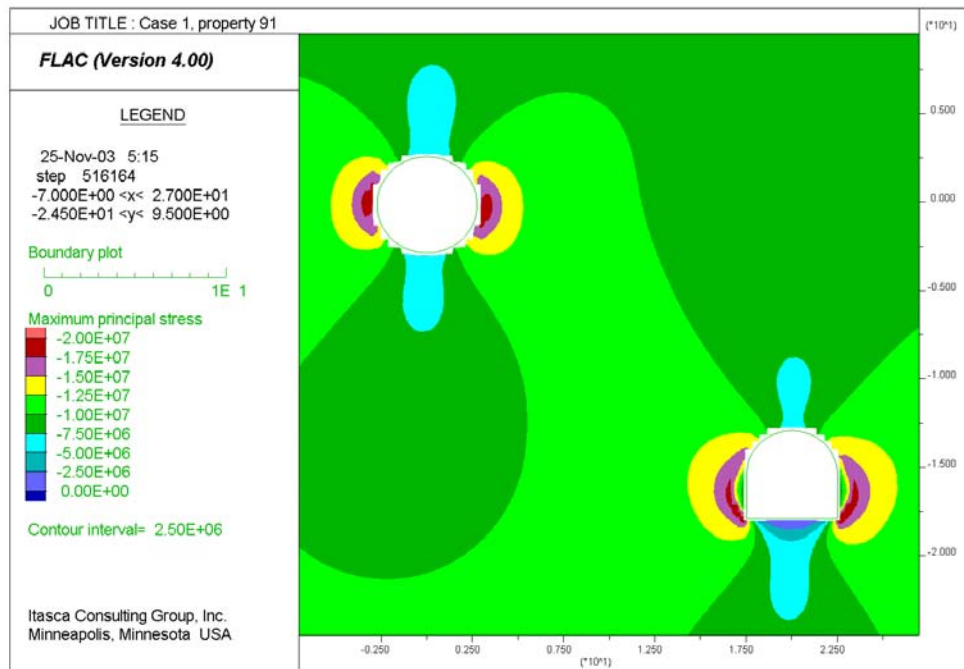


Figure 6-66B. Contours of Major Principal Stress after Excavation of Observation Drift and Emplacement Drift

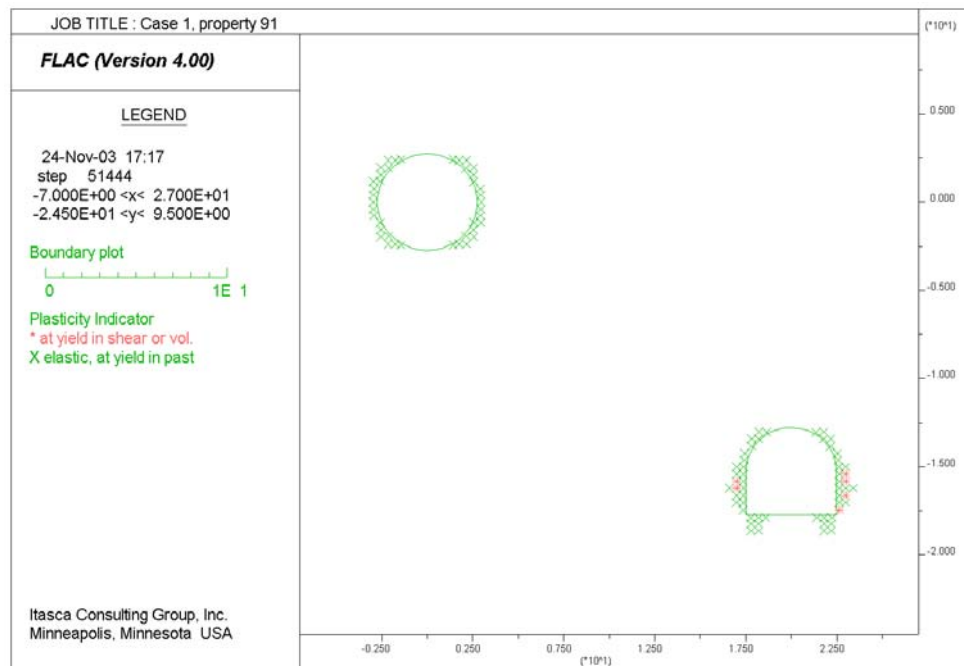


Figure 6-66C. Potential Yield Zone after Excavation of Observation Drift and Emplacement Drift

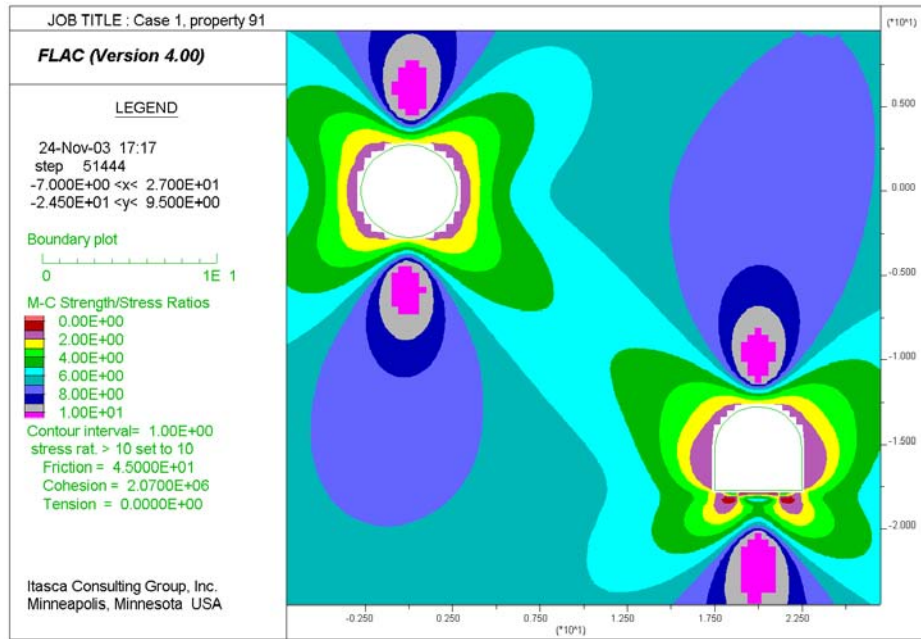


Figure 6-66D. Factor of Safety after Excavation of Observation Drift and Emplacement Drift

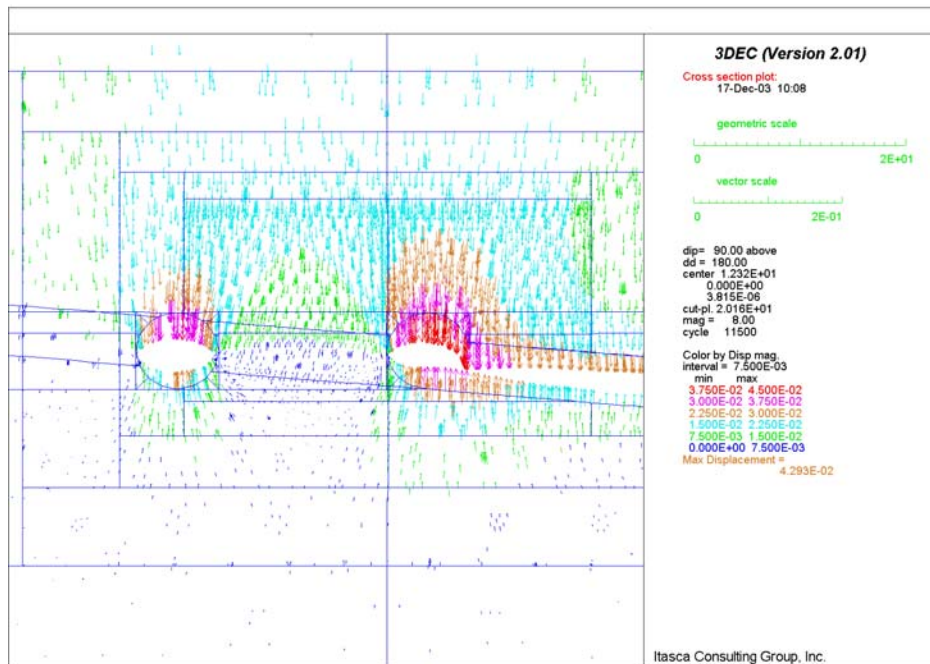


Figure 6-66E. Displacement Field in Vertical Section 1 at Intersection between Observation Drift and Exhaust Main

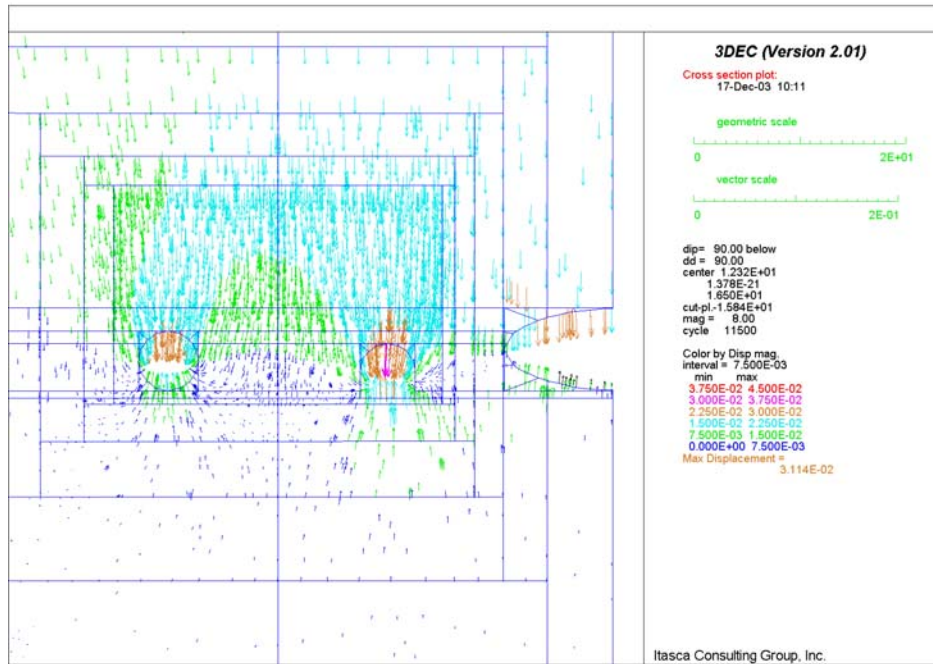


Figure 6-66F. Displacement Field in Vertical Section 2 at Intersection between Observation Drift and Exhaust Main

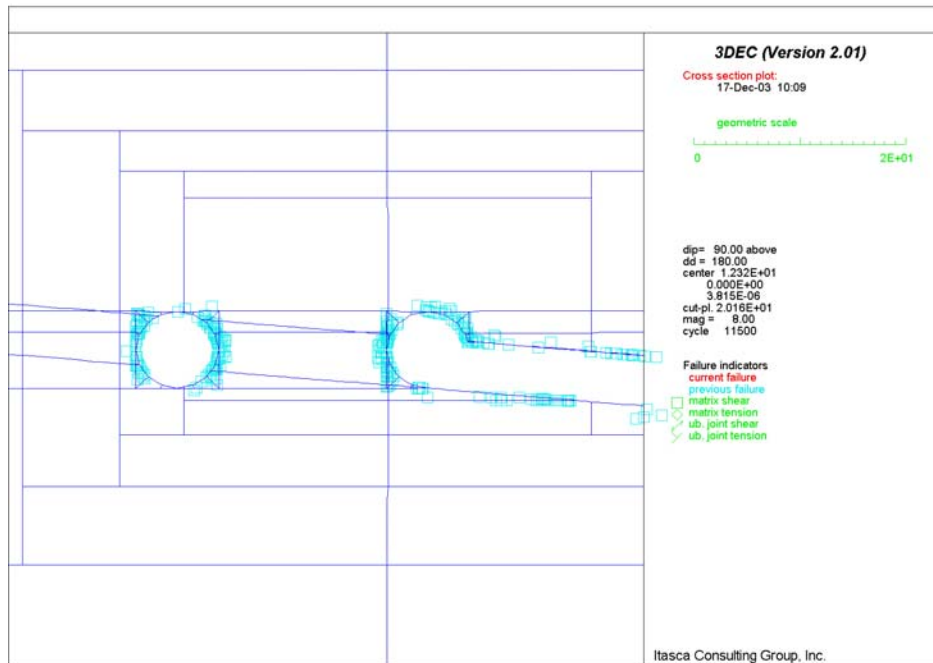


Figure 6-66G. Potential Yield Zone in Intersection between Observation Drift and Exhaust Main in Section 1

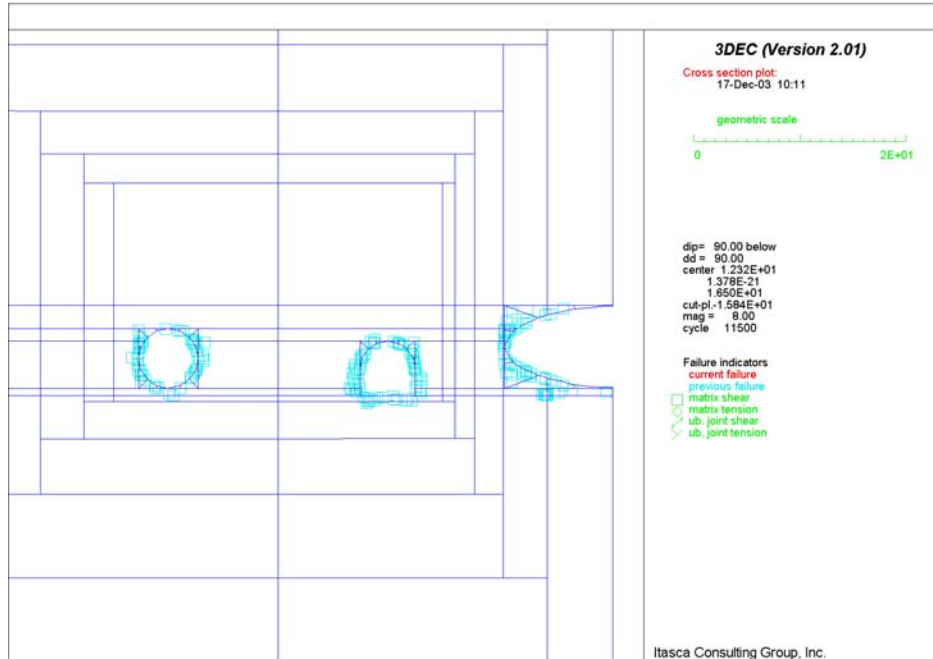


Figure 6-66H. Potential Yield Zone in Intersection between Observation Drift and Exhaust Main in Section 2

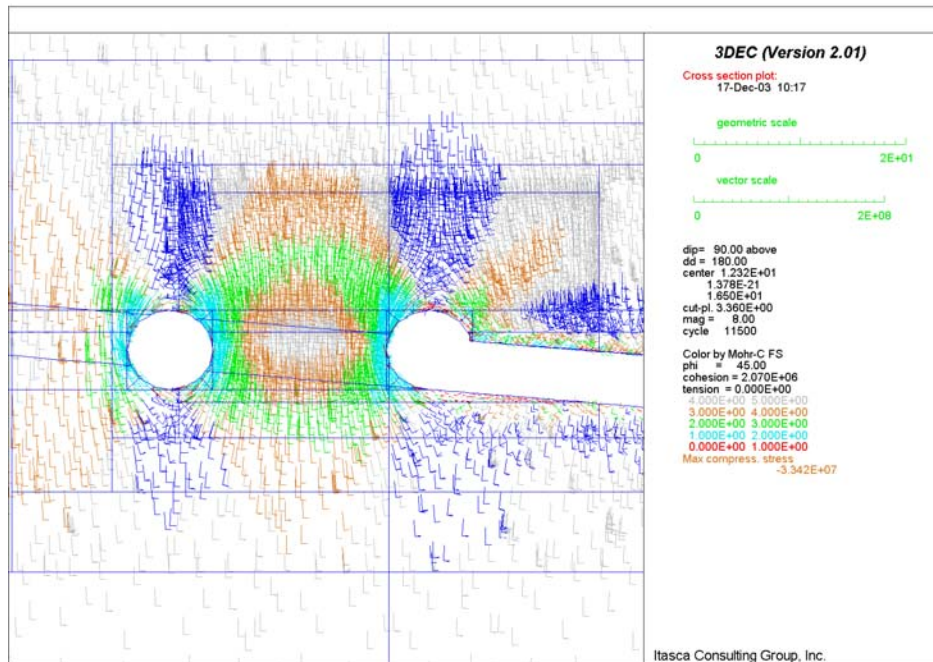


Figure 6-66I. Factor of Safety in Intersection between Observation Drift and Exhaust Main in Section 1

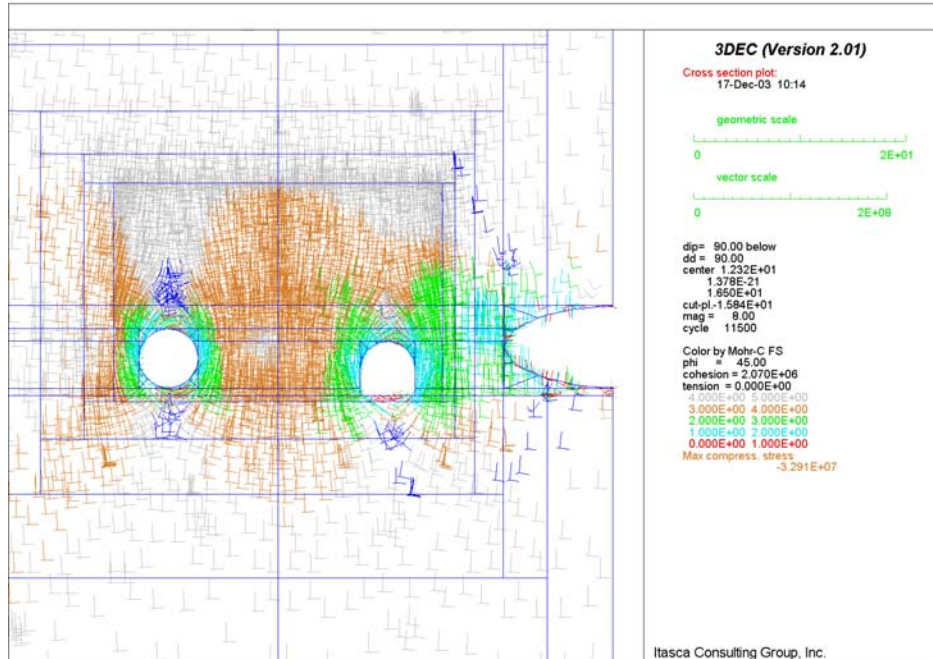


Figure 6-66J. Factor of Safety in Intersection between Observation Drift and Exhaust Main in Section 2

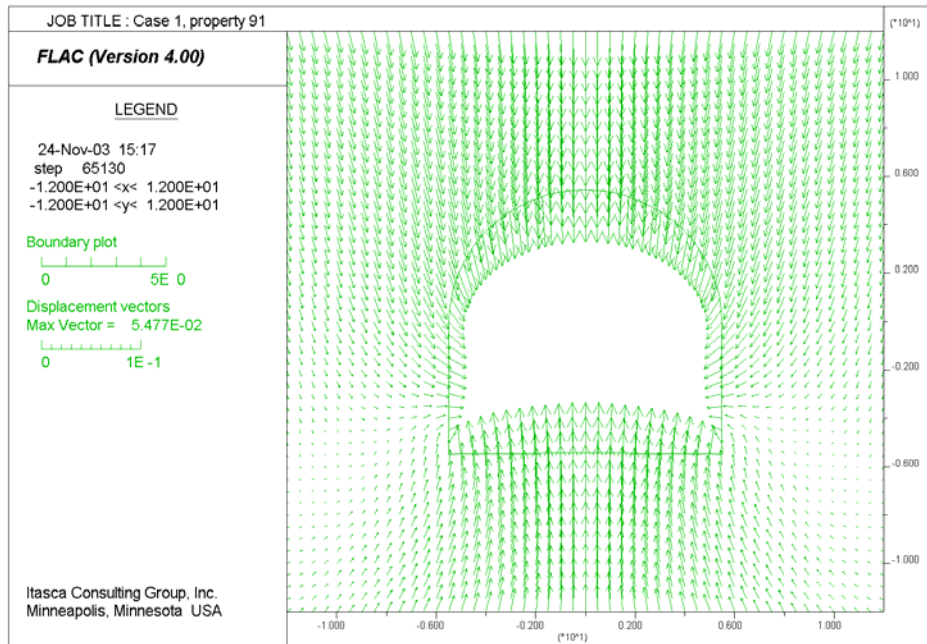


Figure 6-66K. Displacements due to Excavation of TBM Launch Chamber

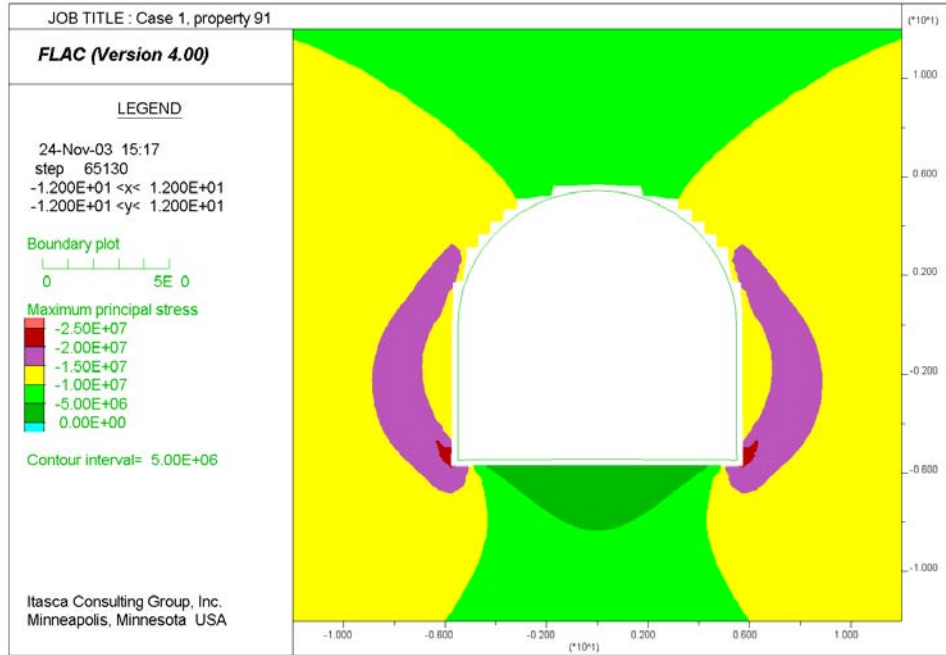


Figure 6-66L. Contours of Major Principal Stress after Excavation of TBM Launch Chamber

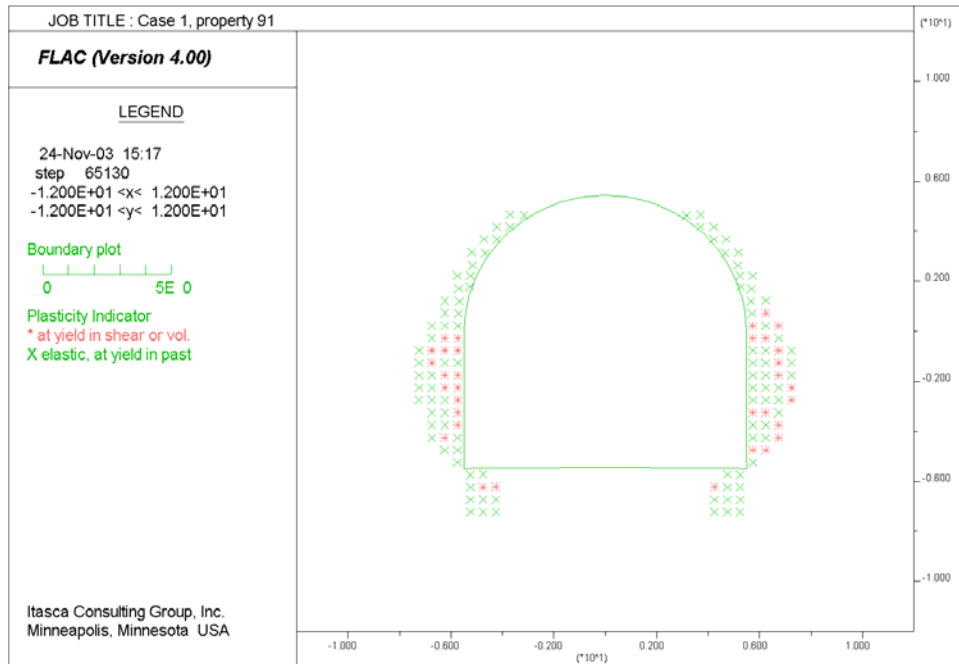


Figure 6-66M. Potential Yield Zone after Excavation of TBM Launch Chamber

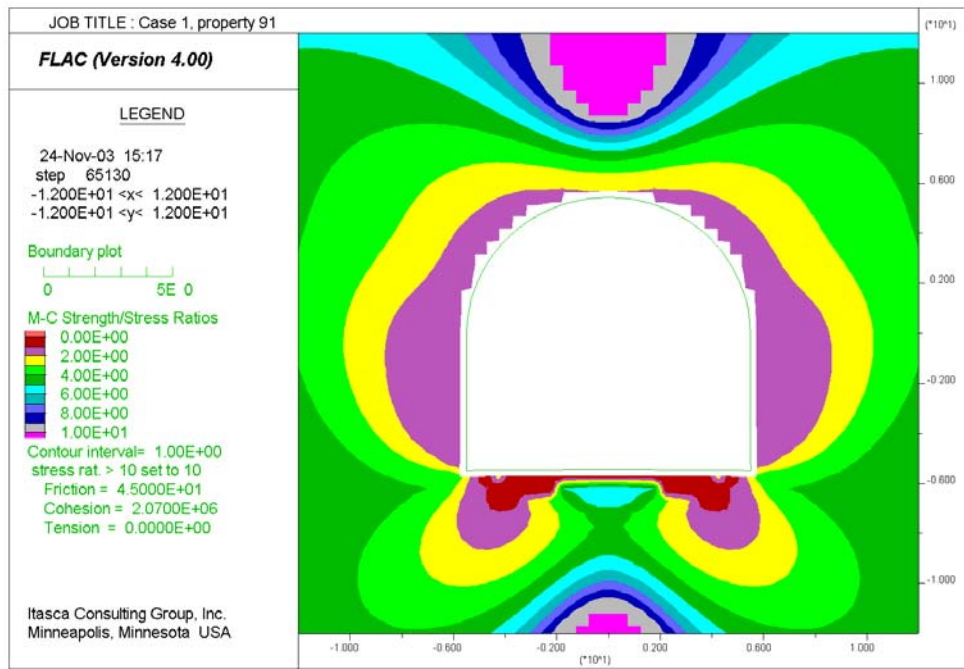


Figure 6-66N. Factor of Safety after Excavation of TBM Launch Chamber

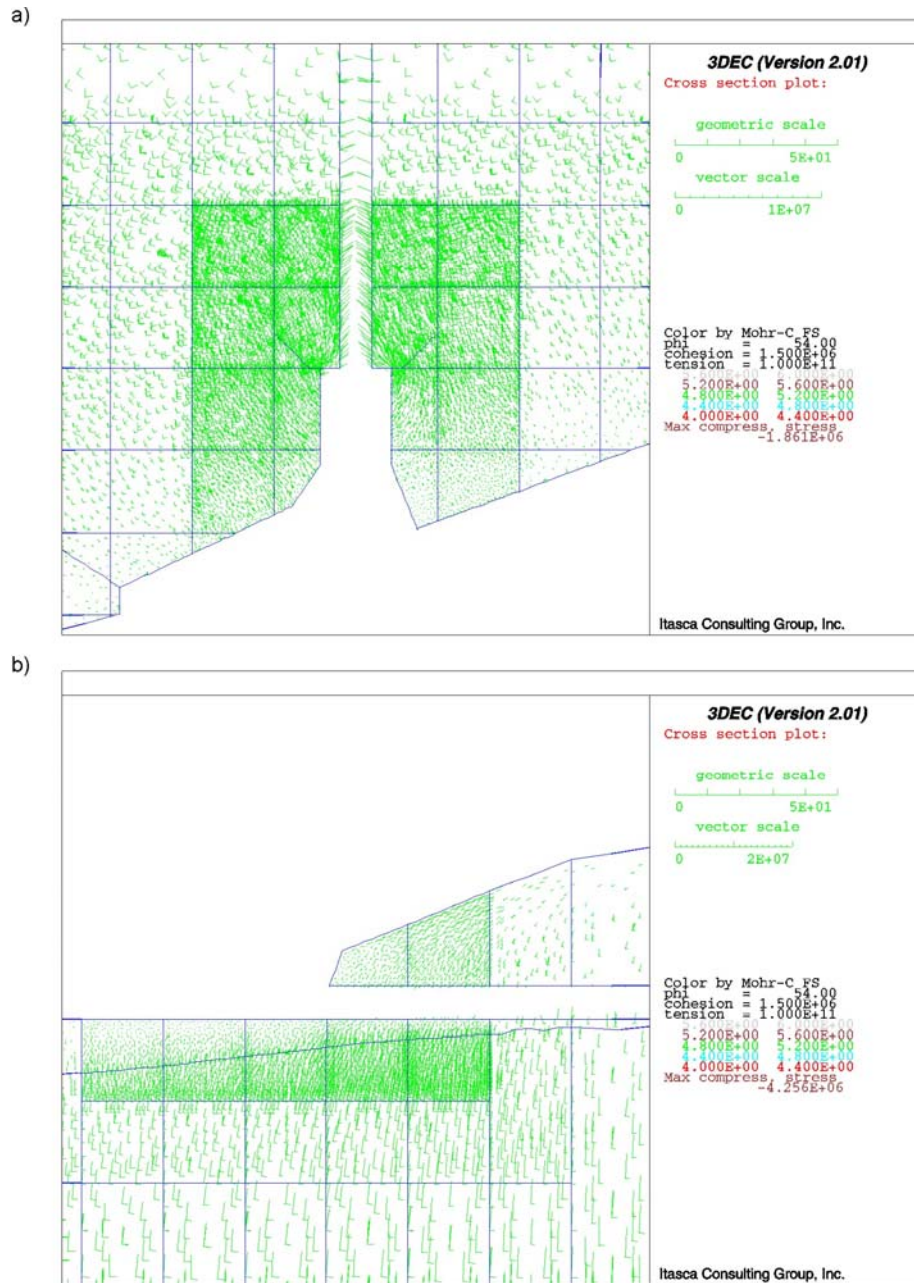


Figure 6-66O. Factor of Safety after Excavation of North Portal Starter Tunnel: a) Horizontal Cross-section at Elevation 1128 m, and b) Longitudinal Cross-section L-L'

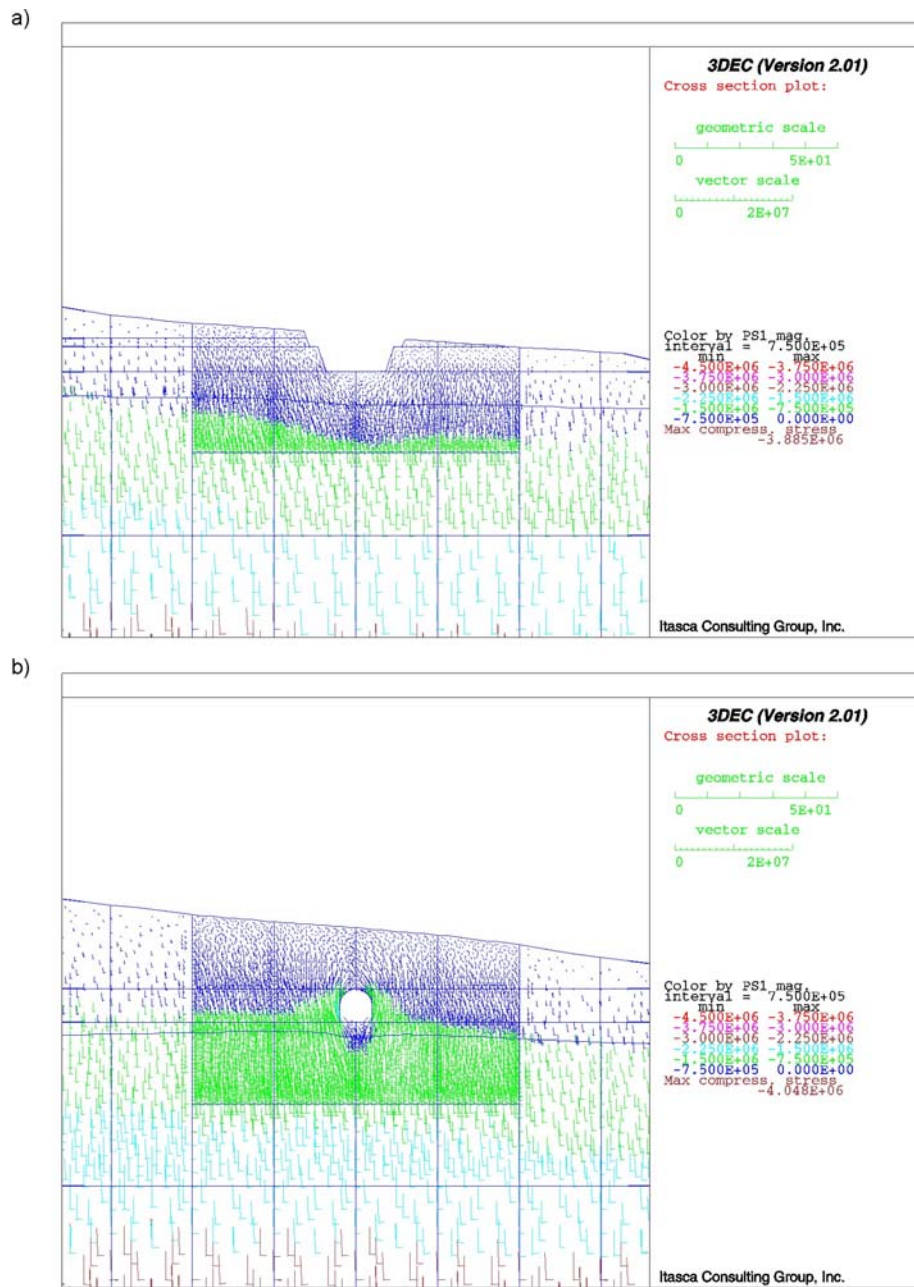


Figure 6-66P. Major Principal Stresses after Excavation of North Portal Starter Tunnel for Cross-sections:  
a) C<sub>1</sub>-C<sub>1</sub>' and b) C<sub>2</sub>-C<sub>2</sub>'

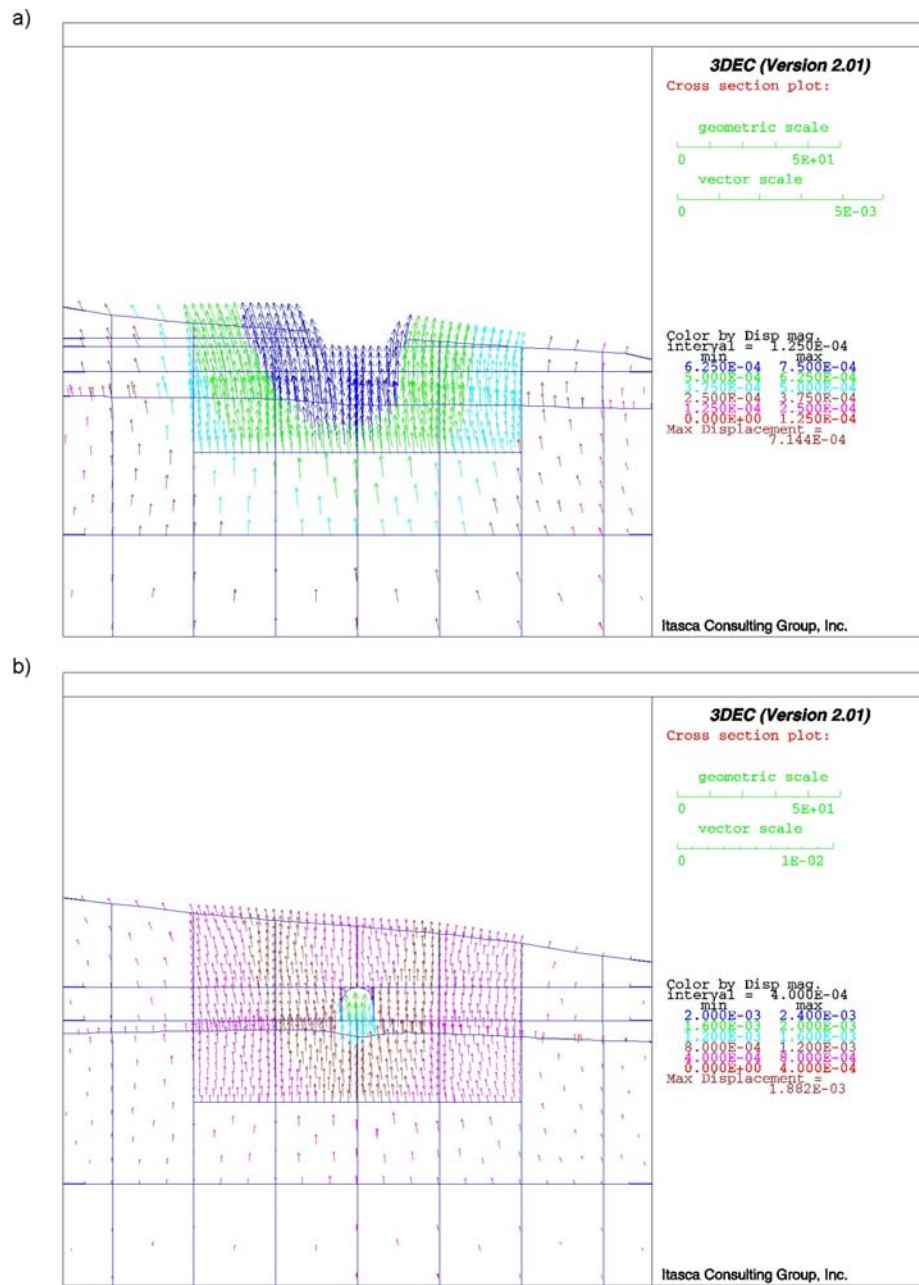


Figure 6-66Q. Displacement Field after Excavation of North Portal Starter Tunnel for Cross-sections:  
a) C<sub>1</sub>-C<sub>1</sub>' and b) C<sub>2</sub>-C<sub>2</sub>'

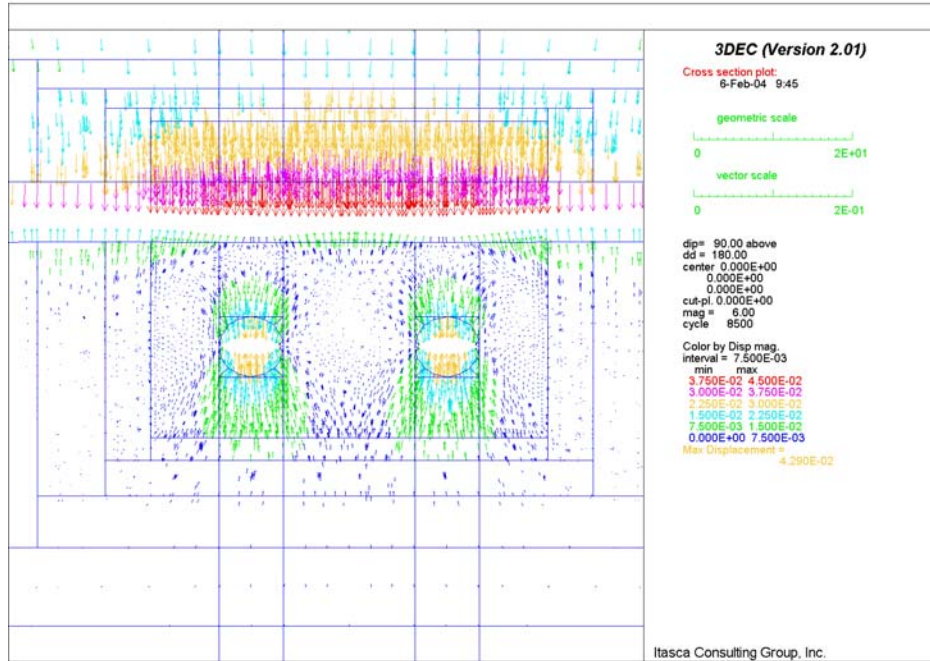


Figure 6-66R. Displacement Field in Vertical Section 1 for Lith. Cat. 1 Rock at Interburden Area

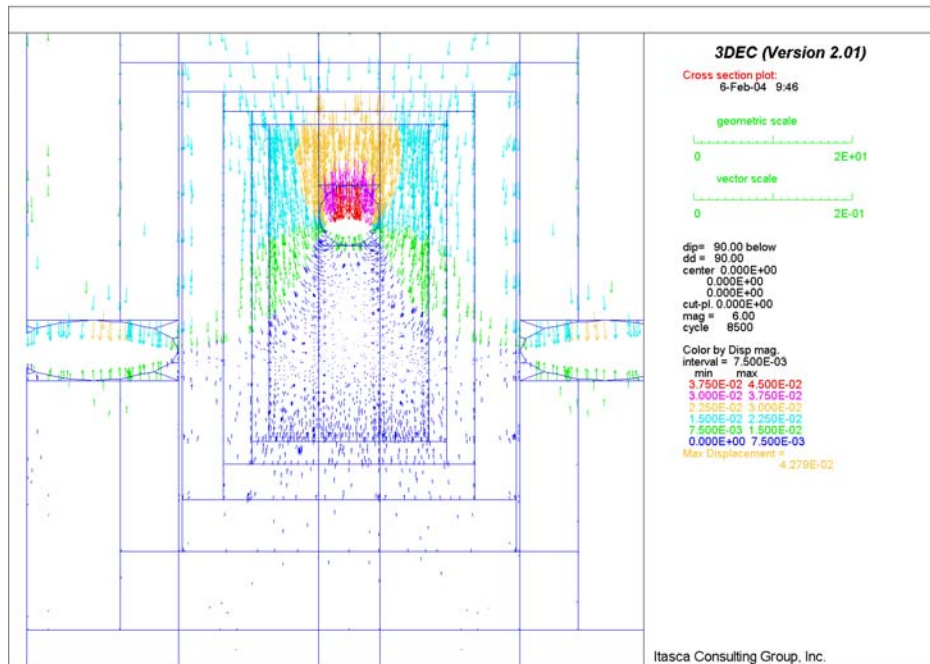


Figure 6-66S. Displacement Field in Vertical Section 2 for Lith. Cat. 1 Rock at Interburden Area

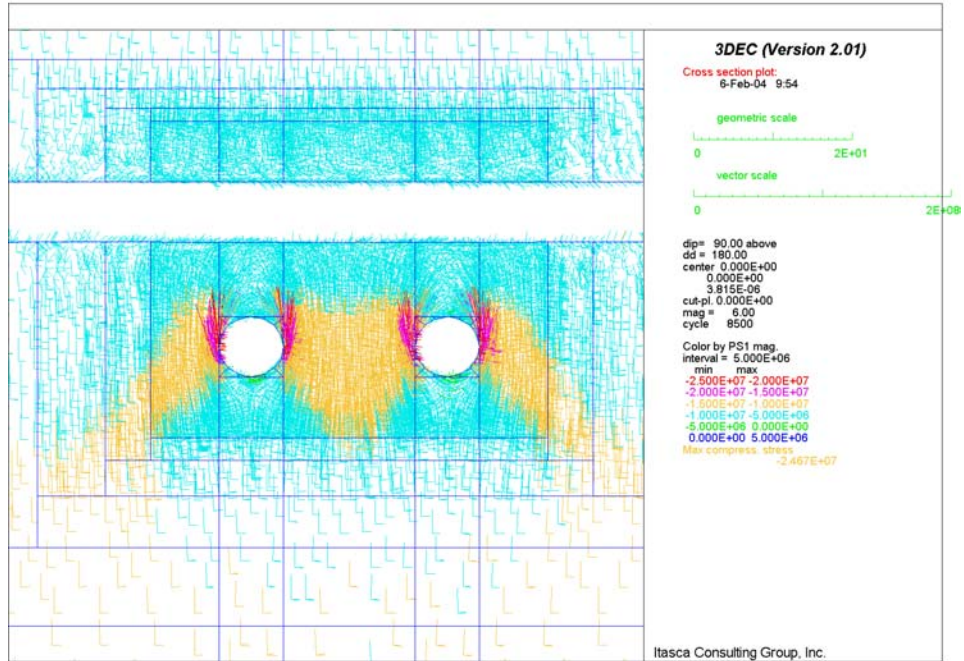


Figure 6-66T. Stress Field in Vertical Section 1 for Lith. Cat. 1 Rock at Interburden Area

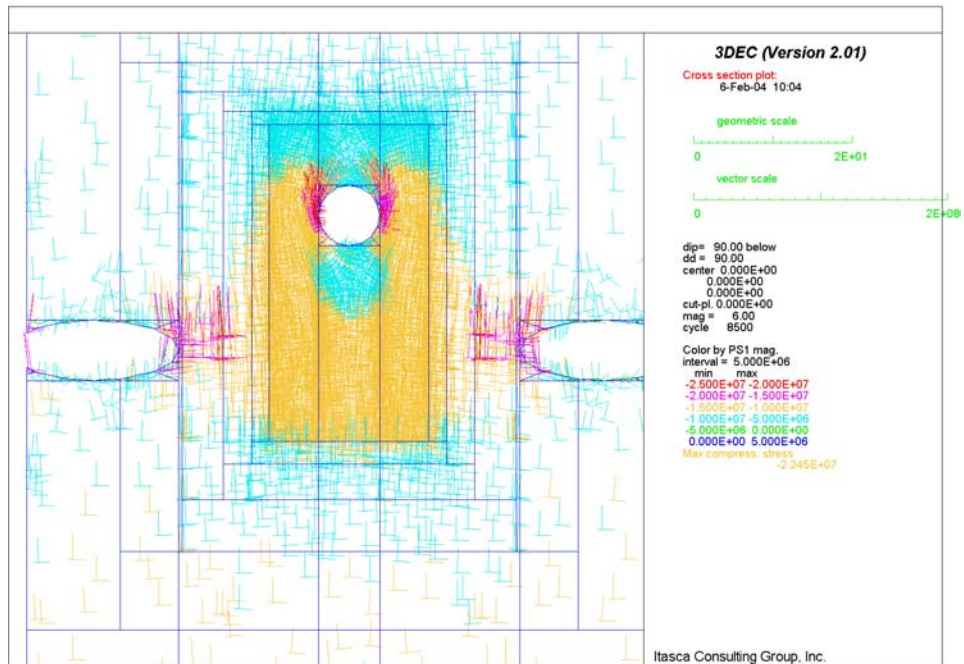


Figure 6-66U. Stress Field in Vertical Section 2 for Lith. Cat. 1 Rock at Interburden Area



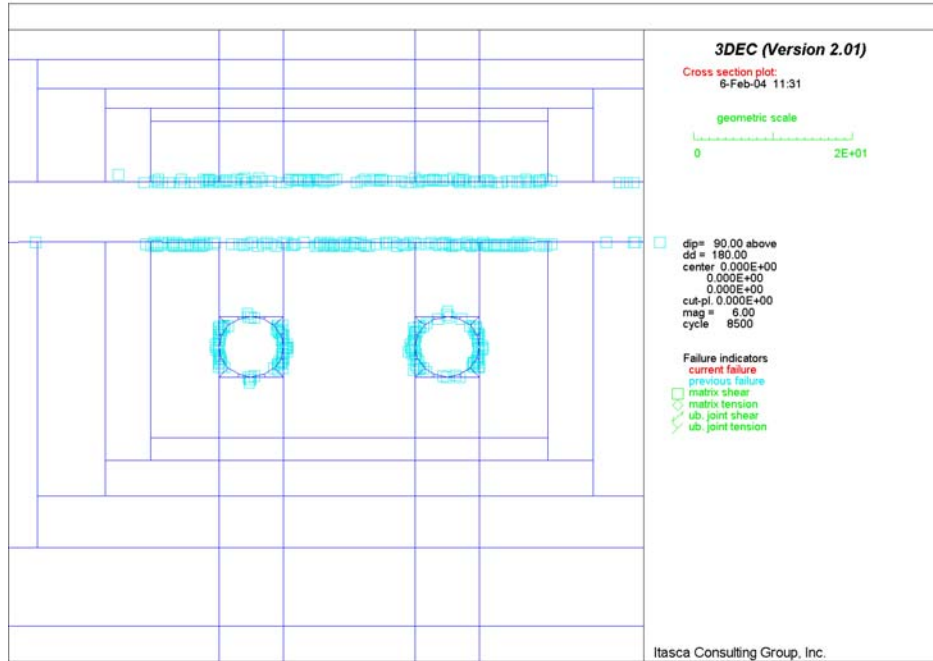


Figure 6-66X. Potential Yield Zone in Vertical Section 1 for Lith. Cat. 1 Rock at Interburden Area

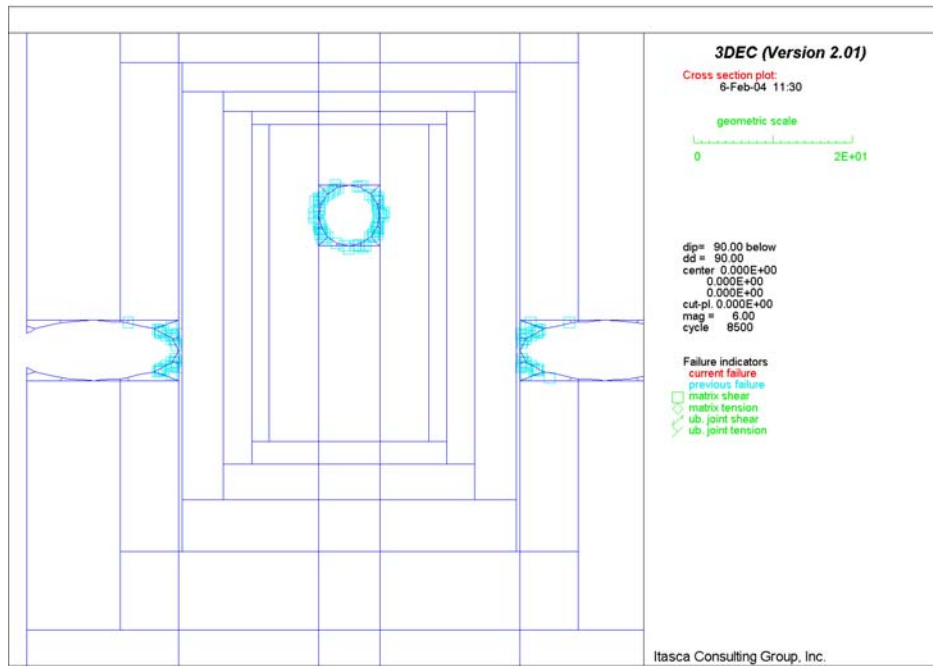


Figure 6-66Y. Potential Yield Zone in Vertical Section 2 for Lith. Cat. 1 Rock at Interburden Area

### **6.5.3.2 Thermal Loading Condition**

It should be noted the thermal loading condition is only applied to intersections of exhaust mains with emplacement drifts, observation drift, intersection of observation drift with exhaust main, and interburden pillar between access to intake shaft #1 and exhaust mains. The discussion in this section is limited to these areas.

#### **6.5.3.2.1 Intersections of Exhaust Mains and Emplacement Drifts**

The temperature fields in intersection B, as calculated in NUFT and imported into 3DEC, after 3 and 20 years of heating are shown in Figures 6-67 and 6-68. The temperature histories at points 1, 2 and 3 (indicated in Figures 6-13 and 6-14) are shown in Figures 6-69 and 6-70 for locations B and D, respectively. Note that the temperatures shown in these two figures are reasonable except temperatures at point 2 in Figure 6-69. The reason that temperatures at this point are higher than those at point 3 is because of the two-dimensional temperature field used in the calculation. In the three-dimensional model, the emplacement drift is not continuous, instead, it intersects and ends at the exhaust main. Consequently, some of the points on the wall of the exhaust main which are located within the projected outline of the emplacement drift have higher temperatures than those of the points on the emplacement drift. However, the impact of this result is insignificant. As indicated in Figure 6-71, thermally induced variation of major principal stress in the preclosure period is relatively small, i.e., about few percent with respect to the initial stress state before heating began.

The thermal stress changes, shown (at points 1, 2 and 3 at locations B and D) in Figures 6-71 through 6-74, are much larger in better quality and stiffer rock masses. The increase in the maximum major principal stress is about 15 MPa in category 5 of the lithophysal and non-lithophysal rock masses. However, the stress change does not change factor-of-safety with respect to the Mohr-Coulomb yield condition throughout the rock mass (Figures 6-75 through 6-78) nor cause significant additional yielding of the rock mass (comparing Figures 6-79 and 6-80 with Figures 6-63 and 6-64). The extent of plastic deformation for both locations, and for the different rock-mass categories remains practically unchanged after 50 years of heating. The heating causes movement of the entire model vertically upward. The change in displacement in the vertical direction of the excavation in the intersection (at point 1) due to temperature change is not significant (Figures 6-81 and 6-82). For locations B and D, it appears that displacement in the vertical direction at point 1 is reduced.

#### **6.5.3.2.2 Observation Drift**

The temperature field after 50 years of heating around the observation drift is shown in Figure 6-82A. Temperature histories during 50 years of heating at three points around the observation drift are shown in Figure 6-82B. The observation drift does not significantly affect heat transport or the predicted temperature fields. This simplification is conservative, resulting in overestimation of the temperatures around the observation drift.

It is predicted that the maximum temperature increase around the observation drift during the 50-yr period after waste emplacement is approximately 13°C. It does not appear that this temperature change (and the corresponding stress change shown in Figure 6-82C) causes any

additional damage around the observation drift (Figures 6-82D and 6-82E). Induced displacements of the points on the drift boundary are of the order of millimeters (Figure 6-82F). Figures 6-82G to 6-82J indicate that thermal loads do not affect the stability conditions of the rock mass around the intersection between the observation drift and the exhaust main.

### **6.5.3.2.3 Interburden Pillar between Shaft Access and Exhaust Mains**

After waste emplacement, the exhaust mains and the pillar between the exhaust mains and the access drifts drift to the ventilation shaft will be subjected to the thermal stresses. The evolution of the temperature field around the pillar was calculated by the NUFT code, conservatively assuming that the emplacement drift is located below the access drift to the ventilation shaft. (In fact, the access drift to the ventilation shaft is located in the plan half way between two emplacement drifts.) The temperature fields (at 1, 2, 3, 5, 10, 20, 30 and 50 years) from the NUFT code were imported into 3DEC in order to calculate the thermal stress around the excavations, according to Equation 6-8.

The temperature fields, as calculated in NUFT and imported into 3DEC, after 3 and 20 years of heating are shown in Figures 6-82K and 6-82L, respectively. As shown in these two figures, the temperatures at the middle of pillar are higher than those near the exhaust mains. This is mainly due to the conservative assumption made in the previous paragraph. The similar temperature distribution is also seen in temperature histories at points 1, 2, 3 and 4 (indicated in Figure 6-17C) shown in Figure 6-82M.

The thermal stress changes are shown (at points 1, 2, 3 and 4) in Figure 6-82N. It is noted that the major principal stresses at points 1 and 2 (i.e., at middle of pillar) are higher than those at points 3 and 4 (i.e., at crown of drifts). The reason of this is due to the higher temperatures assumed in the pillar, which is already described in the previous paragraph. The reason that the stress at point 4 (i.e., at crown of access drift) is higher than that at point 3 (i.e., at crown of exhaust main) is due to the orientation of the major horizontal stress used in the 3-dimensional model. The model  $x$ -axis is aligned with the direction of the two exhaust mains. The orientation of the horizontal principal stresses is adjusted due to rotation of the model axes relative to the global coordinate system. The major horizontal principal stress strikes at N15°E (see Assumption 5.3). Due to rotation of the model horizontal axes by 18° counterclockwise, the major horizontal principal stress strikes in the model at N33°E. However, it should be noted that the stress change due to the thermal load does not change the level of factor-of-safety with respect to the Mohr-Coulomb yield condition due to in situ stress (comparing Figure 6-66V with Figures 6-82O and 6-82P) nor cause significant additional yielding of the rock mass (comparing Figure 6-66X and Figure 6-82Q).

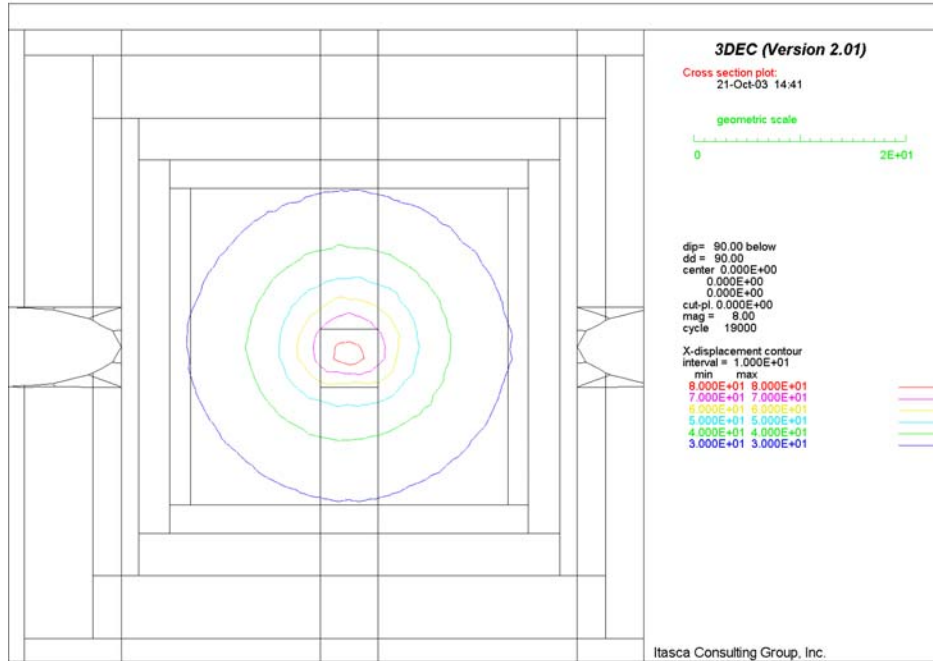


Figure 6-67. Intersection B: Temperature Field in Vertical Section 1 after 3 Years of Heating

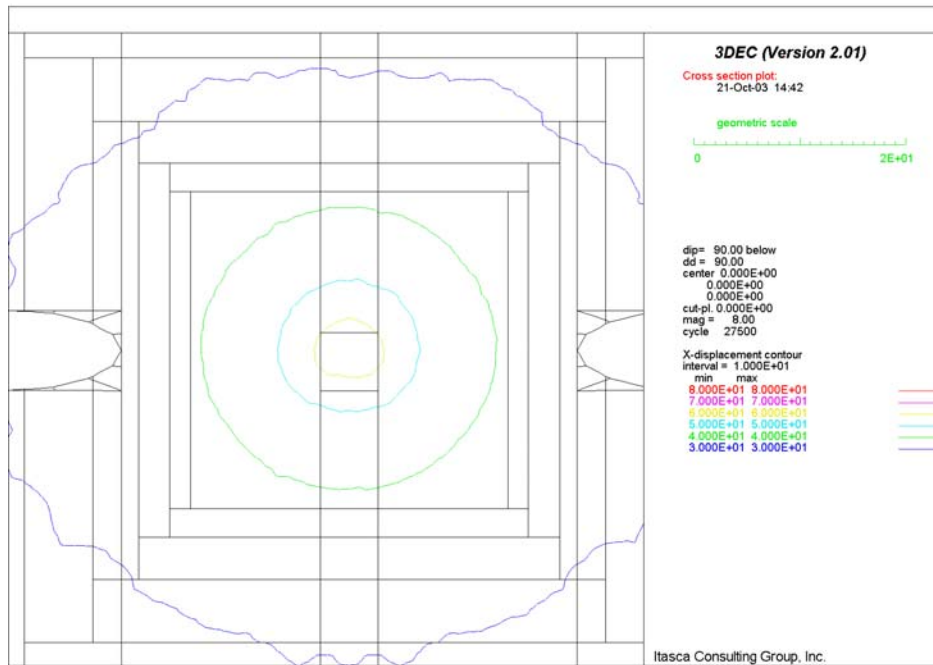


Figure 6-68. Intersection B: Temperature Field in Vertical Section 1 after 20 Years of Heating

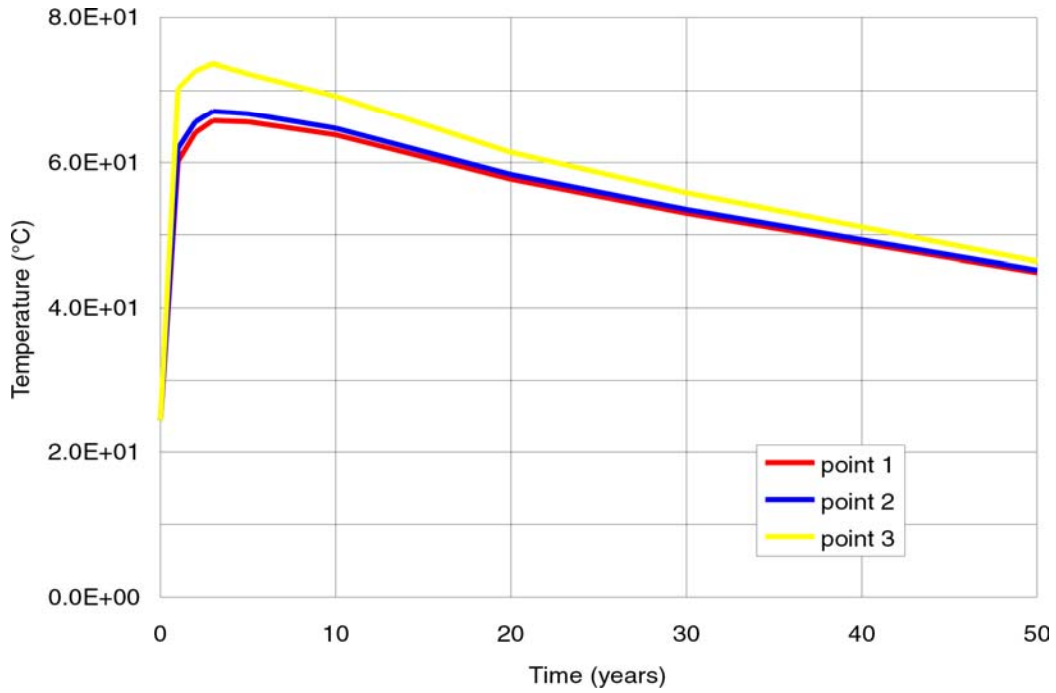


Figure 6-69. Intersection B: Temperature History at Points 1, 2 and 3

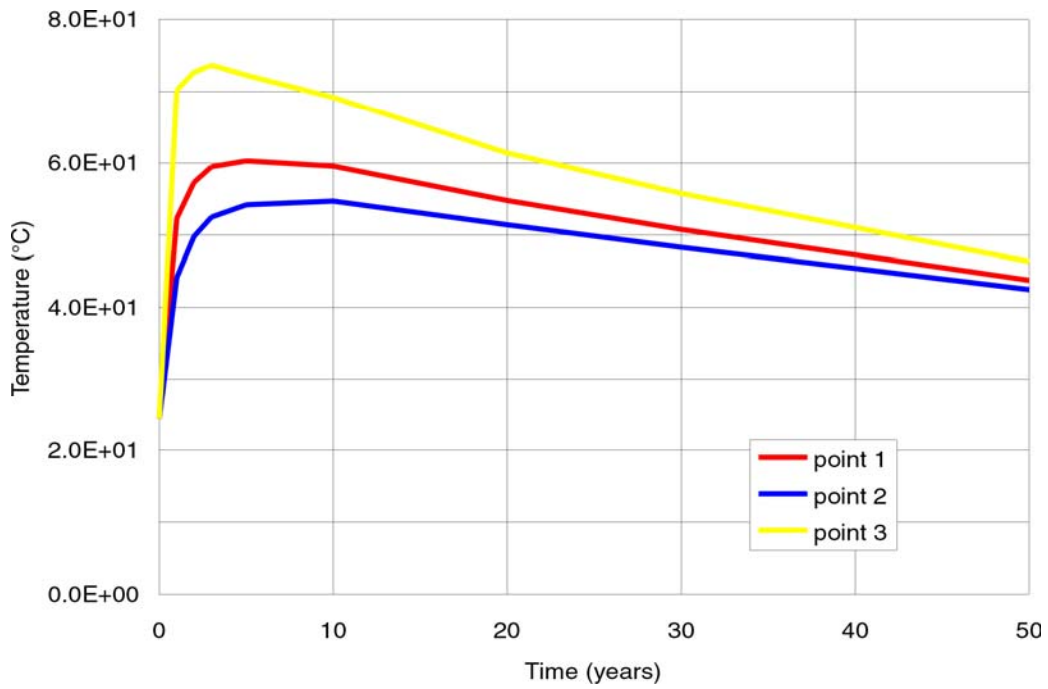


Figure 6-70. Intersection D: Temperature History at Points 1, 2 and 3

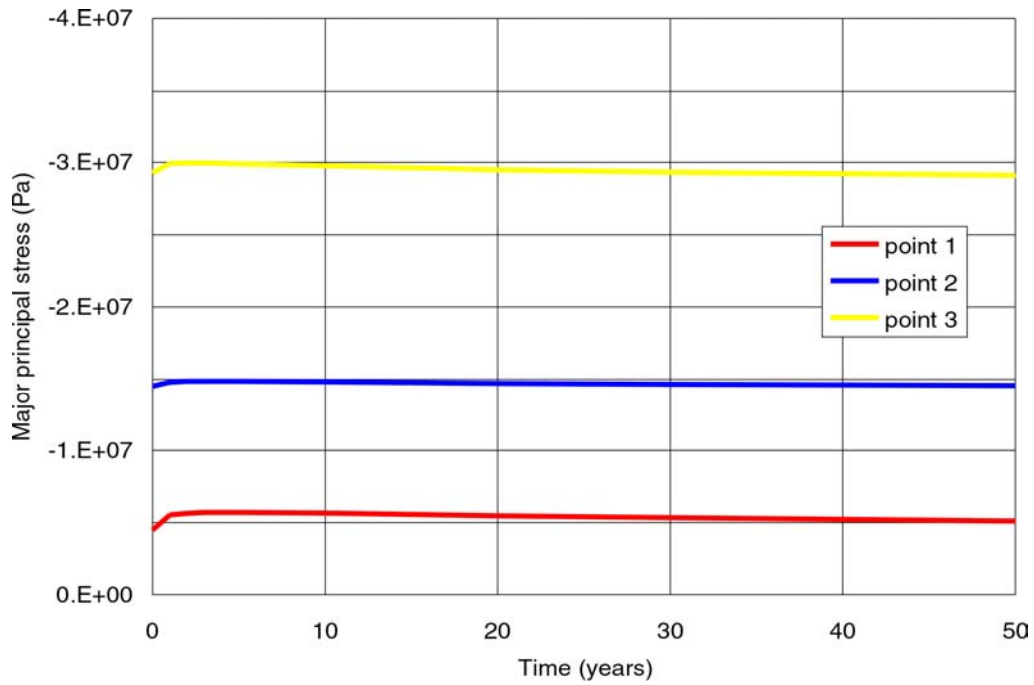


Figure 6-71. Intersection B: Time History of Major Principal Stresses for Lith. Cat. 1 Rock

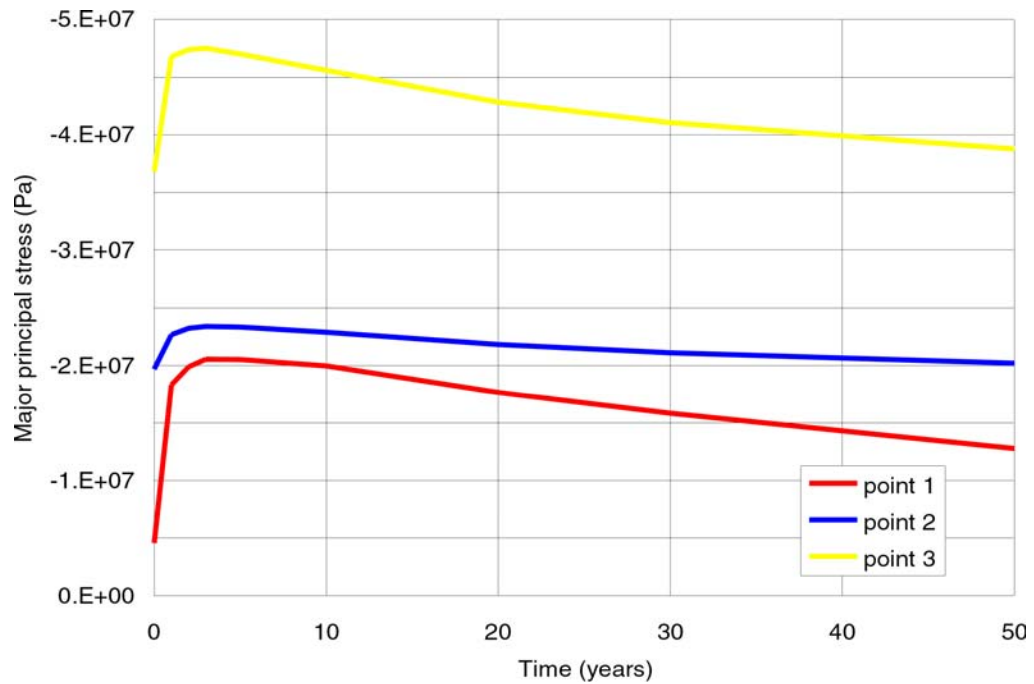


Figure 6-72. Intersection B: Time History of Major Principal Stresses for Lith. Cat. 5 Rock

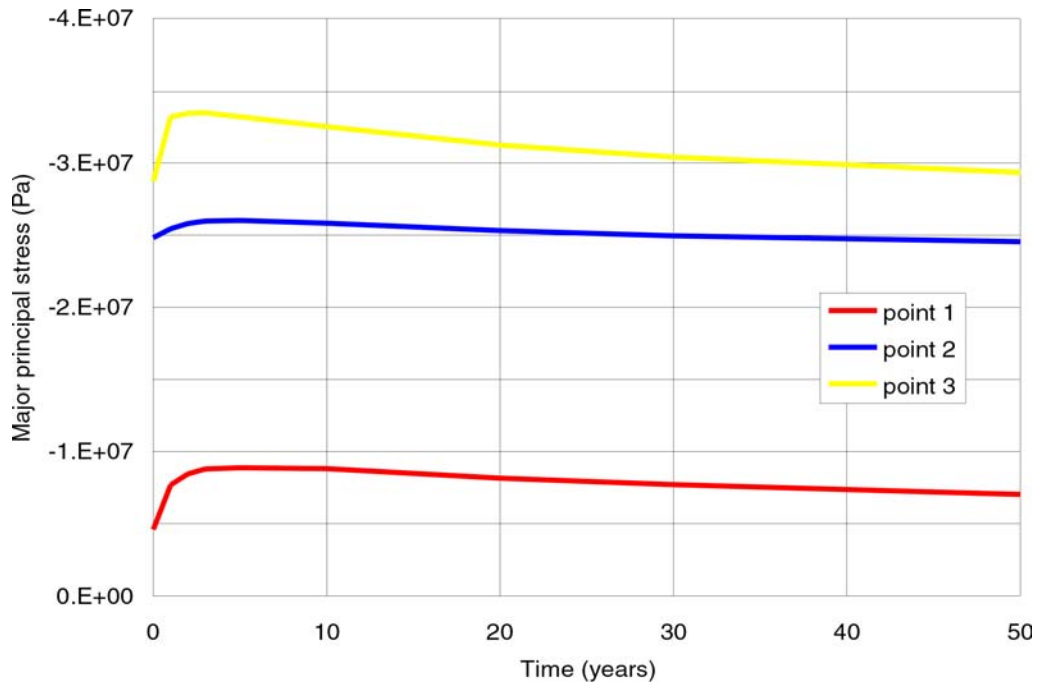


Figure 6-73. Intersection D: Time History of Major Principal Stresses for N. Lith. Cat. 1 Rock

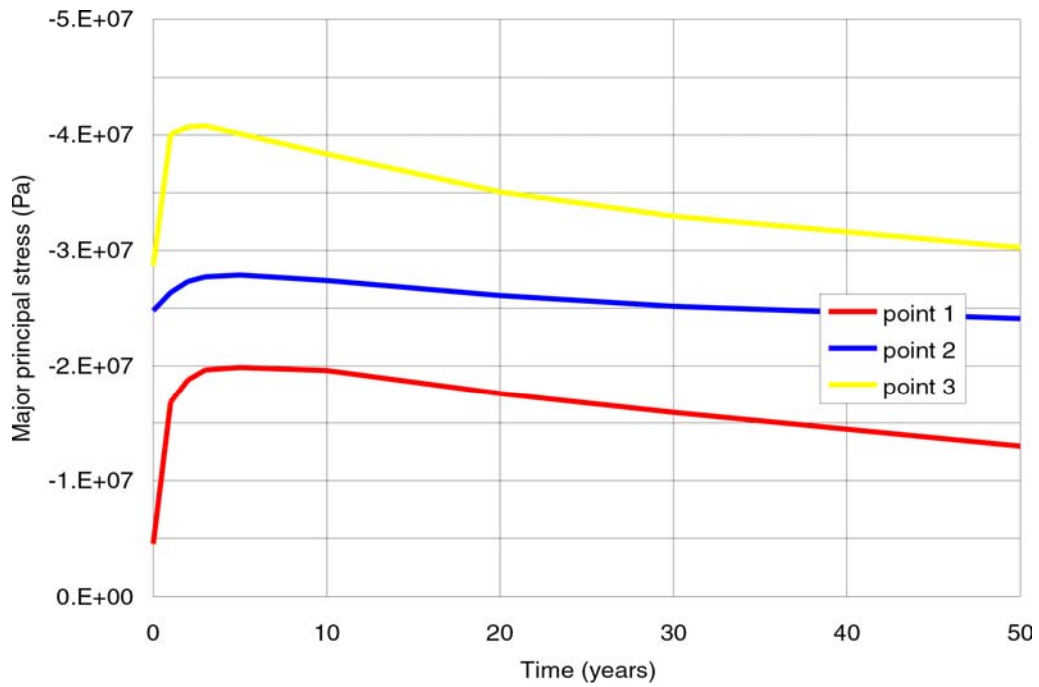


Figure 6-74. Intersection D: Time History of Major Principal Stresses for N. Lith. Cat. 5 Rock

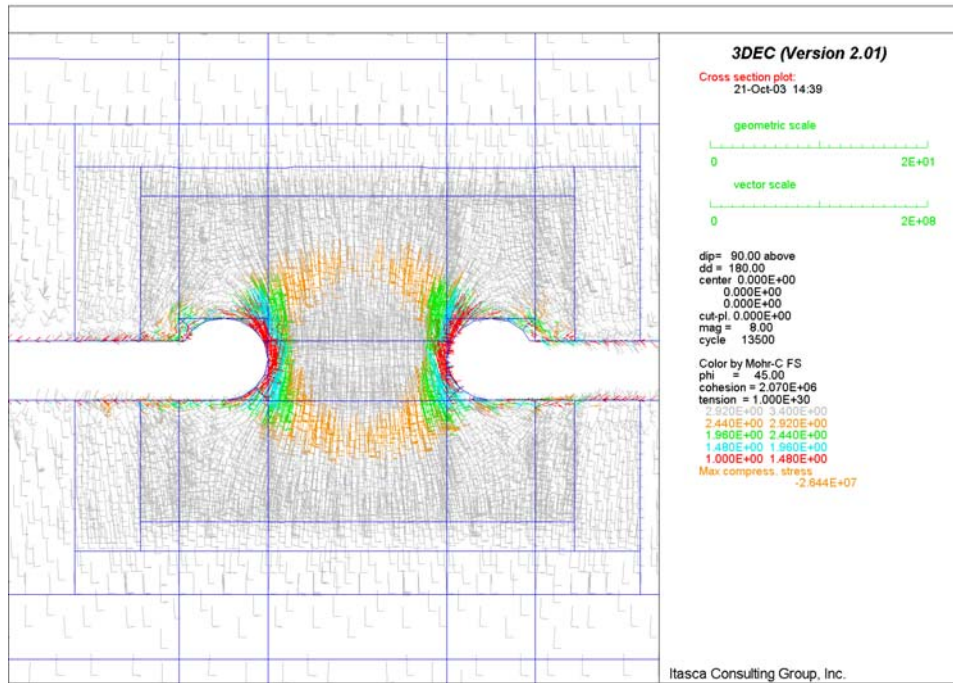


Figure 6-75. Intersection B: Factor of Safety in Vertical Section 1 for Lith. Cat. 1 Rock after 1 Year of Heating

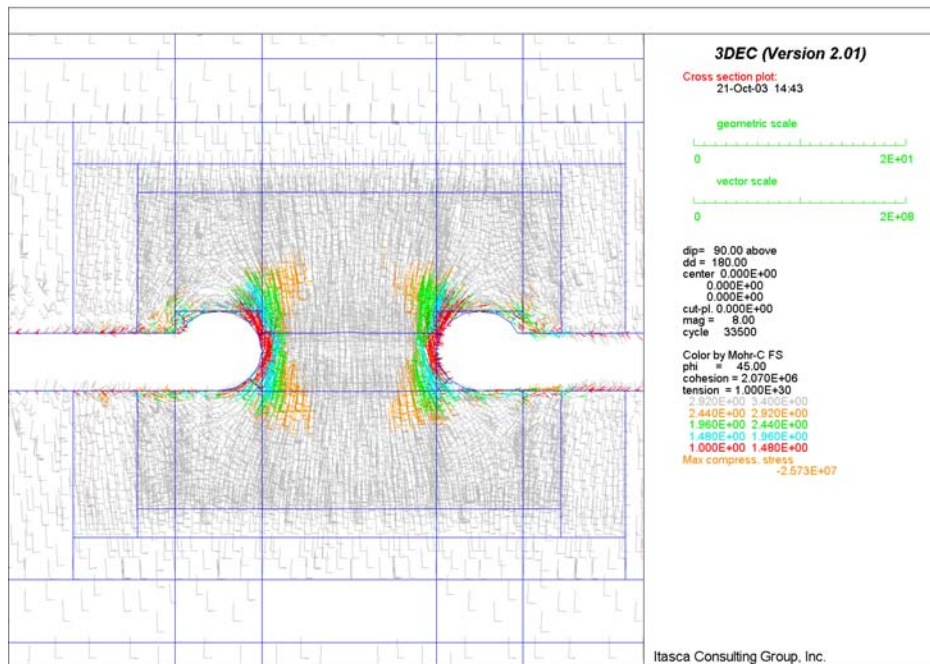


Figure 6-76. Intersection B: Factor of Safety in Vertical Section 1 for Lith. Cat. 1 Rock after 50 Years of Heating

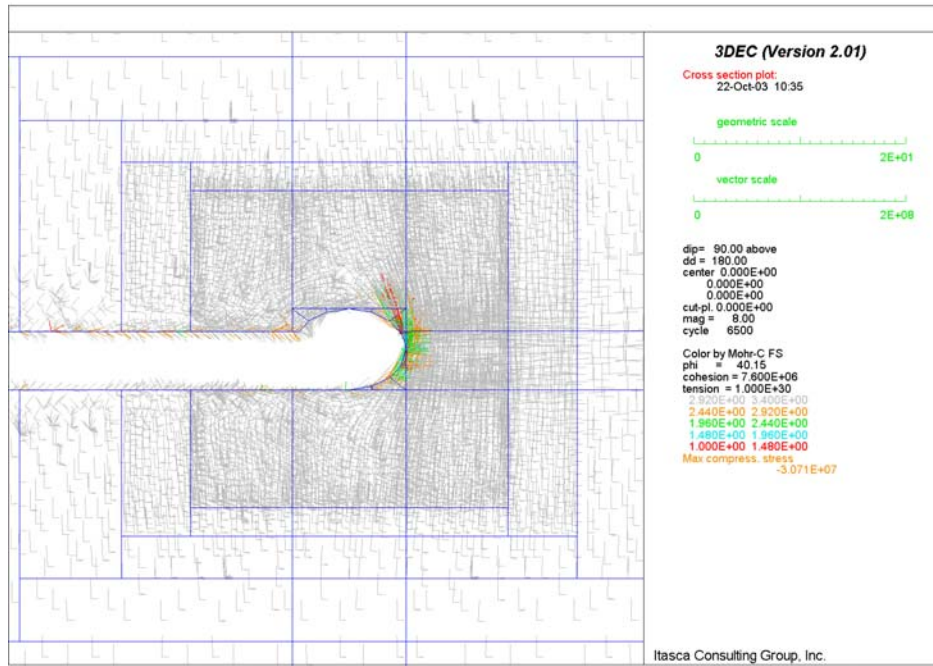


Figure 6-77. Intersection D: Factor of Safety in Vertical Section 1 for N. Lith. Cat. 1 Rock after 1 Year of Heating

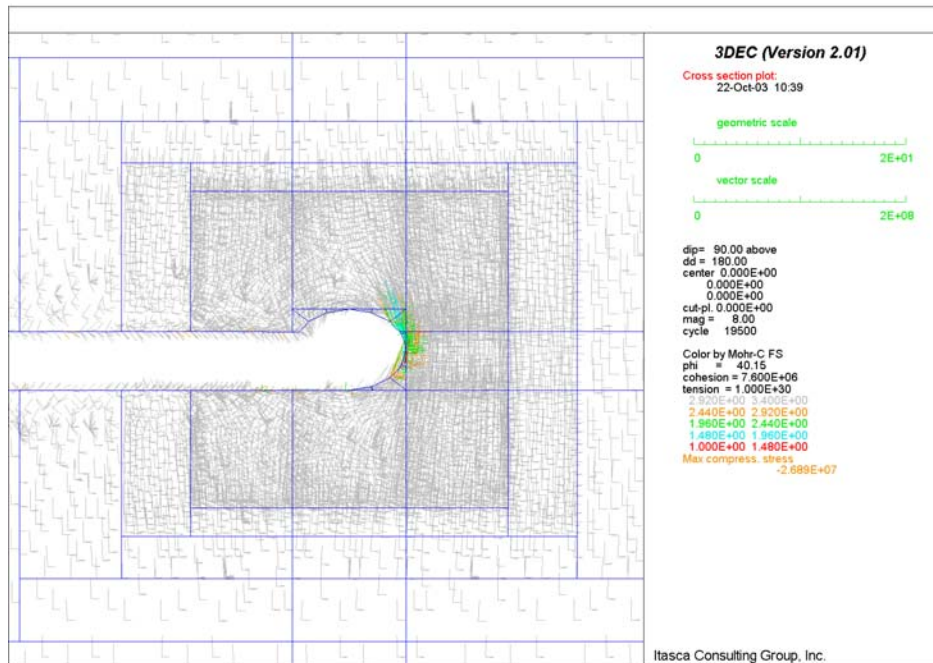


Figure 6-78. Intersection D: Factor of Safety in Vertical Section 1 for N. Lith. Cat. 1 Rock after 50 Years of Heating

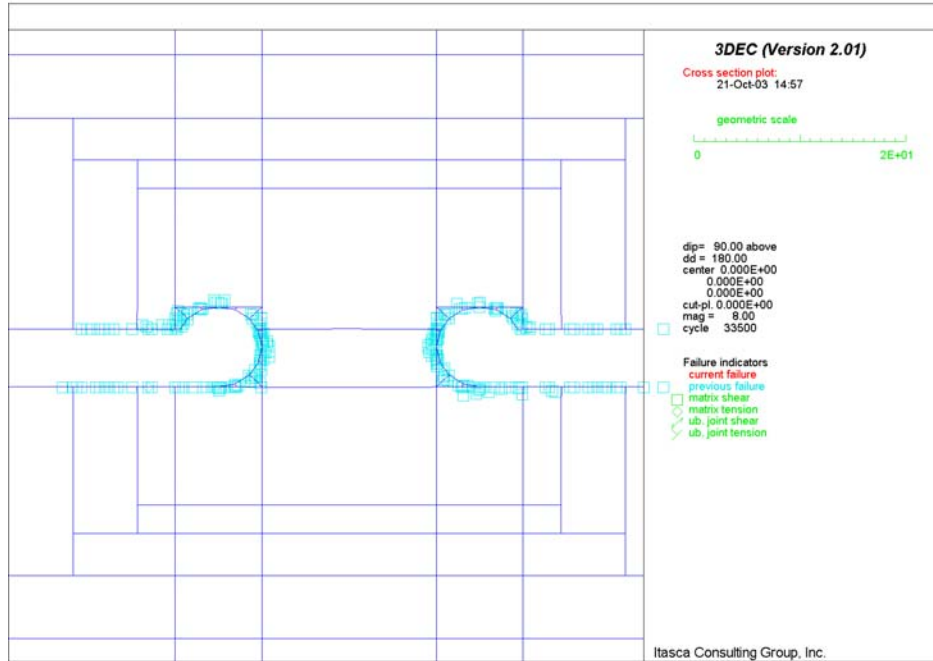


Figure 6-79. Intersection B: Potential Yield Zone in Vertical Section 1 for Lith. Cat. 1 Rock after 50 Years of Heating

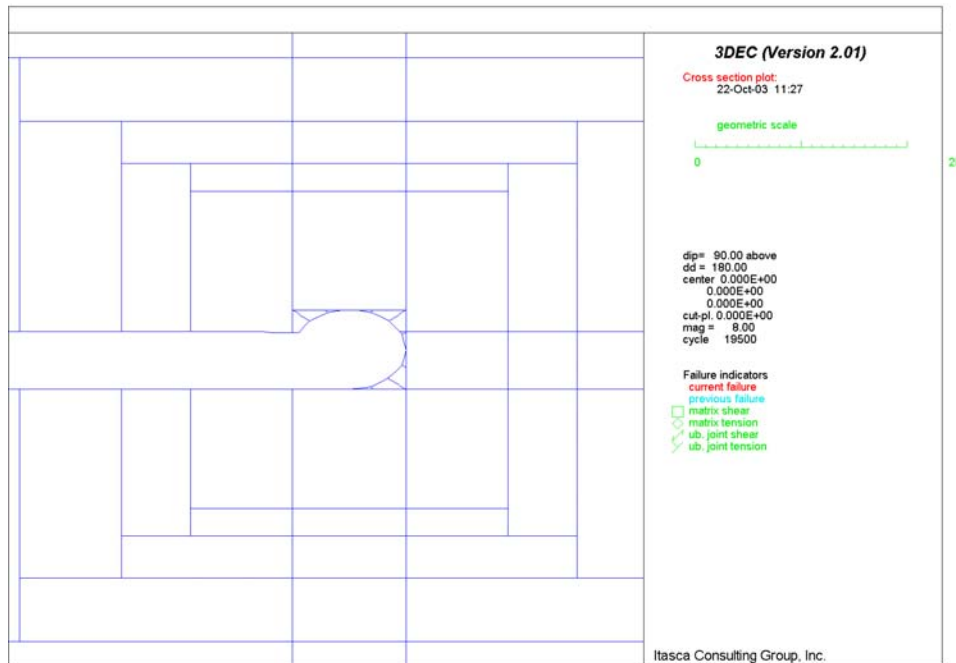


Figure 6-80. Intersection D: Potential Yield Zone in Vertical Section 1 for N. Lith. Cat. 1 Rock after 50 Years of Heating

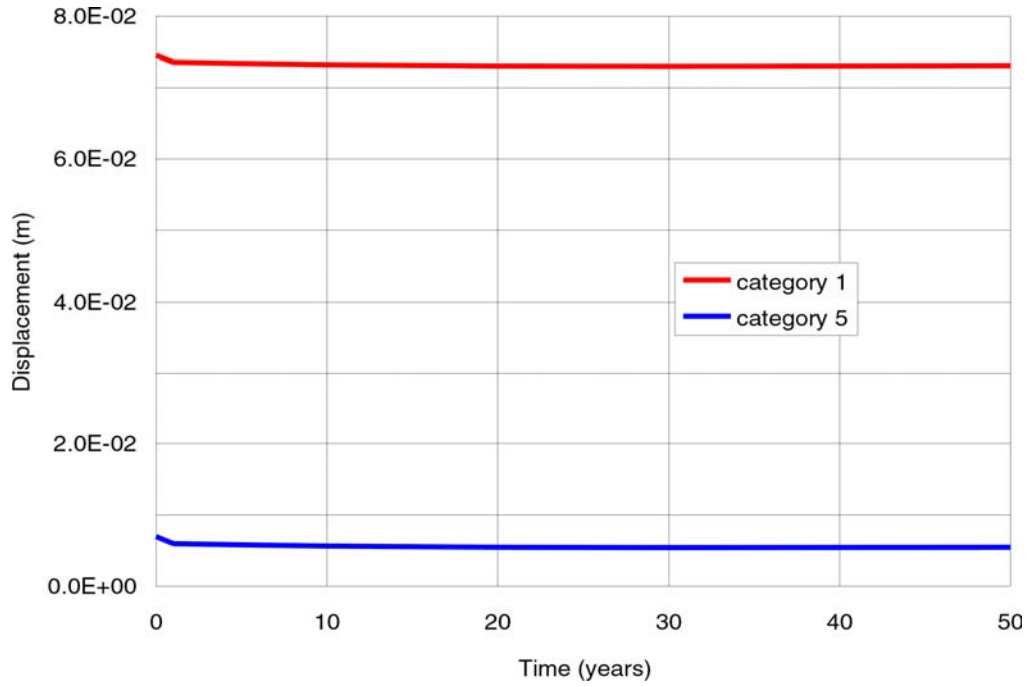


Figure 6-81. Intersection B: Time History of Vertical Displacement at Point 1 for Lith. Rock

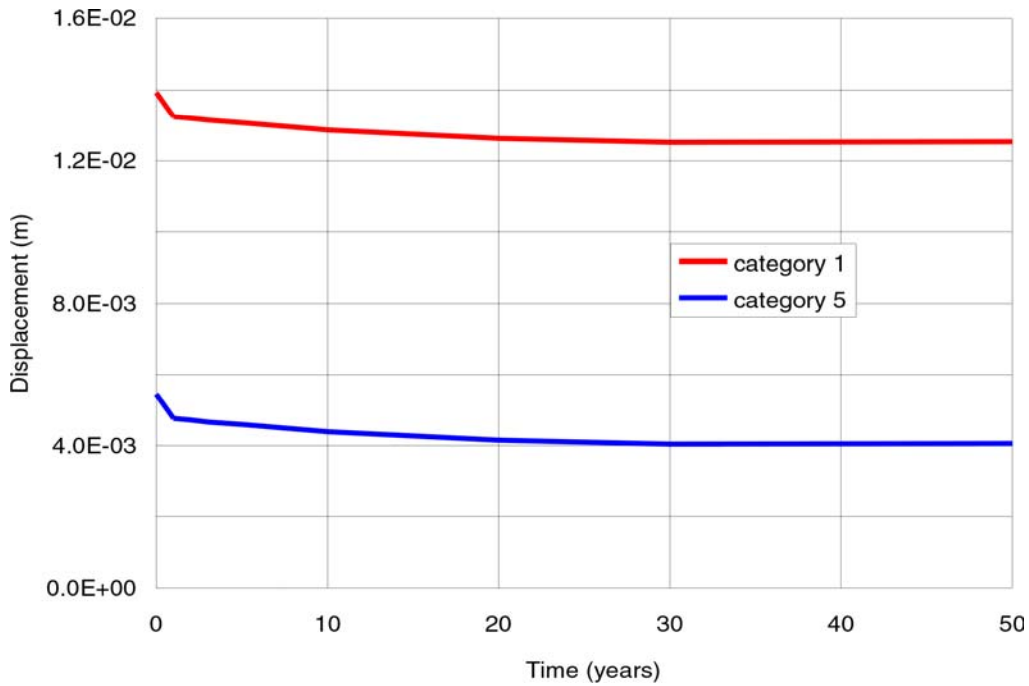


Figure 6-82. Intersection D: Time History of Vertical Closure at Point 1 for N. Lith. Rock

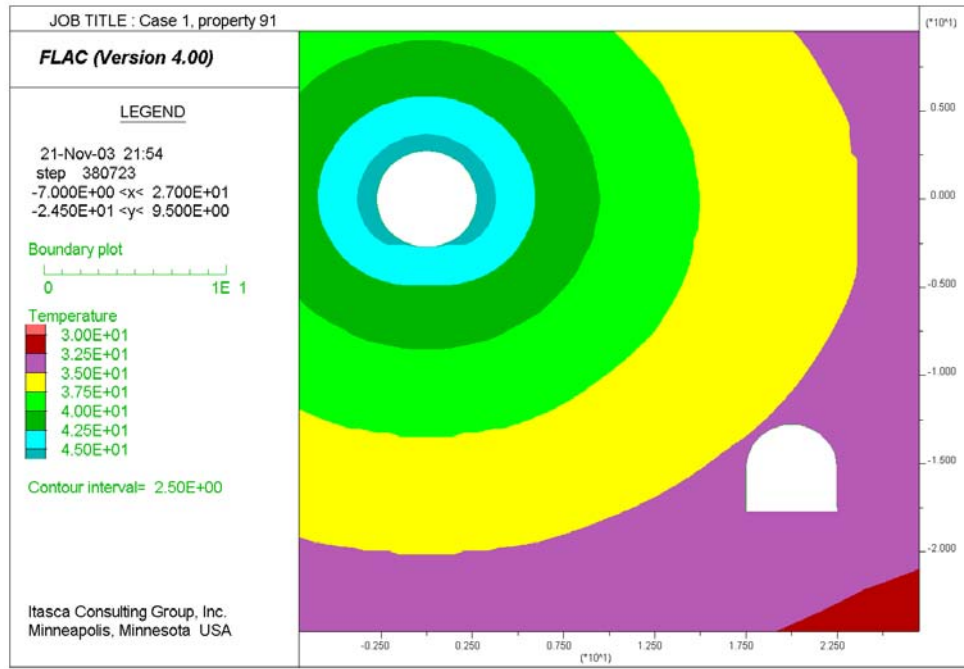


Figure 6-82A. Temperature Contours around Observation Drift after 50 Years of Heating

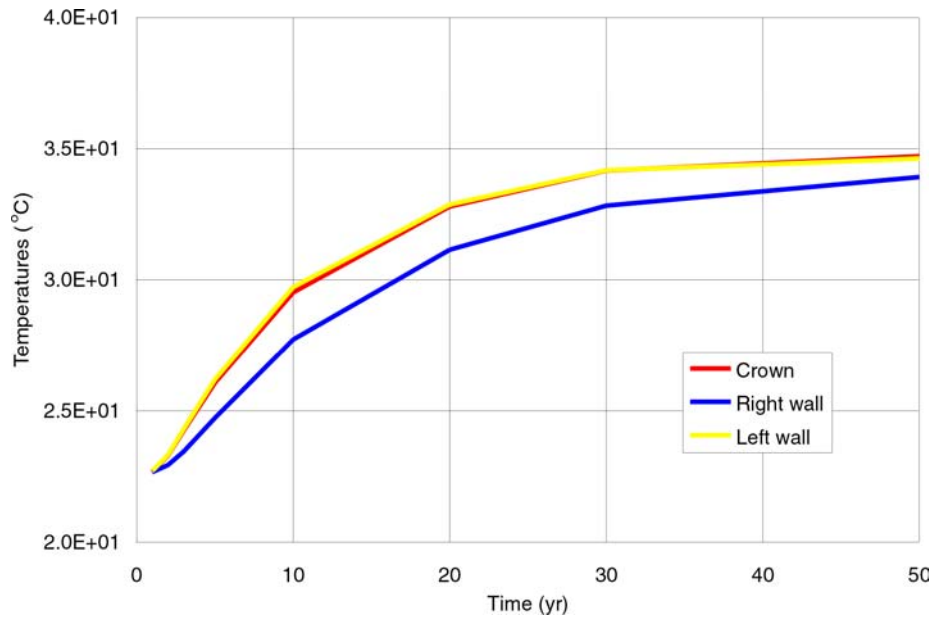


Figure 6-82B. Temperature Histories at Three Points around Observation Drift during 50 Years of Heating

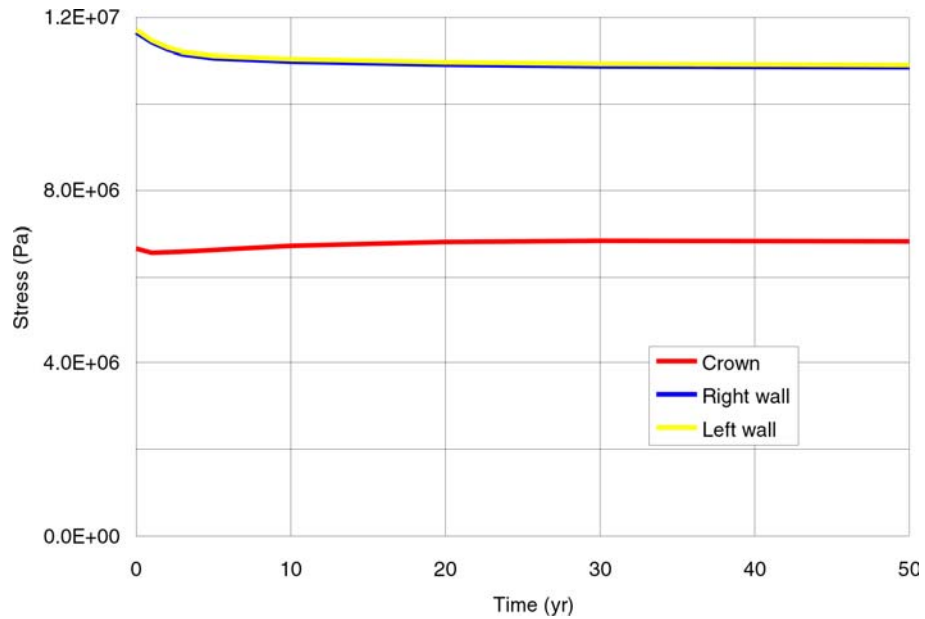


Figure 6-82C. Major Principal Stresses at Three Points around Observation Drift during 50 Years of Heating

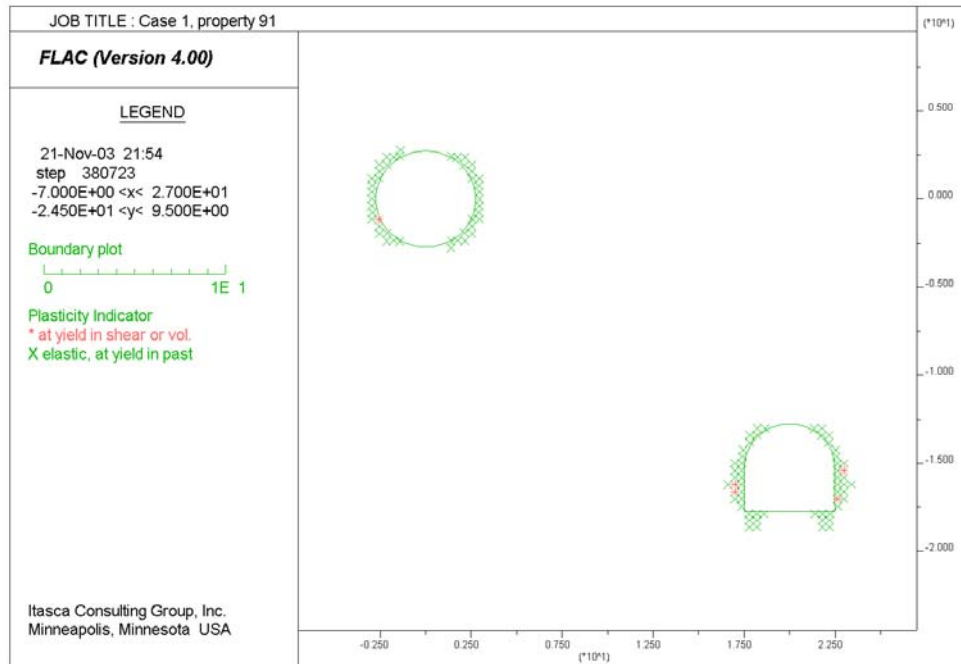


Figure 6-82D. Potential Yield Zone around Observation Drift after 50 Years of Heating

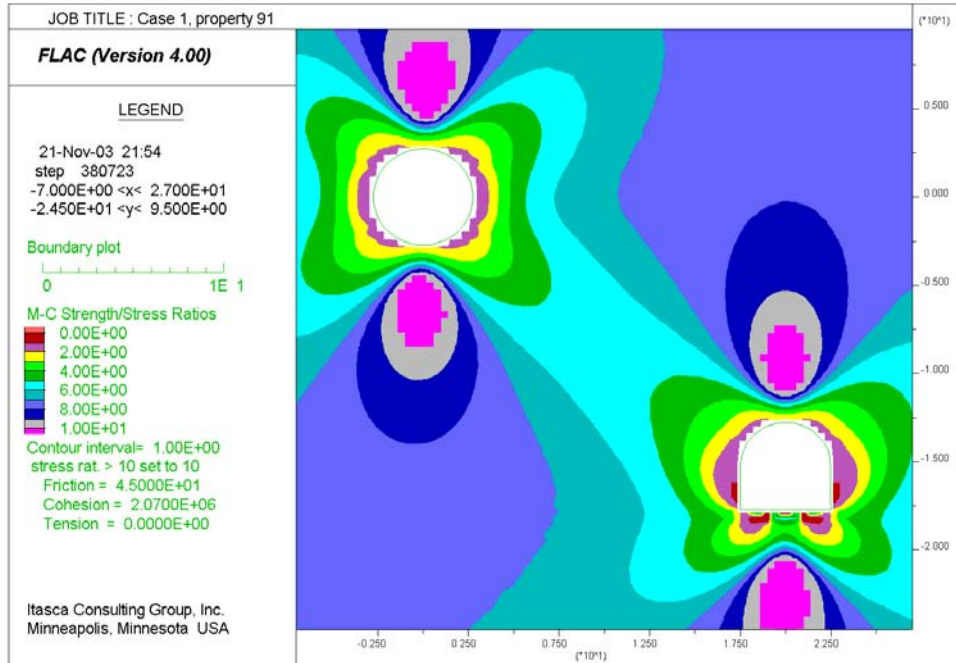


Figure 6-82E. Factor of Safety around Observation Drift after 50 Years of Heating

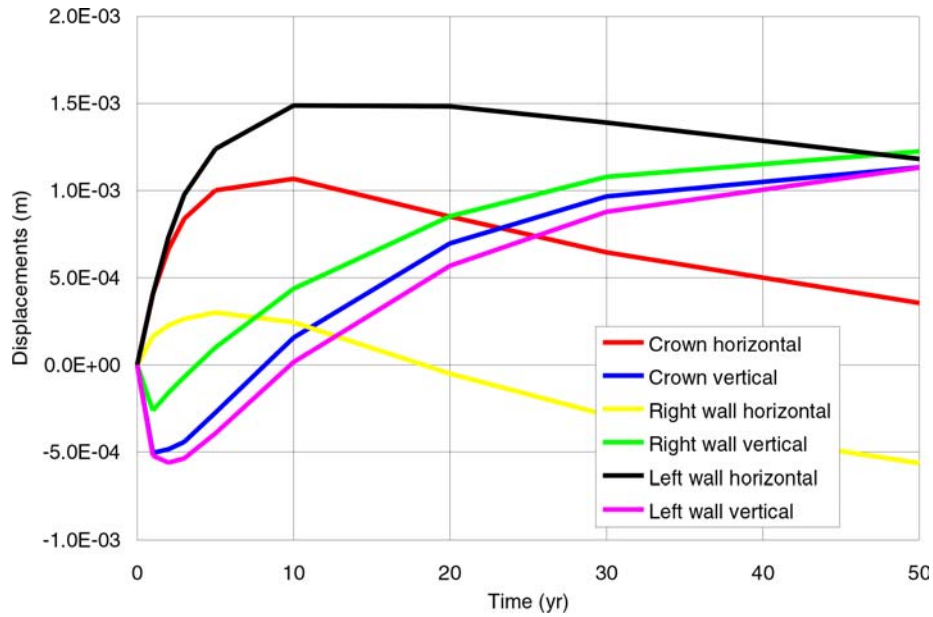


Figure 6-82F. Displacement Histories at Three points around Observation Drift during 50 Years of Heating

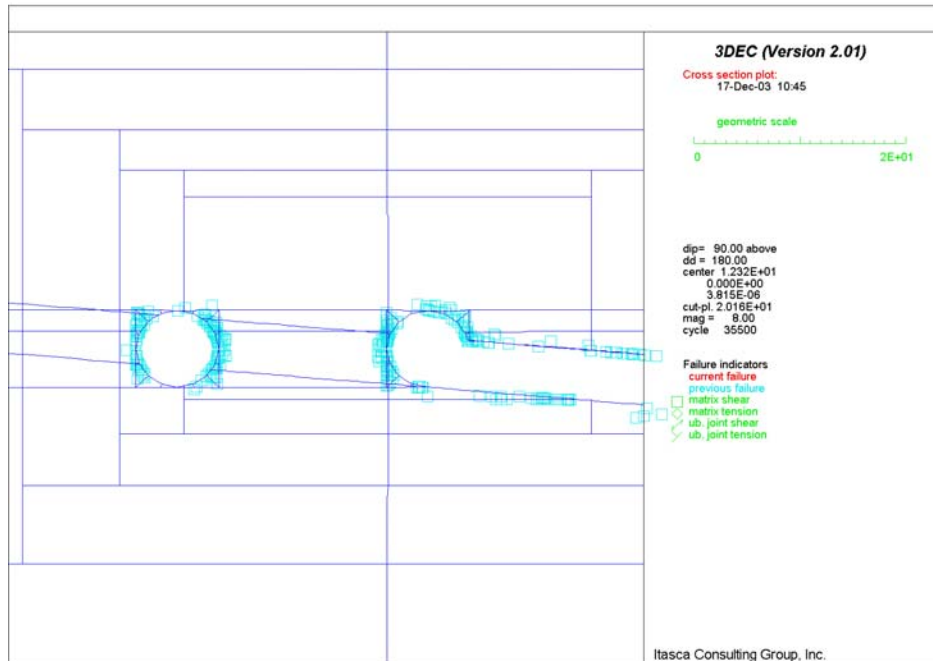


Figure 6-82G. Potential Yield Zone at Intersection between Observation Drift and Exhaust Main in Vertical Section 1 after 50 Years of Heating

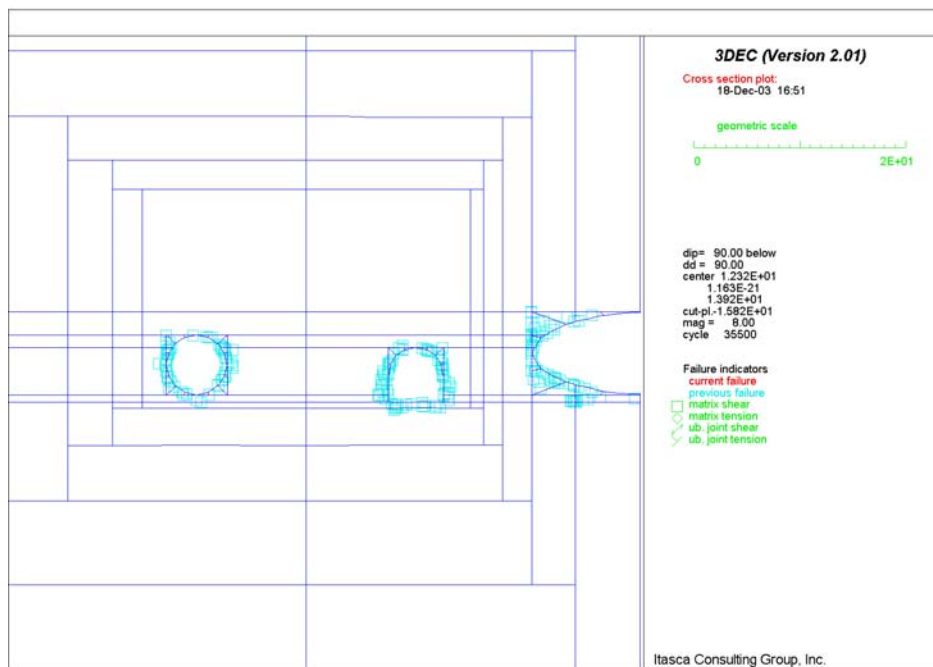


Figure 6-82H. Potential Yield Zone at Intersection between Observation Drift and Exhaust Main in Vertical Section 2 after 50 Years of Heating

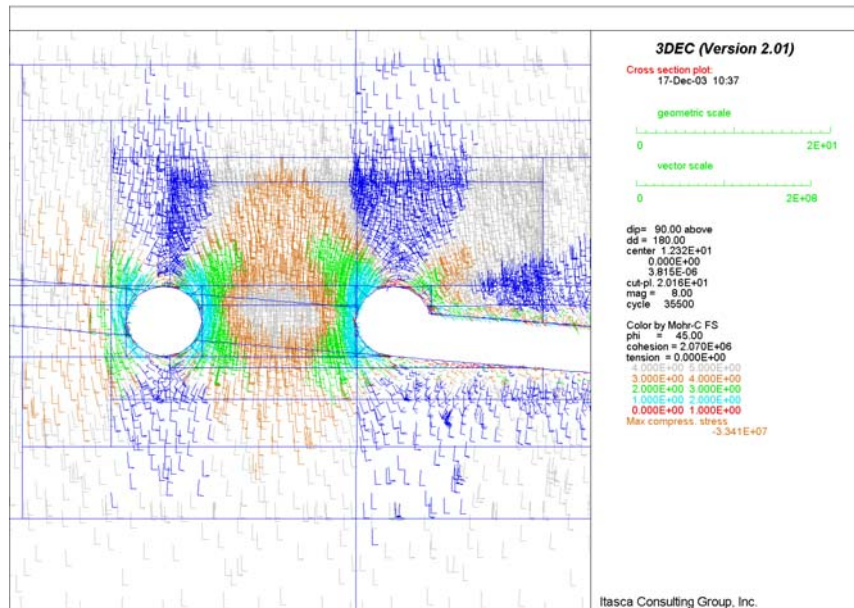


Figure 6-82I. Factor of Safety at Intersection between Observation Drift and Exhaust Main in Vertical Section 1 after 50 Years of Heating

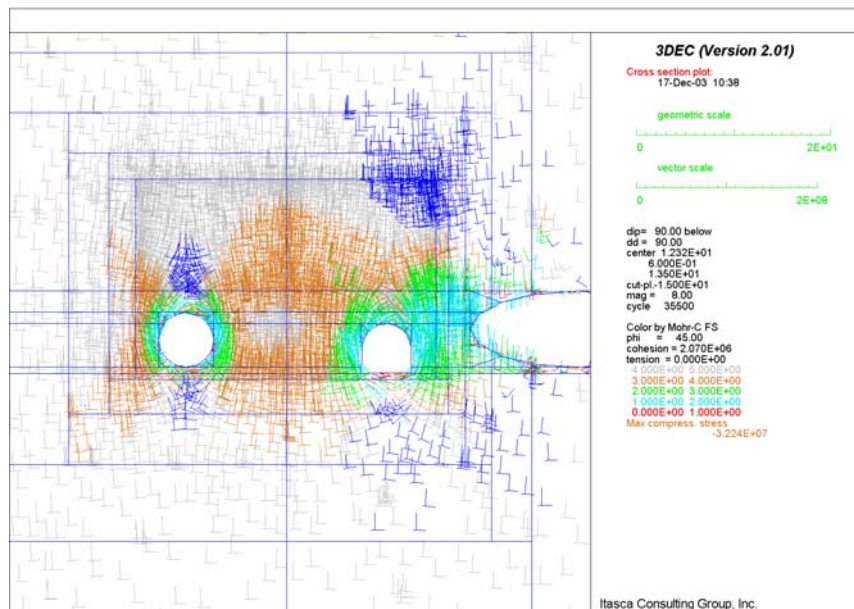


Figure 6-82J. Factor of Safety at Intersection between Observation Drift and Exhaust Main in Vertical Section 2 after 50 Years of Heating

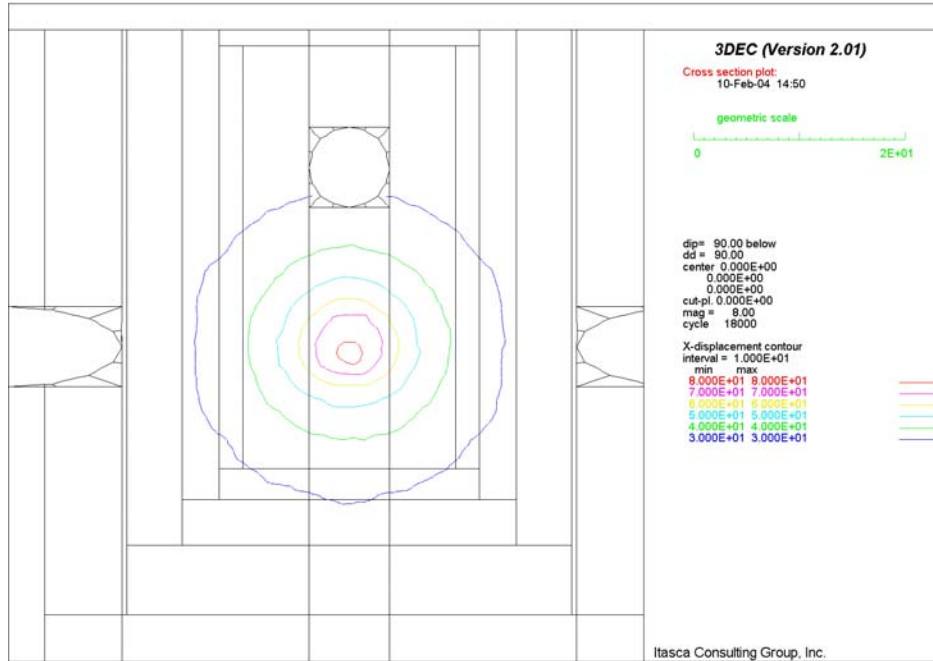


Figure 6-82K. Temperature Field in Vertical Section 1 after 3 Years of Heating at Interburden Area

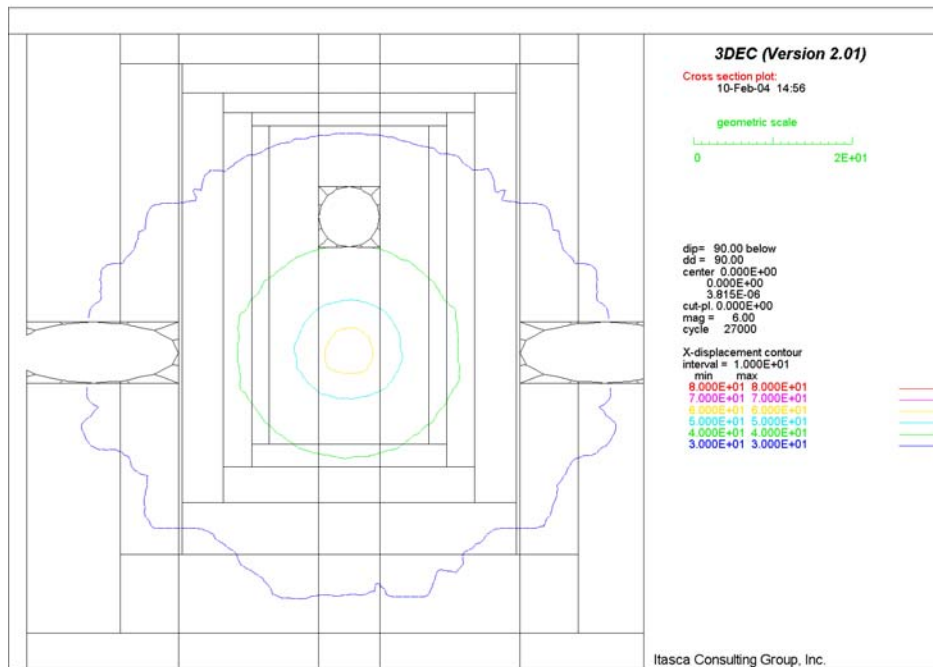


Figure 6-82L. Temperature Field in Vertical Section 1 after 20 Years of Heating at Interburden Area

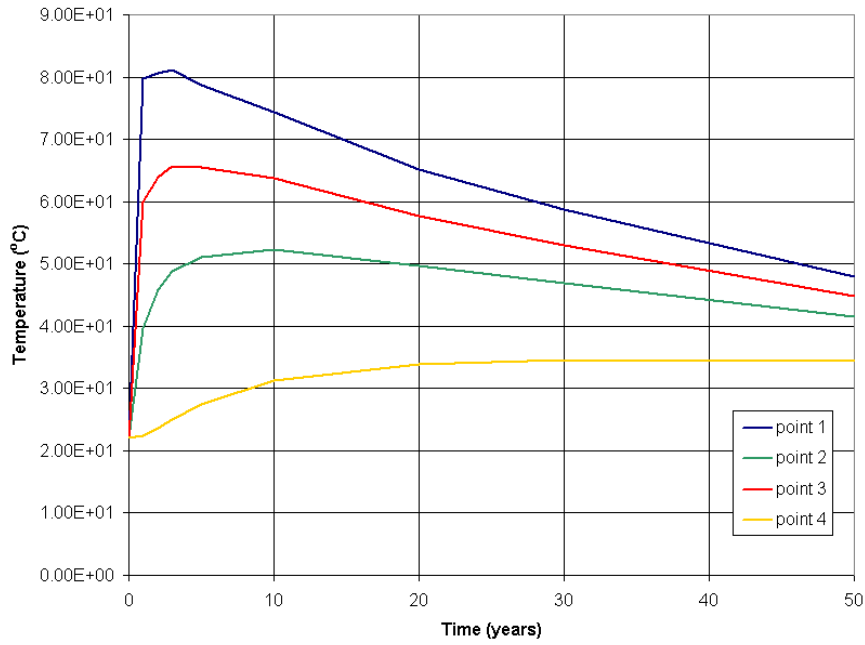


Figure 6-82M. Temperature Histories at Various Points at Interburden Area

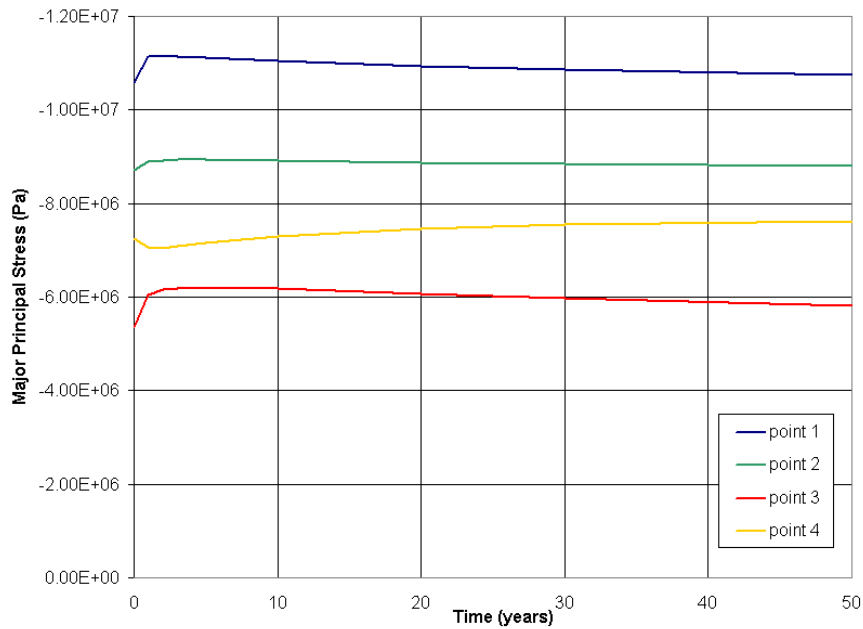


Figure 6-82N. Histories of Major Principal Stresses for Lith. Cat. 1 Rock at Interburden Area

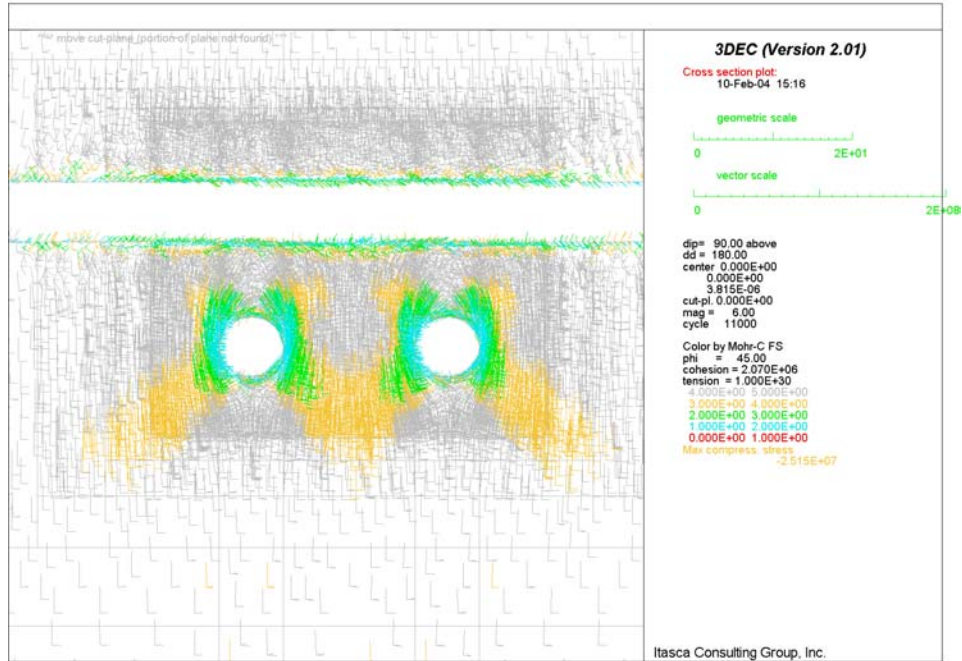


Figure 6-82O. Safety Factor in Vertical Section 1 for Lith. Cat. 1 Rock after 1 Year of Heating at Interburden Area

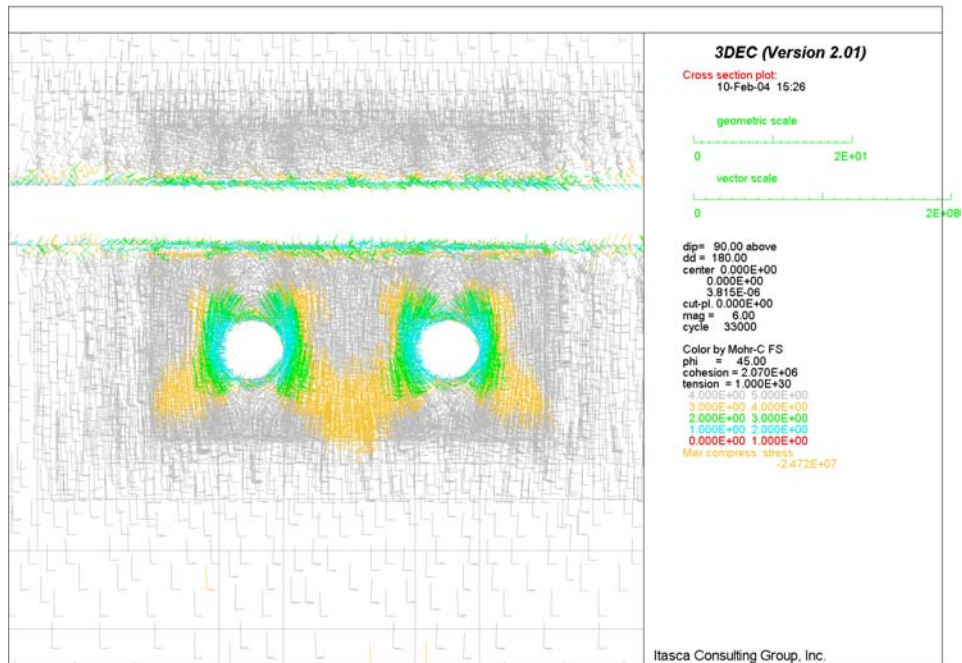


Figure 6-82P. Safety Factor in Vertical Section 1 for Lith. Cat. 1 Rock after 50 Years of Heating at Interburden Area

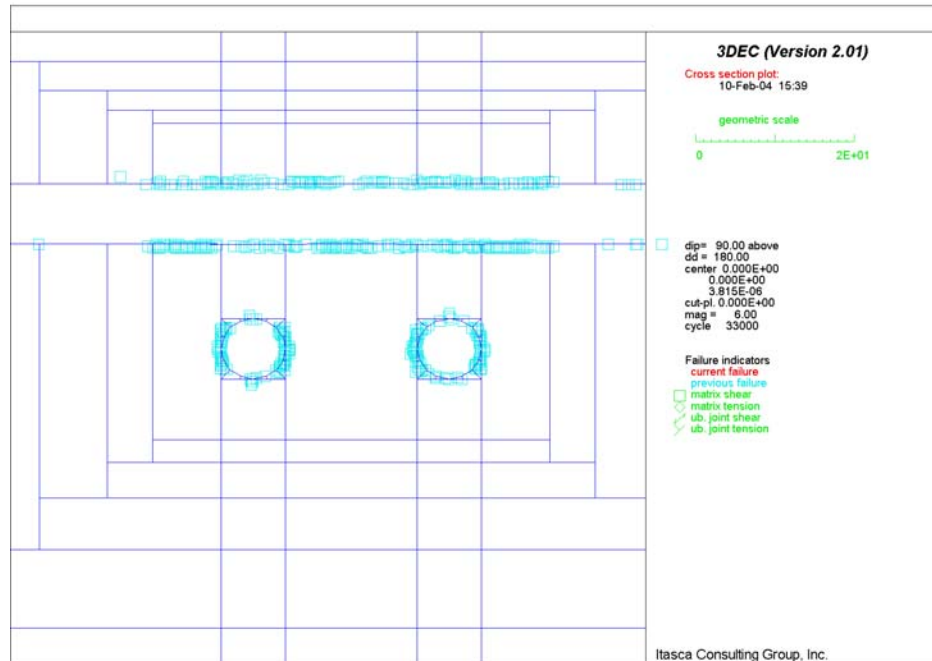


Figure 6-82Q. Potential Yield Zone in Vertical Section 1 for Lith. Cat. 1 after 50 Years of Heating

### 6.5.3.3 Seismic Loading Condition

#### 6.5.3.3.1 Intersections between Access Mains and Turnouts

The non-emplacement excavations including the access main, the turnout and their intersections will be subject to seismic loading during the preclosure period. The stability condition for these underground openings was analyzed for ground motion with a  $10^{-4}$  probability of annual recurrence (i.e., earthquake with 10,000 year return period) (Section 4.1.5). The dynamic analysis was carried out for the intersection at location A (the most critical regarding the size of the span), assuming the intersection to be located in category 1 rock mass (poorest quality), of both the lithophysal and non-lithophysal units.

The results of dynamic analysis are shown in Figures 6-83 through 6-93. Clearly the level of ground shaking due to an earthquake with 10,000 year return period is not expected to cause significant damage to access mains, turnouts, and intersections between access mains and turnouts. The continuum analysis indicates that the extent of inelastic deformation in the surrounding rock mass and, particularly, in the pillar between the two drifts, does not increase with respect to the volume of the rock mass yielded under static conditions (compare Figures 6-83 through 6-86 with Figures 6-28, 6-29, 6-46, and 6-47). During the passage of the seismic waves, the stresses in the model oscillate. The maximum transient stress change caused by an earthquake with 10,000 year return period is approximately 1.1 MP and 2.1 MPa for the lithophysal and non-lithophysal units, respectively. Note that the stress changes are calculated based on Eq. 6-7, without multiplier 2, assuming the velocity amplitude to be 0.5 m/s. However, at the end of the simulation, when oscillations die out, the stresses return to the state that existed

prior to the shaking. Figures 6-87 and 6-88 indicate that there is no permanent stress change, or stress redistribution, indicating loosening or instability of a portion of the rock mass. The stress fields at the end of simulation in the lithophysal rock mass are colored by: a) the factor-of-safety with respect to the Mohr-Coulomb yield condition; and b) indication of tensile and compressive stresses, as shown in Figures 6-89 and 6-90, respectively.

Inspecting these figures and comparing them with static results, it can be concluded that an earthquake with 10,000 year return period does not: a) cause significant, permanent change in the factor-of-safety with respect to the Mohr-Coulomb yield condition throughout the rock mass; or b) increase the volume of the rock mass subject to tensile stresses. The average stresses in the pillar between the drifts are almost unchanged as shown in Figure 6-91. All three components of the velocity histories were monitored during the simulations at four points in the roof and the walls of the intersection. The histories at point A in the roof, shown in Figure 6-92, are almost the same (offset for traveling time from the boundary to the history point) as applied velocities at the bottom boundary. The accumulation of permanent displacement due to inelastic deformation cannot be detected. Such an observation is confirmed by the plot of an increment of the residual displacement at the end of the dynamic simulation as shown in Figure 6-93. The maximum displacement increments are negligible.

Seismic load due to an earthquake with 10,000 year return period does not result in a significant increase in damage of the rock mass around the drifts, nor an increase in the permanent displacements. The dynamic analysis of global stability of the intersections was carried out using the continuum models.

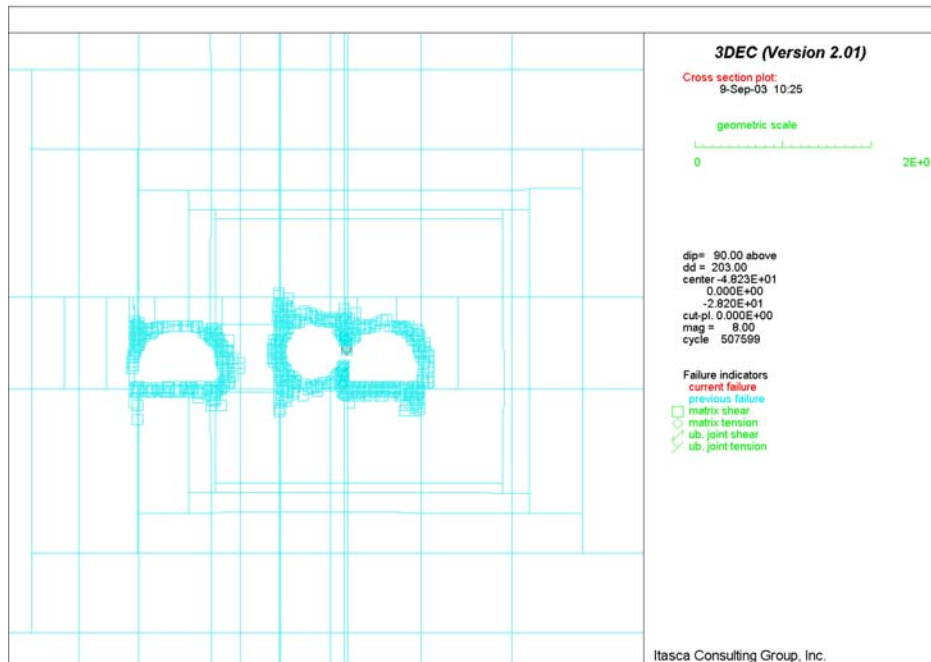


Figure 6-83. Intersection A: Potential Yield Zone in Vertical Section 2 for Lith. Cat. 1 Rock under In Situ and Seismic Loads

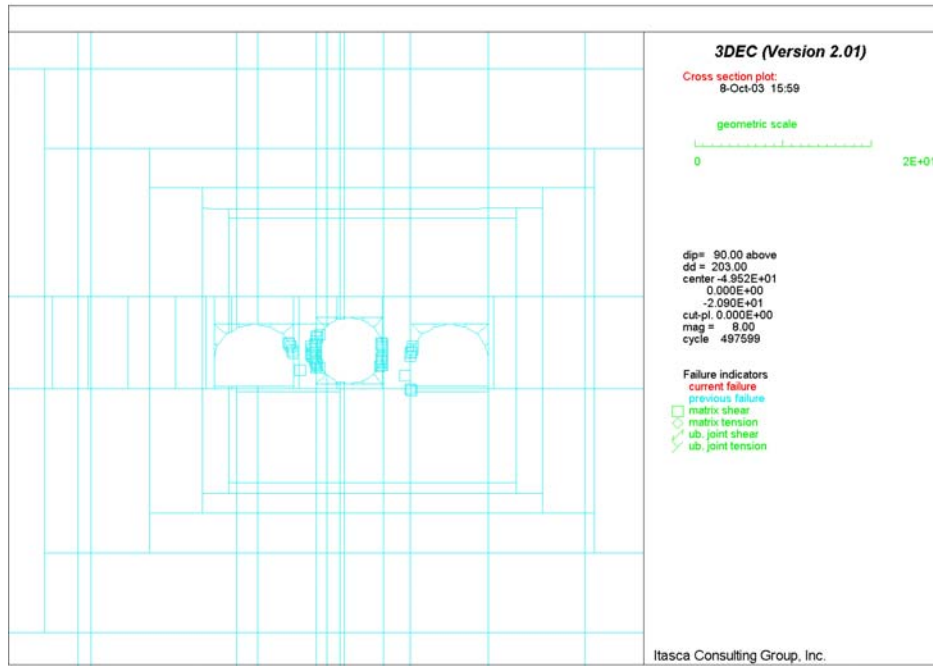


Figure 6-84. Intersection A: Potential Yield Zone in Vertical Section 2 for N. Lith. Cat. 1 Rock under In Situ and Seismic Loads

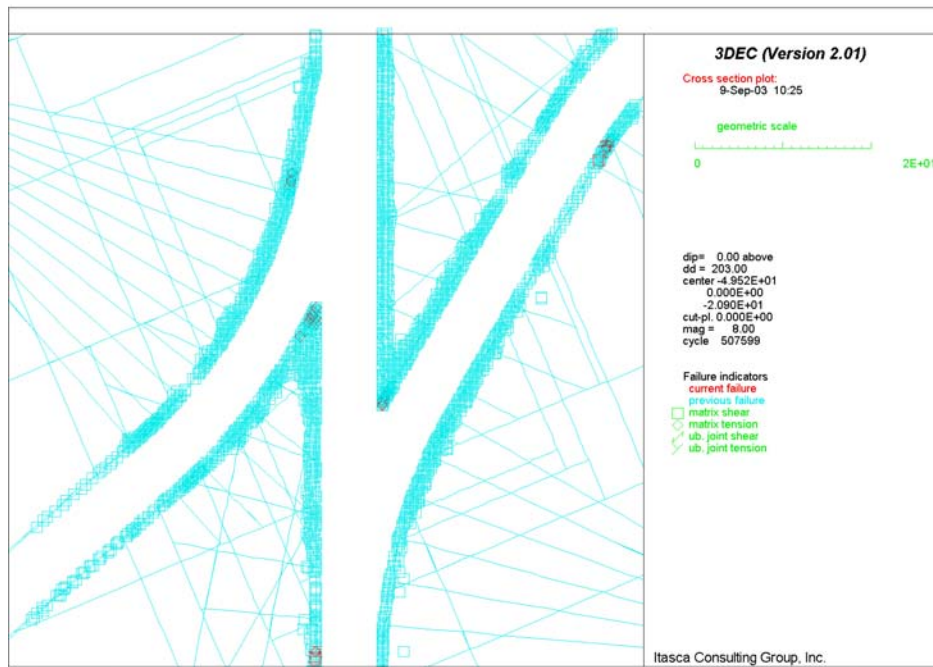


Figure 6-85. Intersection A: Potential Yield Zone in Horizontal Section for Lith. Cat. 1 Rock under In Situ and Seismic Loads

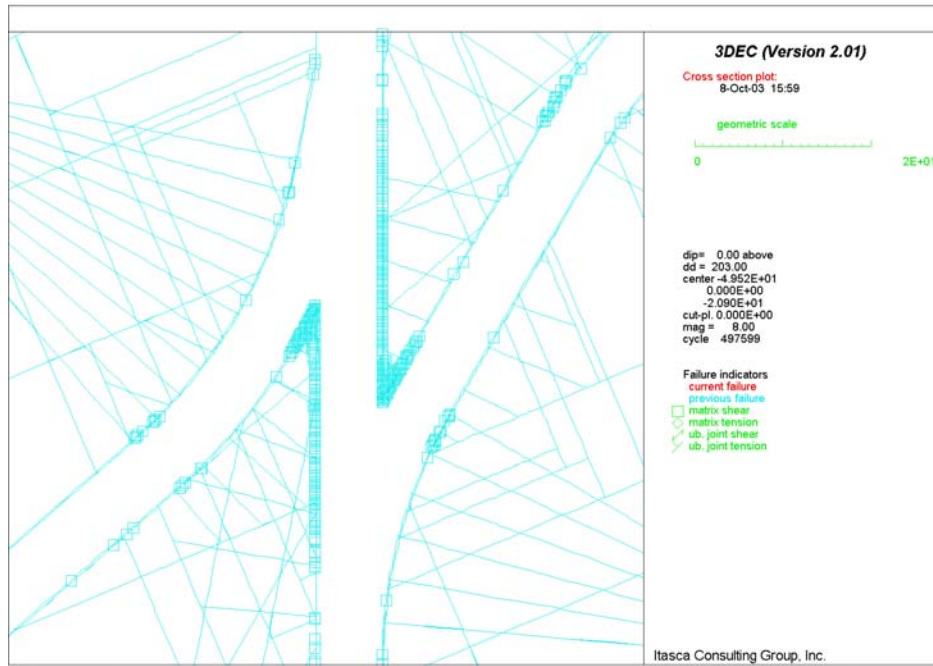


Figure 6-86. Intersection A: Potential Yield Zone in Horizontal Section for N. Lith. Cat. 1 Rock under In Situ and Seismic Loads

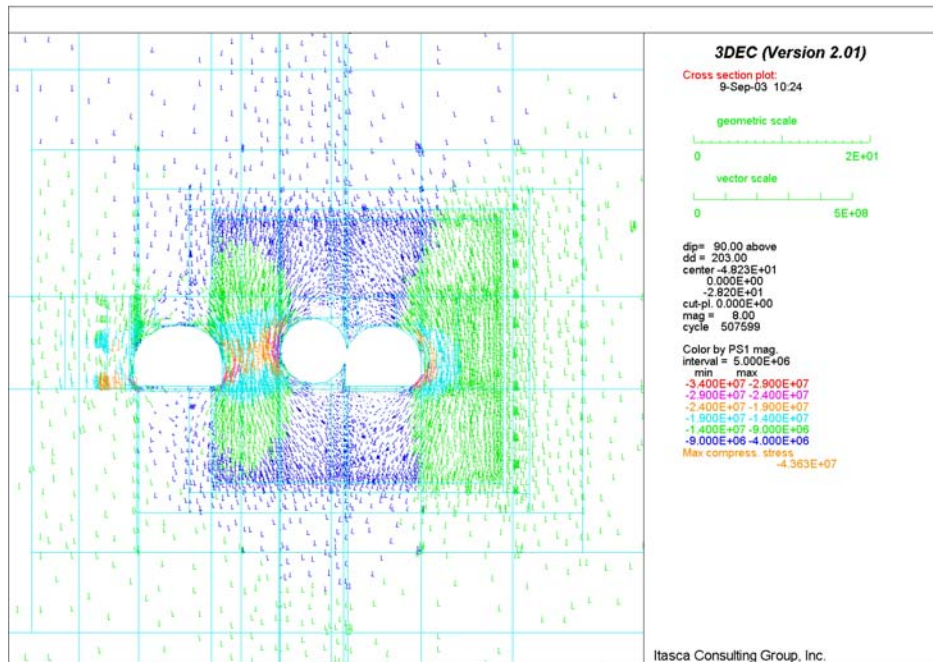


Figure 6-87. Intersection A: Stress Field in Vertical Section 2 for Lith. Cat. 1 Rock under In Situ and Seismic Loads

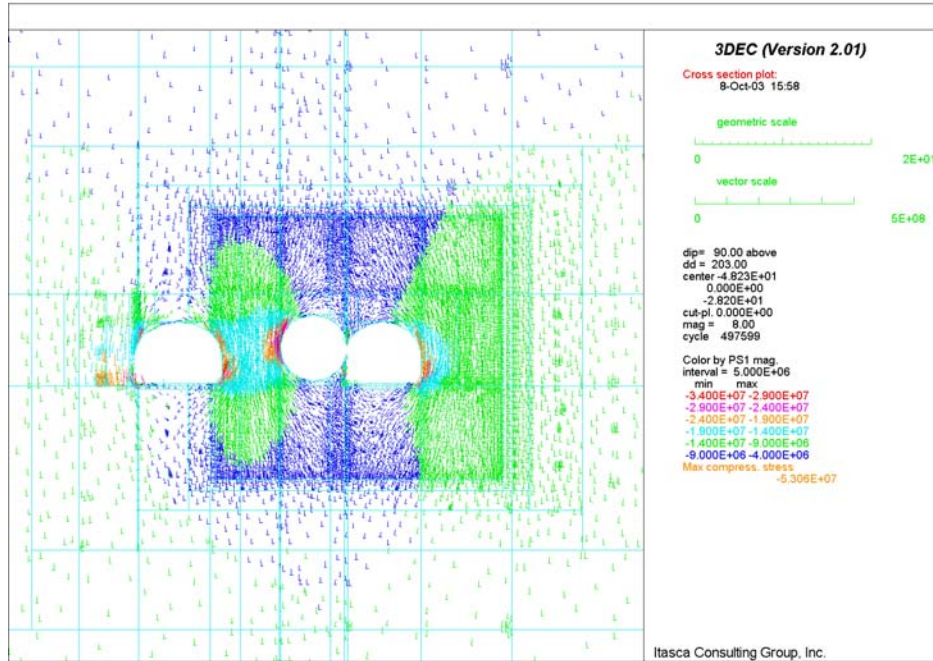


Figure 6-88. Intersection A: Stress Field in Vertical Section 2 for N. Lith. Cat. 1 Rock under In Situ and Seismic Loads

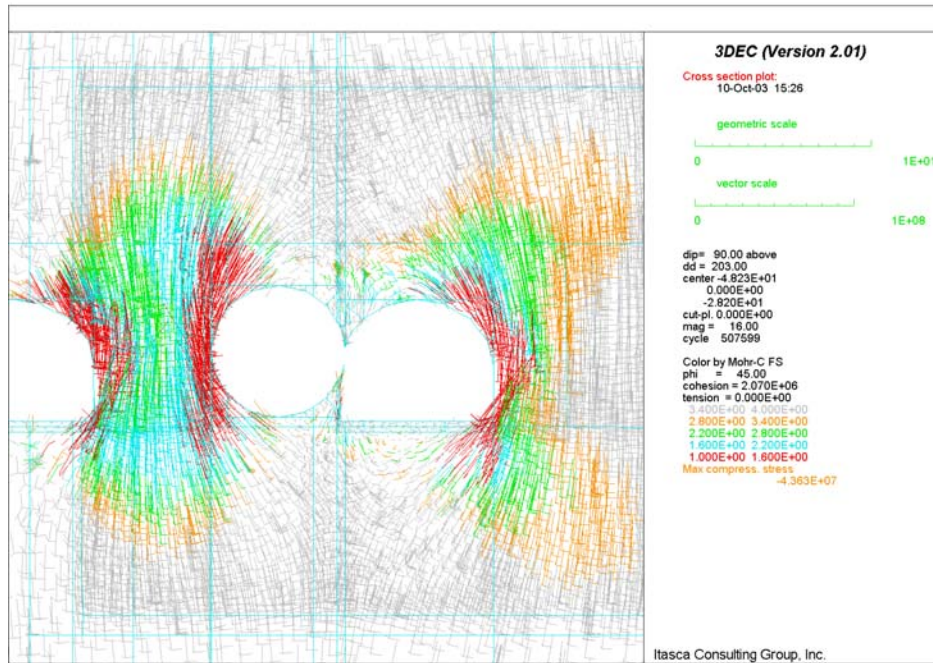


Figure 6-89. Intersection A: Factor of Safety in Vertical Section 2 for Lith. Cat. 1 Rock under In Situ and Seismic Loads

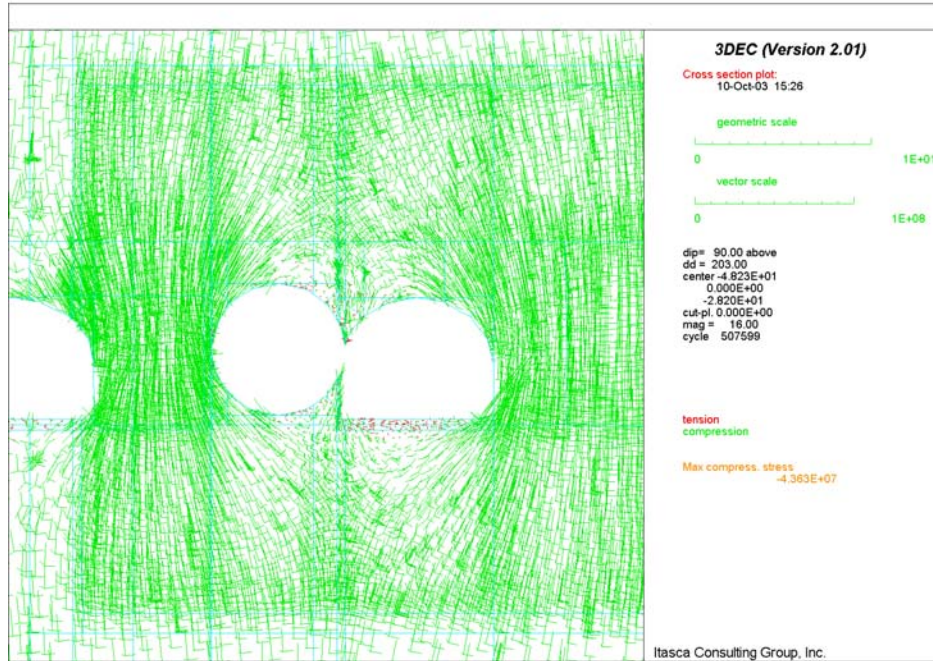


Figure 6-90. Intersection A: Compressive and Tensile Stresses in Vertical Section 2 for Lith. Cat. 1 Rock under In Situ and Seismic Loads

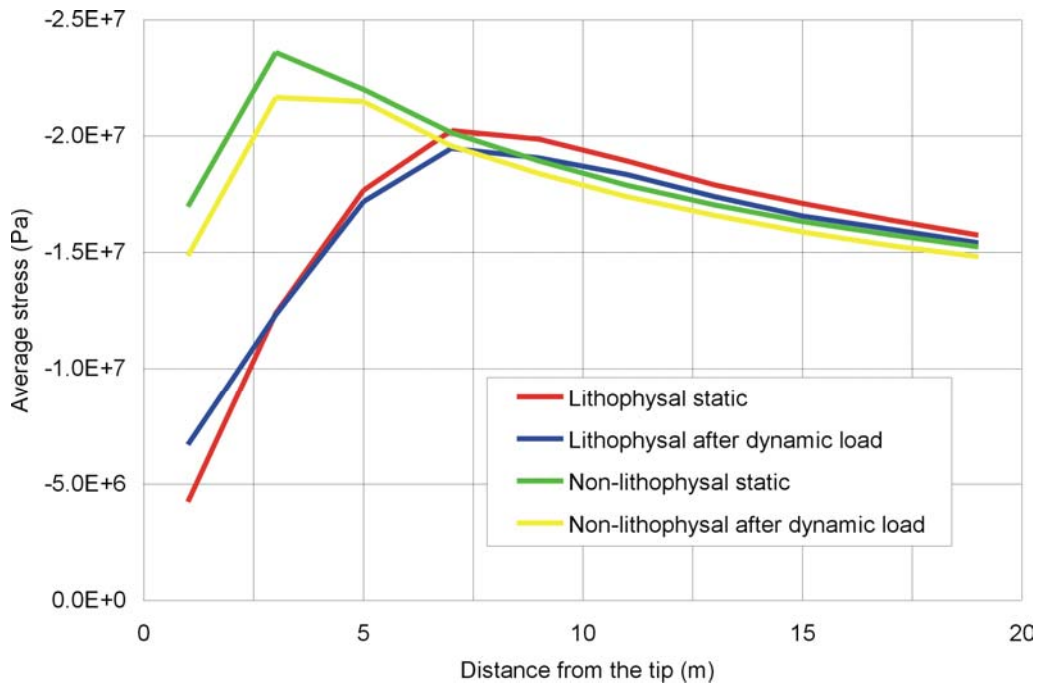


Figure 6-91. Intersection A: Average Pillar Stress vs. Distance from Pillar Tip under In Situ and Seismic Loading

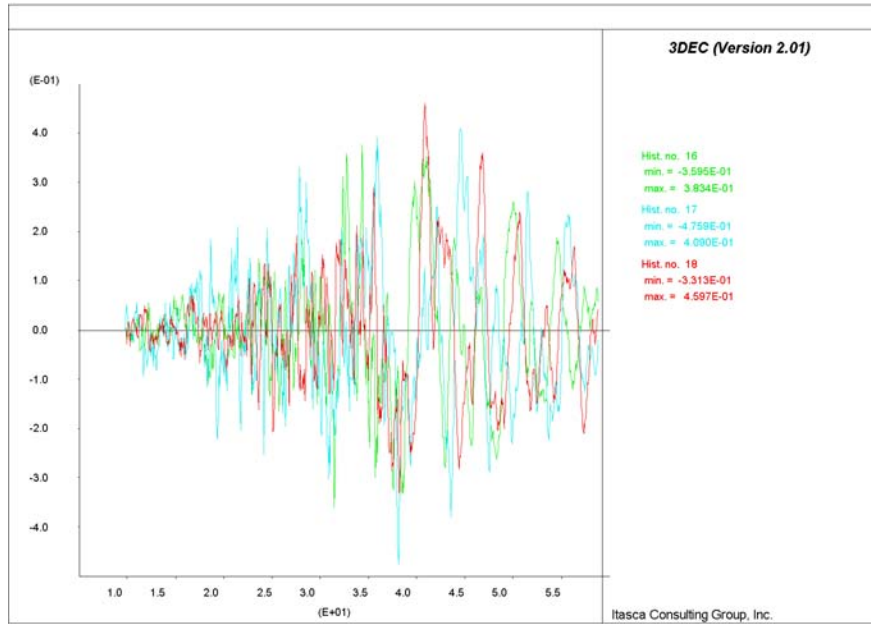


Figure 6-92. Intersection A: Velocity Histories in x, y and z Direction near Point A for Lith. Cat. 1 Rock

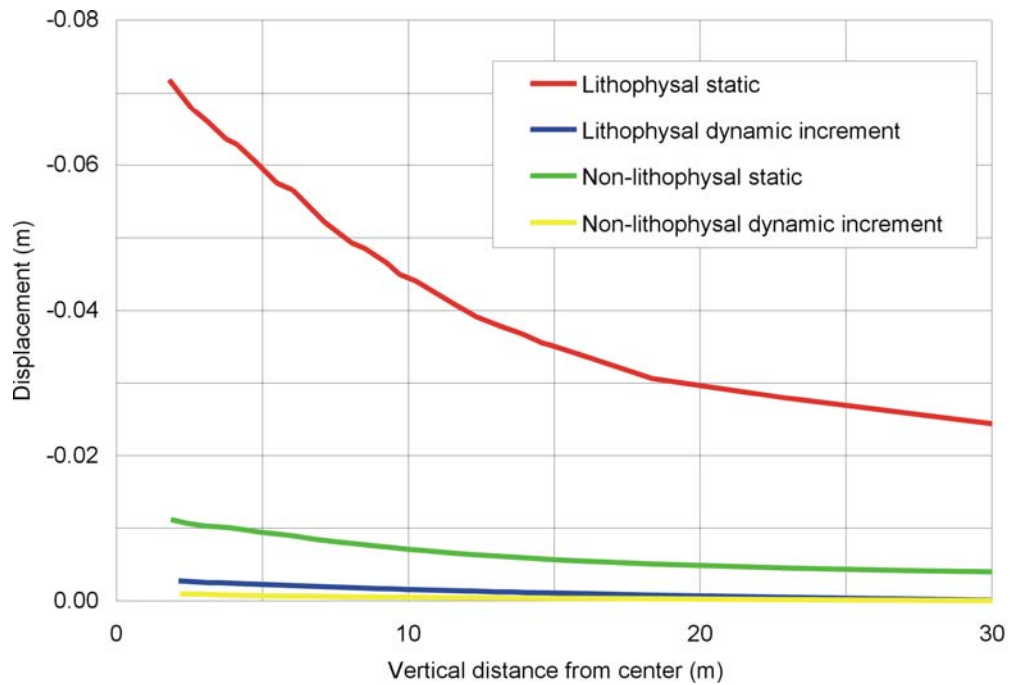


Figure 6-93. Intersection A: Vertical Displacements along Vertical Line through Point A under Static and Seismic Loads

### 6.5.3.3.2 Intersections between Exhaust Mains and Emplacement Drifts

The results of dynamic simulation of the intersections between exhaust mains and emplacement drifts for seismic ground motion with 10,000 year return period are shown in Figures 6-94 through 6-101. Seismic loading was applied on the model at the initial state, after excavation of the drifts but before heating began.

The results are presented for category 1 in both lithophysal (location B) and non-lithophysal (location D) rock masses. The dynamic load causes insignificant additional yielding, which was caused by stress oscillations. After completion of the dynamic simulation, the models for all simulated cases are stable. There is no indication of permanent stress redistribution or destressing of portions of rock mass indicating grounds prone to rockfall. Velocity histories were recorded during the simulations at a number of points throughout the model, particularly at the wall and back of the intersection. The histories near point 1 (located at the intersection of longitudinal axes of exhaust main and emplacement drift) in the intersections at locations B and D are shown in Figures 6-94 and 6-95, respectively. These histories are almost identical to the velocity histories applied at the base of the model due to the vertically propagating seismic wave. Thus, the model deforms elastically under seismic load. There is no indication of accumulation of irreversible, plastic deformation.

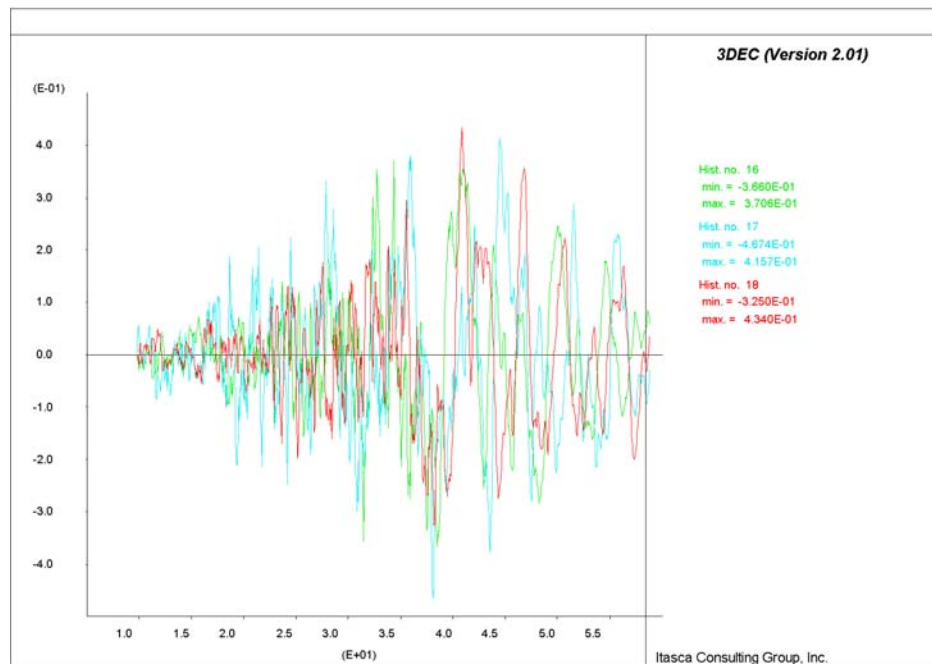


Figure 6-94. Intersection B: Velocity Histories in X, Y and Z Directions near Point 1 for Lith. Cat. 1 Rock

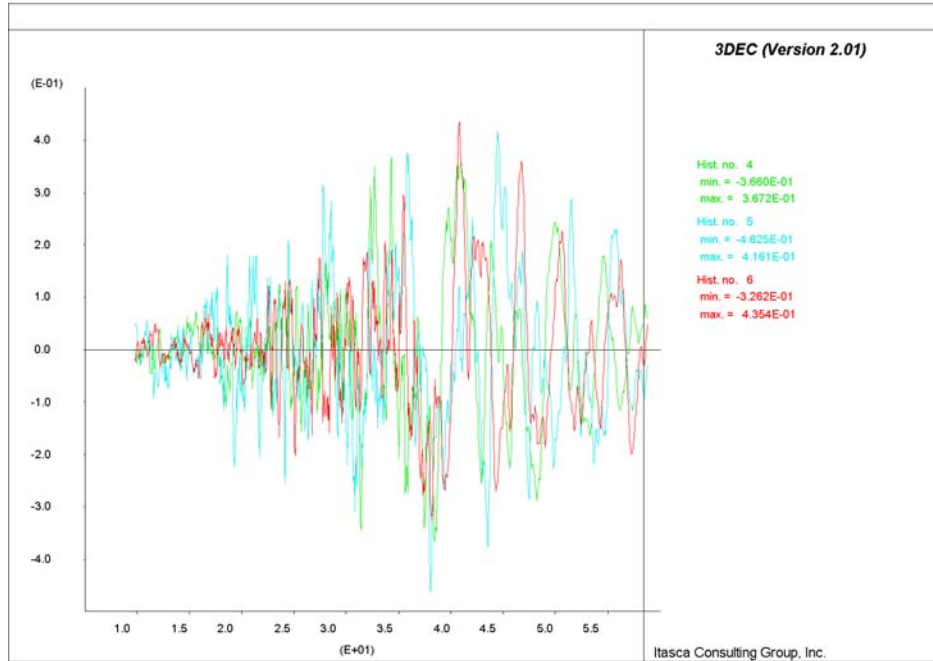


Figure 6-95. Intersection D: Velocity Histories in X, Y and Z Directions near Point 1 for N. Lith. Cat. 1 Rock

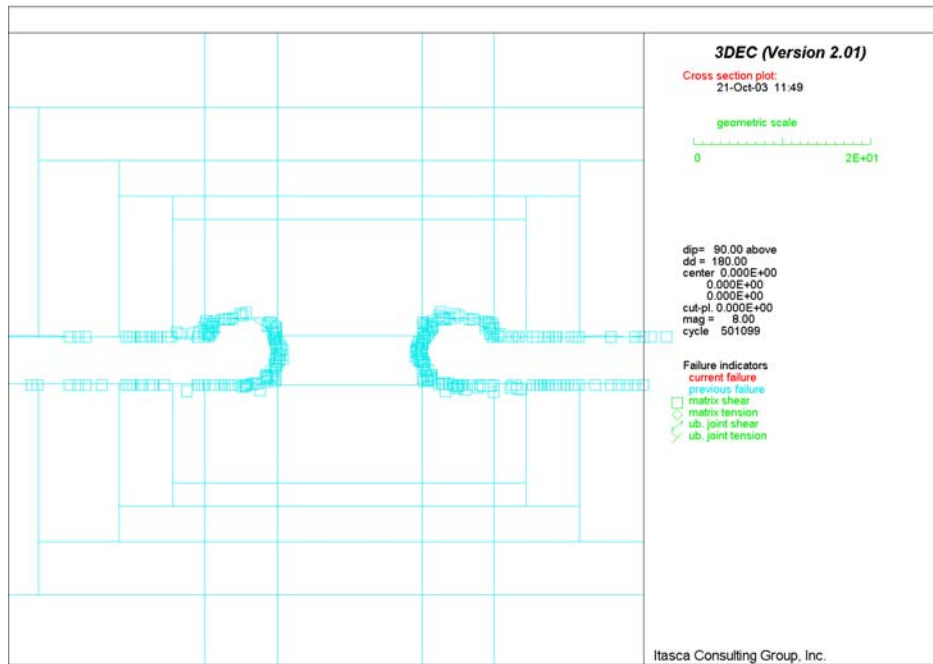


Figure 6-96. Intersection B: Potential Yield Zone in Vertical Section 1 for Lith. Cat. 1 Rock under In Situ and Seismic Loads

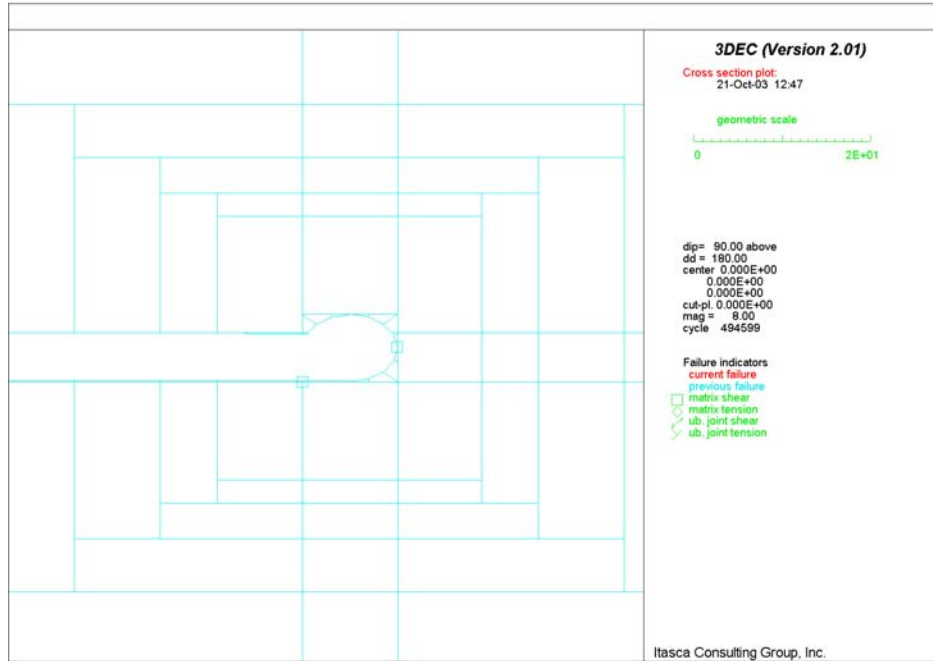


Figure 6-97. Intersection D: Potential Yield Zone in Vertical Section 1 for N. Lith. Cat. 1 Rock under In Situ and Seismic Loads

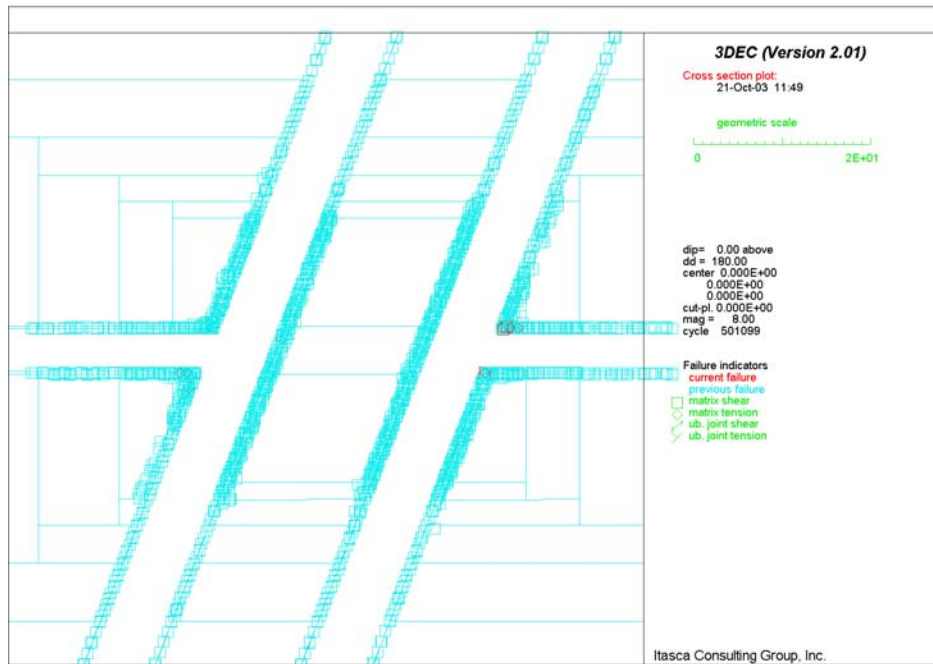


Figure 6-98. Intersection B: Potential Yield Zone in Horizontal Section for Lith. Cat. 1 Rock under In Situ and Seismic Loads

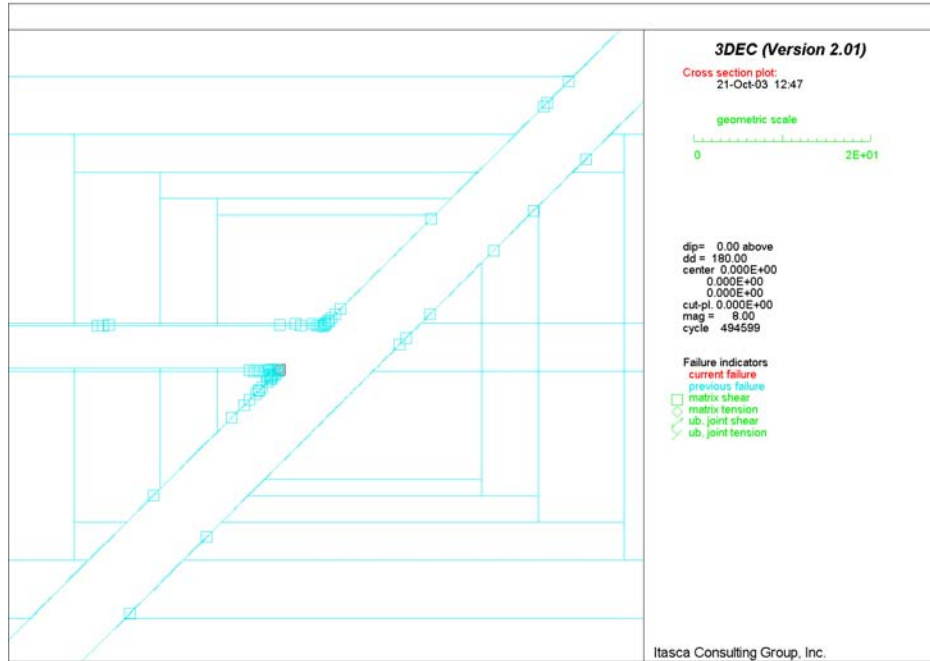


Figure 6-99. Intersection D: Potential Yield Zone in Horizontal Section for N. Lith. Cat. 1 Rock under In Situ and Seismic Loads

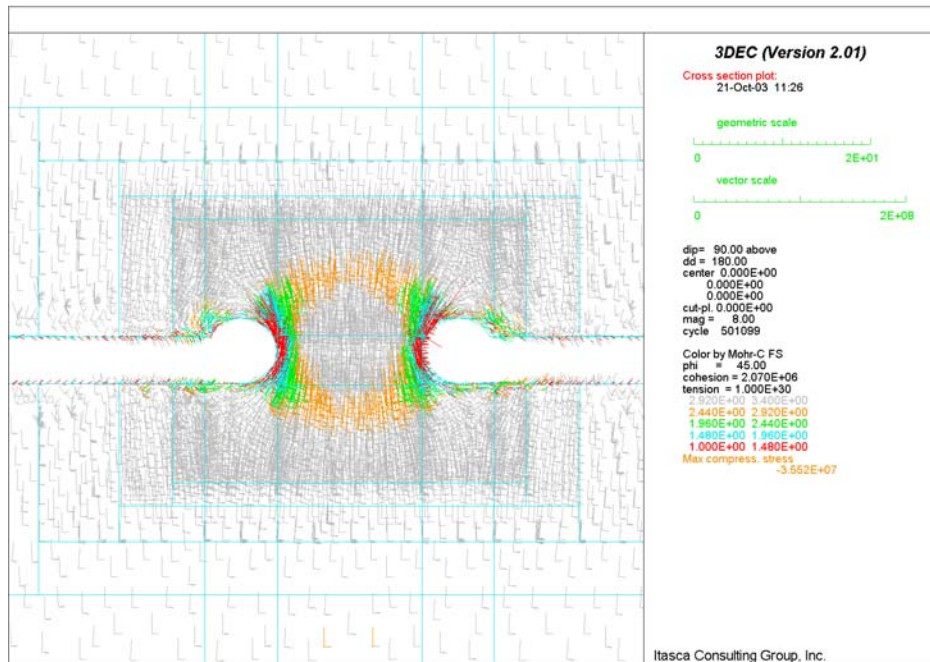


Figure 6-100. Intersection B: Factor of Safety in Vertical Section 1 for Lith. Cat. 1 Rock under In Situ and Seismic Loads

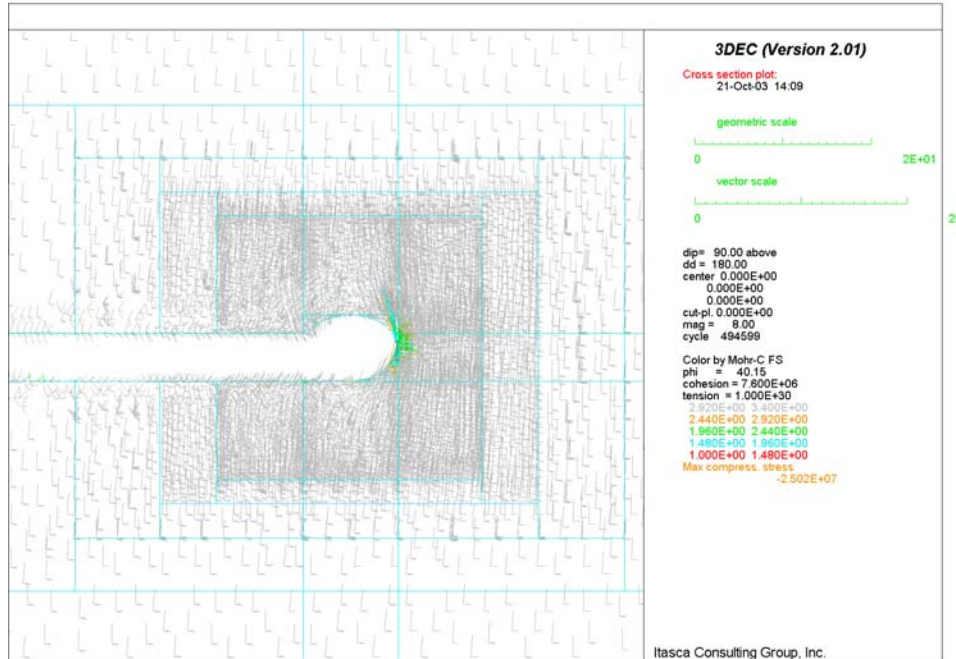


Figure 6-101. Intersection D: Factor of Safety in Vertical Section 1 for N. Lith. Cat. 1 Rock under In Situ and Seismic Loads

### 6.5.3.3.3 Observation Drift

The observation drift was analyzed for seismic loading due to 10,000-yr ground motion in both typical cross-section and at the intersection between the observation drift and the exhaust main. The results are shown in Figures 6-101A to 6-101H. Seismic load causes insignificant increase in damage around the observation drift (compare Figures 6-101A, 6-101E and 6-101F with Figures 6-66C, 6-66G and 6-66H), but there is no indication of large-scale instability. A preclosure level of ground motion could cause some rockfall resulting from shaking down of loose blocks, but designed ground support will be sufficient to prevent most of such rockfall. The velocity histories in the tunnel crown (shown in Figure 6-101C) are almost identical to the velocity histories of the incoming seismic wave. There is no amplification of the velocities due to interaction of the wave with the excavations. The velocities indicate predominantly elastic response. The histories of the principal stress magnitudes (Figure 6-101D) are recorded in the crown and the walls of the observation drift. Variation of the major principal stress in the crown of the observation drift is smaller than the variation of the major principal stress in the walls. The major principal stress in the crown of the tunnel is horizontal and is shielded by the tunnel from the seismic wave propagating vertically upward. Fluctuations of the major principal stresses in the drift walls, which are vertical, are direct consequence of the passage of the P-wave (see comparison between the history of the vertical component of the velocity in Figure 6-101C with histories of the major principal stresses in the walls shown in Figure 6-101D). However, a trend of stress decrease at the points on the walls of the observation drift, within the region that is yielding plastically, can be observed in Figure 6-101D: the major principal stress decreases from approximately 12 MPa to 10 MPa. Seismic load causes some permanent stress redistribution that results in a small increase in the size of the plastic region.

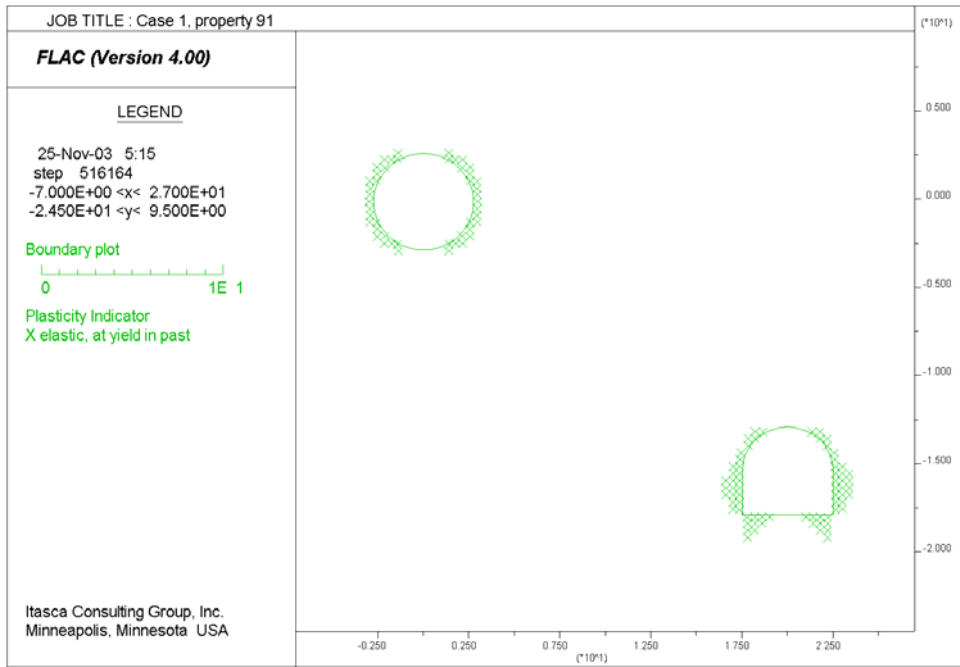


Figure 6-101A. Potential Yield Zone around Observation Drift after Seismic Shaking

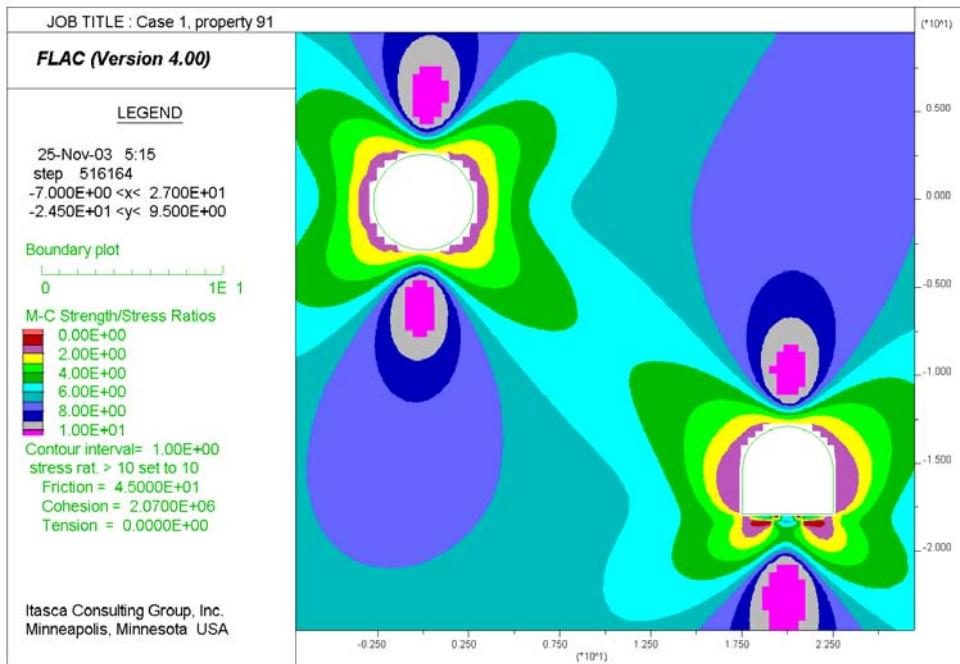


Figure 6-101B. Factor of Safety around Observation Drift after Seismic Shaking

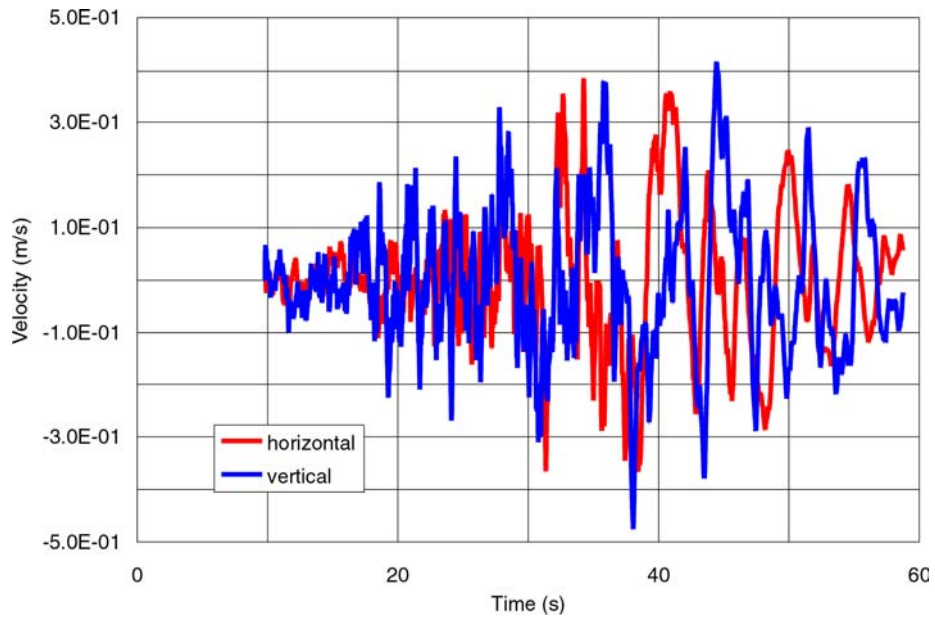


Figure 6-101C. Velocity Histories of Point at Crown of Observation Drift during Seismic Shaking

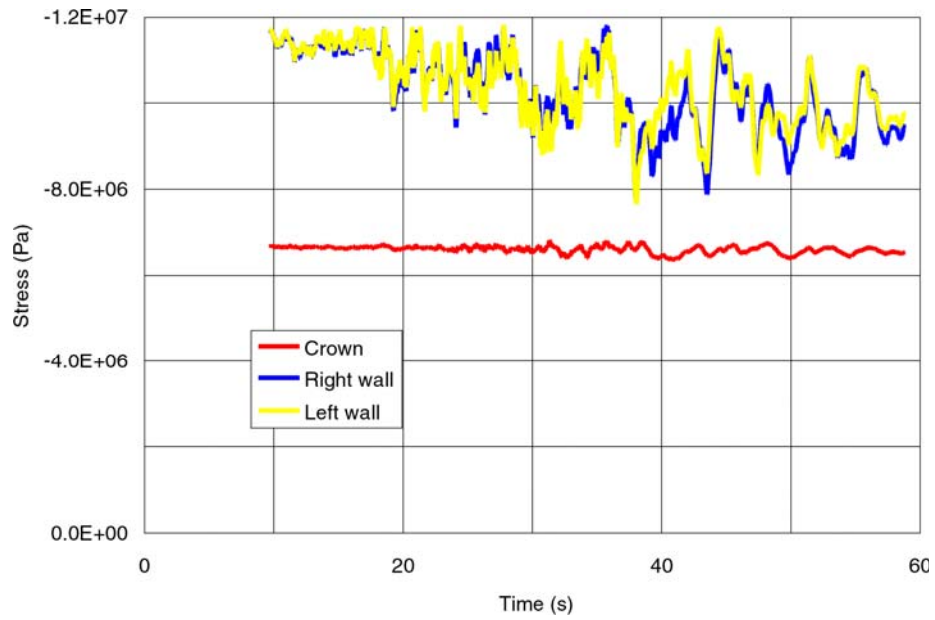


Figure 6-101D. Stress Histories of Points at Observation Drift during Seismic Shaking

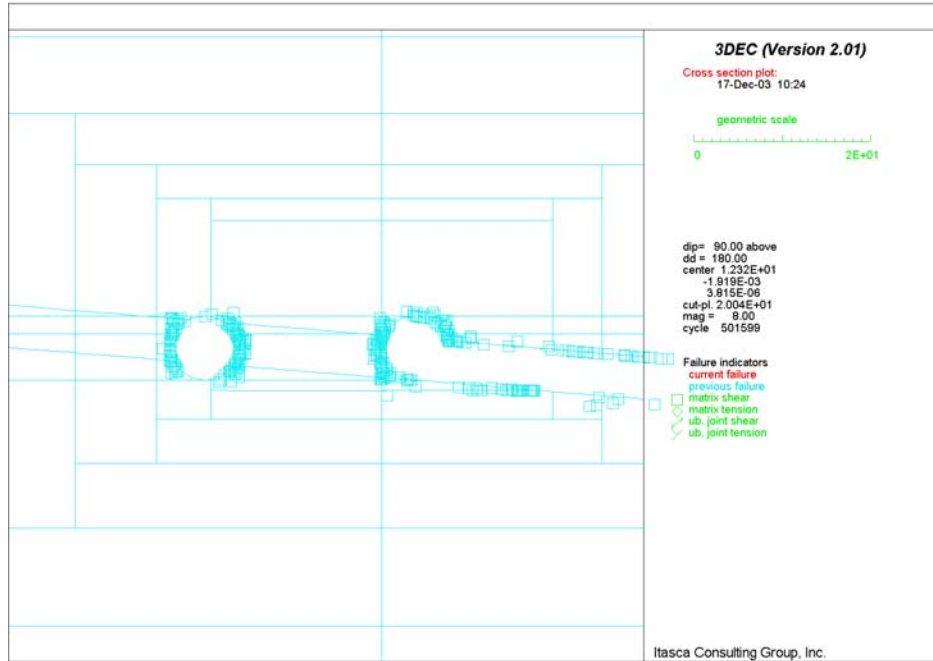


Figure 6-101E. Potential Yield Zone in Intersection between Observation Drift and Exhaust Main in Vertical Section 1 after Seismic Shaking

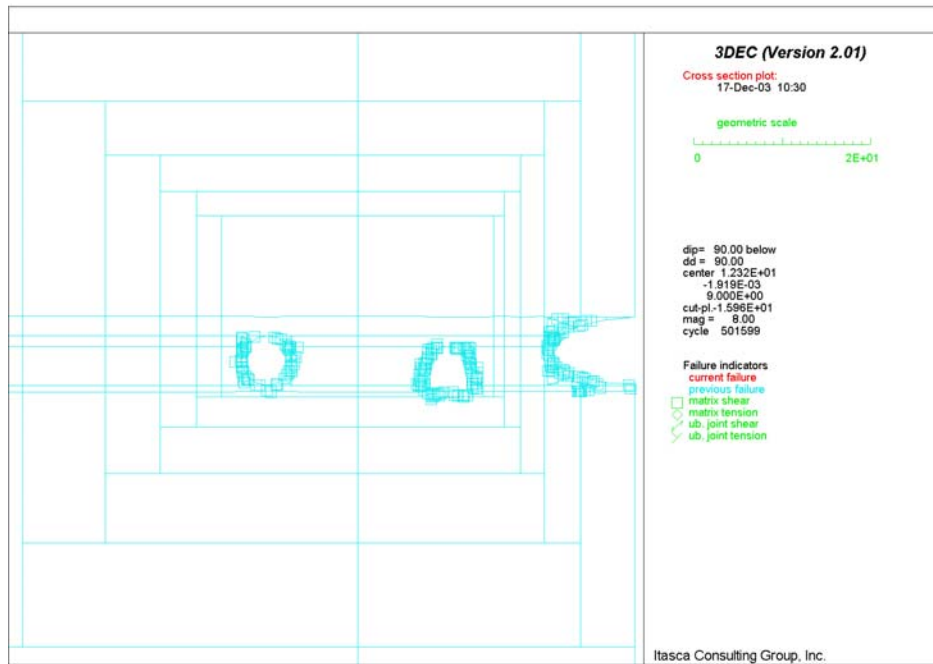


Figure 6-101F. Potential Yield Zone in Intersection between Observation Drift and Exhaust Main in Vertical Section 2 after Seismic Shaking

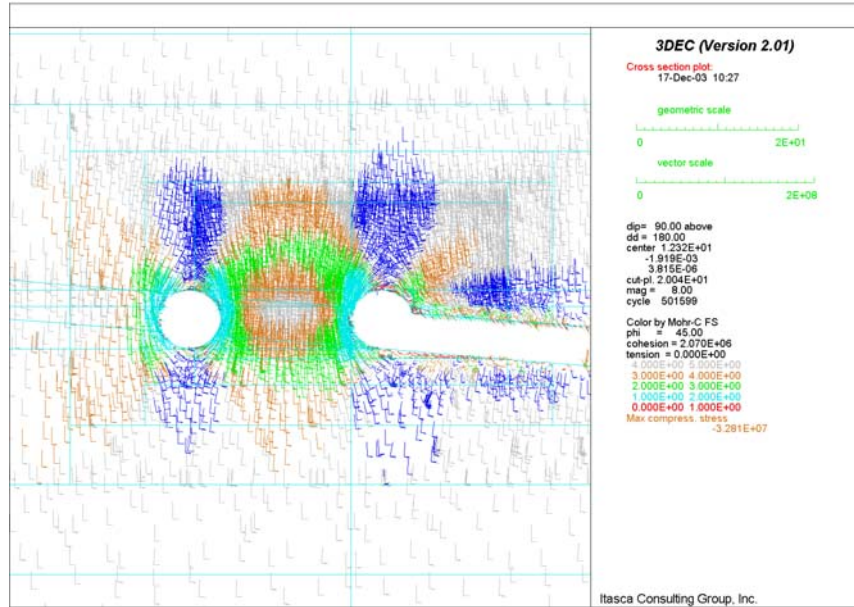


Figure 6-101G. Factor of Safety in Intersection between Observation Drift and Exhaust Main in Vertical Section 1 after Seismic Shaking

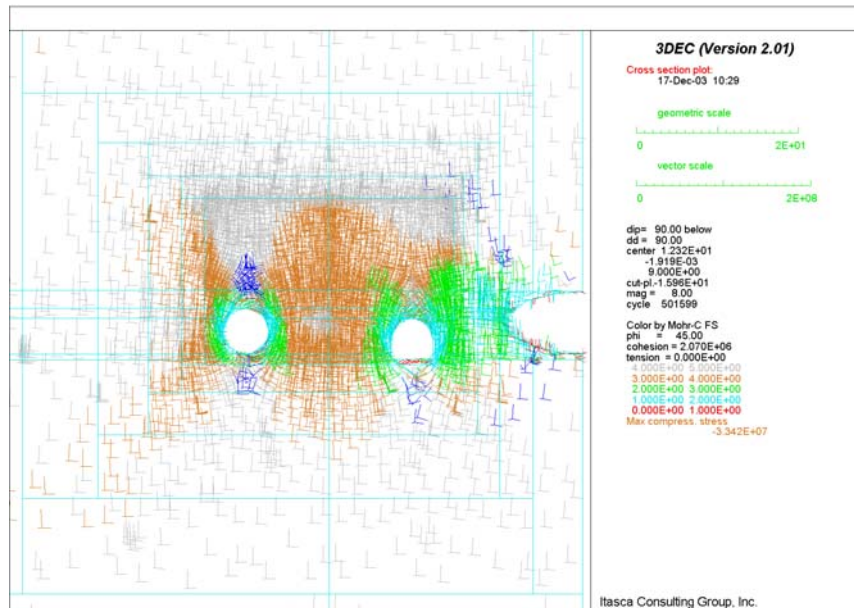


Figure 6-101H. Factor of Safety in Intersection between Observation Drift and Exhaust Main in Vertical Section 2 after Seismic Shaking

#### **6.5.3.3.4 TBM Launch Chamber**

The results of the seismic analysis of the TBM launch chamber, summarized in Figures 6-101I to 6-101L, are very similar to the results obtained for the observation drift. Preclosure seismic shaking (10,000-year earthquake) causes relatively small additional damage of the rock mass (Figure 6-101I), but there is no indication of global instability of the launch chamber during or after the shaking. As expected, based on similarity of the problems, the velocity and stress histories at the points around the excavations are almost identical for the TBM launch chamber (see Figures 6-101K and 6-101L) and the observation drift (see Figures 6-101C and 6-101D).

#### **6.5.3.3.5 North Portal**

The results of dynamic analysis of stability of the North Portal for the seismic ground motion are shown in Figures 6-101M to 6-101R. The velocity histories recorded at the ground surface (Figure 6-101M) are almost identical to the provided velocity histories of the design earthquake (Figure 4-1b). This comparison is a proof that boundary conditions are implemented correctly in the model. The velocity histories recorded at the crown of the starter tunnel (Figure 6-101N) indicate no additional amplification of velocity at the tunnel boundary and elastic model response to the seismic shaking.

Shaking due to the 2,000-year ground motion does not cause any plasticity in the model. Stress tensor fields colored by the major principal stress magnitude and factor-of-safety with respect to Mohr-Coulomb shear failure are shown (Figures 6-101O to 6-101R) at two states during dynamic simulation: after 19.84 seconds, and at the end of dynamic simulation. Ground shaking does not cause residual changes in the stress field, which is consistent with the observation that model behaves elastically. The factor of safety with respect to Mohr-Coulomb shear failure remained large in the entire model throughout the dynamic simulation.

#### **6.5.3.3.6 Interburden Pillar between Shaft Access and Exhaust Mains**

The results of dynamic simulation of the pillar for preclosure seismic ground motion of 10,000-year return period are shown in Figures 6-101S through 6-101W. Seismic loading was applied to the model at the initial state, after excavation of the drifts, before heating began. The results of the thermomechanical analysis indicate that if the seismic load were applied to the model at any stage during 50 years of the preclosure period, the results of the seismic analysis would not be different.

The dynamic load causes insignificant additional yielding caused by stress oscillations (comparing Figures 6-101T and 6-101U with 6-66X and 6-66Y). The contours of safety factor after seismic loading are almost the same as those due to in-situ stress loading (comparing Figures 6-101V and 6-101W with 6-66V and 6-66W). After completion of the dynamic simulation, the models for all simulated cases are stable. There is no indication of permanent stress redistribution or destressing of portions of rock mass indicating areas prone to rockfall. Velocity histories were recorded during the simulation at a number of points throughout the model. The histories near the center of the model are shown in Figure 6-101S. These histories are almost identical to the velocity histories applied at the base of the model due to the vertically

propagating seismic wave (see Figure 4-1a). Thus, the model deforms elastically under seismic load. There is no indication of accumulation of irreversible, plastic deformation.

Based on the results of this section and those from Sections 6.5.3.1.6 and 6.5.3.2.3, it is indicated that the effect of the excavation of an overlying 7.62-m-diameter access drift and two underlying 7.62-m-diameter exhaust mains on the stability of 10-m high interburden pillar is minimum or insignificant.

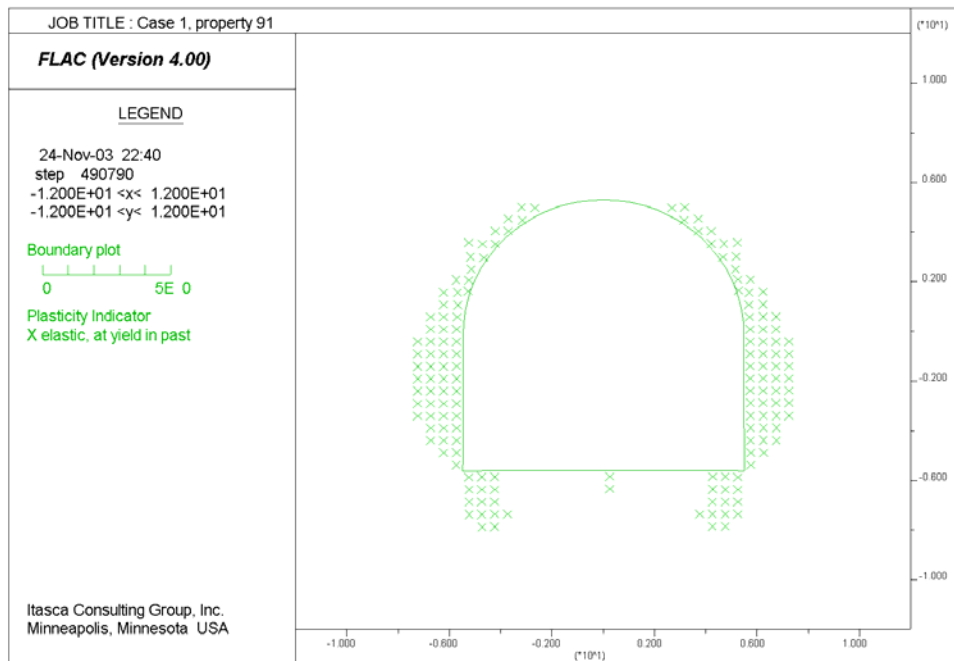


Figure 6-101I. Potential Yield Zone around TBM Launch Chamber after Seismic Shaking

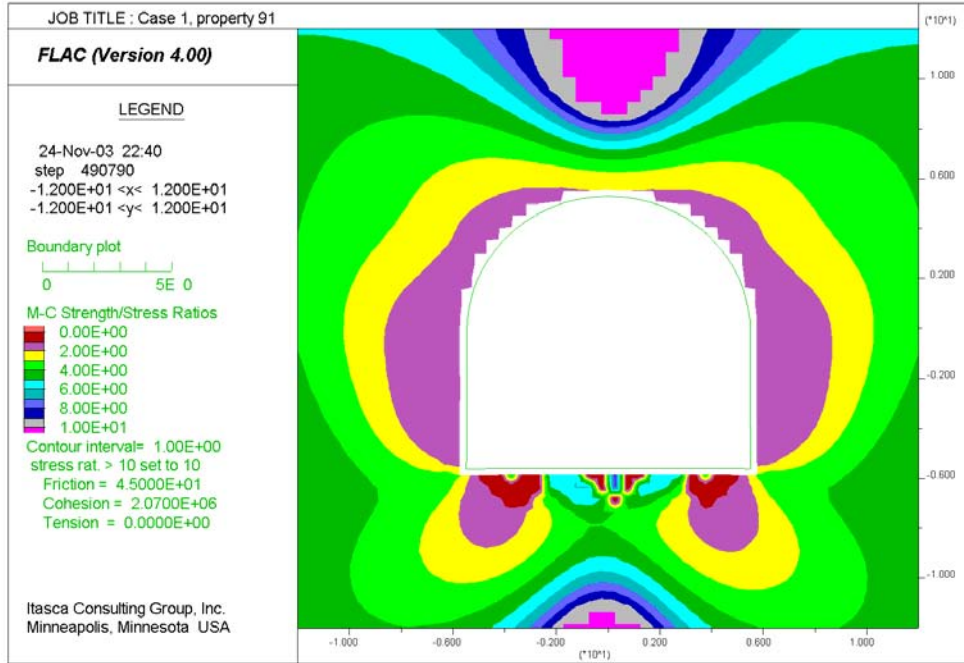


Figure 6-101J. Factor of Safety around TBM Launch Chamber after Seismic Shaking

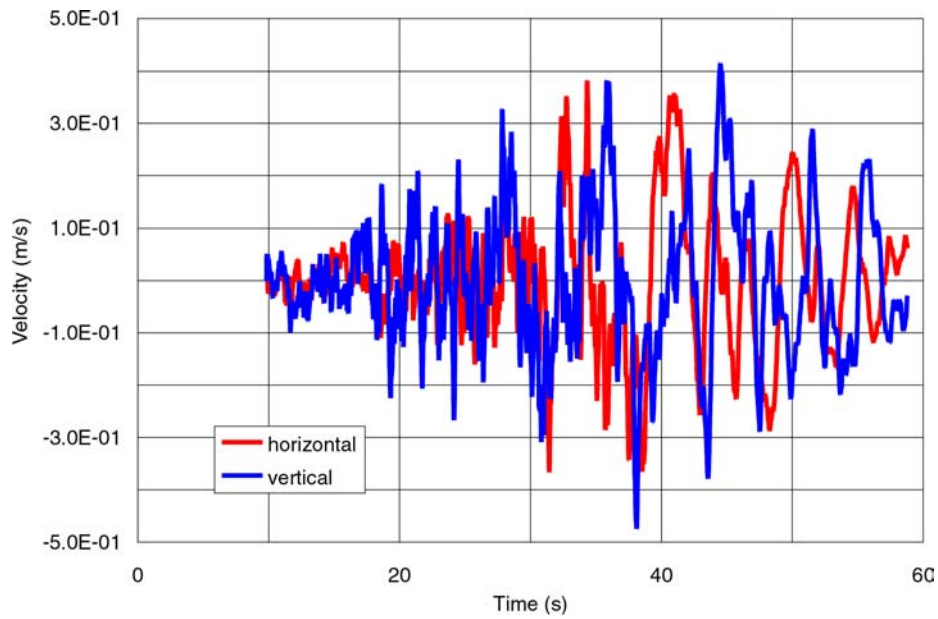


Figure 6-101K. Velocity Histories of Point at Crown of TBM Launch Chamber after Seismic Shaking

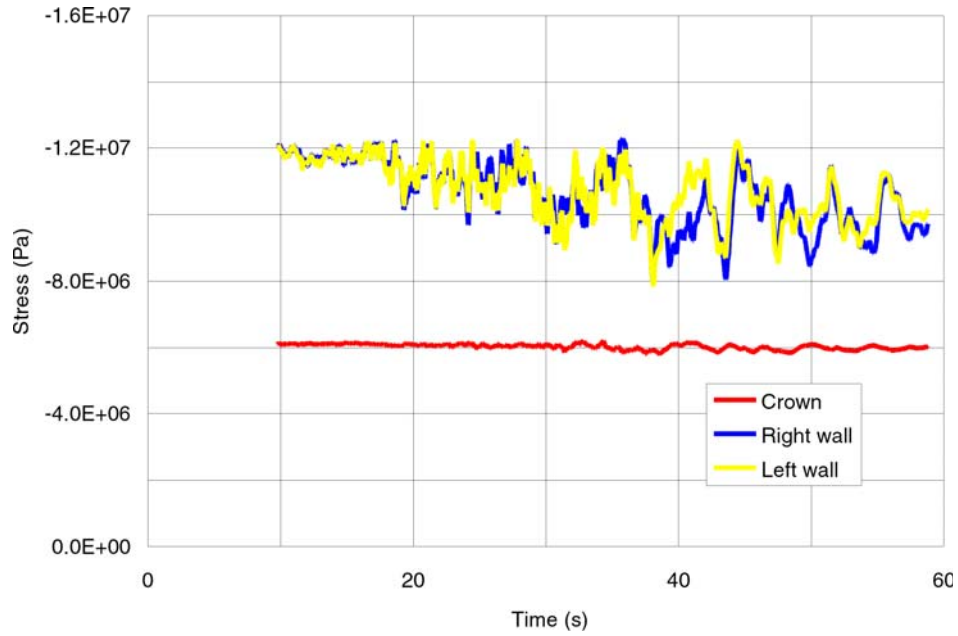


Figure 6-101L. Stress Histories at Three Points around TBM Launch Chamber after Seismic Shaking

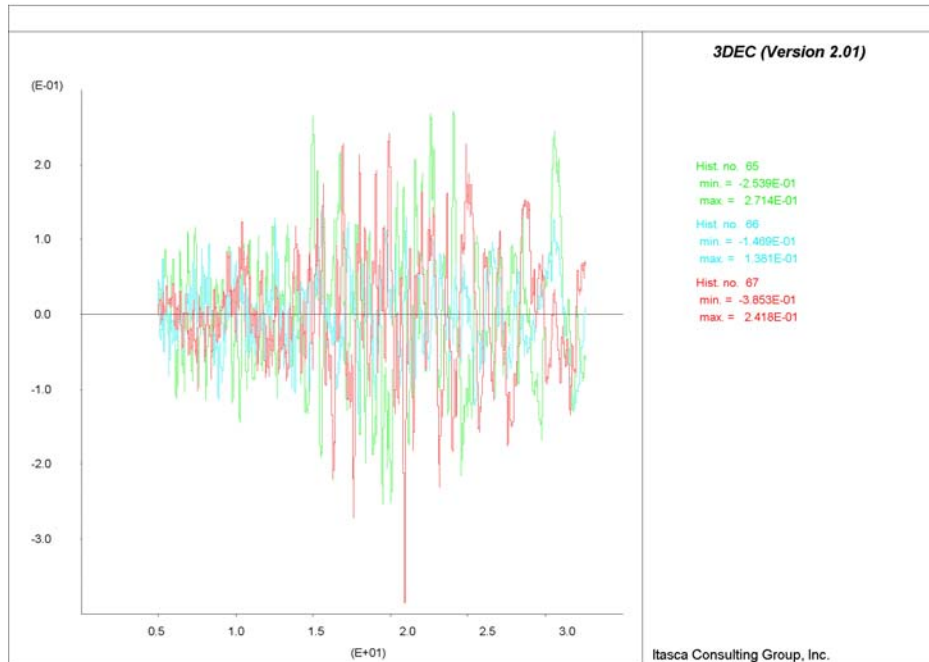


Figure 6-101M. Velocity Histories in X, Y, and Z Directions at Ground Surface

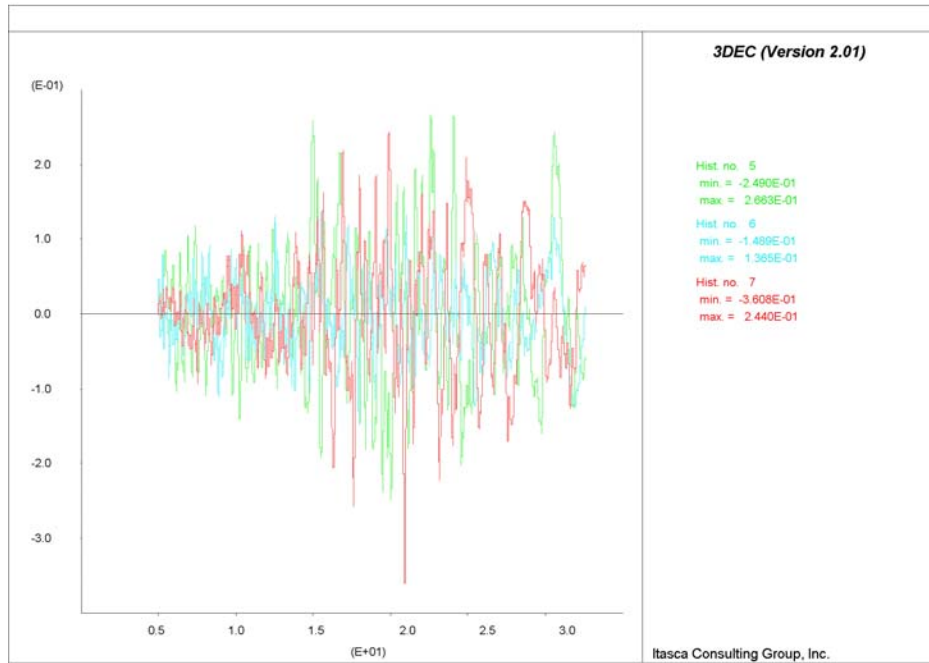


Figure 6-101N. Velocity Histories in X, Y, and Z Directions at Crown of Starter Tunnel

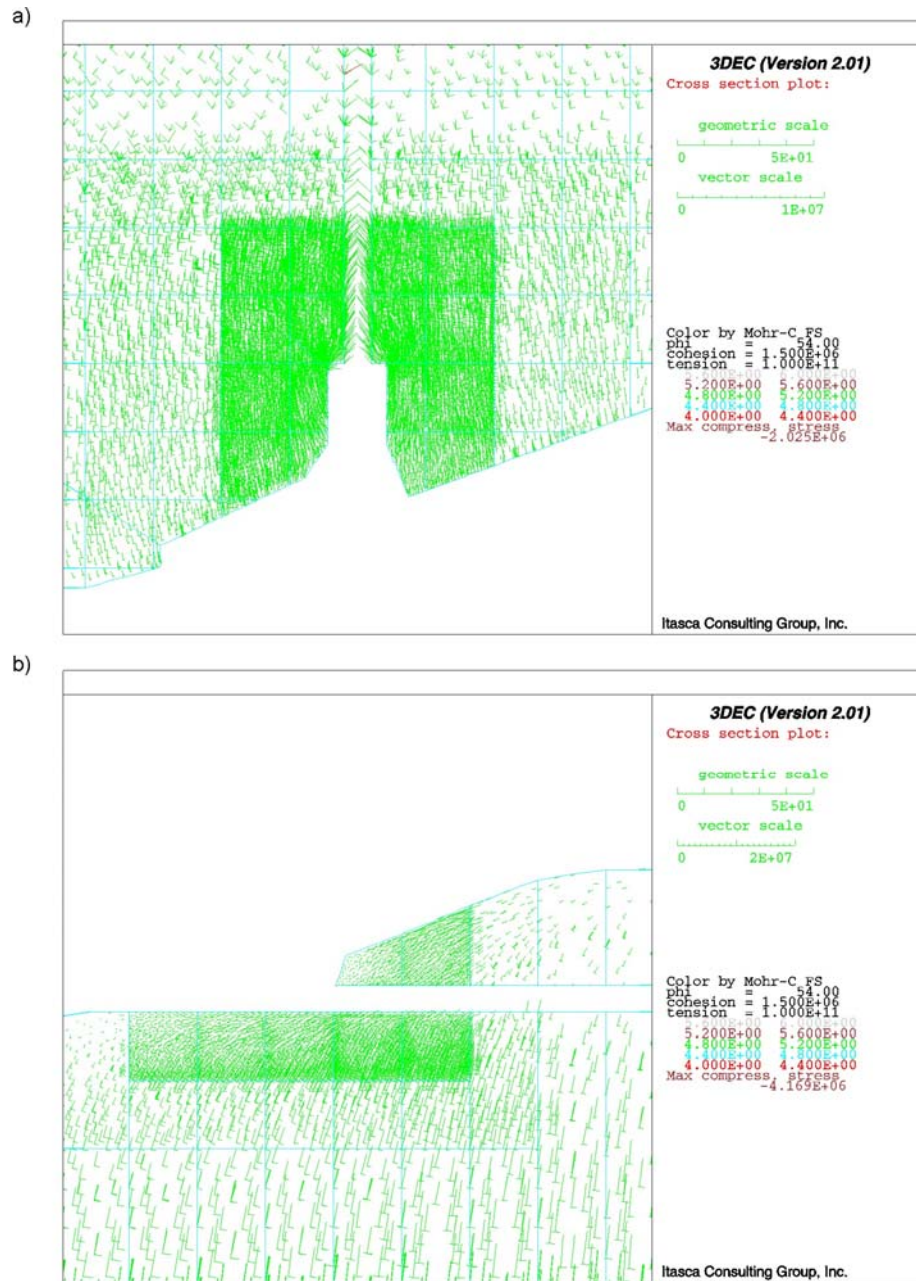


Figure 6-1010. Factor of Safety after 19.84 Seconds of Ground Shaking: a) Horizontal Cross-section at Elevation 1128 m; and b) Longitudinal Cross-section L-L'

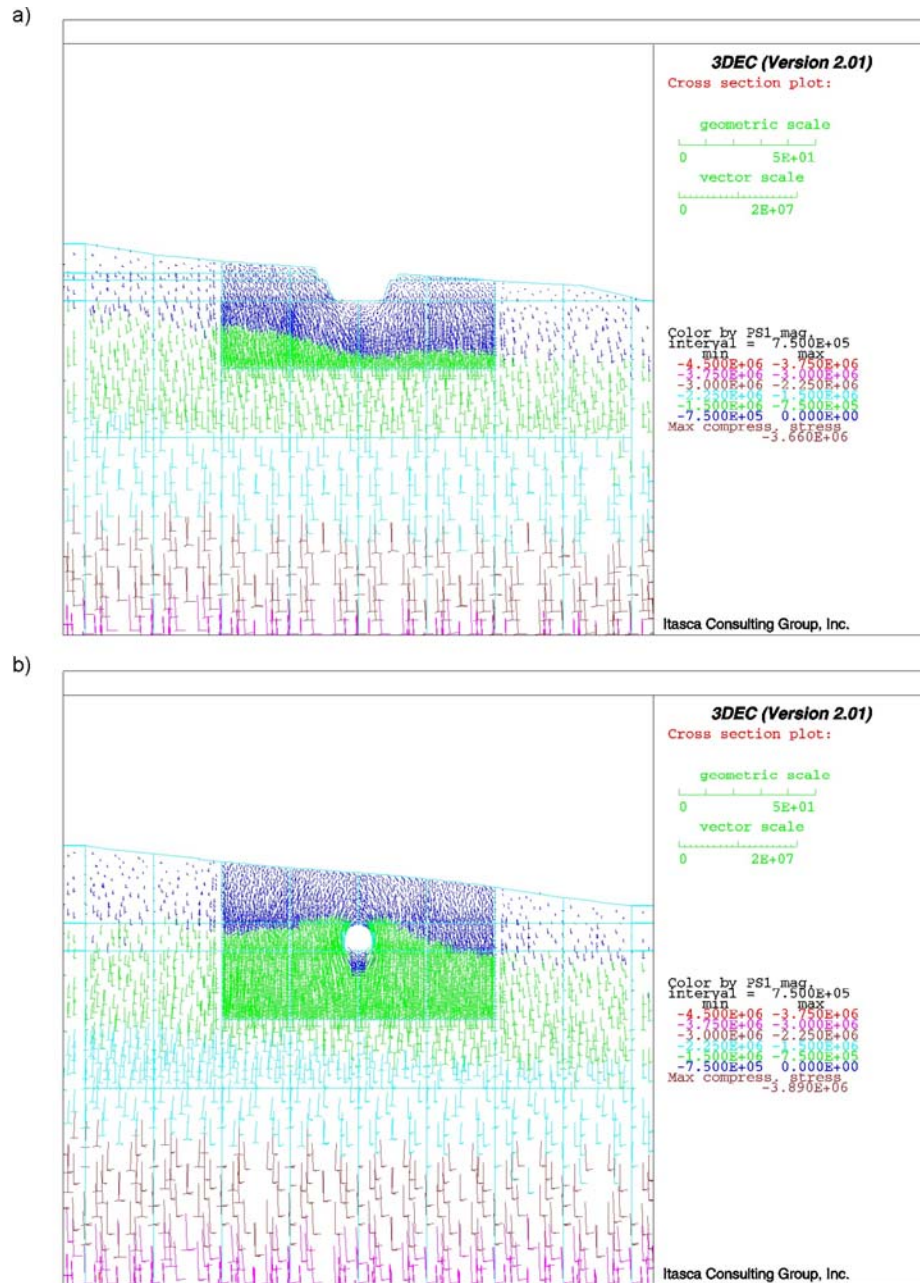


Figure 6-101P. Major Principal Stresses after 19.84 Seconds of Ground Shaking for Cross-sections:  
a) C<sub>1</sub>-C<sub>1</sub>' and b) C<sub>2</sub>-C<sub>2</sub>'

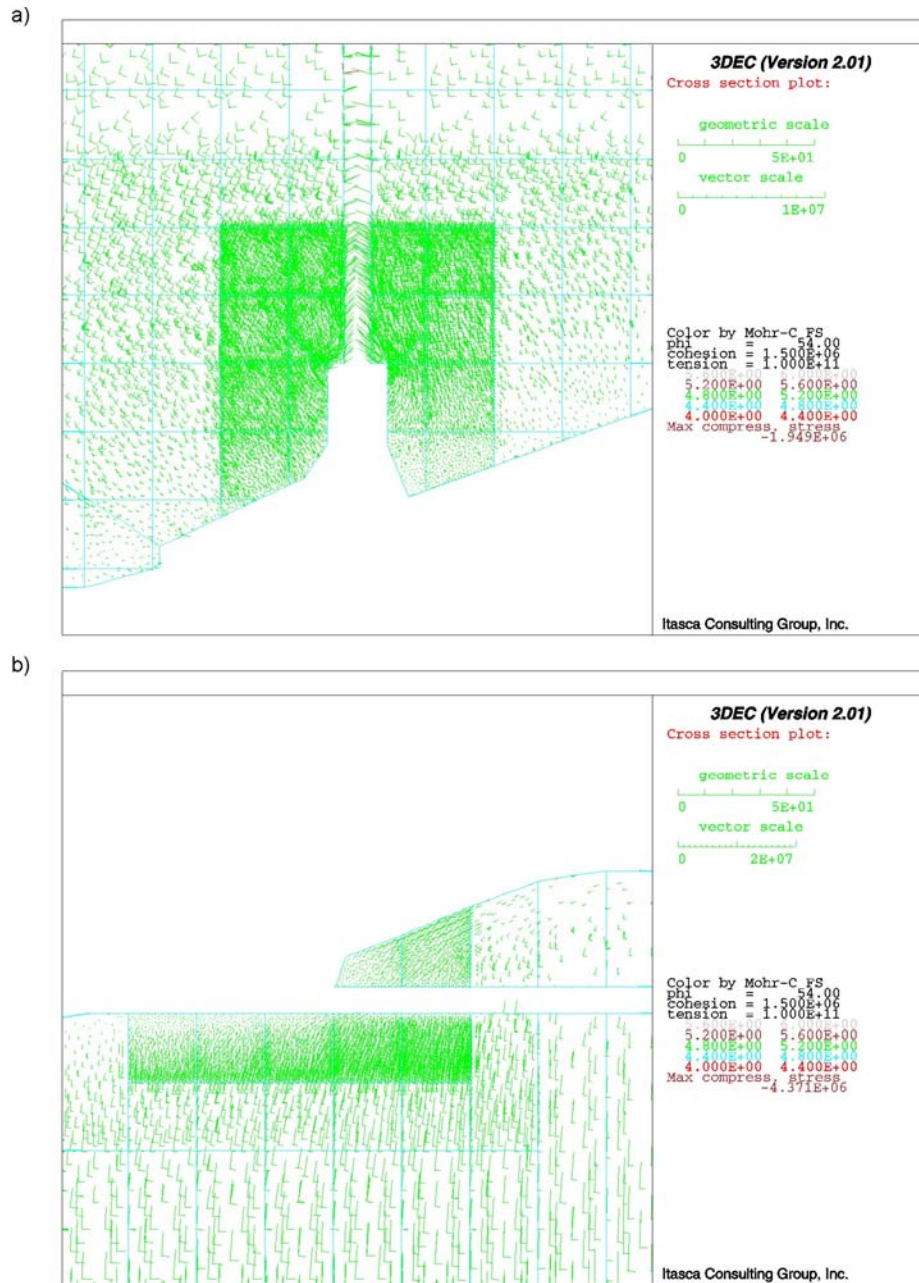


Figure 6-101Q. Factor of Safety at End of Ground Shaking: a) Horizontal Cross-section at Elevation 1128 m; and b) Longitudinal Cross-section L-L'

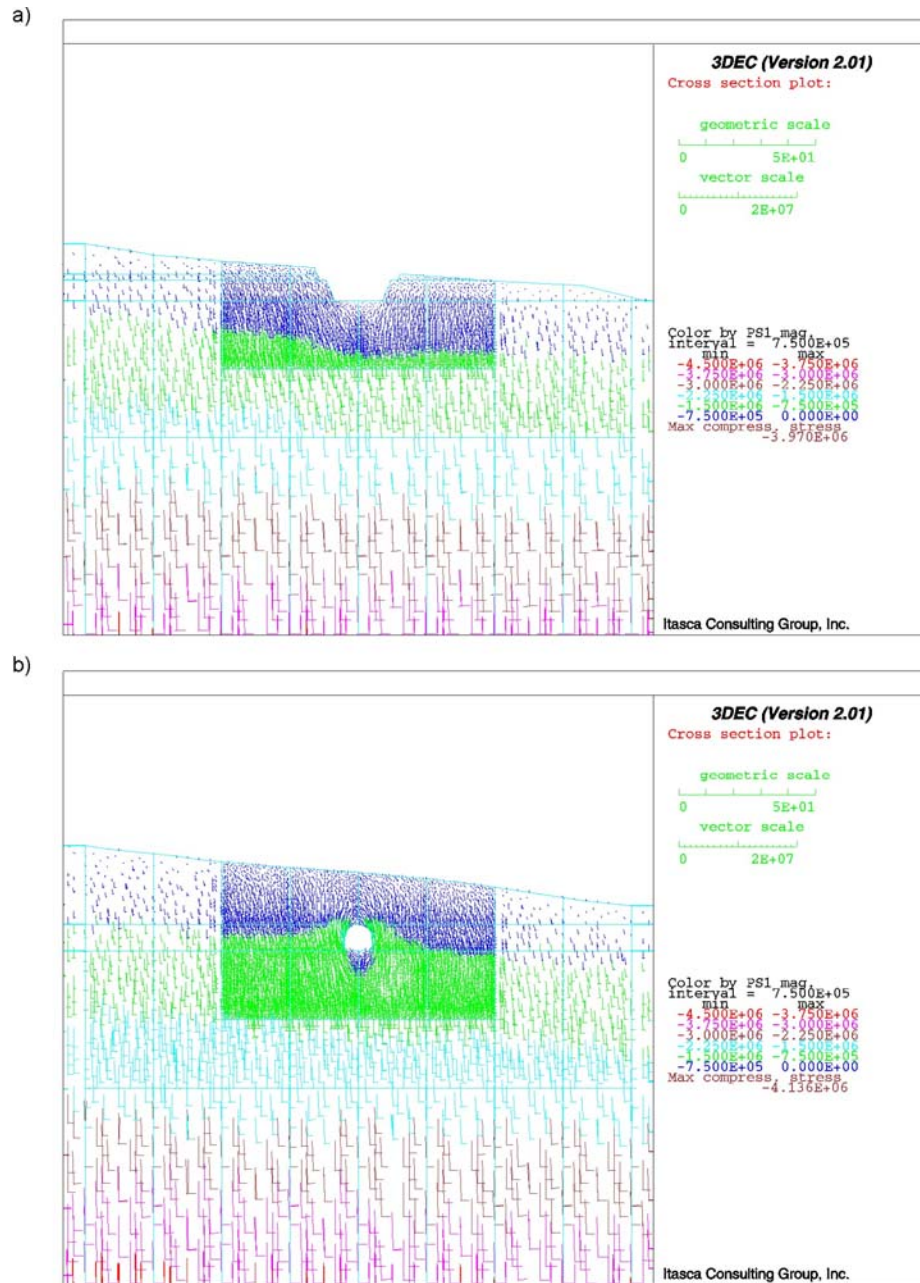


Figure 6-101R. Major Principal Stresses at End of Ground Shaking for Cross-sections: a) C<sub>1</sub>-C<sub>1</sub>' and b) C<sub>2</sub>-C<sub>2</sub>'

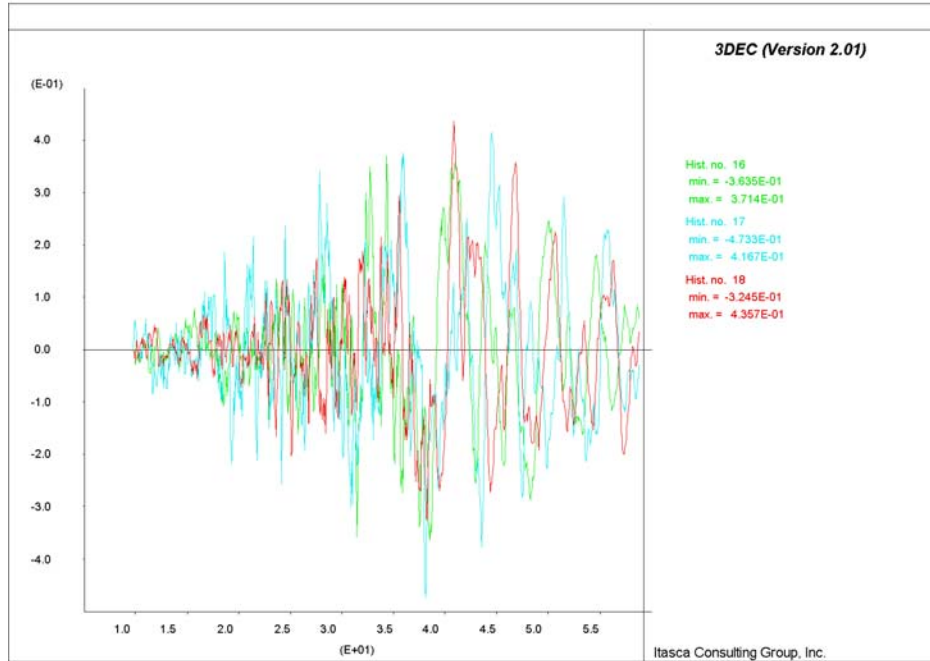


Figure 6-101S. Velocity Histories in X, Y, and Z Directions near Point 1 for Lith. Cat. 1 Rock at Interburden Area

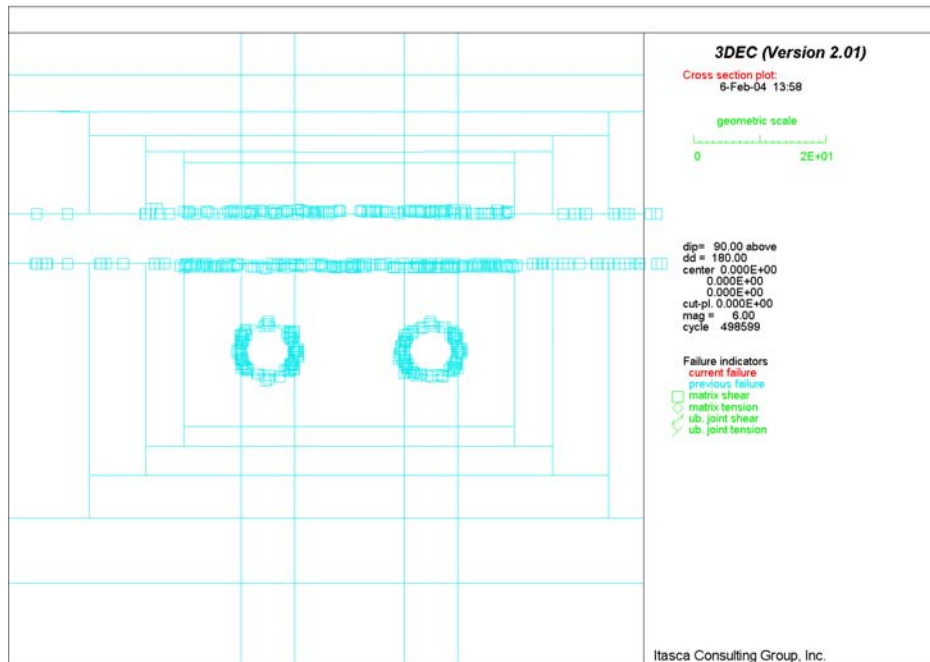


Figure 6-101T. Potential Yield Zone in Vertical Section 1 for Lith. Cat. 1 Rock under In Situ and Seismic Loading at Interburden Area

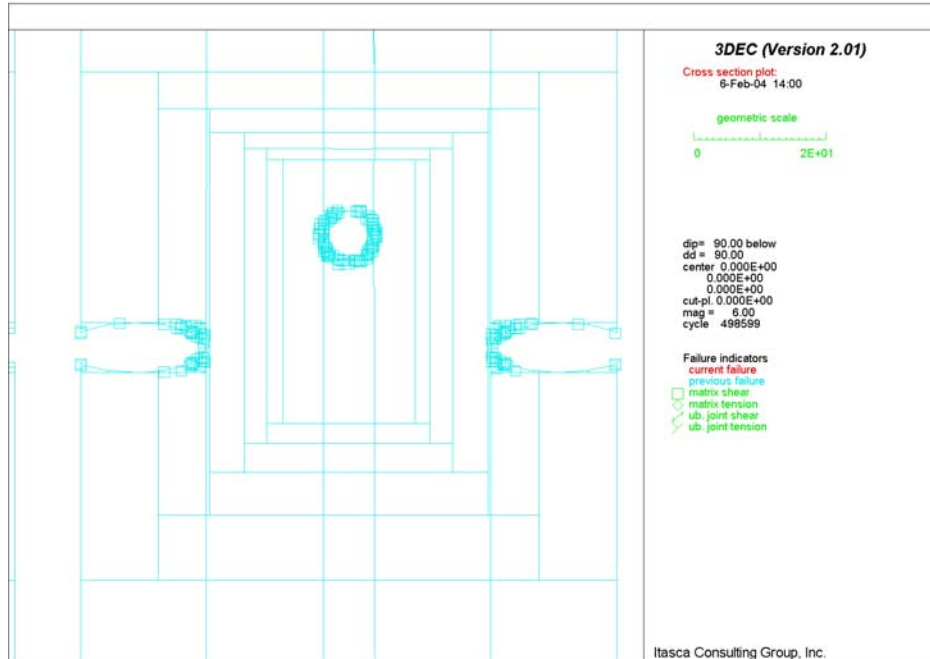


Figure 6-101U. Potential Yield Zone in Vertical Section 2 for Lith. Cat. 1 Rock under In Situ and Seismic Loading at Interburden Area

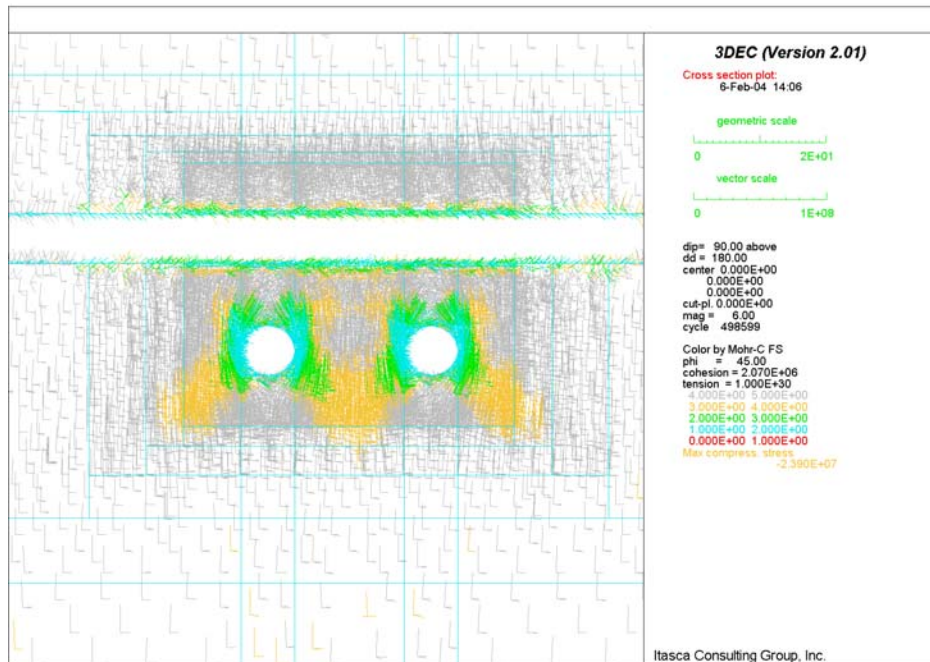


Figure 6-101V. Safety Factor in Vertical Section 1 for Lith. Cat. 1 Rock under In Situ and Seismic Loading at Interburden Area

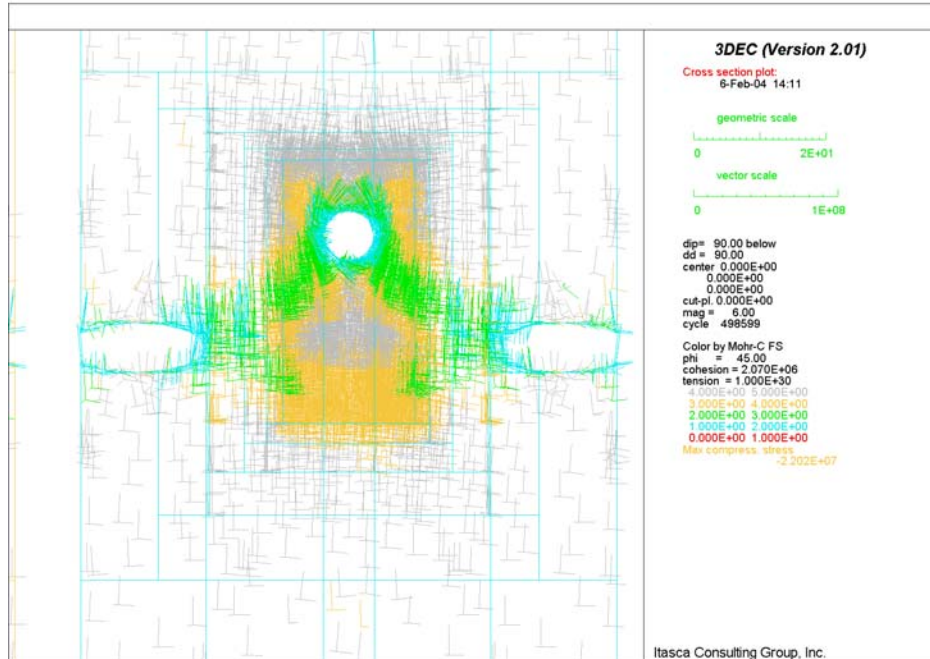


Figure 6-101W. Safety Factor in Vertical Section 2 for Lith. Cat. 1 Rock under In Situ and Seismic Loading at Interburden Area

### 6.5.3.4 Ground Reaction Curves

The Ground Reaction Curve (GRC) is often used for the analysis of ground support requirements or to examine the interaction between ground support components and rock. The visualization of GRC can serve as a check of the stability of unsupported non-emplacement drifts, and to quantify the potential load that may be induced in ground support components due to further ground convergence after ground support component installation. In this calculation, the GRC concepts are described in conjunction with presenting the results of the analysis of the access and exhaust main in category 1 lithophysal rock. This scenario was chosen for demonstration as it represents the worst-case rock mass scenario. The displacements developed around the excavation and resulting loads in the ground support are significantly greater than any other rock mass conditions for these drifts at Yucca Mountain.

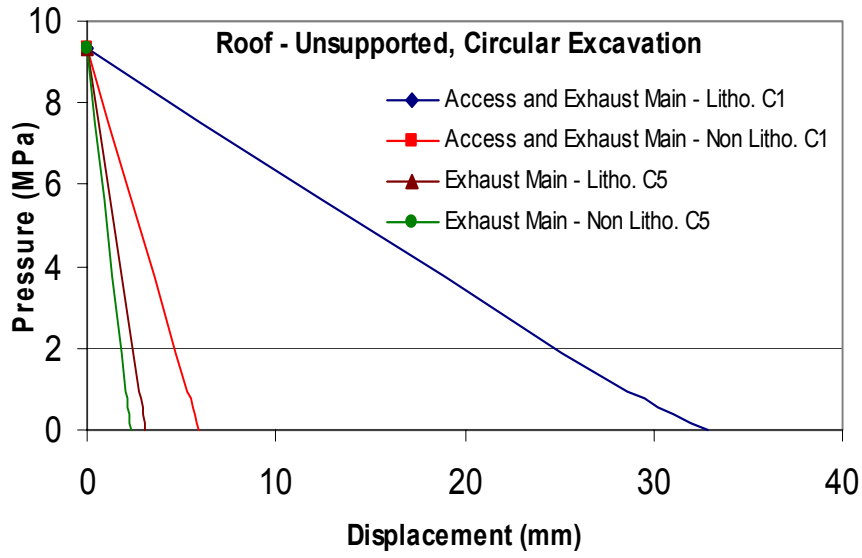
To develop the GRC, forces that are statically equivalent to the initial stresses inside the drift are applied at each of the gridpoints defining the outline of the excavation. The forces are reduced gradually, and the resulting crown and wall displacements are monitored.

Figures 6-102a, 6-102b, 6-103a and 6-103b show the ground reaction curves for unsupported access and exhaust mains and turnouts for roof and wall, respectively, by FLAC.

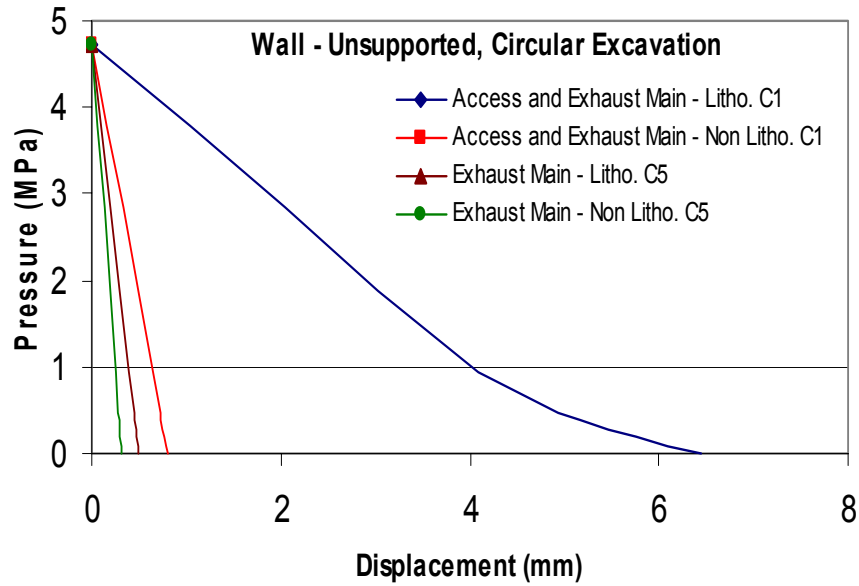
Figures 6-102 and 6-103 indicate that, in all cases, the excavation comes to equilibrium, i.e., GRC reach finite displacement for zero confinement pressure, indicating the drifts are anticipated to be stable. With exception of deformation of wall for the excavations in the

lithophysal category 1 rock, the deformation in all other cases is completely elastic. The horseshoe-shaped turnout in lithophysal category 1 rock shows the largest displacements, i.e., about 37 mm for roof. The circular exhaust main with category 5 non-lithophysal rock shows the smallest displacement, i.e., about 0.3 mm for wall. Non-lithophysal rock shows smaller displacement than that of lithophysal rock. Among lithophysal or non-lithophysal rock, category 1 rock shows larger displacement than that of category 5 rock. Clearly, the circular access and exhaust mains have more stable geometries, resulting in smaller displacements. Also, stronger rock such as non-lithophysal rock with category 5 quality shows smaller deformation compared with that of weaker rock such as lithophysal rock with category 1 quality. The major reason is due to the larger elastic modulus with the former compared with the latter (see Tables 4-2 and 4-1).

It should be noted that equilibrium in the context of modeling with FLAC implies that no active failure planes have developed in the model. However, FLAC does not model the impact the displacements have on the dilation of intersecting joint planes that might cause wedges to loosen and fall under gravity into the excavation. Therefore, the equilibrium in the FLAC model without ground support does not imply that ground support is not necessary.

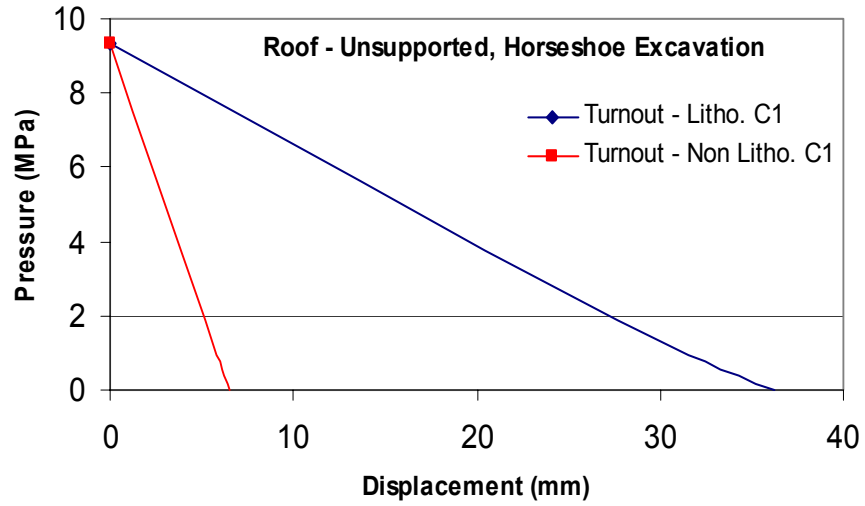


(a)

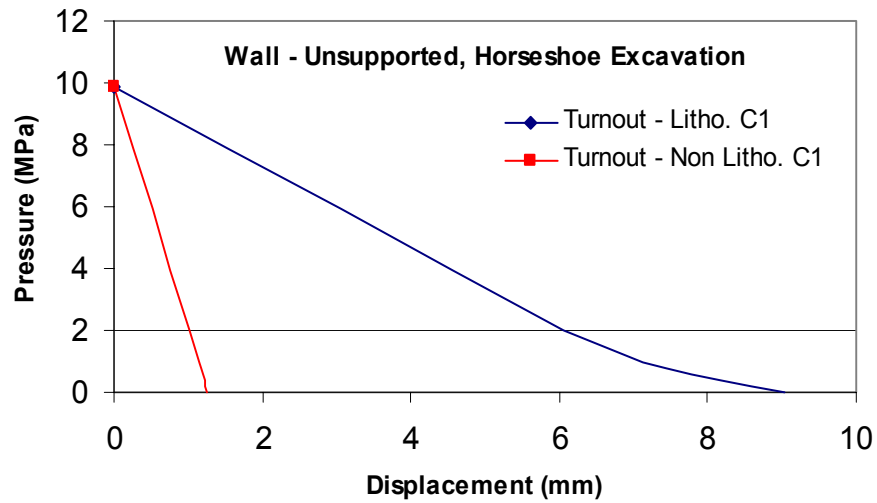


(b)

Figure 6-102. Ground Reaction Curves for Unsupported Access and Exhaust Mains: (a) Roof; (b) Wall.



(a)



(b)

Figure 6-103. Ground Reaction Curves for Unsupported Turnouts: (a) Roof; (b) Wall.

## **6.5.4 Ground Support Systems for Non-Emplacement Drifts**

### **6.5.4.1 Candidate Ground Support System**

The ground support system proposed to be used in non-emplacment drifts is described as follows (Assumption 5.8):

- For non-emplacment openings except intersections between access mains and turnouts and between exhaust mains and emplacment drifts, ramps, and starter tunnel: fully grouted rock bolts with heavy duty welded wire fabric (WWF).
- For intersections between access mains and turnouts and between exhaust mains and emplacment drifts, ramps, and starter tunnel: fully grouted bolts with fiber-reinforced shotcrete, and lattice girders as necessary for roof span control.

Figures 6-104 and 6-105 show the sketch of ground support system in access and exhaust mains and turnouts, respectively. Figure 5-1 shows the typical shotcrete area at intersections.

The fully grouted rock bolts with typical length of 3 m, spaced at 1.25 m with heavy duty WWF are designed to be used for ground support at typical non-emplacment openings, which include access mains, exhaust mains, observation drift and test alcove, TBM launch chambers, and North Portal starter tunnel. In the intersection areas, in order to enhance the opening stability with large roof span, increased bolt length of about 5 m with 0.10 m thick fiber-reinforced shotcrete will be installed, and supplemented with lattice girder as necessary depending on rock mass quality and the associated roof span. It is noted that the same ground support system for the intersections will be applied to ramps except that the bolt length is 3 m long, even though ramps have the same shape and dimension as those of access and exhaust mains. The major reason is that ramps provide access either for men, materials, waste emplacment, or ventilation air. They begin at the interface with the portal and ends at interface with the access mains. Due to their important functions, especially the waste package transportation for North Ramp, it is desirable to supplement fully grouted bolts by shotcrete to enhance the ground support function. It should be noted that the designed ground support system for ramps may be only for North Ramp and may need to be changed for North Construction Ramp and South Ramp as fully grouted rock bolts with heavy duty WWF, with fiber-reinforced shotcrete installed on as-needed basis, depending on the construction schedule.

For the ground support at North Portal, fully grouted rock bolts with fiber-reinforced shotcrete will be installed around the portal frontal and lateral faces. Rock bolts of 3 m long with 1.5 m spacing will be installed at the lateral faces of the portal whereas rock bolts of 5 m long with 1.5 m spacing will be applied at the frontal face. The portal face will be fibercreted to a thickness of 0.1 m. Similar ground support design is expected for North Construction Portal and South Portal if their topographical and ground conditions, geometry, and construction method are similar.

### **6.5.4.2 Candidate Ground Support Materials**

In order to make a proper selection of suitable ground support materials, it is important to know the service life in which these materials will be functional and understand under what kind of environment they will be subjected to during the service life.

For steel ground support components to be used in non-emplacement excavations, carbon steel including high-strength low-alloy steel is considered adequate as long as strength requirements are met. It should be noted that non-emplacement drifts are, in general, accessible during the preclosure period, i.e., proper maintenance of ground support system can be achieved. Steel components that are manufactured based on the following standard specifications included in the American Society for Testing and Materials (ASTM) are expected to perform satisfactorily in the non-emplacement drift environment:

- A 36 *Standard Specification for Carbon Structural Steel,*
- A 242 *Standard Specification for High-Strength Low-Alloy Structural Steel*
- A 588 *Standard Specification for High-Strength Low-Alloy Structural Steel with 50 ksi [345MPa] Minimum Yield Point to 4-in. [100-mm] Thick*
- F 432 *Standard Specification for Roof and Rock Bolts and Accessories*
- A 82 *Standard Specification for Steel Wire, Plain, for Concrete Reinforcement*

For cementitious materials to be used for grouted rock bolts, shotcrete or concrete, it is suggested to use a low pH grout and shotcrete/concrete mix, which will be developed with lesser amounts of portland cement and silica fume or to potentially use other types of grouts and cements which are of non-portland cement types. For information on material and properties and construction of shotcrete, the following documents are recommended:

- ACI 506R *Guide to Shotcrete*
- ACI 506.2 *Specification for Shotcrete*

The typical dimension and material mechanical properties for fully grouted rock bolts and shotcrete are listed in Tables 4-3 and 4-4, respectively.

### **6.5.5 Stability of Supported Non-Emplacement Drifts**

Based on the results presented in Section 6.5.3, static (in-situ stress), thermal (where applicable), and dynamic loads are not going to cause any major instability of the surrounding rock mass. The excavations appear to be stable without any ground support. However, a numerical model based on continuum mechanics does not account for the effects of joints and deformation along the joint due to stress relaxation on the formation of loose blocks, and eventual local rockfall. The access main, the turnout and particularly the intersections will be supported.

The assessment of stability of supported non-emplacement drifts is presented in this section. The bolts and shotcrete were included in the models of the non-emplacement drifts, but the heavy-duty wire mesh was not. The dimensions and mechanical properties of the rock bolts and the shotcrete are listed in Tables 4-3 and 4-4. The calculated loads in the ground support are the result of global deformation of the rock mass, subsequent to installation of the ground support. However, the purpose of the ground support is not to prevent or restrain the global deformation of the excavations, which are stable without any ground support, but to prevent local rock fall. The analysis of the ground support in the non-emplacement drifts except North Portal was carried out mainly for the category 1 lithophysal rock mass, which is the extreme condition of

rock mass quality at the repository level. The analysis of the ground support for North Portal was carried out for the category 1 rock in TCw unit.

### 6.5.5.1 Mechanical Properties of Fully Grouted Rock Bolts and Swellex Bolts

It is important to use appropriate material properties for modeling fully grouted bolts. Two key input parameters in the numerical approach are the bond stiffness ( $K_{\text{bond}}$ ) and the bond shear strength ( $S_{\text{bond}}$ ), which reflect the interaction between bolt and rock and control the bolt behavior. The bond stiffness of  $8.68 \times 10^8$  N/m/m was estimated based on empirical correlation shown in Table 4-3. It is noted that the bond strength is a function of rock modulus; thus, the selection of properties should consider the host rock properties. Based on recommendation by Hutchinson and Diederichs (1996, Figure 2.6.13), the bond strengths for lithophysical category 1 rock (with Young's modulus of 1.92 GPa) and non-lithophysical category 1 rock (with Young's modulus of 10.25 GPa) are 190 and 300 kN/m, respectively, for grout with water/cement ratio of 0.35.

For the Swellex bolts to be used in emplacement drifts, the appropriate values for bond stiffness and bond strength are estimated to be  $3 \times 10^8$  N/m/m and  $2.75 \times 10^5$  N/m, respectively (see detailed discussion in Section 6.4.1 of BSC 2003f).

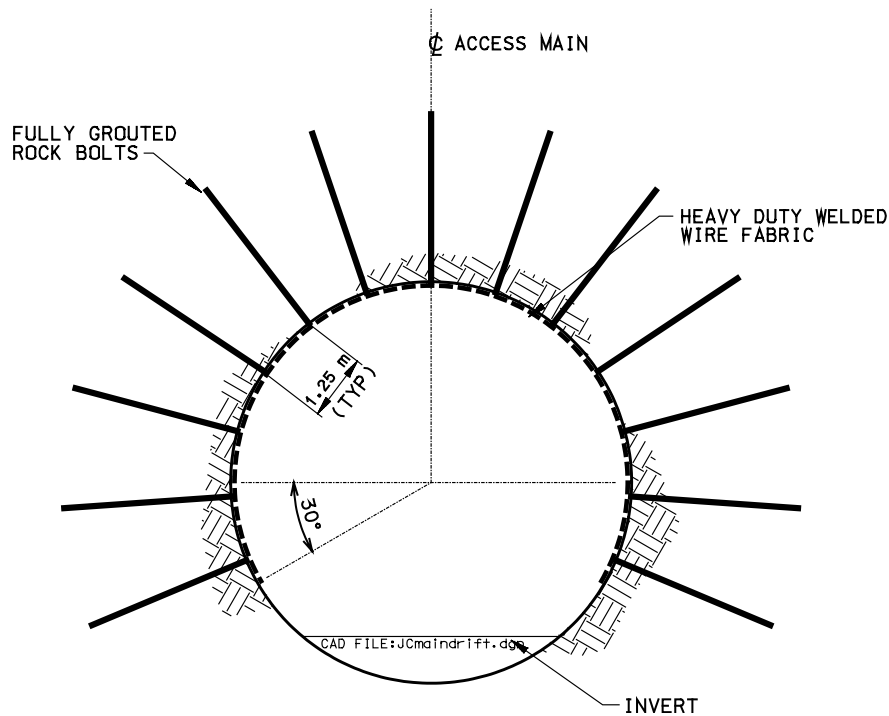
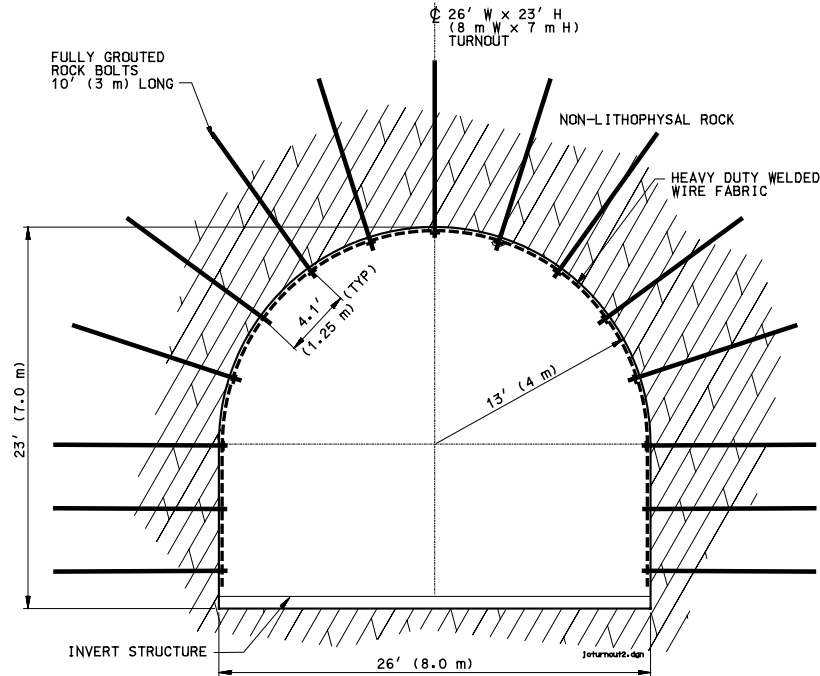


Figure 6-104. Ground Support System in Access or Exhaust Mains



Note: same ground support for lithophysal rock

Figure 6-105. Ground Support System in Turnouts

## 6.5.5.2 In Situ Stress Loading Condition

### 6.5.5.2.1 Access and Exhaust Mains and Turnouts

The planned ground support for the access mains, exhaust mains and turnouts is analyzed using the FLAC code.

Figure 6-106 shows the displacements around supported access mains for lithophysal category 1 rock. Comparing this figure with Figure 6-18, the displacements are nearly identical in both figures, with the maximum displacement about 3.28 and 3.27 cm for unsupported and supported drifts, respectively. Figure 6-107 shows the axial load along fully grouted rock bolts around access mains for lithophysal category 1 rock. Note that the negative value in bolt load signifies tensile force in FLAC. The predicted load in the center bolt is  $2 \times 37.5$  kN, or 70 kN/ meter of excavation. To account for the out-of-plane spacing by multiplying by 1.25; thus, the predicted bolt load for a center cable is 87.5 kN, which is much smaller than the yield strength of fully grouted bolt, i.e., 264 kN (see Table 4-3). Figures 6-108 and 6-109 show the safety factors of supported openings for access and exhaust mains in lithophysal and non-lithophysal rock, respectively. Figures 6-110 and 6-111 show the safety factors of supported openings for turnouts in lithophysal and non-lithophysal rock, respectively.

Comparing Figures 6-108 through 6-111 with Figures 6-19 through 6-22, it appears that the safety factor contours for supported openings are almost identical to those of unsupported cases,

i.e., the effect of adding ground support to the modeled openings has minimal impact. This demonstrates an important point regarding the role of fully grouted rock bolt system in deep underground excavations. Ground support such as rock bolts should not be expected to arrest movement of the rock or reduce the rock mass stresses. Rather, it is there to support the loose blocks that result from the slip and dilation of joint planes intersecting the excavation surface.

#### **6.5.5.2.2 Intersections between Access Mains and Turnouts**

The analysis of the ground support in the access main intersections was carried out using 3DEC for the category 1 lithophysal rock mass, which is the extreme condition of rock mass quality at the repository level.

The elements of ground support are simulated in the numerical model, following the expected sequence of their installation during tunnel construction. The bolts will be installed at a certain distance behind the excavation face. From the three-dimensional model, which simulated the face advance, it is assumed that 75% of stress relaxation is completed before the bolts are installed (if the face advance is not explicitly considered). The bolts are loaded due to displacements caused by the remaining 25% of stress relaxation. Although the model of the intersection is three-dimensional, simulation of the face advance and sequential installation of the bolts behind the face would be a very time-consuming process.

The following are modeling steps performed during the analysis of the ground support in the intersection to simulate the consequence sequence.

1. 75% of stress relaxation in the access main.
2. Support of the access main with the grouted rock bolts and complete excavation of the access main.
3. 75% of stress relaxation in the first turnout.
4. Support of the first turnout with the grouted rock bolts and complete excavation of the first turnout.
5. 75% of stress relaxation in the second turnout.
6. Support of the second turnout with grouted rock bolts and complete excavation of the second turnout.
7. Installation of the shotcrete in the intersection.

According to this construction sequence, it is clear that shotcrete in the intersection is not going to be loaded due to stress relaxation, which is caused by the excavation of the drifts under in-situ stresses. The shotcrete will be loaded by deformation due to time-dependent strength degradation or seismic loading subsequent to installation of the shotcrete. In order to examine the effect of sequential turnout excavation on the forces in the rock bolts already installed in the access main, the excavation of the second turnout was simulated following the expected sequence of face advance and bolt installation behind the advancing face.

The bolt forces in the view along the access main, due to 25% of stress relaxation after excavation of the access main, are shown in Figure 6-112. Locally, in the bolts installed just above the springline, the forces reach 143 kN. However, the bolt forces are predominantly lower than 100 kN. The bolts in the back are loaded to almost 100 kN, while the bolts in the walls (with the exception of those above the springline) are loaded to less than 50 kN. This gives a safety factor of about 2.6 ( $264/100 = 2.64$ ). In other words, the bolts have a reserve of at least 150 kN (i.e.,  $264 - 100 = 164 > 150$ ) to take the load by loose, locally unstable blocks.

The effect of excavation of the first turnout on the bolt forces in the access main is illustrated in Figures 6-113 and 6-114. As expected, excavation of the turnout has the largest effect on the bolts already installed above the intersection. The force in the bolts circled in Figure 6-113 increases from approximately 100 kN (shown in Figure 6-112 after excavation of the access main) to less than 200 kN. In the limited number of bolts that undergo the maximum force increase, the reserve available for additional load due to loose blocks is 50 kN (i.e.,  $264 - 200 = 64 > 50$ ). A plot of the bolt forces in the plan view (Figure 6-114) indicates that the bolts that are additionally loaded due to excavation of the turnouts are located in the area above the intersection. The effect of the excavation of the turnout on the bolts in the access main rapidly decays as a function of distance in the plan view. That effect is illustrated in the plot (Figure 6-115) of the bolt forces after both intersections are excavated. The region of interested bolt forces above the first intersection does not increase, nor do the forces in the bolts within that region increase due to excavation of the second turnout. Displacement vector fields shown in Figure 6-116 are in the vertical cross-section normal to the access main, through the center of the first intersection, for the model states before and after excavation of the second turnout. Any increase in displacements in this cross-section due to excavation of the second turnout is relatively small (shown at Figure 6-116b). Consequently, the excavation of the second turnout has little effect on the load in the bolts in the first intersection.

### 6.5.5.2.3 Intersections between Exhaust Mains and Emplacement Drifts

The ground support in the exhaust main is the same as the ground support used in the access main. The emplacement drifts will be supported by 3-m long Super Swellex rock bolts, at 1.25 m spacing, and Bernold-type perforated sheets (BSC 2003f, Section 8). The mechanical properties of the Super Swellex bolts used in the simulation of the ground support in the intersections between the exhaust main and the emplacement drifts are listed in Table 4-5. Bernold-type sheets were not included in the model. The ground support in the intersection (i.e., about 15-m length along the exhaust main and 5 m from the intersection into the emplacement drift) includes 5-m long rock bolts and 0.10-m thick steel-fiber reinforced shotcrete. The ground support analysis was carried out only for the intersection at location B, and using lithophysal rock mass category 1, as the most unfavorable conditions for the load in the ground support.

The loads in the bolts in the exhaust main after excavation of the exhaust main, looking along the exhaust main and in plan view, are shown in Figures 6-117 and 6-118, respectively. With the exception of a few bolts affected by the local conditions, the maximum bolt force is around 100 kN. The forces in the bolts after excavation of both exhaust mains and the emplacement drifts are shown in Figures 6-119 through 6-121. The maximum force increases to approximately 120 kN in the regions above the intersection. Those loads are well within the limit of the elastic

deformation of the bolts, which have yield strength of 264 kN, which gives a safety factor of 2.2. Note that the sign convention in 3DEC is that tensile force is positive.

#### **6.5.5.2.4 Observation Drift**

The ground support for the observation drift and the intersection between the observation drift and the exhaust main is described in Section 6.5.4.1. The ground support will be used even though the numerical models show that the observation drift will be stable without any ground support (see Section 6.5.3). The used models are based on continuum theory and do not consider stability of the blocks created by joints in the walls and the crown of the drift. The used numerical models provide assessment of the global stability of the excavation. The designed ground support will prevent rockfall due to local instability.

The stability of supported observation drift was analyzed numerically. The objective was to assess performance of the ground support during the preclosure period for the expected loading conditions. Although the ground support is not designed to prevent (or reduce) deformation of the drift due to stress relaxation or thermal or seismic loading, it is important to demonstrate that such loads are not going to damage the ground support and make it ineffective in preventing local rockfall. The heavy-duty wire mesh was not included in the models. The observation drift is planned to be excavated using the drill-and-blast method. Consequently, it is assumed that ground relaxation due to excavation of the observation drift will be completed before the ground support inside the observation drift is installed.

Two different excavation sequences that have an effect on rockbolt loads were considered with regard to the sequence of drift excavation: in one case, the observation drift was excavated first; in the other, the emplacement drift was excavated first. The analysis has shown that the sequence of excavation has minor effect on the rockbolt forces. However, because the rockbolt forces are larger if the emplacement drift is excavated after excavation and support of the observation drift, the results in this section are presented for that case only.

The bolt forces after excavation of the emplacement drift are shown in Figure 6-121A. Note that the bolt forces in a two-dimensional model are presented per unit thickness of the model. The actual bolt forces can be obtained by multiplying values in the plot with spacing of the rows, which, in this case, is 1.25 m. These forces are insignificant considering the bolt yield strength of 264 kN.

#### **6.5.5.2.5 TBM Launch Chamber**

The designed ground support in the launch chamber includes 3-m long grouted rockbolts and heavy-duty wire mesh. Only the grouted rockbolts are included in the numerical model. The analysis was carried out for the seismic load induced by the preclosure earthquake only. It is assumed that the rockbolts do not take any load due to rock mass deformation caused by the relaxation of in situ stresses, as the launch chamber will be excavated using the drill-and-blast method.

### 6.5.5.2.6 North Portal

Although it is demonstrated that the North Portal and the starter tunnel are stable under static and dynamic loading conditions, both excavations will be supported. The objective of the ground support is to prevent local instability (of blocks created by joints not accounted for in the models) and to slow deterioration of rock mass properties with time.

For the North Portal modeling, shotcrete and rockbolt reinforcement have been considered (see Figure 6-105A). Three different regions, denoted as a) Lateral surfaces, b) Frontal surface and c) Tunnel surface, can be distinguished in Figure 6-105A.

The ground support is installed after complete relaxation of the in situ stresses due to excavation of the North Portal and the starter tunnel. Consequently, the ground support does not take any load under static conditions.

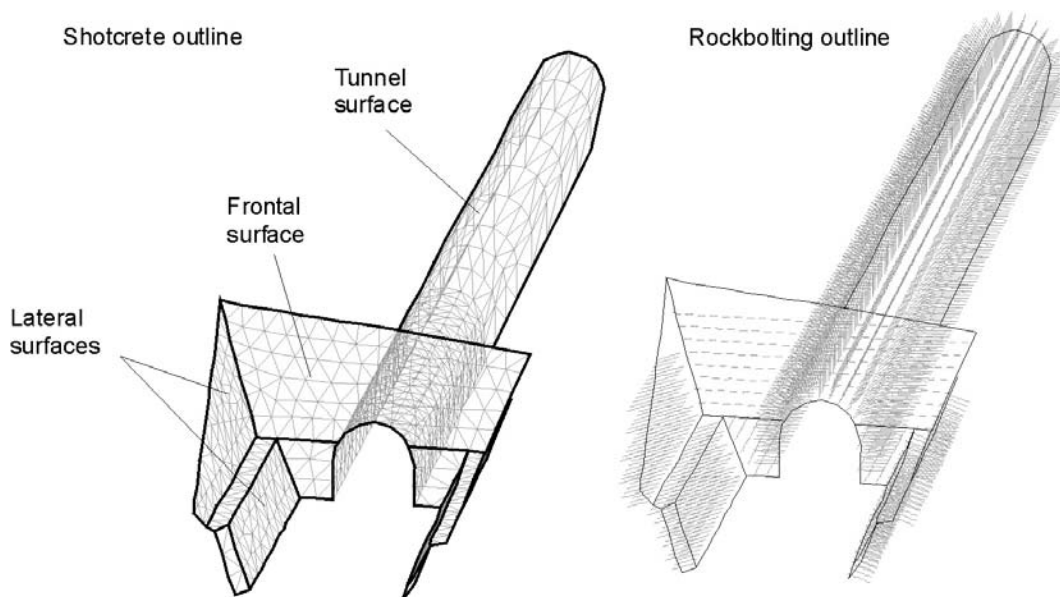


Figure 6-105A. Isometric View of Shotcrete and Rockbolts in North Portal Model

### 6.5.5.3 Thermal Loading Condition

The thermal loading condition for supported non-emplacment drifts is only applied to intersections between exhaust mains and emplacement drifts, observation drift, and intersection of observation drift with exhaust main.

### **6.5.5.3.1 Intersections between Exhaust Mains and Emplacement Drifts**

As illustrated in Figures 6-122 through 6-125, the forces in the bolts increase during the preclosure period due to heating. The predicted maximum force increases are between about 20 kN and 35 kN (Figure 6-122). The predicted maximum forces in the rock bolts are between 180 kN and 190 kN (i.e., at a safety factor of about 1.4) during the preclosure period, which are less than the yield strength.

### **6.5.5.3.2 Intersection between Observation Drift and Exhaust Main**

Thermal load causes an increase in bolt forces, as indicated in Figure 6-125A, which shows the bolt forces after 50 years of heating, and in Figure 6-125B, which shows histories of bolt forces along three bolts: one in the crown, and two in the walls. Note that the number within the parenthesis in the legend indicates bolt number shown in Figure 6-125A. However, after 50 years of heating, the loads are well within the range of elastic deformation of the rockbolts. Figure 6-125C shows the extent of inelastic deformation predicted around the observation drift. The designed bolt length of 3 m appears to be sufficient to provide anchoring into the elastic (undamaged) rock.

## **6.5.5.4 Seismic Loading Condition**

### **6.5.5.4.1 Intersections between Access Mains and Turnouts**

The intersection between Access Mains and Turnouts supported with rock bolts and shotcrete is simulated for dynamic loading due to earthquake with 10,000 year return period. The shotcrete is represented in the model with triangular shell elements, which can take axial and bending forces. The shell elements are generated in such a way to coincide with triangular faces of zones exposed on the walls of the excavations. The geometry of the shotcrete support is shown in the plan view in Figure 6-126 (together with the bolts), and in the view along the access main in Figure 6-127. Prior to seismic loading, the shotcrete carries no load; the forces in the bolts are as described in Section 6.5.5.2.2.

The unsupported intersection is stable after earthquake with 10,000 year return period even in category 1 lithophysal rock mass, the poorest quality rock mass. The increase in the permanent displacement is insignificant. Consequently, the residual load increase in the ground support after the seismic event predicted by this model is small. However, transient variations of the load (stresses) in the ground support could be a concern. Figures 6-128, 6-129 and 6-130 show bolt forces before shaking, after 40 seconds of shaking and at the end of shaking, respectively. The maximum transient bolt force increase during shaking to more than 200 kN (Figure 6-129) after 40 seconds of ground shaking when one horizontal and the vertical component of velocity are approximately 0.4 m/s (as shown in Figure 6-92). Even the maximum transient load in the bolts is less than their yield strength. Knowing that steel is quite ductile (it can undergo substantial strain after yield before it breaks), it is not expected that earthquake with 10,000 year return period will cause significant damage of the rockbolts in the intersections, even in the poorest quality rock mass (i.e., category 1, lithophysal rock mass). Note in Figure 6-130 that two bolts, pulled out during the dynamic simulation, shown inside the access main, are yielding (indicated maximum force of 264 kN). These bolts are consequence of a local effect. All other bolts in the

model behave properly, with the maximum force less than 200 kN, i.e., a safety factor greater than 1.3.

The shell elements used for simulation of the shotcrete are linearly elastic. The forces in the elements are checked during the simulation and they indicate that earthquake with 10,000 year return period will cause localized damage in the shotcrete, consisting mostly of tensile fractures. Figures 6-131 and 6-132 show the contours of the major principal membrane stress in the shotcrete after 40 seconds and at the end of ground shaking, respectively. Note that compression is positive in these two figures. It shows that there is indication of tensile stresses in the significant portion of the shotcrete during ground shaking. However, at the later stage of ground motion, i.e., at the end of dynamic simulation, the tensile forces do not exist in the shotcrete, except in local areas. It should be noted that shotcrete liner is not part of the ground support as a structural element, intended to carry the force. Its function is mainly to prevent weathering of the rock and hold small pieces of the rock from falling out. So, even if shotcrete fails (cracks) it does not affect its functionality.

#### **6.5.5.4.2 Intersections between Exhaust Mains and Emplacement Drifts**

For stability analysis of supported openings in intersections between exhaust mains and emplacement drifts, the maximum bolt forces, after 40 seconds of dynamic loading caused by ground motion with 10,000 year return period (applied after drift excavation but before heating began), are shown in Figure 6-133. The maximum increase in bolt forces compared to the static condition is approximately 55 kN in the region above the intersection, resulting in a maximum bolt force of about 185 kN (comparing Figure 6-133 to Figure 6-117) with a safety factor of about 1.4.

#### **6.5.5.4.3 Observation Drift**

The bolt forces in observation drift after seismic shaking is shown in Figure 6-134. The histories of bolt forces along three bolts in observation drift during seismic shaking is shown in Figure 6-135. The extent of the potential yield zone around the observation drift after seismic shaking is shown in Figure 6-136. The maximum bolt force after seismic shaking is 73.1 kN ( $1.25\text{m} \times 58.47 \text{ kN/m}$ ), much less than the bolt yield strength of 264 kN.

The ground support in the intersection between observation drift and exhaust main was analyzed using a three-dimensional model. The predicted bolt forces after 50 years of heating and after seismic ground shaking are shown in different views in Figures 6-137 to 6-141. The forces in the rockbolts installed in the exhaust main at the intersection with the observation drift are approximately 150 kN after thermal loading and during seismic loading. These loads are of the same order, but less than those predicted by the forces in the rockbolts at the intersection between the exhaust main and the emplacement drift (see Section 6.5.5.4.2). In the same time, the forces in the rockbolts in the observation drift in the intersection are quite small, less than 50 kN.

#### **6.5.5.4.4 TBM Launch Chamber**

The forces in the rockbolts at the end of dynamic simulation, shown in Figure 6-142, are small relative to the yield strength of the rockbolts. Note that the values indicated in the figure need to be multiplied by the 1.25-m spacing of the bolt rows to obtain the forces in the bolts. Figure 6-143 indicates that the forces in the bolts installed in the wall (in the region of the largest damage of the rock mass) have a residual component in addition to transient oscillation after seismic loading. Comparison of the bolt lengths and the size of the region of damaged rock suggests that the designed bolt length is sufficient, because the anchoring length into the elastic rock mass is approximately at least 1 m (see Figure 6-144).

#### **6.5.5.4.5 North Portal**

The forces and stresses in the ground support at North Portal and starter tunnel induced by the seismic loading at two stages during simulation are shown in Figures 6-145 and 6-146. The forces in the bolts are less than 10 kN. The yield strength of the fully grouted bolts is 264 kN. The compressive stresses in the shotcrete are very small, i.e., less than about 1.7 MPa (see Figures 6-147 and 6-148). However, the considered ground motion could cause localized tensile failure in the shotcrete. The failure will occur in the form of fractures that will not affect functionality of the shotcrete either on the slopes or in the starter tunnel.

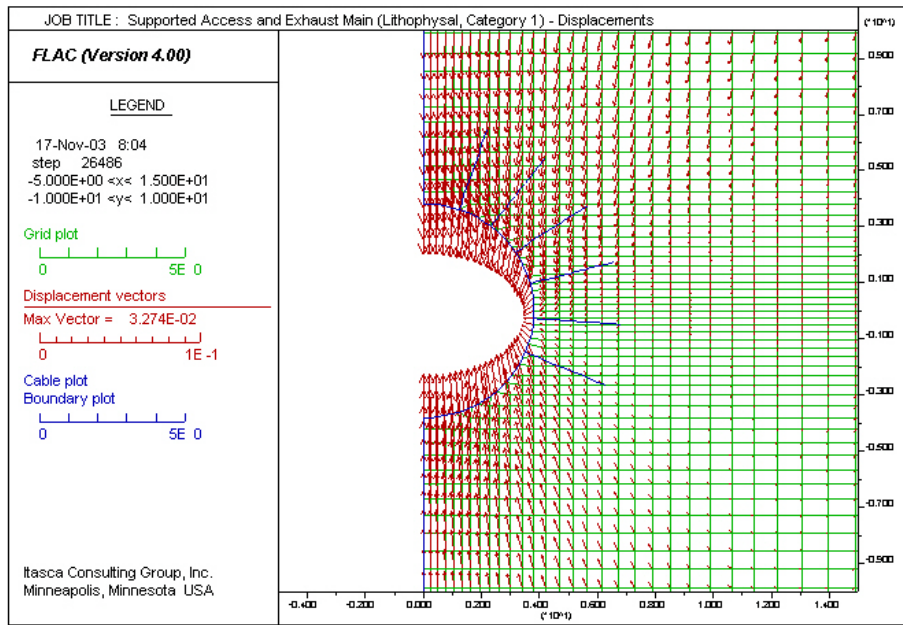


Figure 6-106. Displacements around Supported Access Main for Lith. Cat. 1 Rock

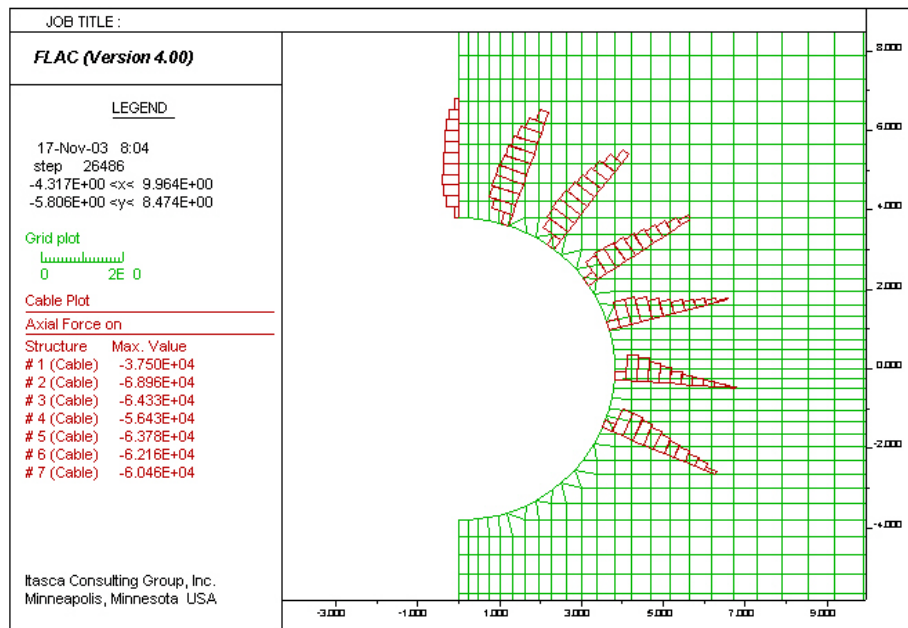


Figure 6-107. Axial Force along Bolts at Access Main for Lith. Cat. 1 Rock

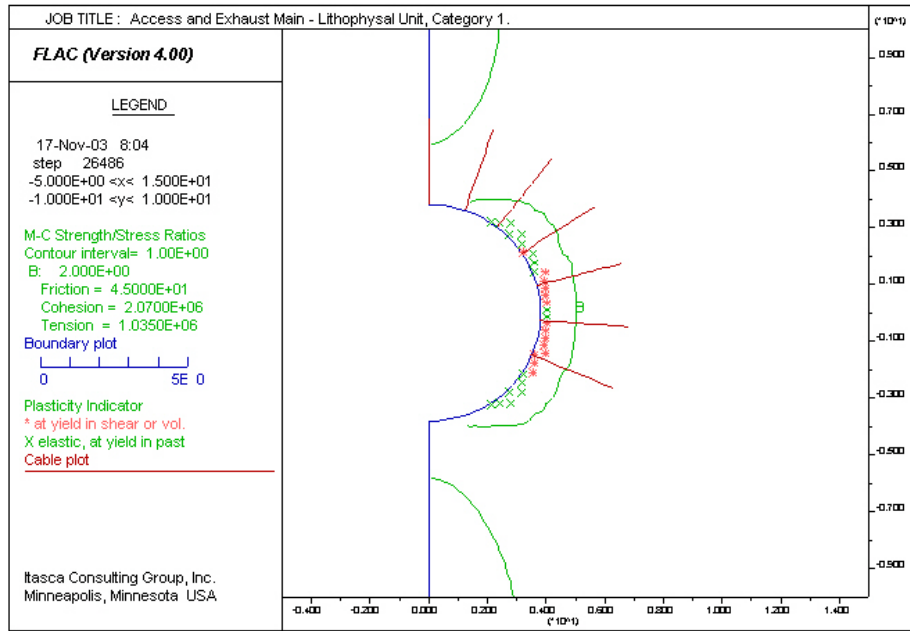


Figure 6-108. Contours of Safety Factor around Supported Access/Exhaust Main for Lith. Cat. 1 Rock

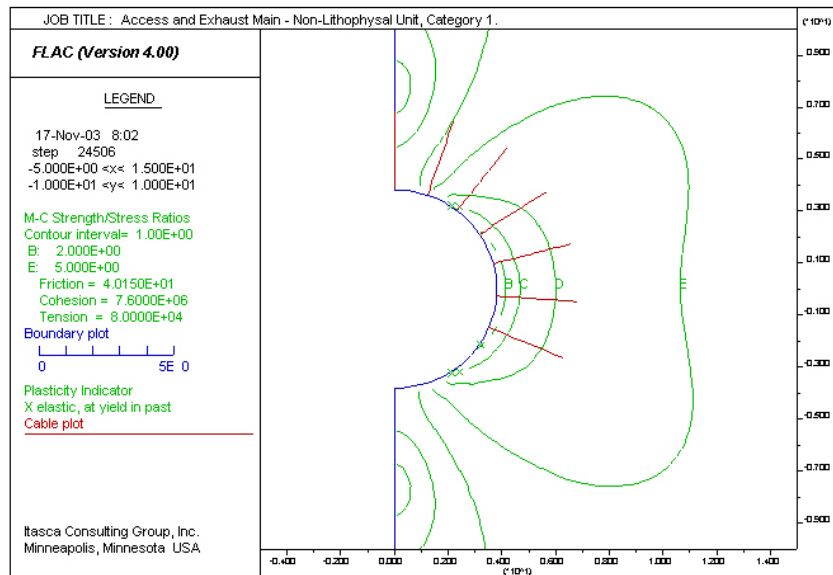


Figure 6-109. Contours of Safety Factor around Supported Access/Exhaust Main for N. Lith. Cat. 1 Rock

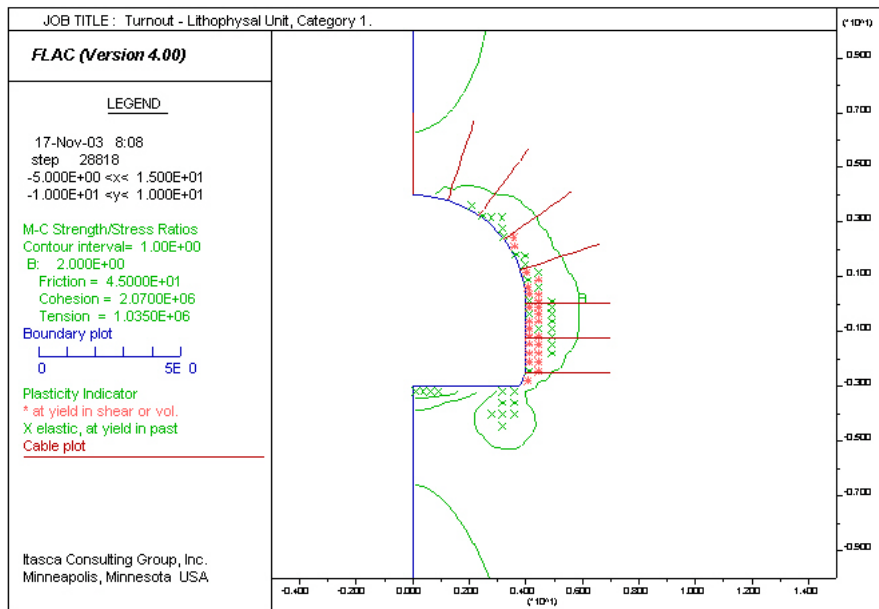


Figure 6-110. Contours of Safety Factor around Supported Turnout for Lith. Cat. 1 Rock

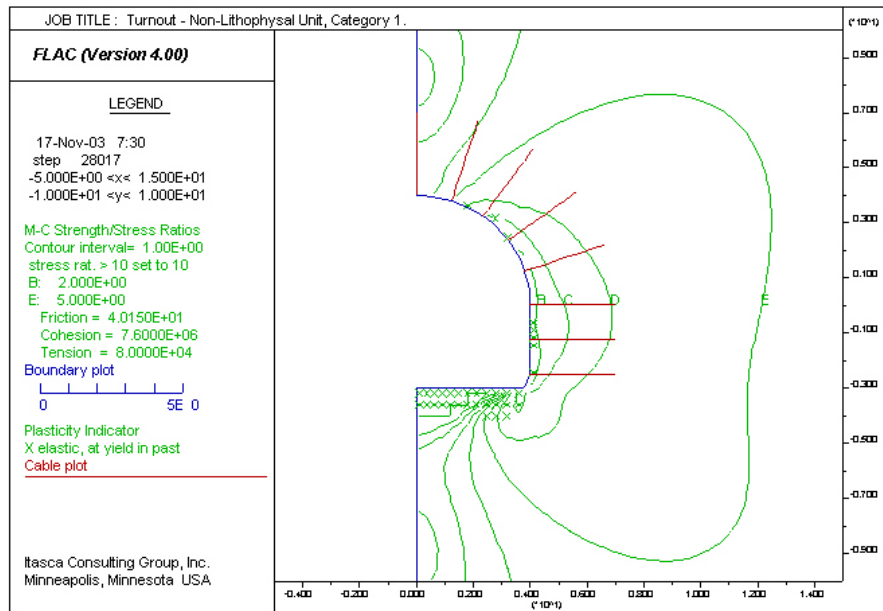


Figure 6-111. Contours of Safety Factor around Supported Turnout for N. Lith. Cat. 1 Rock

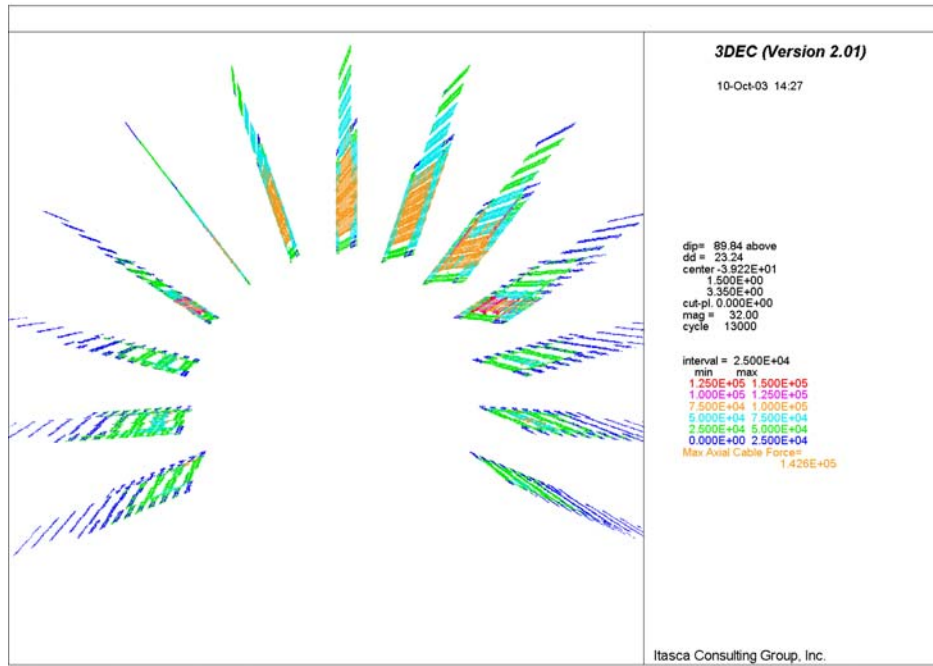


Figure 6-112. Axial Forces in Bolts along the Access Main after Excavation

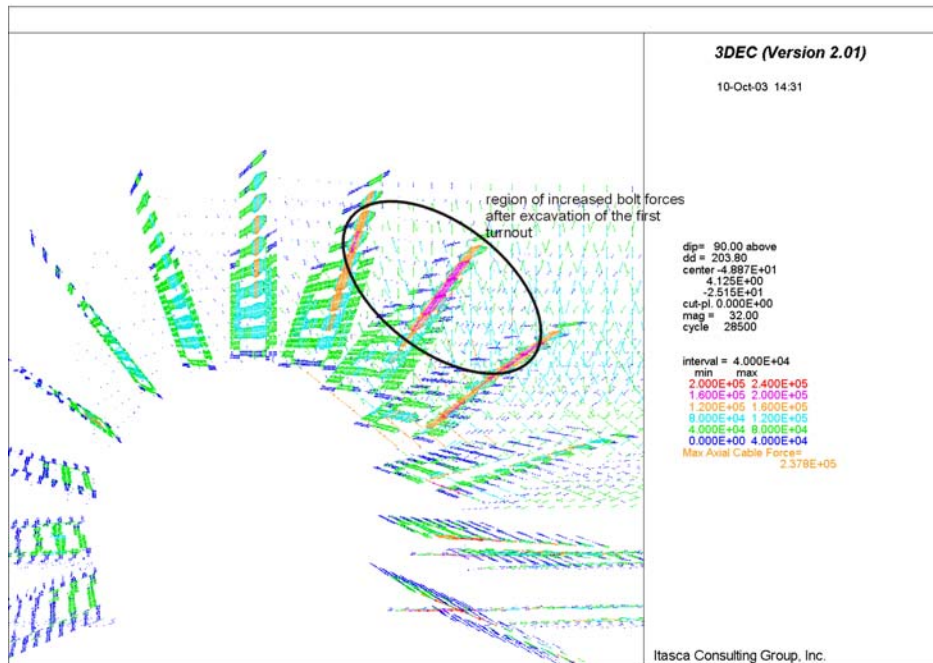


Figure 6-113. Axial Forces in Bolts along the Access Main after Excavation of First Turnout

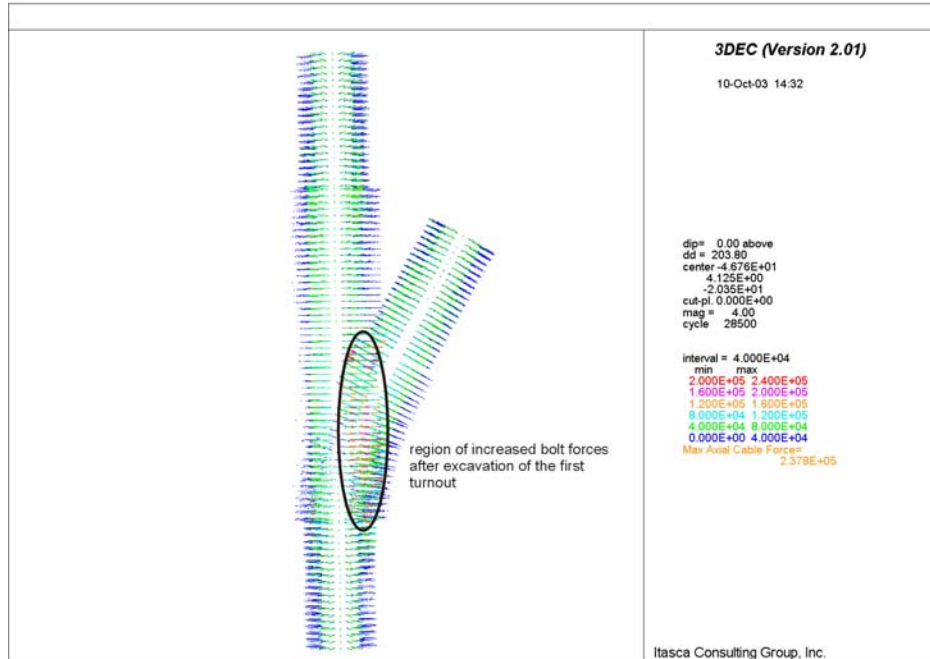


Figure 6-114. Plan View: Axial Forces in Bolts along the Access Main after Excavation of First Turnout

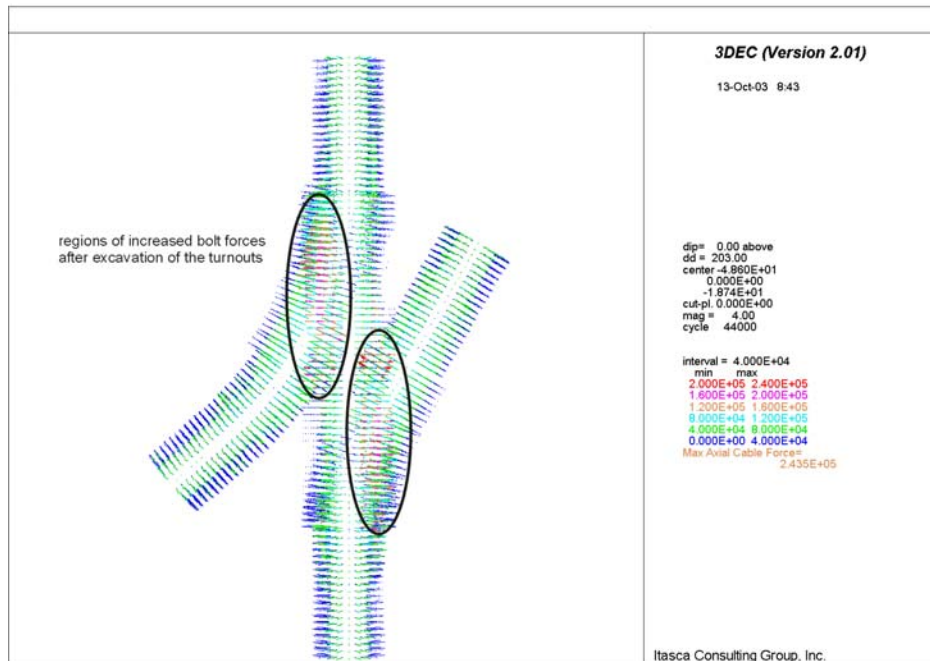
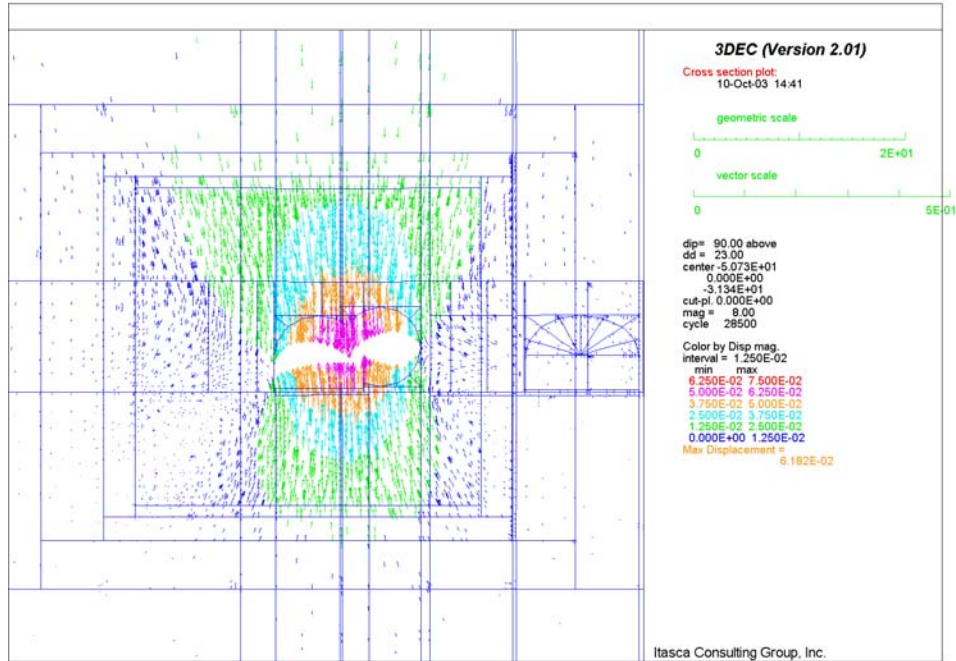
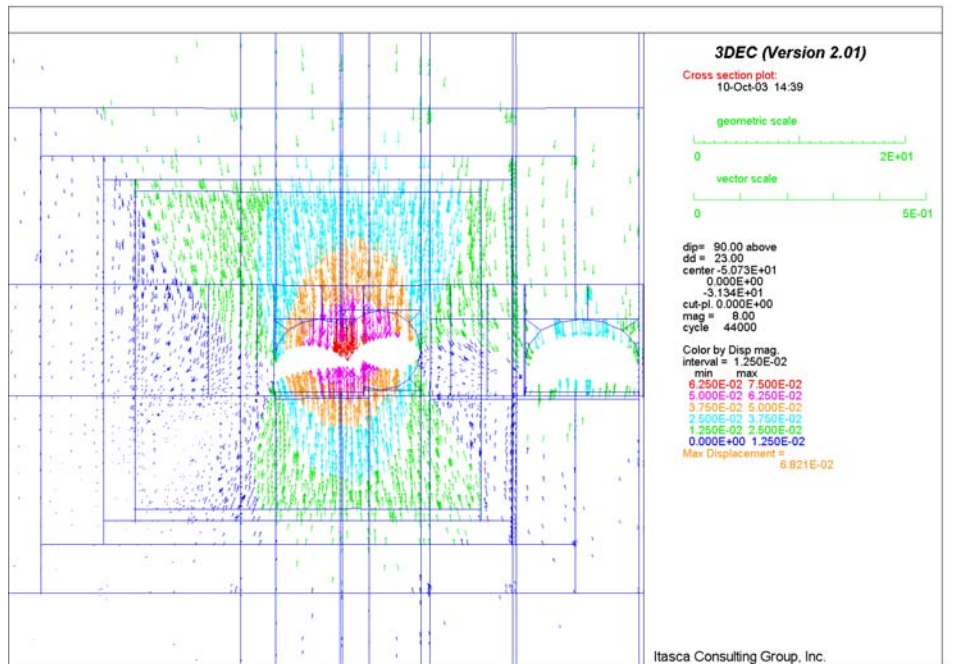


Figure 6-115. Plan View: Axial Forces in Bolts along the Access Main after Excavation of both Turnouts



(a)



(b)

Figure 6-116. Displacement in Vertical Section 2 through First Intersection: a) before, b) after Excavation of Second Turnout

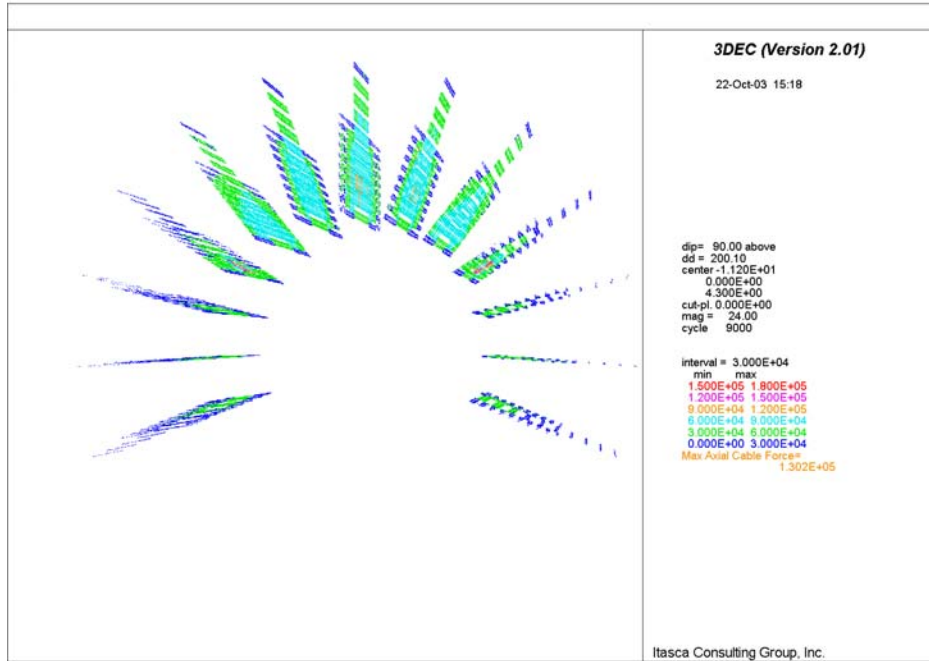


Figure 6-117. Axial Forces in Bolts along Exhaust Main after Excavation

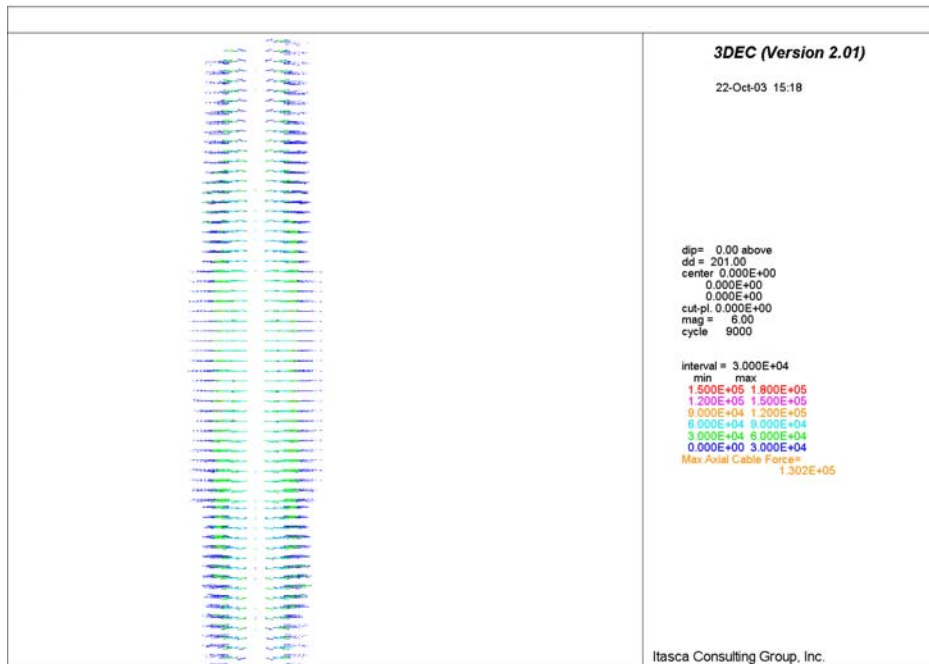


Figure 6-118. Plan View of Axial Forces in Bolts along Exhaust Main after Excavation

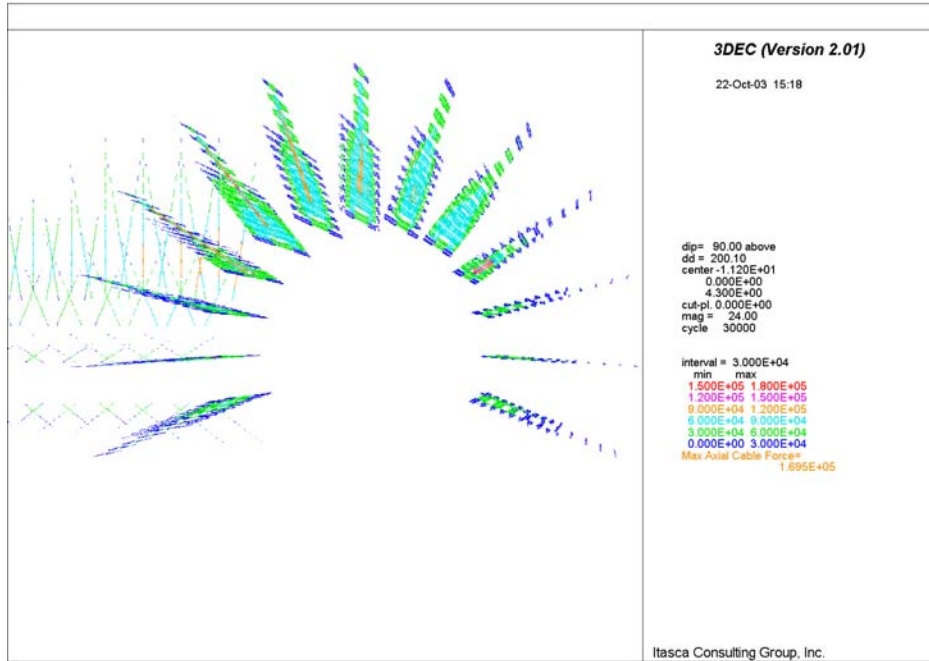


Figure 6-119. Axial Forces in Bolts along Exhaust Main after Excavation of Exhaust Main and Emplacement Drift

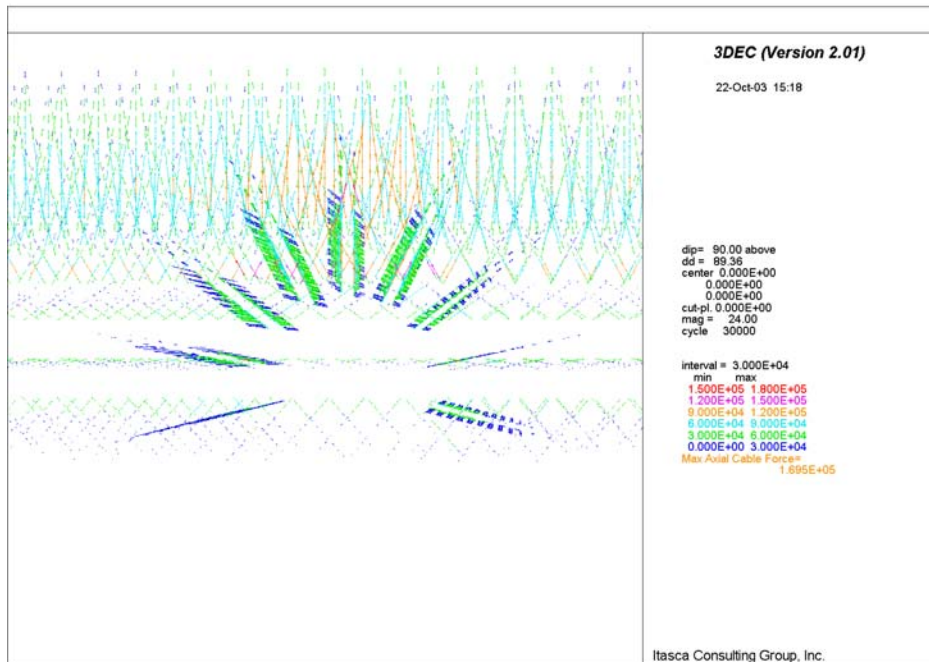


Figure 6-120. Axial Forces in Bolts along Emplacement Drift after Excavation of Exhaust Main and Emplacement Drift

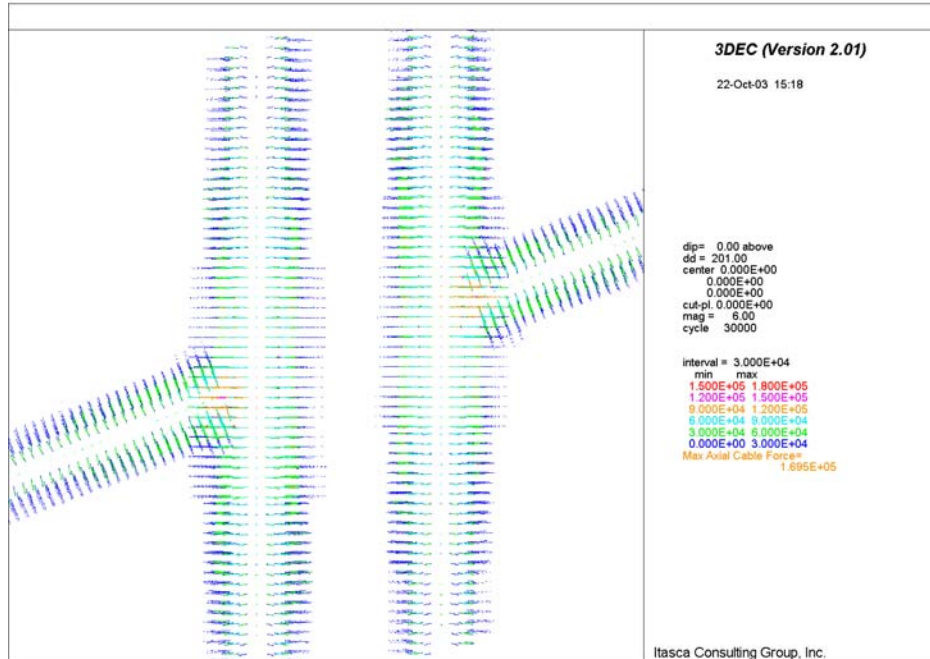


Figure 6-121. Plan View of Axial Forces in Bolts along Exhaust Main after Excavation of Exhaust Main and Emplacement Drift

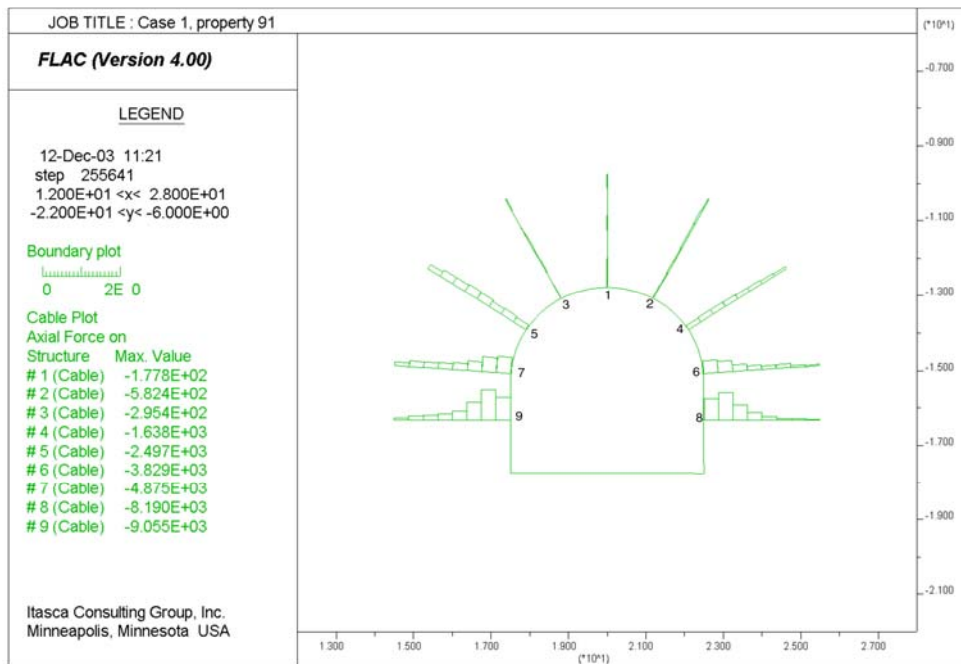


Figure 6-121A. Bolt Forces in Observation Drift after Excavation of Emplacement Drift

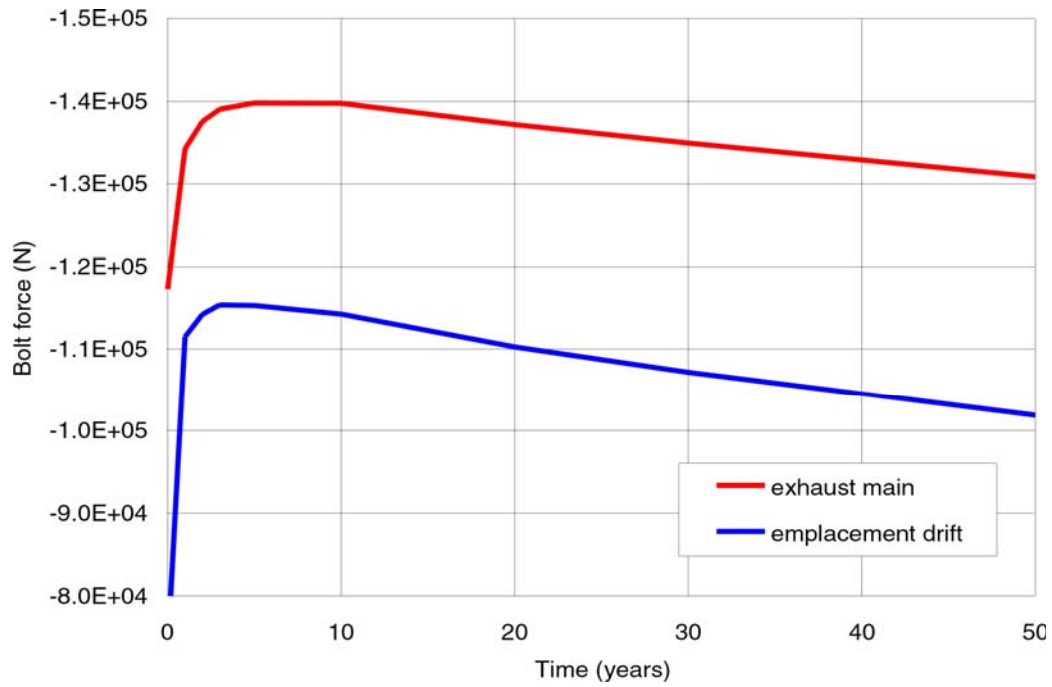


Figure 6-122. Time History of Bolt Forces at Exhaust Main and Emplacement Drift during Preclosure

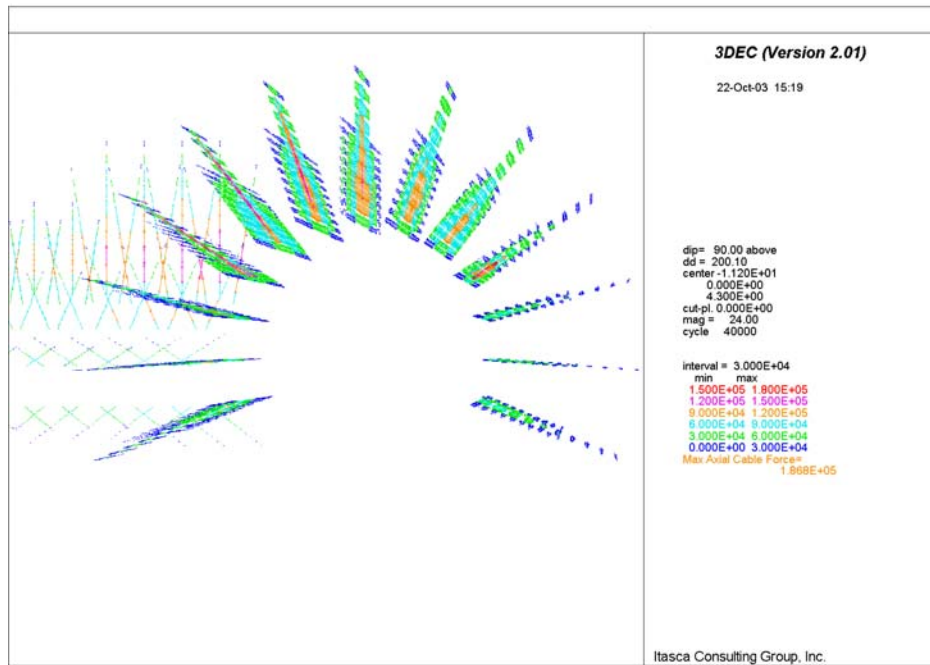


Figure 6-123. Intersection B: Forces in Bolts along Exhaust Main after 5 Years of Heating

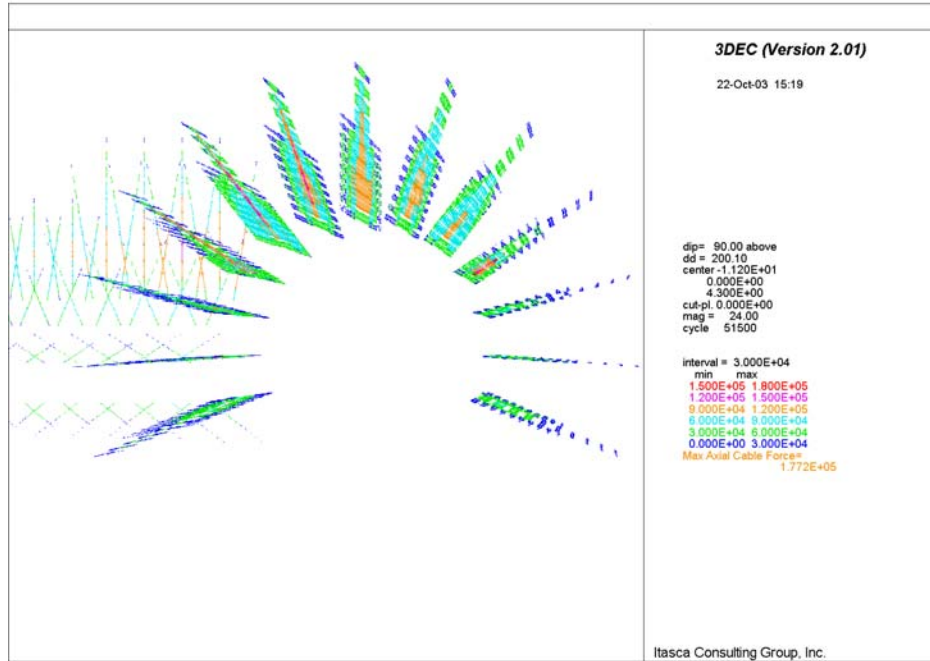


Figure 6-124. Intersection B: Forces in Bolts along Exhaust Main after 50 Years of Heating

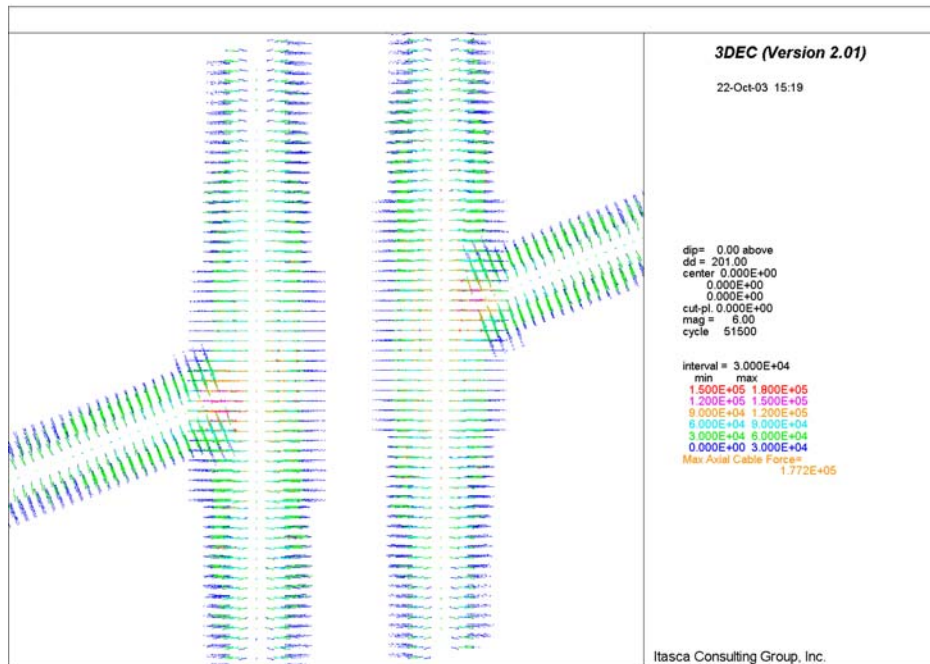


Figure 6-125. Plan view of Forces in Bolts along Exhaust Main after 50 Years of Heating

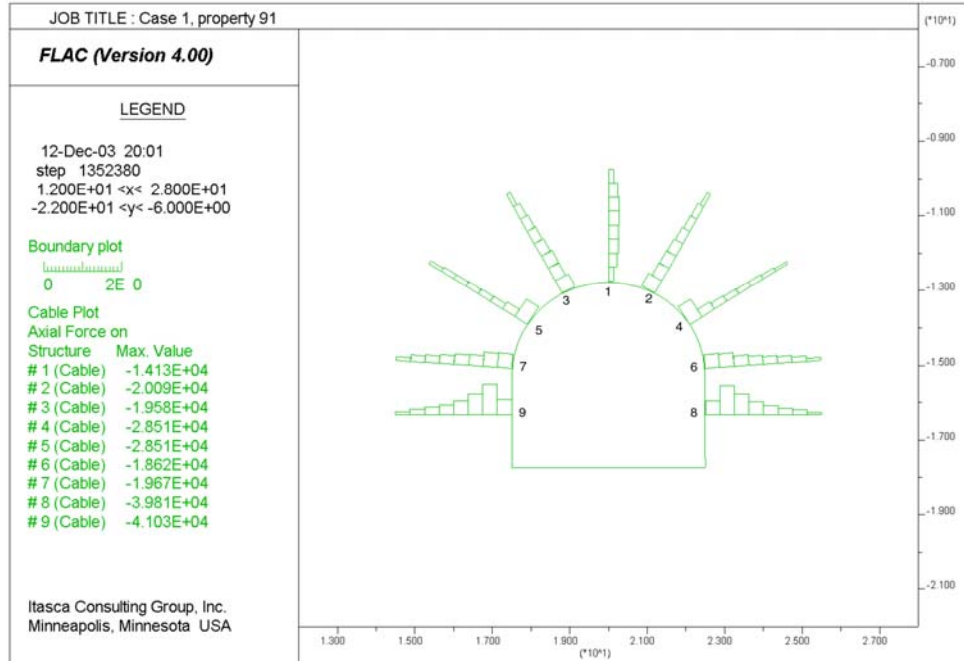


Figure 6-125A. Bolt Forces in Observation Drift after 50 Years of Heating

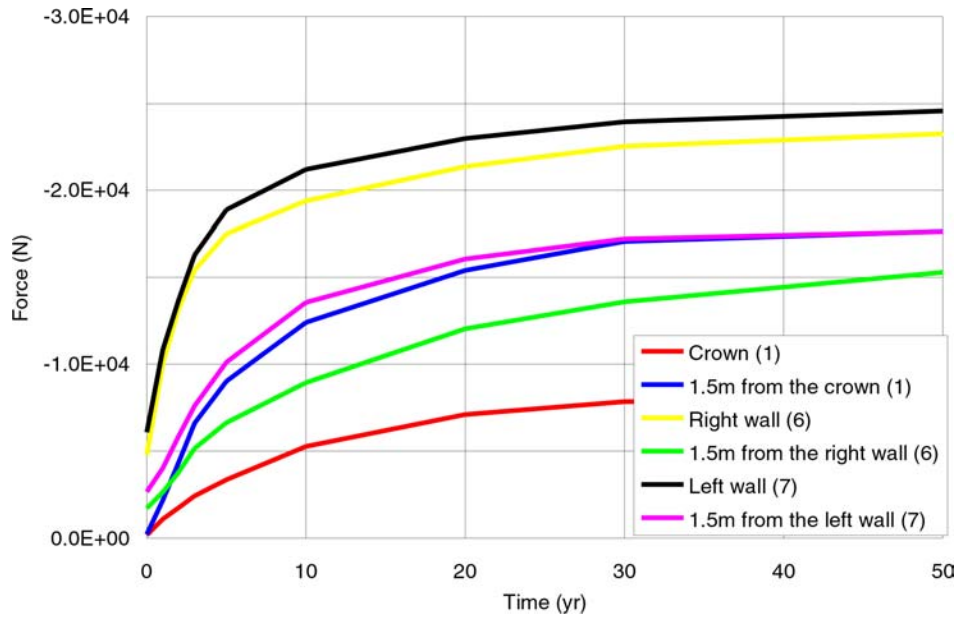


Figure 6-125B. Bolt Forces in Three Points of Observation Drift after 50 Years of Heating

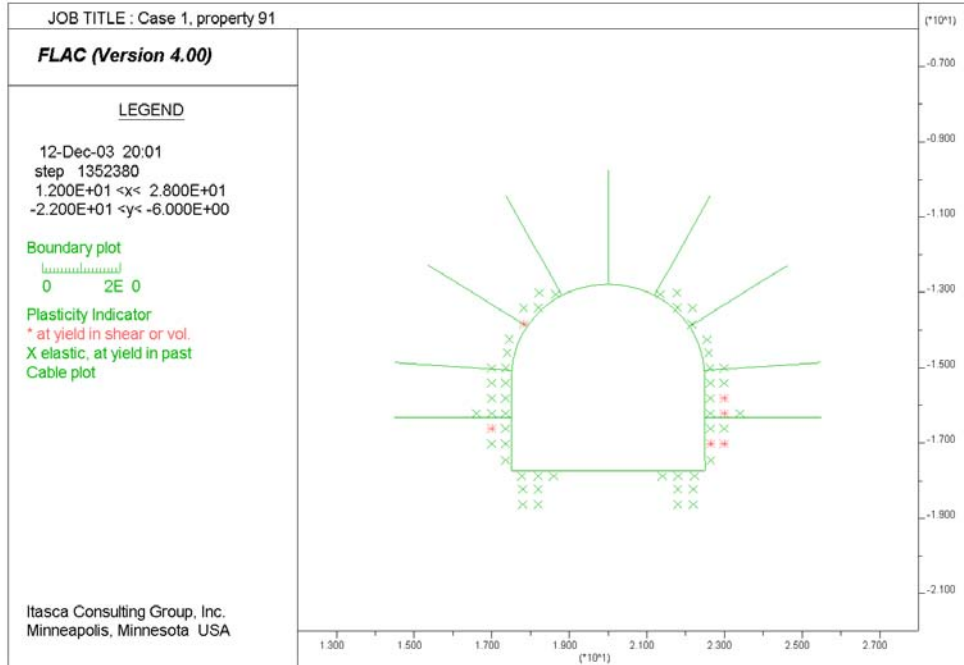


Figure 6-125C. Potential Yield Zone around Observation Drift after 50 Years of Heating

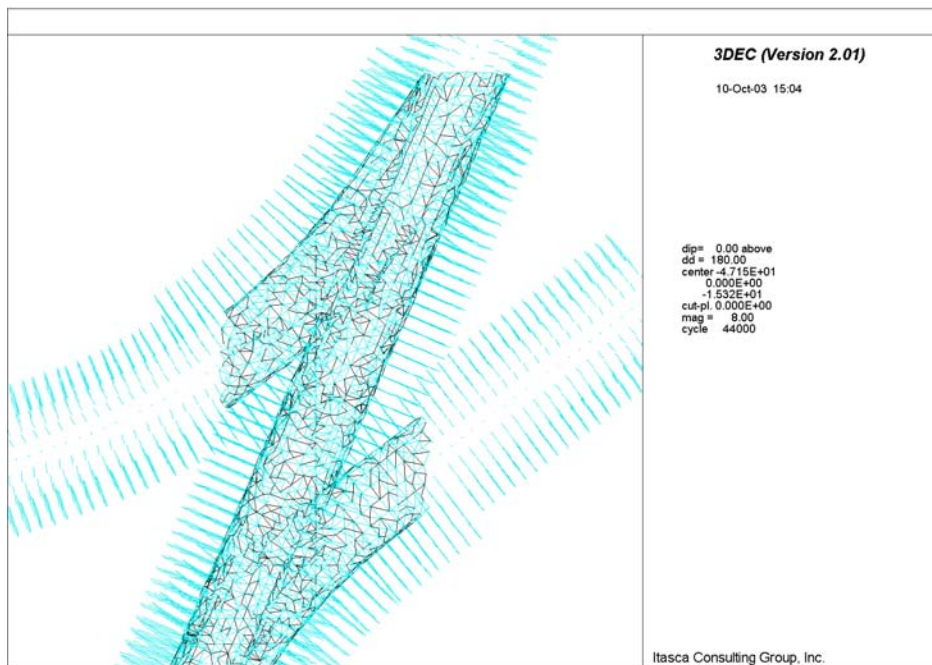


Figure 6-126. Plan View of Rock Bolts and Shotcrete at Intersection of Access Main and Turnout

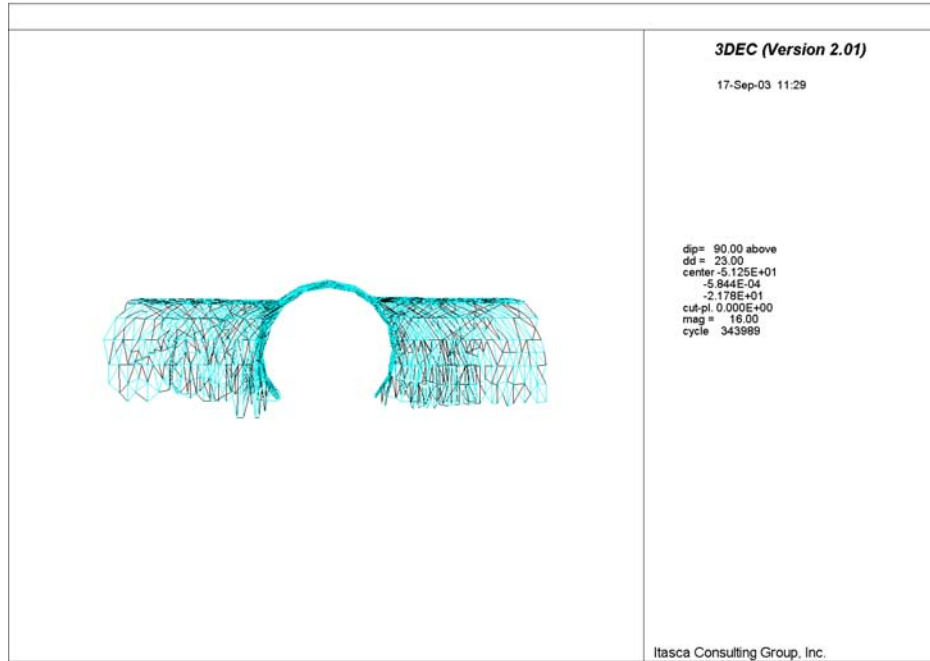


Figure 6-127. Perspective View along Access Main showing Geometry of Shotcrete

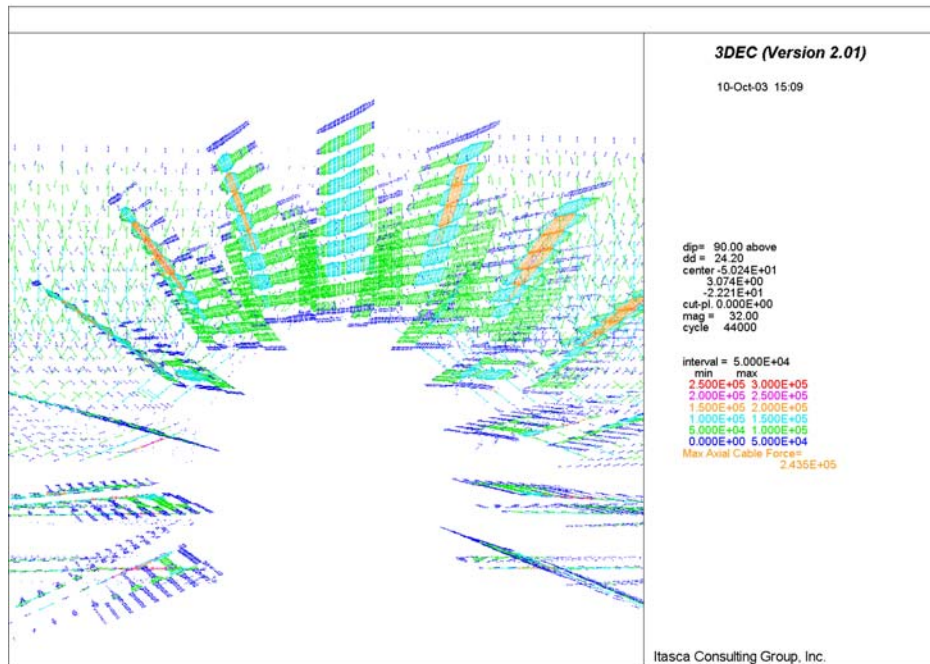


Figure 6-128. Axial Forces in Bolts along Access Main before Ground Shaking

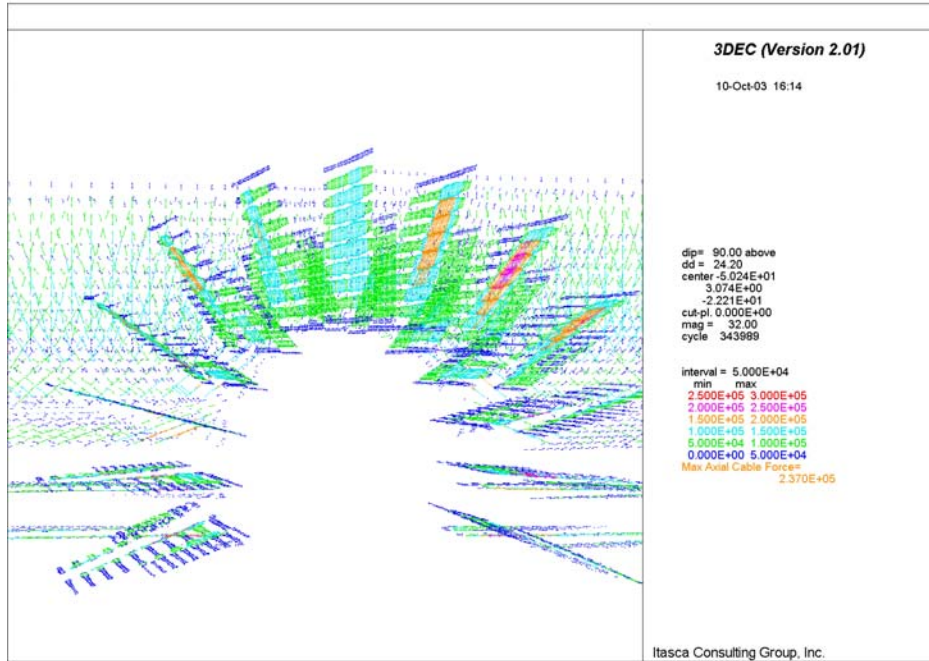


Figure 6-129. Axial Forces in Bolts along Access Main after 40 seconds of Ground Shaking

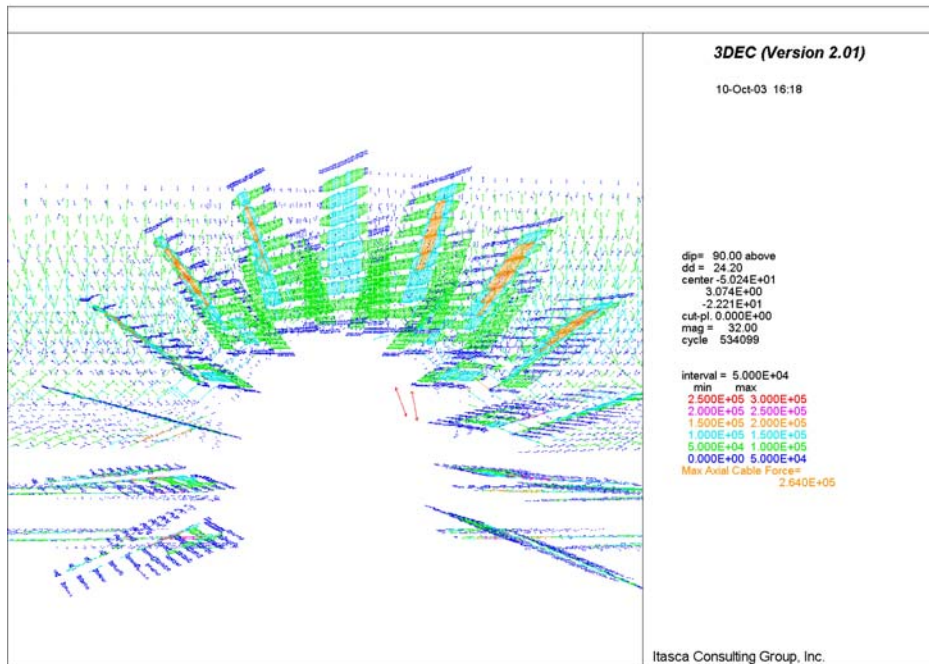


Figure 6-130. Axial Forces in Bolts along Access Main at End of Ground Shaking

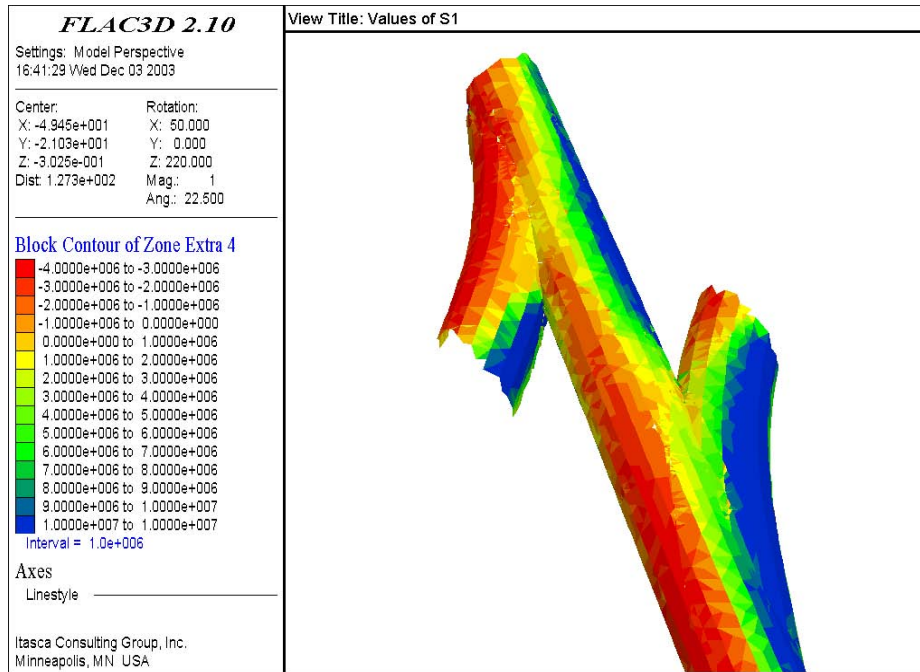


Figure 6-131. Contours of Major Principal Stresses in Shotcrete after 40 Seconds of Ground Shaking

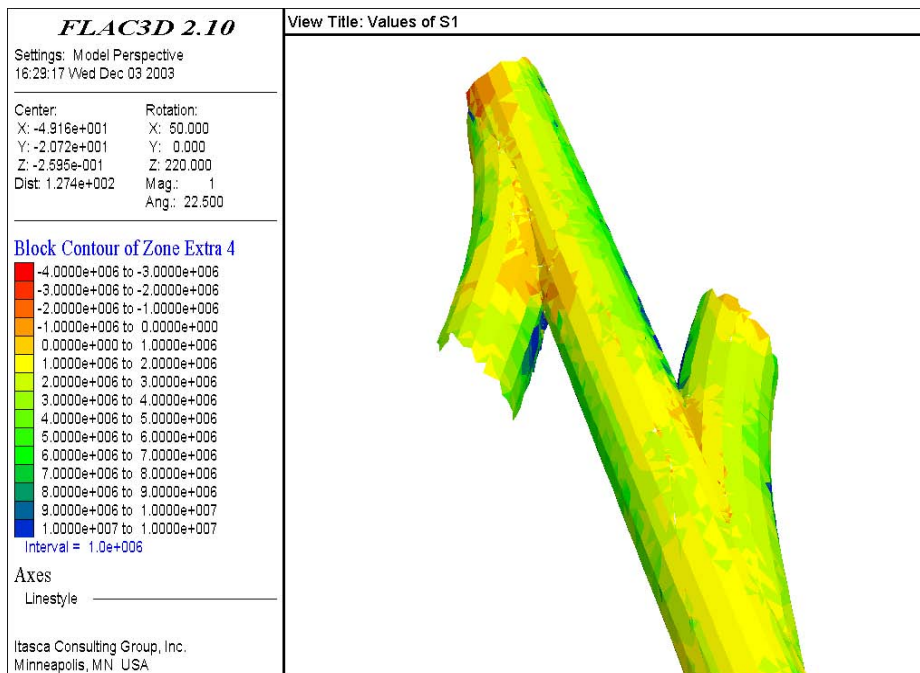


Figure 6-132. Contours of Major Principal Stresses in Shotcrete at End of Ground Shaking

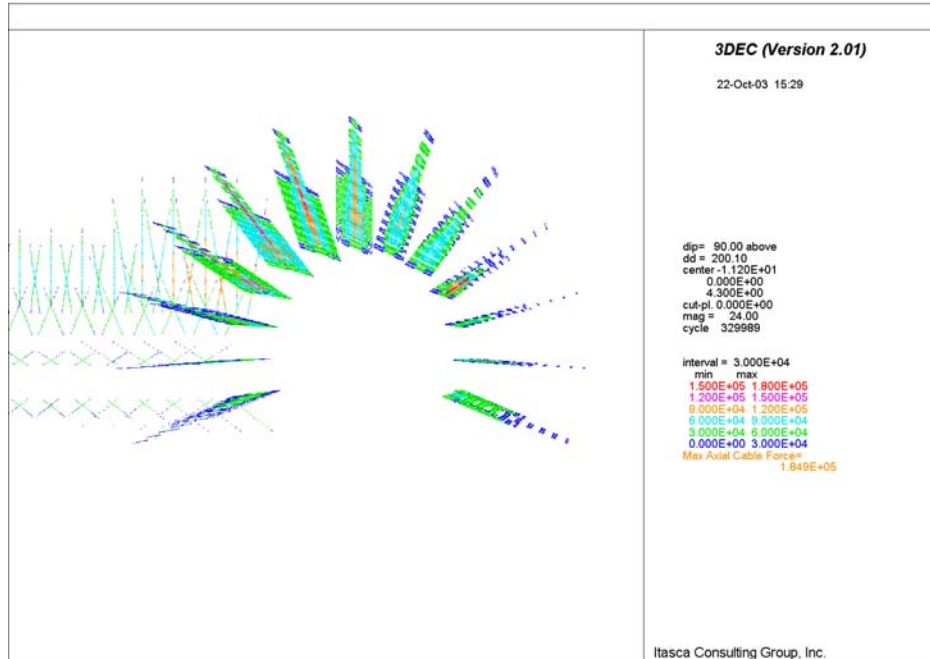


Figure 6-133. Forces in Bolts along Exhaust Main after 40 Seconds of Ground Shaking

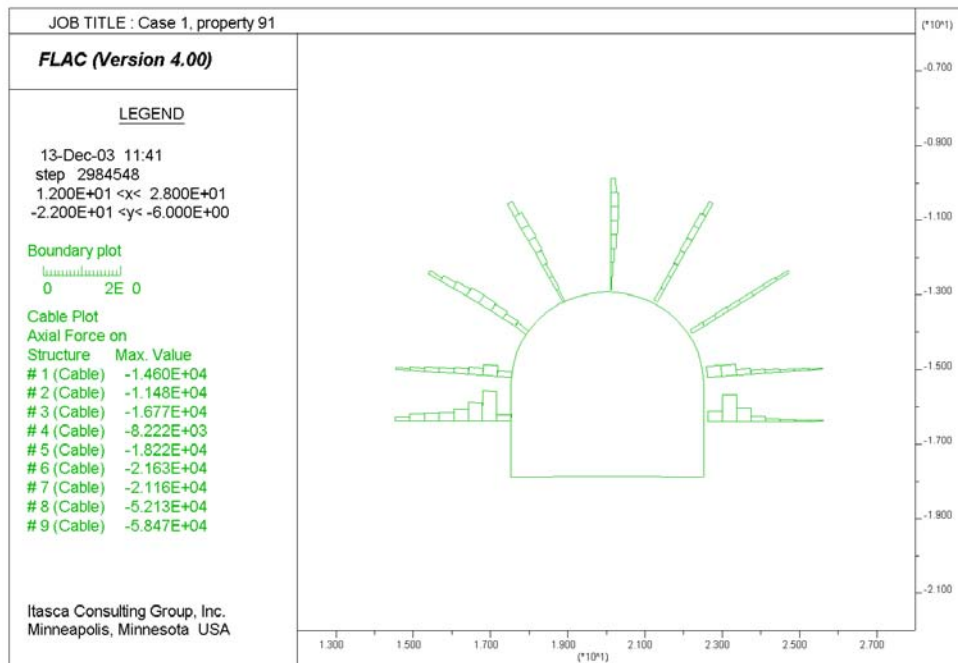


Figure 6-134. Bolt forces in Observation Drift after Seismic Shaking

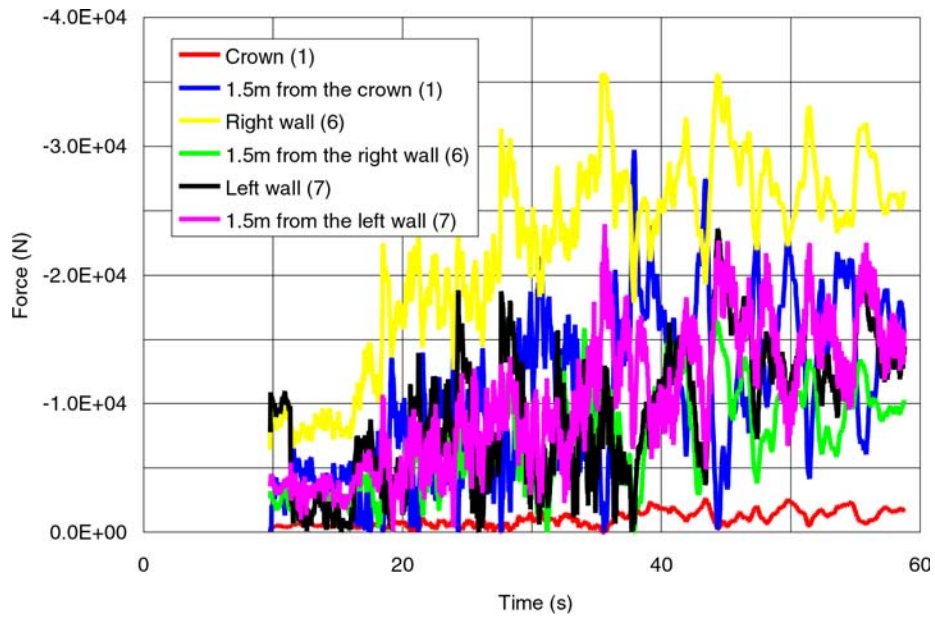


Figure 6-135. Histories of Forces in Three Bolts in Observation Drift during Seismic Shaking

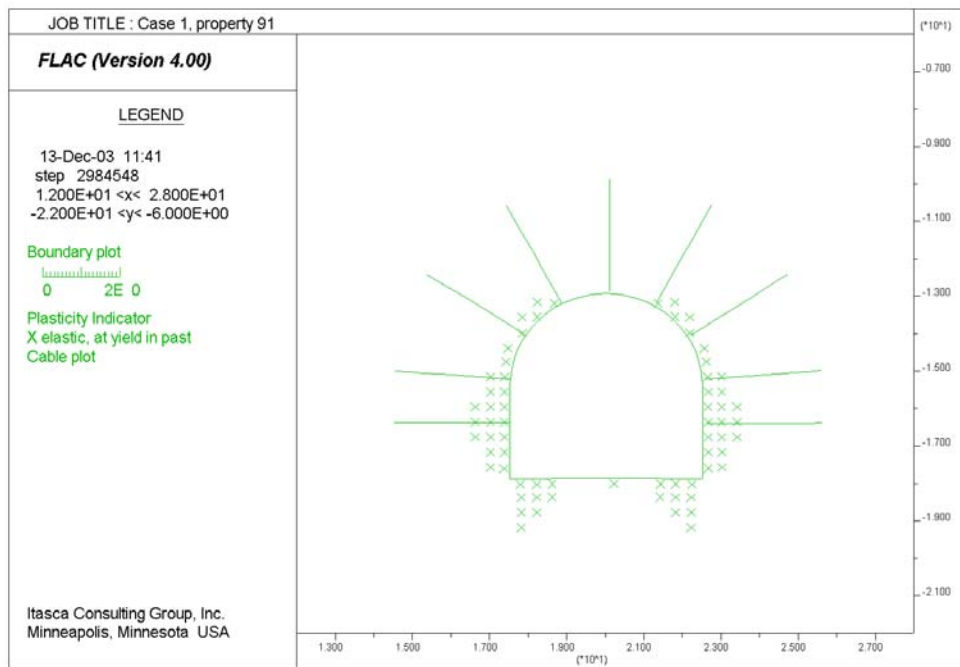


Figure 6-136. Potential Yield Zone around Observation Drift after Seismic Shaking

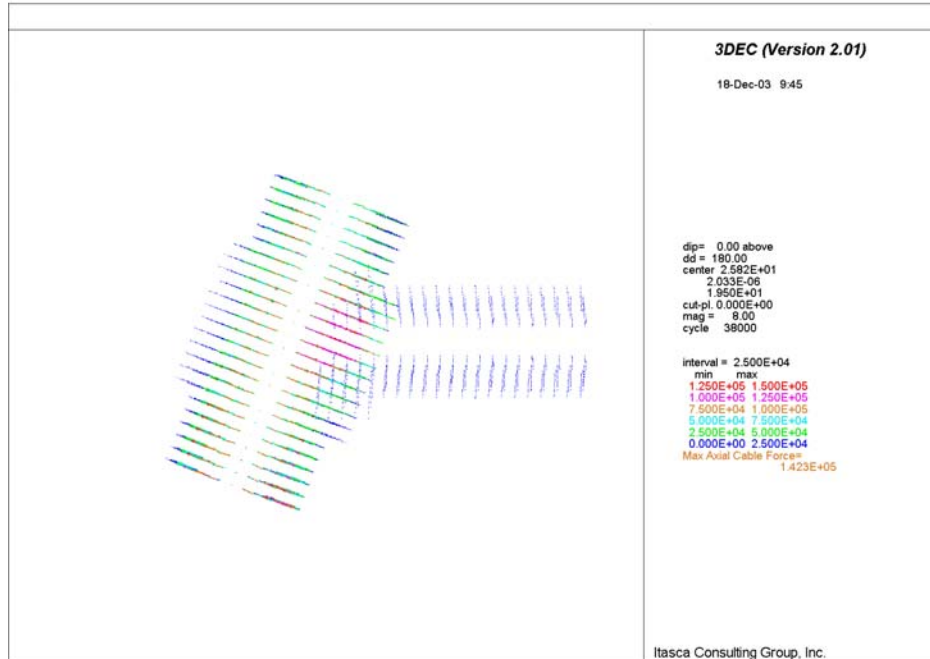


Figure 6-137. Plan View of Bolt Forces in Intersection between Observation Drift and Exhaust Main after 50 Years of Heating

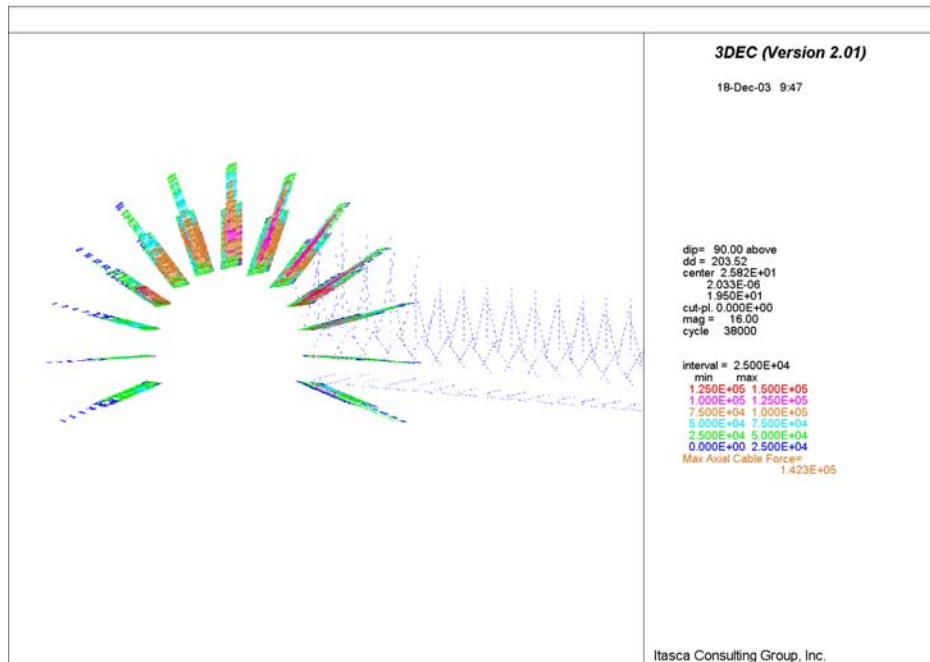


Figure 6-138. Bolt Forces in Intersection between Observation Drift and Exhaust Main after 50 Years of Heating – View along Exhaust Main

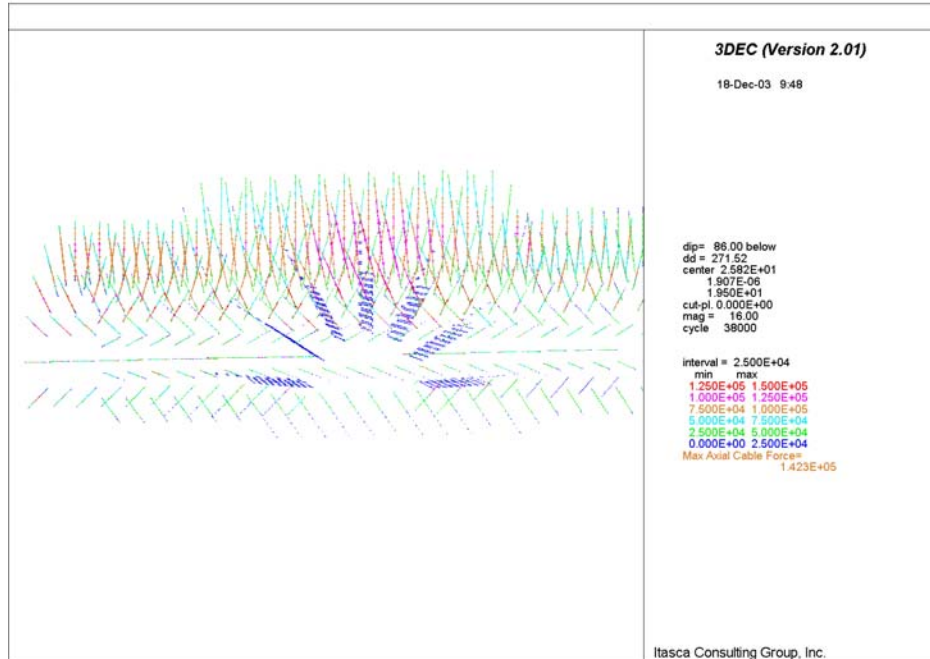


Figure 6-139. Bolt Forces in Intersection between Observation Drift and Exhaust Main after 50 Years of Heating – View along Observation Drift

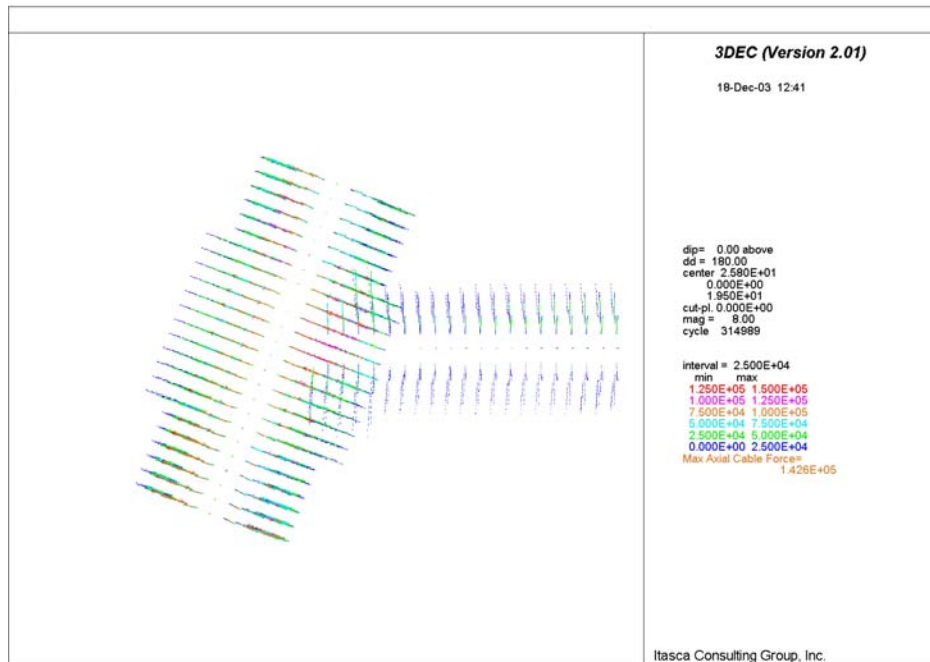


Figure 6-140. Plan View of Bolt Forces in Intersection between Observation Drift and Exhaust Main after 40 Seconds of Seismic Shaking

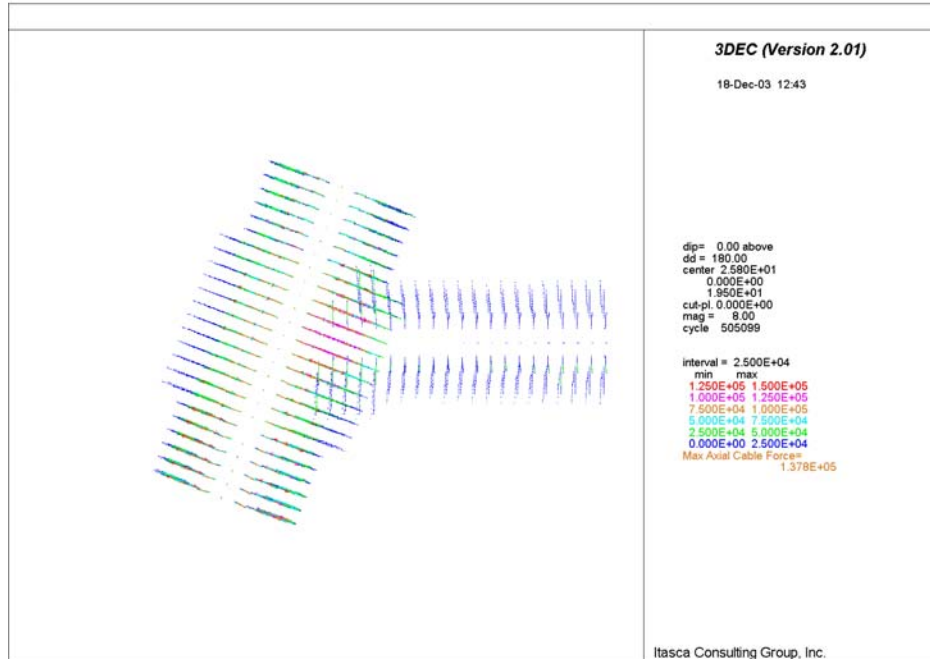


Figure 6-141. Plan View of Bolt Forces in Intersection between Observation Drift and Exhaust Main at End of Seismic Shaking

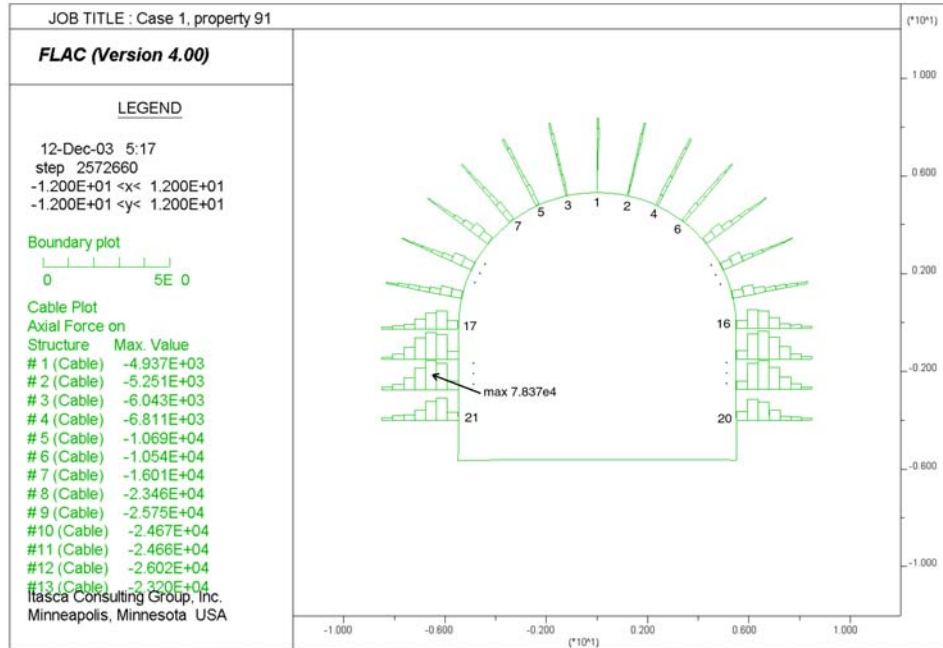


Figure 6-142. Bolt Forces in TBM Launch Chamber after Seismic Shaking

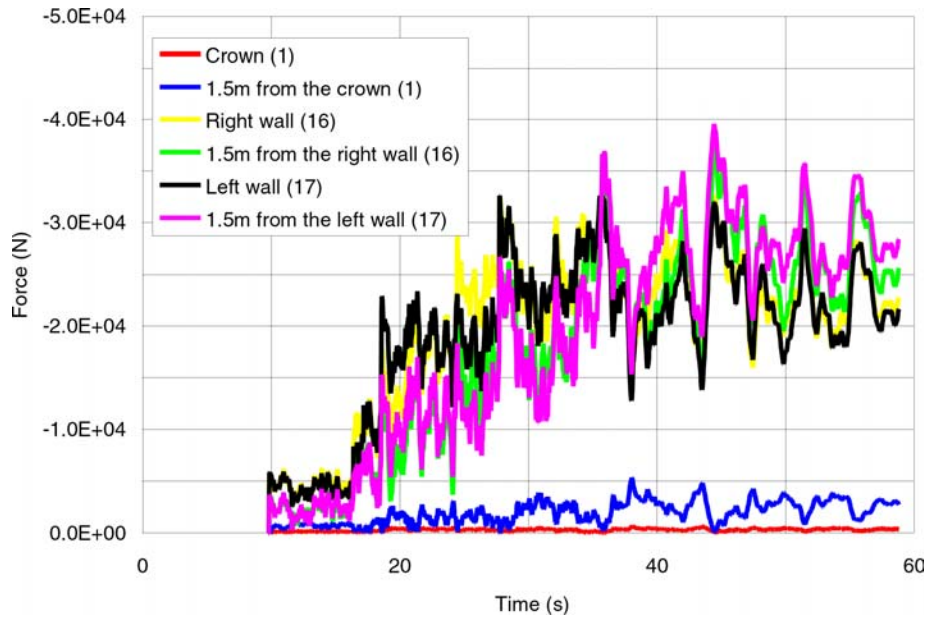


Figure 6-143. Histories of Forces in Three Bolts in TBM Launch Chamber during Seismic Shaking

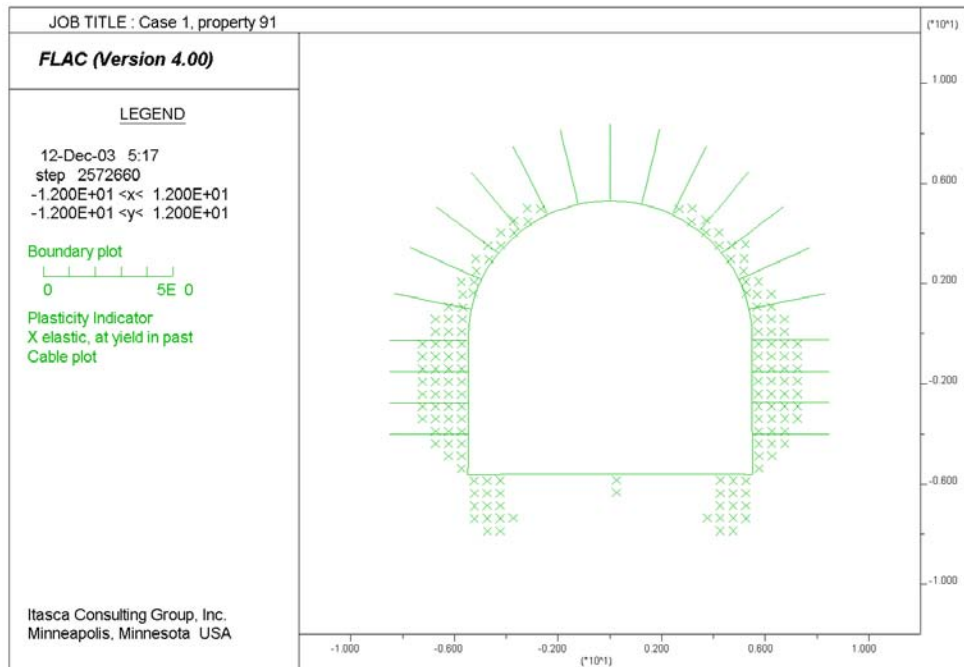


Figure 6-144. Potential Yield Zone around TBM Launch Chamber after Seismic Shaking

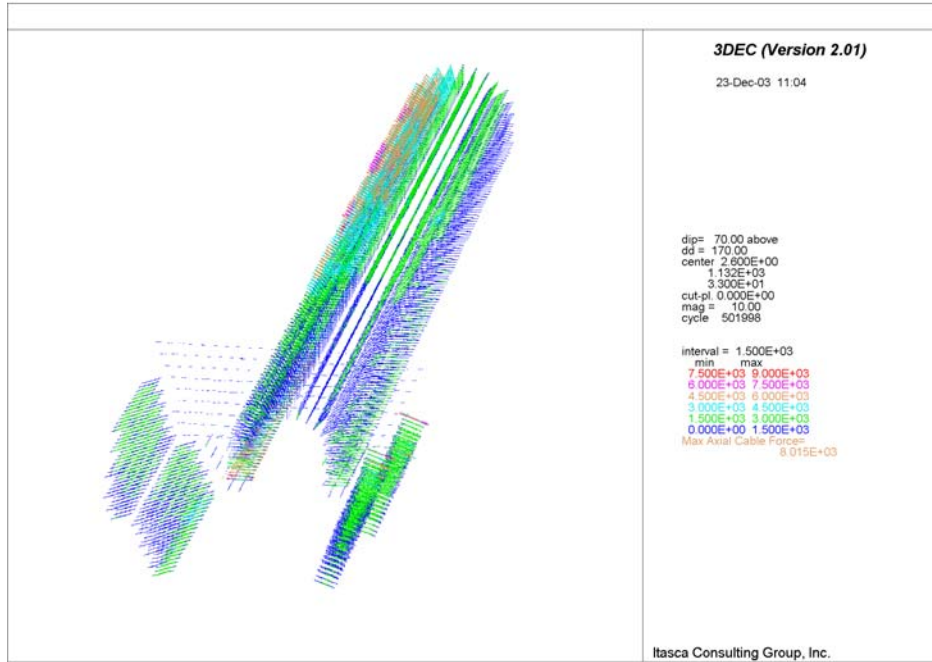


Figure 6-145. Bolt Forces in North Portal after 19.84 Seconds of Ground Shaking

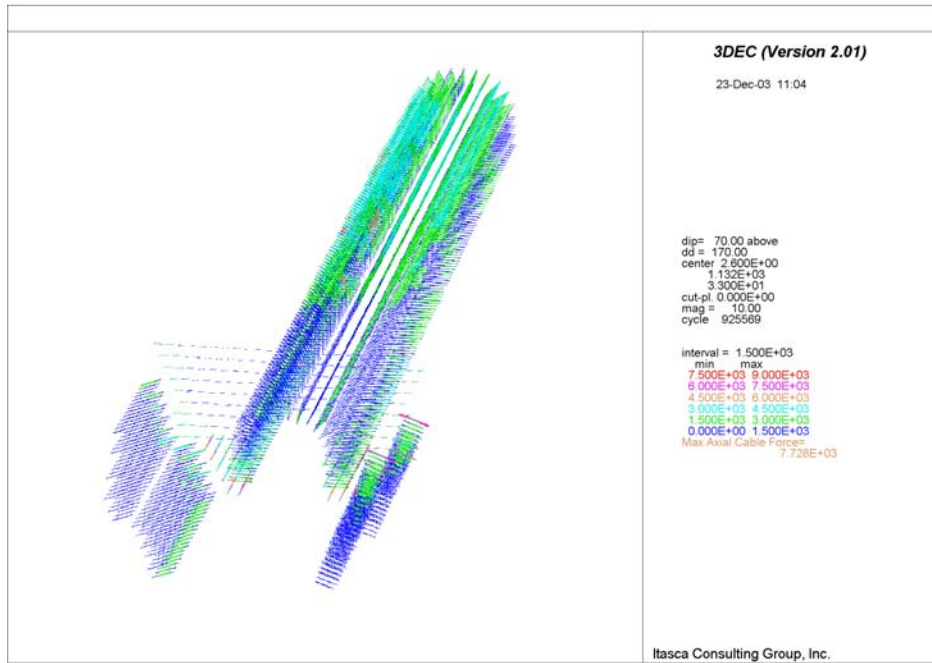


Figure 6-146. Bolt Forces in North Portal at End of Ground Shaking

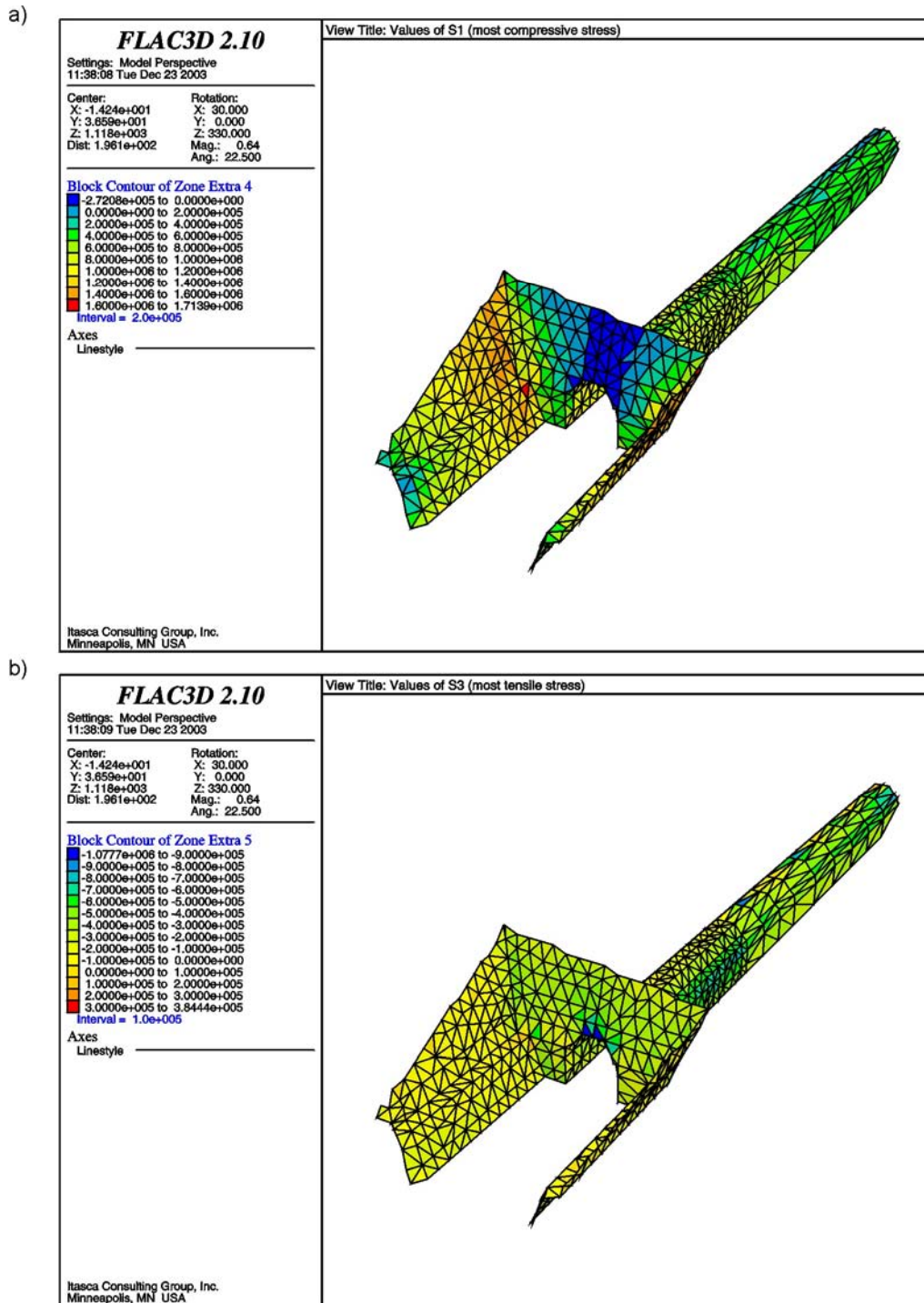


Figure 6-147. Contours of a) Major and b) Minor Principal Membrane Stresses in Shotcrete after 19.84 Seconds of Ground Shaking

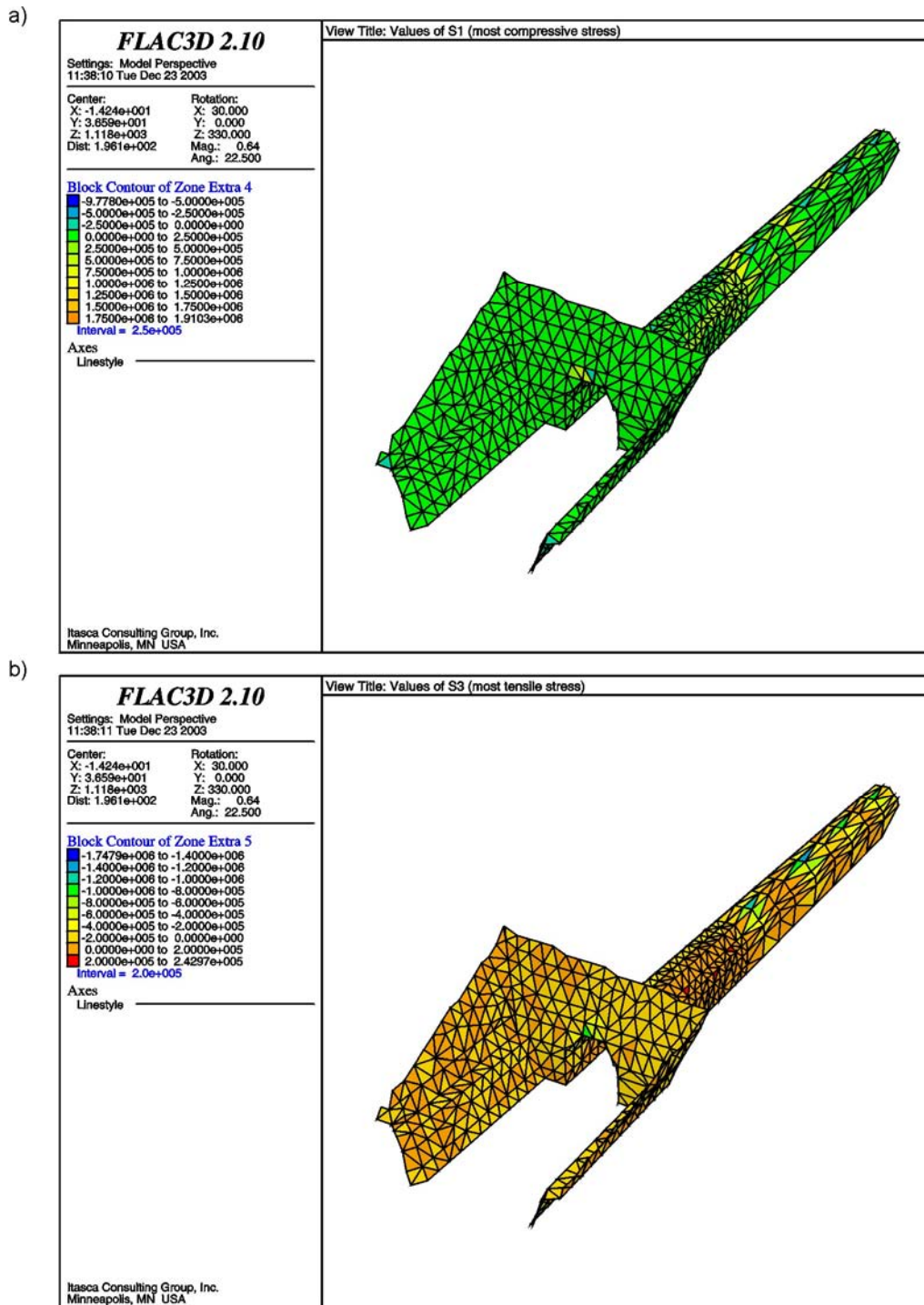


Figure 6-148. Contours of a) Major and b) Minor Principal Membrane Stresses in Shotcrete at End of Ground Shaking

## **6.6 UNCERTAINTY DISCUSSION**

There are uncertainties associated with this calculation. These uncertainties are discussed primarily in the following areas: empirical approach, numerical modeling methods, and input data.

### **6.6.1 Uncertainties with Empirical Approach**

As discussed in Section 6.4, there are two empirical approaches adopted in this calculation for estimating the ground support need for openings at non-lithophysal rock in non-emplacment drifts, i.e., RMR and Q approaches.

For RMR approach, the ground support recommendation shown in Table 6-1 was based on a 10-m wide, horseshoe-shaped tunnel and mainly for conventional excavation method, i.e., not TBM operation. Since most tunnels or openings related to non-emplacment drifts are circular and will be excavated by TBM, therefore, there exist some uncertainties associated with the recommended ground support system based on RMR approach. In particular, the opening sizes for access and exhaust mains and turnouts are smaller than 10 m, which was based for Table 6-1. Therefore, although the recommended ground support system based on RMR approach provides good design guidance, it is considered very conservative.

For Q approach, the most important value for estimating the ground support need is the Q value. However, in order to derive the appropriate Q value there are a number of steps to estimate various parameters as shown in Section 6.4.3, in which uncertainties are involved with each step. Moreover, in applying Q value to Figure 6-4, the corresponding bolt spacing and shotcrete thickness are estimated from ranges of values covered by various intervals. Again, uncertainties are associated with the selection of appropriate bolt spacing and shotcrete thickness.

Since uncertainties are associated with both empirical approaches, their use will provide us the design guidance. The final selection ground support system will depend on numerical analysis as well as the experience obtained from construction of ESF and ECRB.

### **6.6.2 Uncertainties with Numerical Modeling Method**

In this calculation, two-dimensional FLAC is used to simulate any long tunnels compared with its dimension. 3DEC is used to simulate the intersection area, which is appropriate for three-dimensional layout configuration. FLAC3D is also run for very limited cases for comparison purposes.

For numerical analysis of stability of underground openings, there are two major modeling methods, i.e., continuous and discontinuum. In a continuum approach, the geologic features in the rock mass are “lumped” into the constitutive model that represents the overall equivalent effect of these features. In a discontinuum approach, fractures or lithophysae are modeled explicitly as interfaces or cavities. Note that FLAC and FLAC3D are continuous approaches whereas 3DEC is a discontinuum one. However, for 3DEC approach used in this calculation, the joints between blocks are glued together to behave as a continuous one.

As mentioned before, all intersection areas were modeled with 3DEC except that FLAC3D run for very limited cases. The analysis using 3DEC has the advantage of generating model geometry easily and quickly. However, because of the tetrahedral zones with constant strain used in 3DEC, the calculation of plastic deformation is sometimes inaccurate. The advantage of FLAC3D is that it performs more accurate calculations of plastic deformation, particularly in the case of softening plasticity. However, FLAC3D models for such complex geometries as those of the intersections are very time consuming to generate. Although there are some uncertainties associated with these approaches, the difference between these techniques is therefore the level of detail that is necessary in the model to adequately capture the deformation and failure mechanisms. As shown in Section 6.5.3.1.2.1, the maximum displacements calculated based on FLAC3D are comparable to that of 3DEC results. From a ground support design perspective, stability of non-emplacment drifts is judged by overall rock mass displacements and stresses. Therefore, the adoption of the approaches used in the calculation is considered adequate.

### **6.6.3 Uncertainties with Input Data**

The uncertainties associated with input data for the numerical analyses are mainly involved in the following areas: material properties, overburden depth, and opening sizes.

The effect of the rock mass quality variability within the lithophysal and non-lithophysal units at the repository level was accounted for by considering different rock mass categories. As shown in Tables 4-1 and 4-2, there are six and five rock mass categories for lithophysal and non-lithophysal rock, respectively. Category 6 lithophysal rock is representative of extremely poor quality lithophysal rock mass in the disturbed rock zone around excavations, which was not considered in the simulations because it would result in excessively conservative, unrealistic predictions of deformation and damage of the rock mass. The computer simulations in this calculation were mainly carried out for the most conservative conditions, category 1 rock (the poorest quality rock mass), both in lithophysal and non-lithophysal units. Stability analysis for category 5 rock (the strongest quality rock mass) was also included mainly for intersection between exhaust main and emplacement drift since thermally induced stress is more in rock with higher Young's modulus. Therefore, the ground support design based on the poorest quality is conservative and should also cover the good rock condition.

The average depth of repository host horizon is assumed to be 400 m for all the model calculations. Although depth of non-emplacment drifts varies from drift to drift. The depths of emplacement drifts range from 215 to 450 m with the majority between 300 to 400 m. As discussed in Assumption 5.2 that the emplacement drift stability results for the maximum value of 450 m would be similar to those for the bounding case of 400 m. The overburden depth of the majority of non-emplacment drifts are less than 400 m, use of a depth of 400 m for calculating in situ stress at the non-emplacment drift horizon is considered adequate for the purpose of this calculation.

There are several configurations in intersections between access mains and turnouts and between exhaust mains and emplacement drifts, with roof spans at openings varying from about 10 m to greater than 20 m. The intersection A at intersections between access mains and turnouts represents the critical conditions with respect to the maximum span of the roof and stress concentrations in the pillars whereas intersection C represents a typical layout. The intersections

B at intersections between exhaust mains and emplacement drifts represent intersection locations in the middle of the repository with large roof span whereas D represents locations at the edge of the repository. Temperature changes at the edge of the repository (location D) are overpredicted by NUFT's two-dimensional results, resulting in conservative estimate of stress increase and more unfavorable stability conditions. Also, the diameter of exhaust mains are assumed as 7.62 m throughout the analysis, even though it is 5.5 m in Panel 1 of the repository. With large roof span, the larger stresses will be resulted, which will give conservative estimate on ground support system.

Based on the above discussion, the model layout in terms of locations and opening sizes should result in conservative results regarding the on stability of non-emplacment drifts.

## **7. SUMMARY AND CONCLUSIONS**

### **7.1 SUMMARY**

This analysis for ground support design at non-emplacement drifts demonstrates that a satisfactory ground control system can be developed for the Yucca Mountain repository. The repository ground support design was based on both empirical approaches and analytical methods using acquired computer codes, and focused on the final support systems.

Empirical approaches using RMR value and Q index were used to estimate the ground support need for openings in non-lithophysal rock. For analytical methods, both continuum and discontinuum modeling approaches were employed in the analyses of the rock mass behavior for both lithophysal and non-lithophysal rock and in the evaluation of the stability of the openings.

Stability of the unsupported and supported non-emplacement drifts was evaluated in this analysis. The stability analysis was conducted for access mains, ramps, exhaust mains, turnouts, and intersections between main drifts with turnouts and emplacement drifts, observation drift, TBM launch chambers, and North Portal. The stability analysis of unsupported drifts at the interburden area between access drift to intake shaft #1 and two underlying exhaust mains was also performed.

The excavation effects (i.e., state of the stress change due to excavation), thermal effects (i.e., due to heat output from waste packages), and seismic effects (i.e., from potential earthquake events) were evaluated, and stress controlled modes of failure were examined for representing rock mass categories of 1 and 5. The focus was on the category 1 rock because this rock mass is generally weaker than other categories of rock mass.

No credit or account was given for the initial or temporary ground support in modeling the final ground support systems for non-emplacement drifts in this analysis.

It should be noted that the results presented in this calculation are based on the adopted methods, input data and assumptions. If any input information is changed, the output information may vary. Also, as the design of ground support systems for LA progresses, the evaluation of ground control for non-emplacement drifts will be updated as necessary.

### **7.2 STABILITY OF UNSUPPORTED NON-EMPLACEMENT DRIFTS**

For unsupported access/exhaust mains under in situ stress loading, a very narrow zone adjacent to wall (about 0.2 m into wall) is shown with potential yield for lithophysal rock. At distance of 1.5 m into wall SF increases to 2. For non-lithophysal rock, almost no yield is observed near the wall and SF increases to 2 with a very short distance (about 0.2 m) into wall. There is no indication of instability of the rock surrounding the unsupported access/exhaust mains and turnouts.

For unsupported intersection between access mains and turnouts, the 3DEC models predict similar deformation and stability conditions for intersections with large and small roof spans. The rock mass deformation around intersections will be predominantly elastic. The damage is

expected to extend approximately 1 m from the drift walls into the rock mass, in the worst case, for the poorest quality rock mass. A relatively large displacement of 7 cm predicted for the lithophysal rock mass, category 1, is a consequence of the very low Young's modulus used. There are no indications of loosening and instability of the rock mass in the crown for any of the analyzed cases. The roof in the intersections appears to be stable, even for the largest spans.

The tips of the pillars between the access main and the turnouts will be damaged due to stress concentrations. The extent of this damage from the pillar tip will depend on the rock mass quality. Rounding of the pillars and additional ground support will resolve the problem of pillar instability.

Similar stability condition for intersections and pillars between exhaust mains and emplacement drifts as those at intersections at access mains are also obtained based on the computer results.

The thermal stress changes are much larger in better quality and stiffer rock masses. The increase in the maximum major principal stress is about 15 MPa in category 5 of the lithophysal and non-lithophysal rock masses. However, the stress change does not change factor-of-safety with respect to the Mohr-Coulomb yield condition throughout the rock mass nor cause significant additional yielding of the rock mass. The extent of plastic deformation for locations B and D, and for the different rock-mass categories remains practically unchanged after 50 years of heating.

The results of seismic analysis can be concluded that the seismic events with a mean annual exceedance probability of  $1 \times 10^{-4}$  does not cause significant, permanent change in the factor-of-safety with respect to the Mohr-Coulomb yield condition or increase the volume of the rock mass subject to tensile stresses. The average stresses in the pillar between the drifts are almost unchanged.

For unsupported observation drift, excavations of the emplacement drift and the observation drift do not interact with each other. The predicted extent of the damage of the rock mass surrounding the observation drift and the emplacement drift is similar. There is a little more damage in the walls and the floor of the observation drift because of mechanically less-favorable shape. However, the factor-of-safety with respect to Mohr-Coulomb shear failure increases very quickly as a function of distance from the drift boundary; the factor-of-safety is larger than 2 only a couple of meters from the drift walls.

It does not appear that the temperature change causes any additional damage around the observation drift. It also indicates that thermal loads do not affect the stability conditions of the rock mass around the intersection between the observation drift and the exhaust main.

The observation drift was analyzed for seismic loading due to 10,000-yr ground motion in both typical cross-section and at the intersection between the observation drift and the exhaust main. The results indicate that seismic load causes insignificant increase in damage around the observation drift, but there is no indication of large-scale instability.

For unsupported TBM launch chamber, due to the span (or height) of the launch chamber is approximately two times of the span of the observation drift, the depth of the damaged rock in the wall of the launch chamber is about 2 m, compared to the depth of about 1 m predicted in the

wall of the observation drift. Outside the yielded region, the factor-of-safety to shear failure increases rapidly as a function of distance from the drift wall, indicating overall stability of the excavation.

The results of the seismic analysis of the TBM launch chamber are very similar to the results obtained for the observation drift. Preclosure seismic shaking causes relatively small additional damage of the rock mass, but there is no indication of global instability of the launch chamber during or after the shaking.

The stability analysis for interburden pillar between access drift to intake shaft #1 and two underlying exhaust mains subjected to in-situ stress, thermal, and seismic loading has been performed. The results indicate that the effect of the excavation of an overlying 7.62-m-diameter access drift and two underlying 7.62-m-diameter exhaust mains on the stability of 10-m high interburden pillar is minimum or insignificant.

For unsupported North Portal including starter tunnel, the model under static in situ conditions after both the slope and the starter tunnel are excavated indicate that the stress state is completely elastic. Small overburden and slope heights result in stresses that are small compared to cohesion, even in the case of the poorest-quality rock mass, category 1, which was considered in the calculation. The factor-of-safety with respect to Mohr-Coulomb shear failure is quite large (approximately 5) throughout the entire model. The magnitude of the displacements due to the excavation of the starter tunnel is very small, of the order of 0.002 m or less. It appears from the results of the numerical modeling that the North Portal and the starter tunnel would be stable for the considered mechanical properties of the rock mass even if no ground support was used.

### **7.3 GROUND SUPPORT SYSTEM FOR NON-EMPLACEMENT DRIFTS**

The ground support system designed for non-emplacement drifts is described as follows:

- For non-emplacement openings except intersections between access mains and turnouts and between exhaust mains and emplacement drifts, ramps, and starter tunnel: fully grouted rock bolts with heavy duty welded wire fabric (WWF).
- For intersections between access mains and turnouts and between exhaust mains and emplacement drifts, ramps, and starter tunnel: fully grouted bolts with fiber-reinforced shotcrete, and lattice girders as necessary for roof span control.

The fully grouted rock bolts with typical length of 3 m, spaced at 1.25 m with heavy duty WWF are designed to be used for ground support at typical access mains, exhaust mains, turnouts, observation drift and test alcove. For ground support system in intersection areas, bolting pattern with the same bolt spacing as that for access mains with increased bolt length of about 5 m and 0.10 m thick fiber-reinforced shotcrete will be installed, and supplemented with lattice girder as necessary, depending on rock mass quality and control of roof span.

It is noted that the same ground support system for the intersections will be applied to starter tunnel and ramps except that the bolt length is 3 m long. The designed ground support system for ramps may be only for North Ramp and may need to be changed for North Construction Ramp

and South Ramp as fully grouted rock bolts with heavy duty WWF, with fiber-reinforced shotcrete installed on as-needed basis, depending on the construction schedule.

For the ground support at North Portal, 3 m long fully grouted rock bolts on 1.5 m spacing will be installed around the portal lateral faces whereas 5 m long bolts with the same spacing will be installed at the frontal face. The portal face will be fibercreted to a thickness of 0.1 m. Similar ground support design is expected for North Construction Portal and South Portal if their topographical and ground conditions, geometry, and construction method are similar.

Candidate ground support components to be used in non-emplacment excavations will be carbon steels including high-strength low-alloy steel, which are considered adequate as long as they are manufactured based on the proper ASTM standard specifications and the strength requirements are met. For cementitious materials to be used for grouted rock bolts, shotcrete or concrete, a low pH grout and shotcrete/concrete mix or use of other types of grouts and cements made of non-portland cement types is proposed.

#### **7.4 STABILITY OF SUPPORTED NON-EMPLACEMENT DRIFTS**

For stability condition of supported non-emplacment openings, the computer models do not indicate formation of a failure mechanism, or the accumulation of residual displacement, which is a result of plastic deformation of the rock mass during shaking. However, the results do not imply that rockfall of any kind will not occur during an earthquake with 10,000 year return period. The limitation of this model is that it is formulated based on continuum mechanics. Consequently, it is not possible to simulate the formation of new or reopening of existing fractures, which could form loose blocks, resulting in a rockfall. The analysis implies that, if there is no ground support, the rockfall will be fairly limited and confined to the drift boundary. The designed ground support would prevent any potential rockfall.

To a large extent the load in the rock bolts is determined by the percentage of total relaxation completed at the moment of bolt installation, and by the stiffness and shear strength of the grout. Assuming 75% of stress relaxation due to a stand-off between the advancing face and installed rock bolts, the maximum forces in the bolts in the access main before excavation of the turnouts is predicted to be 143 kN. However, the majority of the bolts are loaded to less than 100 kN. Excavation of the turnouts results in an increase in load to less than 200 kN in the bolts above the turnouts. The bolts will remain elastic due to the loads generated by the convergence of the drifts for in-situ stresses. The forces in the rock bolt generated by the convergence of the drifts will act as an active force, as if the bolts are pre-tensioned. However, the bolts will have a reserve between 50 kN and 100 kN for the additional loading.

Seismic load has insignificant effect on the rock bolts. It appears that the shotcrete would be damaged during an earthquake with 10,000 year return period, but that damage (mostly tensile cracks) would be localized.

The stability condition of supported exhaust mains and their intersections are similar to those of access mains and the adjacent intersections. The maximum load in the bolts in the exhaust main after excavation of the exhaust main is around 100 kN, with exception of a few bolts affected by the local conditions. The maximum force in the bolts increases to approximately 120 kN in the

regions above the intersection after excavation of both exhaust mains and the emplacement drifts. Those loads are well within the limit of the elastic deformation of the bolts, which have yield strength of 264 kN.

The forces in the bolts increase during the preclosure period due to heating. However, even using the conservative analysis, the predicted maximum force in the rock bolts is about 185 kN during the preclosure period, which is less than the yield strength. The maximum increase in bolt forces due to seismic loading compared to the static condition is approximately 55 kN in the region above the intersection, with the bolt load less than the yield strength. Note that the dynamic analysis of global stability of the intersections was carried out using the continuum models. In the simulations of intersections, the blocks were glued together to behave effectively as a continuum. Thus, the local stability of blocks created by joints around the excavation was not considered. However, such blocks will be of limited size and number and will be effectively supported by the designed ground support.

For supported observation drift under static loading, the forces in bolts are insignificant considering the bolt yield strength of 264 kN. Thermal load causes an increase in bolt forces, however, the loads are well within the range of elastic deformation of the rockbolts after 50 years of heating. The designed bolt length of 3 m appears to be sufficient to provide anchoring into the elastic (undamaged) rock. The maximum bolt force after seismic shaking is much less than the bolt yield strength of 264 kN.

For supported TBM launch chambers, the rockbolts do not take any load due to rock mass deformation caused by the relaxation of in situ stresses, as the launch chamber will be excavated using the drill-and-blast method. The forces in the rockbolts at the end of dynamic simulation are small relative to the yield strength of the rockbolts. Comparison of the bolt lengths and the size of the region of damaged rock suggests that the designed bolt length is sufficient, because the anchoring length into the elastic rock mass is approximately at least 1 m.

For supported North Portal, the ground support is installed after complete relaxation of the in situ stresses due to excavation of the North Portal and the starter tunnel. Consequently, the ground support does not take any load under static conditions. The forces and stresses in the ground support at North Portal and starter tunnel induced by the seismic loading at two stages during simulation are analyzed. The forces in the bolts are less than 10 kN, which is much smaller than the yield strength of the fully grouted bolts, i.e., 264 kN. The compressive stresses in the shotcrete are very small. However, the considered ground motion could cause localized tensile failure in the shotcrete. The failure will occur in the form of fractures that will not affect functionality of the shotcrete either on the slopes at the portal surface or in the starter tunnel.

## 8. REFERENCES

### 8.1 DOCUMENTS CITED

ASM International 1990. *Properties and Selection: Irons, Steels, and High-Performance Alloys*. Volume 1 of *Metals Handbook*. 10th Edition. Materials Park, Ohio: ASM International. TIC: [245666](#).

Atlas Copco. 2003. Swellex® – The Engineered Rock Reinforcement System, Extending the Traditional Role of Rock Bolts. [Commerce City, Colorado]: Atlas Copco. TIC: [254198](#).

Barton, N.; Lien, R.; and Lunde, J. 1974. "Engineering Classification of Rock Masses for the Design of Tunnel Support." *Rock Mechanics*, 6, (4), 189-236. New York, New York: Springer-Verlag. TIC: 219995.

Barton, N. 2002. "Some New Q-Value Correlations to Assist in Site Characterization and Tunnel Design." *International Journal of Rock Mechanics & Mining Sciences*, 39, (2), 185-216. New York, New York: Elsevier. TIC: 252648.

Bieniawski, Z.T. 1984. *Rock Mechanics Design in Mining and Tunneling*. Rotterdam, The Netherlands: A.A. Balkema. TIC: [4281](#).

Bieniawski, Z.T. 1989. *Engineering Rock Mass Classifications*. New York, New York: John Wiley & Sons. TIC: 226350.

Board, M. 2003. *Resolution Strategy for Geomechanically-Related Repository Design and Thermal-Mechanical Effects (RDTME)*. REV 00. Las Vegas, Nevada: Bechtel SAIC Company. ACC: [MOL.20030708.0153](#).

BSC (Bechtel SAIC Company) 2001. *Ground Control for Emplacement Drifts for SR*. ANL-EBS-GE-000002 REV 00 ICN 01. Las Vegas, Nevada: Bechtel SAIC Company. ACC: [MOL.20010627.0028](#).

BSC 2003a. *Input Parameters for Ground Support Design*. 800-K0C-TEG0-00500-000-00A. Las Vegas, Nevada: Bechtel SAIC Company. ACC: [ENG.20030515.0002](#).

BSC 2003b. Not used.

BSC 2003c. *Subsurface Geotechnical Parameters Report*. 800-K0C-WIS0-00400-000-00A. Las Vegas, Nevada: Bechtel SAIC Company. ACC: ENG.20040108.0001.

BSC 2003d. *Q-List*. TDR-MGR-RL-000005 REV 00. Las Vegas, Nevada: Bechtel SAIC Company. ACC: [DOC.20030930.0002](#).

BSC 2003e. *Underground Layout Configuration*. 800-P0C-MGR0-00100-000-00E. Las Vegas, Nevada: Bechtel SAIC Company. ACC: [ENG.20031002.0007](#).

BSC 2003f. *Ground Control for Emplacement Drifts for LA*. 800-K0C-TEG0-00100-000-00A. Las Vegas, Nevada: Bechtel SAIC Company. ACC: [ENG.20031016.0001](#).

BSC 2003g. *Scoping Analysis on Sensitivity and Uncertainty of Emplacement Drift Stability*. 800-K0C-TEG0-00600-000-000. Las Vegas, Nevada: Bechtel SAIC Company. ACC: [ENG.20031125.0002](#).

BSC 2004. *Committed Ground Support Materials for LA Design*. 800-K0C-WIS0-00100-000-00C. Las Vegas, Nevada: Bechtel SAIC Company. ACC: [ENG.20040119.0011](#).

CRWMS M&O (Civilian Radioactive Waste Management System Management and Operating Contractor) 1997. *ESF North Portal Stability Analysis*. BABEE0000-01717-0200-00015 REV 00. Las Vegas, Nevada: CRWMS M&O. ACC: [MOL.19970711.0032](#).

Deere, D.U. and Deere, D.W. 1988. "The Rock Quality Designation (RQD) Index in Practice." *Rock Classification Systems for Engineering Purposes*. Kirkaldie, L., ed. ASTM STP 984. Pages 91-101. Philadelphia, Pennsylvania: American Society for Testing and Materials. TIC: [216484](#).

DOE 2003. *Quality Assurance Requirements and Description*. DOE/RW-0333P, Rev. 13. Washington, D.C.: U.S. Department of Energy, Office of Civilian Radioactive Waste Management. ACC: [DOC.20030422.0003](#).

Dowding, C.H. 1979. "Earthquake Stability of Rock Tunnels." *Tunnels & Tunnelling*, 11, 15-20. London, England: Morgan-Grampian Publishing. TIC: [242115](#).

DSI (Dywidag-Systems International) "DYWIDAG Threadbar." *DSI Ground Support Systems*. Bolingbrook, Illinois: Dywidag-Systems International. TIC: [255197](#).

Hardy, M.P. and Bauer, S.J. 1991. *Drift Design Methodology and Preliminary Application for the Yucca Mountain Site Characterization Project*. SAND89-0837. Albuquerque, New Mexico: Sandia National Laboratories. ACC: NNA.19910808.0105.

Hoek, E.; Kaiser, P.K.; and Bawden, W.F. 2000. *Support of Underground Excavations in Hard Rock*. Rotterdam, The Netherlands: A.A. Balkema. TIC: 252991.

Hutchinson, D.J. and Diederichs, M.S. 1996. *Cablebolting in Underground Mines*. Richmond, British Columbia, Canada: BiTech Publishers. TIC: [249146](#).

Itasca Consulting Group. [2002]. *Itasca Software—Cutting Edge Tools for Computational Mechanics*. Minneapolis, Minnesota: Itasca Consulting Group. TIC: [252592](#).

Jaeger, J.C. and Cook, N.G.W. 1979. *Fundamentals of Rock Mechanics*. 3rd Edition. New York, New York: Chapman and Hall. TIC: [218325](#).

Merritt, F.S., ed. 1983. *Standard Handbook for Civil Engineers*. 3rd Edition. New York, New York: McGraw-Hill. TIC: [206892](#).

Minwalla, H.J. 2003. *Project Design Criteria Document*. 000-3DR-MGR0-00100-000-001. Las Vegas, Nevada: Bechtel SAIC Company. ACC: [ENG.20030402.0001](#).

Onofrei, M.; Gray, M.N.; Pusch, R.; Borgesson, L.; Karnland, O.; Shenton, B.; and Walker, B. 1993. *Sealing Properties of Cement-Based Grout Materials Used in the Rock Sealing Project*. AECL-10815. Pinawa, Manitoba, Canada: Atomic Energy of Canada Limited, Whiteshell Laboratories. TIC: [210964](#).

Ruest, M. and Martin, L. 2002. *FLAC Simulation of Split-Pipe Tests on an Instrumented Cable Bolt*. CIM Vancouver 2002, Paper No. 287. Montreal, Canada: Canadian Institute of Mining, Metallurgy and Petroleum. TIC: [255291](#).

Wickham, G.E.; Tiedemann, H.R.; and Skinner, E.H. 1972. "Support Determinations Based on Geologic Predictions." *Proceedings: North American Rapid Excavation and Tunneling Conference, Chicago, Illinois, June 5-7, 1972*. 43-64. New York, New York: American Institute of Mining, Metallurgical, and Petroleum Engineers. TIC: [226274](#).

## **8.2 CODES, STANDARDS, REGULATIONS, AND PROCEDURES**

ACI (American Concrete Institute) 506R-90(95). 1995. *Guide to Shotcrete*. Farmington Hills, Michigan: American Concrete Institute. TIC: [238721](#).

ACI 506.2-95. 1995. *Specification for Shotcrete*. Detroit, Michigan: American Concrete Institute. TIC: [226412](#).

AISC (American Institute of Steel Construction) 1997. *Manual of Steel Construction, Allowable Stress Design*. 9th Edition, 2nd Revision, 2nd Impression. Chicago, Illinois: American Institute of Steel Construction. TIC: [240772](#).

AP-3.12Q, Rev. 2, ICN 1. *Design Calculations and Analyses*. Washington, D.C.: U.S. Department of Energy, Office of Civilian Radioactive Waste Management. ACC: DOC.20030827.0013.

ASTM (American Society for Testing and Materials) ASTM A 36/A 36M-03a. 2003. *Standard Specification for Carbon Structural Steel*. West Conshohocken, Pennsylvania: American Society for Testing and Materials. TIC: [254846](#).

ASTM A 82-97a. 1998. *Standard Specification for Steel Wire, Plain, for Concrete Reinforcement*. West Conshohocken, Pennsylvania: American Society for Testing and Materials. TIC: [246400](#).

ASTM A 242/A 242M-03a. 2003. *Standard Specification for High-Strength Low-Alloy Structural Steel*. West Conshohocken, Pennsylvania: American Society for Testing and Materials. TIC: [254844](#).

ASTM A 276-03. 2003. *Standard Specification for Stainless Steel Bars and Shapes*. West Conshohocken, Pennsylvania: American Society for Testing and Materials. TIC: [254842](#).

ASTM A 588/A 588M-03. 2003. *Standard Specification for High-Strength Low-Alloy Structural Steel with 50 ksi [345MPa] Minimum Yield Point to 4-in. [100-mm] Thick*. West Conshohocken, Pennsylvania: American Society for Testing and Materials. TIC: [254843](#).

ASTM F 432-95 (Reapproved 2001). 1995. *Standard Specification for Roof and Rock Bolts and Accessories*. West Conshohocken, Pennsylvania: American Society for Testing and Materials. TIC: [253986](#).

BSC 2002. *Software Code: 3DEC*. V2.01. PC WINDOWS 2000/NT 4.0. 10025-2.01-00.

BSC 2002. *Software Code: FLAC*. V4.0. PC WINDOWS 2000/NT 4.0. 10167-4.0-00.

BSC 2002. *Software Code: FLAC3D*. V2.1. PC WINDOWS 2000/NT 4.0. 10502-2.1-00.

### 8.3 SOURCE DTNS

[MO0306SDSAVDTH.000](#). Seismic Design Spectra and Acceleration, Velocity, and Displacement Time Histories for the Emplacement Level at 10<sup>-4</sup> Annual Exceedance Frequency. Submittal date: 06/26/2003.

[MO0402SDSTMHIS.004](#). Seismic Design Spectra and Time Histories for the Surface Facilities Area (Points D/E) for 5E<sup>-4</sup> Annual Exceedance Frequency. Submittal date: 02/09/2004.

[SNL01B05059301.006](#). Laboratory Thermal Expansion Data for Boreholes UE25 NRG-4, NRG-5; USW NRG-6 and NRG-7/7A. Submittal date: 02/07/1996.

SNF37100195002.001. Hydraulic Fracturing Stress Measurements in Test Hole: ESF-AOD-HDFR1, Thermal Test Facility, Exploratory Studies Facility at Yucca Mountain. Submittal date: 12/18/1996.